NDOT Research Report

Report No: RDT-01-003

Dynamic Testing and Analysis of Non-Prismatic Reinforced Concrete Bridge Columns Retrofitted with FRP Jackets

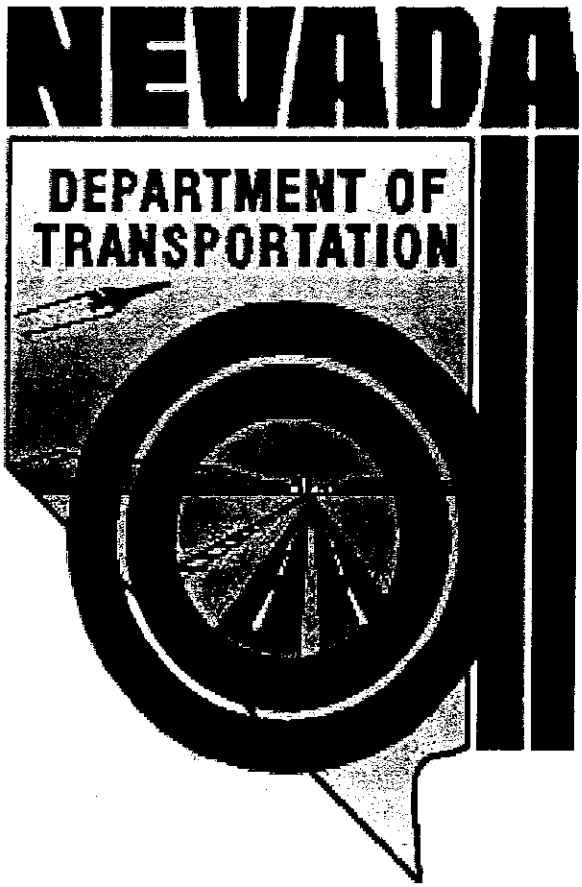

April 11, 2001

TECHNICAL REPORT DOCUMENTATION PAGE

1. Report No.	2. Government Accession No.	3. Recipient's Catalog No.
RDT-01-003		

4. Title and Subtitle	5. Report Date
Dynamic Testing and Analysis of Non-Prismatic Reinforced Concrete Bridge Columns Retrofitted with FRP Jackets	**January 2000**
	6. Performing Organization Code
7. Author(s)	8. Performing Organization Report No.
F. Martinovic, M. Saiidi, D. Sanders, and F. Gordaninejad	**CCEER-00-4**
9. Performing Organization Name and Address	10. Work Unit No.
Center for Civil Engineering Earthquake Research **Department of Civil Engineering/258** **University of Nevada, Reno** **Reno, NV 89557**	
	11. Contract or Grant No.
12. Sponsoring Agency Name and Address	13. Type or Report and Period Covered
Nevada Department of Transportation **1263 S. Stewart** **Carson City, NV 89712**	
	14. Sponsoring Agency Code

15. Supplementary Notes

16. Abstract

This document presents the development and experimental validation of seismic retrofitting of non-prismatic (flared) reinforced concrete bridge columns. Fiber reinforced plastic (FRP) jacketing was installed on the non-prismatic columns to enhance the shear capacity and improve the seismic response of the columns. Two .03-scale columns, one encased with a glass fiber-epoxy and the other with a carbon fiber-epoxy fabrics were tested. A shake table was used to load the column with a strong motion accelerogram from the 1994 Northridge earthquake. The measured results were compared to those from testing of an as-built and steel-jacketed specimen to evaluate the effectiveness of the retrofit methods. The FRP jacket design and installation methods, as well as shear capacity calculation are presented. The experimental data indicated that both FRP jackets significantly improved the shear capacity and ductility. The performance of the columns retrofitted with FRP was very similar to that of a steel-jacketed column.

17. Key Words	18. Distribution Statement
carbon, composites, earthquakes, glass, reinforced concrete, retrofit	**Unrestricted. This document is available through the National Technical Information Service, Springfield, VA 21161**

19. Security Classif. (of this report)	20. Security Classif. (of this page)	21. No. Of Pages	22. Price
Unclassified	Unclassified	**154**	

ACKNOWLEDGEMENTS

This study was funded by the Nevada Department of Transportation (NDOT). However, the opinions, findings and conclusions presented in this thesis are those of the author and do not necessarily represent the views of NDOT.

The authors would like to express their appreciation for the helpful comments of Mr. Bill Crawford, Chief Bridge Engineer and NDOT. Thanks are due to Dr. Nadim Wehbe of South Dakota State University for his original work in the study of flared columns and his assistance in this project. Special thanks are due to John Drumm, Jesus Pedroarena, and the staff of the Civil Engineeing Department for their help and support. Messrs Ed Fyfe and Scott Arnold of the Fyfe Co. are thanked for their close interaction in selection and application of the fiber reinforced plastic composites.

This report is based on a M.S.C.E. thesis by the first author supervised by the other authors.

ABSTRACT

This document presents the development and experimental validation of seismic retrofitting of non-prismatic (flared) reinforced concrete bridge columns. Fiber reinforced plastic (FRP) jacketing was installed on the non-prismatic columns to enhance the shear capacity and improve the seismic response of the columns. Two 0.3-scale columns, one encased with a glass fiber-epoxy and the other with a carbon fiber-epoxy fabrics were tested. A shake table was used to load the column with a strong motion accelerogram from the 1994 Northridge earthquake. The measured results were compared to those from testing of an as-built and steel jacketed specimen to evaluate the effectiveness of the retrofit methods. The FRP jacket design and installation methods are presented. The experimental data indicated that both FRP jackets significantly improved the shear capacity and ductility. The performance of the columns retrofitted with FRP was very similar to that of a steel jacketed column.

TABLE OF CONTENTS

LIST OF TABLES

LIST OF FIGURES

Chapter 1

Introduction

1.1 General Perspective

Many existing highway bridges were constructed prior to understanding of seismic actions[22]. Hence, in nearly every recent major earthquake, bridge failures have occurred resulting in extensive bridge damage, collapse, and in some cases loss of life. The knowledge gained through observation and evaluation of damage in highway structures after recent strong earthquakes is used as a basis for assessing the ability of the existing infrastructure to withstand future event. Based on these assessments, seismic retrofitting of highway bridges has become commonplace to ensure public safety. Much of our recent seismic retrofitting has been based on lessons learned from the 1989 Loma Prieta and 1994 Northridge earthquakes.

Current highway bridge seismic design provisions outline a stringent procedure which has been developed since the 1971 San Fernando earthquake. The provisions have the purpose of safeguarding against major structural failures that can lead to the loss of life and service during a large earthquake[1]. The seismic design philosophy comes from the desire to allow large inelastic deformations, without significant strength degradation of the bridge and without major structural failure. Since the bridge superstructure in concrete bridges remains essentially linear during earthquakes, the bridge columns must be designed such that they allow a ductile behavior well into post-elastic deformations caused by strong earthquake motions.

The seismic response of reinforced concrete highway bridge columns is dominated by providing a ductile behavior through the non-linear deformations, thus allowing the column to dissipate significant earthquake energy prior to strength degradation. In reinforced concrete column design, high levels of ductility are achieved through the proper detail of transverse steel to provide sufficient confinement and to prevent longitudinal bar buckling. The confinement prevents the column core from dilating, thus ensuring high compressive stresses can be accommodated after the spalling of the cover concrete. This allows the bridge superstructure to still be supported by the column. The high capacity of column core also delays buckling of the longitudinal reinforcement. Buckling of longitudinal bars occurs in two different modes: (1) over a large segment length of the column resulting from yield and fracture of one or more layers of transverse reinforcement, (2) in the spacing between the two transverse steel layers. The first type of buckling typically presents a more desired mode of failure, as the column damage is not limited to a discrete location, thus significant energy dissipation can take place prior to column failure. The second type of failure is undesirable due to the low levels of energy dissipation associated with the failure of the

column in a very localized manner. This mode of buckling is prevented in the current design of columns as the spacing between transverse steel is very small.

In order to achieve large inelastic deformations, and thus high levels of ductility, brittle failure modes must be prevented. In reinforced concrete columns the most critical type of failure to prevent is shear failure. It occurs in a brittle mode, presenting very little warning prior to the failure. Shear failure occurs with the formation of inclined cracks once the tensile strength of concrete is exceeded. The extension and opening of these cracks creates large stresses on the transverse reinforcement, thus leading to the yield and fracture of the bars. The failure of the transverse steel then allows the longitudinal steel to buckle, leading to the disintegration of the column core and brittle column failure. Furthermore, large inelastic deformations in the plastic hinge reduce the shear capacity of the column.

Many of the reinforced concrete highway bridge columns built prior to the 1971 San Fernando earthquake lack sufficient transverse steel to ensure a ductile response and accommodate the seismic deformation demands. As a result many highway bridges have been retrofitted. For reinforced concrete columns with substandard reinforcement details, retrofit systems consisting of concrete, steel, and advanced composite jackets have been developed and installed. The method used most often for enhancing ductility and shear strength is steel jacketing. The use of advanced composite jacketing, typically called fiber reinforced plastics (FRP), has become increasingly popular over the last 3-5 years.

During the 1994 Northridge earthquake several highway bridge structures failed in non-ductile shear failure modes. One of these bridges was the SR-118 Mission/Gothic undercrossing that was supported on one-way flared columns[33,34]. The column flares were designed to be non-structural, and thus were assumed not to contribute to the response of the column. An experimental study of those columns was completed by the University of California, San Diego, which determined that the column flare contributed to a significant flexural enhancement in the column, forcing the column to fail in shear[28].

In California and Nevada, the use of non-prismatic reinforced concrete highway bridge columns (one-way and two-way flared columns) has been extensive. The surprising failure of the SR-118 Mission/Gothic undercrossing prompted the Nevada Department of Transportation (NDOT) to fund an evaluation of flared bridge columns in Northern Nevada. A series of studies involving an analytical and experimental assessment of seismic vulnerability of flared highway bridge columns and the development of retrofit methods was undertaken at the University of Nevada, Reno[5,17,37]. The part reported in this document is the fourth part of the series. The benefits of using FRP jacketing was investigated in this study to test validity of this method on retrofitting non-prismatic columns. A comparison of the steel jacketing from a previous study[17] is made with FRP jacketing to help determine the differences between the retrofit methods.

1.2 Previous Work

The experimental research pertaining to the seismic behavior of reinforced concrete highway bridge columns is quite extensive. The majority of the published research address the retrofit of circular and rectangular columns, and very little research has been conducted on the seismic response of octagonal, non-prismatic bridge columns. There is a considerable amount of research on the retrofit of prismatic reinforced concrete columns using advanced composite jackets. The research is widely varied with respect to types of composites used and methods of installation.

This is the first study to consider the use of advanced composite jackets on non-prismatic reinforced bridge columns. The discussion of previous work that follows is limited to the experimental research on each of these components to present some background on: (1) the seismic performance of non-prismatic bridge columns, and (2) the effects of FRP jacketing of reinforced concrete columns.

1.2.1 Non-Prismatic Bridge Columns

Prior to the 1994 Northridge earthquake very little attention was paid to one-way and two-way flared columns. The effect of column flares was considered to be minimal due to its design and purpose being primarily non-structural. The shear failure of several one-way flared columns in the 1994 Northridge earthquake prompted research to determine the seismic response of one-way flared columns as these columns are widely used in the western United States.

A preliminary analytical study of the SR-118 Mission/Gothic undercrossing was conducted by the National Institute of Standards and Technology (NIST)[19] and the University of California, San Diego (UCSD)[24].

The main longitudinal reinforcement in the columns consisted of bars placed in a circular manner throughout the height of the column, with very little reinforcement in the flared portion of the column. It was thought that the column flares would spall off during severe lateral loading, thus not increasing the flexural capacity of the column. Both studies concluded that the flares contributed to the flexural enhancement of the column, and that the spalling of the flare would not occur as planned.

USCD continued to investigate these columns with a study completed by Sanchez et al. which consisted of testing both as-built and retrofitted columns[28]. The study outlined the testing of ten, forty percent scale specimens in two phases. Phase one outlined the testing of four specimens modeled after the typical column detail on the SR-118 Mission/Gothic undercrossing, while phase two involved testing the other six specimens which were constructed using the current California Department of Transportation (CALTRANS) design methods. In both cases the main longitudinal steel was oriented in a circular pattern confined with spiral transverse reinforcement.

In that study, an increase in flexural capacity was measured in both phases of the testing. The predicted failure mode from the analytical analysis was verified with the plastic hinge being developed at the junction of flared and non-flared segments rather than the end of the column. The study suggested a retrofit method of decoupling the effect of the flared portion of the column through cutting the flare at the soffit, leaving a gap between the flare and the soffit. This type of retrofit would reduce the effect of the flare and possibly lead to the spalling of the flared portion of the column during a seismic event, as previously thought.

Webhe et al.[37] investigated the seismic behavior of four highway bridges with flared columns located in northern Nevada. The one-way flared columns, in general, were constructed using two different reinforcement details. The first type of columns is somewhat similar to those that failed during at the Mission/Gothic undercrossing in that they consist of a longitudinal steel distributed in a prismatic circular pattern through the core of the column. However, unlike the columns in Mission/Gothic undercrossing, these columns have heavily reinforced (longitudinal and transverse) flares. In the second type of columns, the primary longitudinal reinforcement follows the column flare without a core longitudinal reinforcement or spirals, and the transverse reinforcement consisted solely of lateral ties. A non-linear analysis was completed in this study which indicated the first type of column has sufficient shear capacity, and would respond well to seismic excitation[36]. However, the second type of column clearly showed an insufficient shear capacity, indicating probable brittle failure in a seismic event.

The results of the analytical study led to phases two to four of research that involved testing of large-scale flared columns at the University of Nevada, Reno. In the second phase, Webhe et al.[37] investigated two forty-percent scale as-built specimens subjected to quasi-static cyclic lateral loads. The results confirmed the need for the development of a retrofit system for the columns. Caywood et al.[5] studied two additional forty percent scale specimens that were retrofitted with steel jackets and tested subjected to slow cyclic loads. This study showed the steel jackets were effective in retrofitting the test specimens. The results from the first two parts of this series are outlined in more detail in Section 2.2.2.

The availability of the shake tables at the University of Nevada, Reno, allowed further testing of the flared columns to consider variation in the response of the columns due to a more realistic dynamic loading effects. The third phase study was conducted by McElhaney et al.[17], in which two thirty-percent scale specimens were tested. One specimen modeling the as-built columns while the other was retrofitted with a steel jacket. The purpose of the study was to verify the results of the first two studies and quantify the effects of the dynamic loading as compared to the quasi-static loading. The third study showed generally good correlation with the first two studies, while some variation existed due to the dynamic loading. A more detailed explanation of the results of the third study is discussed in Section 2.2.3, with some of the experimental data presented within this study to compare different retrofit methods. This study constitutes the fourth and final phase of research, in which two additional thirty-percent scale specimens were retrofitted with FRP jackets and tested using a shake table.

1.2.2 Advanced Composite Retrofit of Highway Bridge Columns

The use of advanced composites for seismic retrofit has become an increasingly popular area of research over the last several years. Many studies have considered the effects of FRP jacketing on columns for confinement, flexural behavior, shear strength and lap splice reinforcement. The research widely varies with respect to the type of composites used and configuration used to install the jacketing. A majority of the early research on advanced composite retrofit systems considered both active and passive confinement of the bridge column. The composite wrap in an active confinement system is prestressed during installation on the column, thus exerting confinement stresses even when the column is not deformed. In contrast, in a passive system, the jacket is simply attached to the column and its confining effect is not realized until the column undergoes lateral deformations. An active confinement system is no longer considered as an acceptable retrofit method[4,8]. This section outlines some of the relevant research to this test project relating to highway bridge columns retrofitted with advanced composites used in a passive manner.

USCD was one of the first research institutions to delve into the retrofit of reinforced concrete columns with advanced composites. Seible and Priestley[29] tested four 3.65-m (12-ft) rectangular cantilever columns 730 mm by 489 mm (28.75 in by 19.25 in). The specimens consisted of two retrofitted with a steel jacket and the other two with glass fiber-epoxy jacket. The jackets were installed in the plastic hinge region at the base of the column. The specimens were tested both in the weak and strong directions to determine the level of flexural increase experienced by the retrofit. The test results showed that the advanced composite and steel jackets performed very well, providing a ductility greater than $\mu_\Delta = 8$. The glass fiber-epoxy jackets showed slightly better confinement than the steel jackets, and were found to be a suitable retrofit method for reinforced concrete columns.

At the University of Utah, Salt Lake City, Gergely et al.[7], completed field-testing of a full-scale reinforced concrete column-cap beam connection retrofitted with carbon fiber-epoxy wrap to improve the shear strength of the system. The bridge pier consisted of three 0.914 m (36 in) diameter circular columns monolithically connected to a 1.067 m (42 in) square cap beam. The beam-cap connection required a seismic retrofit to overcome the transverse steel deficiencies. This study primarily tested the effectiveness of the beam-column joint rather than retrofitting the column. It was found that the shear capacity of the cap beam and columns were improved significantly by the advanced composite retrofit increasing the ductility of the bridge pier.

Xiao et al.[39], at the University of Southern California (USC), tested three fifty-percent scale circular column specimens. The specimens were 2440 mm (96 in) tall circular columns with a diameter of 610 mm (24 in). The reinforcement consisted of 2 percent longitudinal steel distributed in a circular manner, with hoops placed at a spacing of 150 mm (5.9 in). One specimen was tested as-built, with the other two retrofitted for enhanced shear strength with prefabricated glass fiber reinforced composite jackets consisting of: (1) individual shells, and (2) continuous shells. Both fiberglass jackets succeeded in improving the hysteretic response of the as-built column and improving the ductility.

The University of Arizona, Tucson has completed several studies in the use of advanced composites to retrofit reinforced concrete bridge columns. Two of these studies are presented below. In the first study discussed, Jin et al.[10] created a glass fiber jacket system that was used to retrofit reinforced concrete columns. The experimental study consisted of ten reinforced concrete columns, with five circular columns and five rectangular columns. The specimens were a twenty-percent scale of typical bridge columns constructed prior to 1971. Four as-built specimens and six retrofitted specimens with glass fiber composite jackets were tested. The as-built specimens had serious deficiencies in shear strength and lap splice detail. The test results showed that the advanced composite jackets greatly increased the columns ductility capacity and shear resistance, preventing brittle shear failure and bond failure witnessed in the as-built specimens.

In the second study at the University of Arizona, Saadatmanesh et al.[25] used a parametric study to present a method of using fiber reinforced straps to increase the strength and ductility of reinforced concrete columns. The goal was to provide a method using composite straps to increase the column confinement without impacting the flexural strength. In that study, the proposed method accomplished the goal of increasing confinement by placing straps at intervals along the column height leaving gaps between the straps. The parametric study indicated that this method of strapping the column was effective in both increasing the column ductility and strength.

USCD has completed several studies on the use of composite wrap jackets on reinforced concrete columns. Seible et al.[30]considered both steel jacketing and carbon fiber tow jackets to retrofit reinforced concrete bridge columns. The purpose of the study was to retrofit the column for deficiencies in shear strength, flexural ductility and lap splice bond failure. The experimental program consisted of forty-percent scale specimens subjected to cyclic loading. The specimens were 3.658 m (144 in) tall, with circular cross-sections of a diameter of 0.610 m (24 in). The longitudinal reinforcement was twenty-six 19-mm (#6) bars, with 6 mm (#2) lateral ties at a spacing of 127 mm (5 in). Four specimens were tested representing one as-built, one steel jacketed and two carbon fiber jacketed specimens. The carbon fiber tow jackets had a tensile strength of 1.29 MPa (188 ksi) with a Young's modulus of 124 GPa (18000 ksi). The carbon fiber jacketed specimens exceeded the measured displacement ductility and ultimate flexural strength of the steel jacketed specimens. The carbon fiber specimens reached a ductility of nearly $\mu_\Delta = 10$ prior to failure, while the steel jacketed column reached a ductility of $\mu_\Delta = 8$.

1.3 Objective and Scope

The primary objective of this study was to develop and experimentally validate a seismic retrofit system using advanced composite fabrics for non-prismatic reinforced concrete bridge columns. The study involves two different advanced composite materials, featuring both glass fiber-epoxy and carbon fiber-epoxy systems. The measured results from each of the test specimens was then compared to the as-built and steel jacketed specimens from a previous test[17], to identify possible advantages gained through the use of composites to retrofit highway bridge columns.

An experimental study was completed using two thirty-percent scale specimens of a prototype one-way flared reinforced concrete bridge column. The specimens constructed represent a scaled version of the columns with the highest steel ratio used on the prototype bridge because these columns were the most vulnerable to shear failure. Representative material properties of the prototype columns were used in the construction of the specimens. A new method of installation of composite fabrics on flared columns was developed. The composite jackets were installed in a similar manner on each specimen, with the only difference being jacket thickness and type of composite materials installed. The experimental procedure consisted of shake table testing using the measured strong motion accelerogram from the 1994 Northridge earthquake as measured at the Sylmar Hospital to excite the specimens.

Chapter 2

Test Background and Specimens

2.1 Introductory Remarks

The purpose of the experimental program was to complete the study series of the seismic behavior of flared highway bridge columns in bridge I-1250 in Reno, Nevada. The previous studies of flared columns involved testing of both as-built and retrofitted specimens with steel jackets[5,17,37]. This study outlines the testing of two additional thirty- percent scale flared column test specimens retrofitted with fiber reinforced plastic (FRP) jackets. A dynamic test program of the specimens was completed using an earthquake history and state-of-the-art shake table to load the columns.

The purpose of this chapter is to present: (1) selection of test specimens, (2) design of test specimens, (3) selection and design of FRP retrofit materials, (4) construction of test specimens, (5) material properties, and (6) test setup and instrumentation.

2.2 Selection of Test Specimens

This study is the fourth and final part of the series studying the seismic behavior of non-prismatic bridge columns at the University of Nevada, Reno. The first study in the series completed an in-depth analysis of several highway bridges located in Reno, Nevada[37]. This study identified bridge I-1250 on U.S. 395 as being of significant seismic risk, which prompted the Nevada Department of Transportation to fund an experimental study of the seismic response and retrofit of the bridge columns.

2.2.1 Details of Bridge I-1250

Bridge I-1250 is a sixteen-span reinforced concrete box girder structure. Each bent consists of six or seven one-way flared columns, with a total of 94 columns for the entire bridge. The column connections to the super structure are monolithic but are two-way hinges at the footing. The column heights vary from 6.1 m (20 ft) to 7.0 m (23 ft). The shape of the column is octagonal, with the cross-section dimensions varying with the column height in a parabolic manner. Details of the prototype bridge columns are shown in Figs. 2-1 and 2-2. The lower part of the columns is prismatic and the flared segments are over the upper 4.8 m (16 ft) part of the columns. The column width is constant over the entire height.

The longitudinal reinforcement ratio varies among different columns. In the previous studies, the steel ratios were described as low, medium, and high corresponding to 1.0, 1.4, and 1.8 percent at the top of the columns respectively. The longitudinal reinforcement follows the parabolic shape of the column giving way to four cross-sections within columns

of high steel ratio. The difference among different sections is the amount of longitudinal reinforcement, as the number of bars varies with the height of the column. The transverse reinforcement amount and detail were the same in all columns.

2.2.2 Specimens Tested Under Quasi-static Loads

The purpose of the first two phases of the four-part study was to test the seismic response of the bridge columns and provide a seismic retrofit method[5,37]. The analytical study of the bridge indicated that the columns lacked sufficient shear capacity. Both the low (LS) and high steel (HS) ratio columns were tested in phase two using a forty-percent scale prototype. These specimens were tested under a slow-cyclic loading with gradually increasing displacements.

Two as-built specimens were tested[37]. The test results indicated that neither test specimen failed in shear, but extensive shear cracking occurred at failure that presented cause for concern. The possibility of brittle shear failure warranted the design of a retrofit method and further testing of the specimens. Two additional specimens were constructed (R-LS and R-HS) and retrofitted with a steel jacket. The test results indicated that the steel jacketing was effective in controlling the shear cracking and reducing stresses in the transverse steel. The measured displacement of the retrofitted specimens was the same as the ductility capacity of the corresponding as-built specimens. The measured displacement ductility capacity of the as-built and retrofitted specimens with low longitudinal steel was $\mu_\Delta = 8$, which is considered acceptable under strong earthquake motions. Based on the measured data the factor of safety against shear failure in LS was approximately 1.35. As a result it was recommended not to retrofit columns with low steel ratio. The measured displacement ductility capacity of HS and R-HS was $\mu_\Delta = 6$, and the margin against shear failure of these columns was fifteen percent. Retrofit of these columns was considered necessary. With the availability of the shake tables, it was decided to conduct shake table studies of the columns that have a high steel ratio.

2.2.3 Specimens Tested on Shake Table

The third and fourth phases of the study series only considered the columns with high-steel ratio due to the acceptable seismic response of the columns with low steel ratio. In these phases the method of testing was changed to incorporate a true dynamic testing using a shake table and earthquake records. The forty-percent scale test specimens from the first two phases were too large to be tested on the shake table due to the capacity limits of the shake table. A non-linear dynamic computer simulation was performed on various scale specimens using RC-Shake[12,17]. The primary goal of the computer simulation was to find a smaller scale test specimen that would reach the same ultimate ductility level as in the first two studies, and not exceed the fundamental limitations of the shake table such as maximum displacement, maximum velocity, and actuator capacity. Each model of the test specimen was subjected to several different earthquake histories trying to achieve the same failure ductility level that was achieved during the first two studies. The analysis showed that the largest specimen that could be tested to failure was a thirty-percent scale of the prototype column.

2.3 Design of Shake Table Specimens

Thirty-percent scale test specimens were used in the final two phases of the study. In the third phase, two thirty percent scale specimens to represent an as-built and steel jacketed retrofitted column were tested. This study used two additional thirty percent scale test specimens that were retrofitted with FRP jackets. The specimens were labeled FA (as-built specimen), FR (steel jacketed retrofitted specimen), FRG (glass fiber-epoxy retrofitted specimen), and FRC (carbon fiber-epoxy retrofitted specimen). The column and footing details of the four specimens were identical.

2.3.1 Column Design

The column was built inverted with the largest cross-section attached to a footing and the smallest cross-section attached to an inertial mass rig. The footing was designed to rigidly attach the column to the shake table, simulating the prototype column connection to the bentcap. Figures 2-3 and 2-4 show the column test specimen detail. The top of the column was designed to be connected to the inertial mass rig, simulating the two-way pinned connection of the prototype column to the footing. The specimen effective height was 1778 mm (70 in) which was measured from the centerline of the applied inertial force to the top of the footing. This height represented a thirty percent scale of the clear height of the shortest (and hence the most critical) prototype columns. The shape of the test specimen was octagonal, with a one-way flare in the strong direction beginning with the largest section at the footing elevation decreasing in size from 1422 mm (56 in), and remaining prismatic for 38 mm (1.5 in). The top of the column consisted of a concrete block that provided a mounting surface for the mass rig connection. The weak direction of the column had a constant width of 356 mm (14 in) from footing to mass rig connection block.

As in the prototype, there were four typical cross-sections in the thirty-percent scale test specimen. The difference among the cross-sections is the amount of longitudinal reinforcement as the number of bars varied with the height of the column due to the non-prismatic shape, as shown in Fig. 2-4. The longitudinal reinforcement was Ø13 mm (#4) bars, which were nearly an exact scale of the prototype, the column bars are Ø35 mm (#11) in the prototype. The section at the connection to the footing had a longitudinal reinforcement ratio of 1.8. The reinforcing ratio then varied depending upon the elevation and termination of longitudinal bars. The bar cutoffs within the column height occurred at 508 mm (20 in) and 800 mm (31.5 in) corresponding to the typical cross-sections as seen in Fig. 2-3.

The transverse reinforcement was more difficult to scale due to the availability of typical bar sizes. The smallest available rebar size was Ø6 mm (#2) which did not scale well due to the volumetric ratio requiring a larger spacing than was required to prevent longitudinal bar buckling. A Ø4.5 mm (7 gage) smooth wire was used in order to provide sufficient bar spacing. Use of the smooth wire allowed the transverse reinforcement spacing to be 51 mm (2 in) along the length of the column, which modeled the Ø13mm (#4) bars at 102 mm (4 in) reasonably well. The smooth wire did create additional modeling concerns such as: (1) the difference in bond strength of smooth wire, and (2) finding smooth wire with

a yield strength of approximately 414 MPa (60 ksi). The smoothness of the wire was addressed by increasing both the lap length and hook length in the reinforcement detail to provide similar anchorage strength to that of deformed rebar. In the third phase these effects were considered and the increase in lap length and hook length was determined[17]. The lap lengths were increased from 36 bar diameters in the prototype to 45 bar diameters in the test specimens. The hook lengths were increased from 18 bar diameters in the prototype to 22.6 bar diameters in the test specimens.

A galvanized steel wire was chosen because it had sufficient yield strength and was. However, the zinc coating created the problems of substantially increasing the yield strength of the wire and potentially providing additional smoothness of the wire as compared to bare wire, which was not desired. The increase in the yield stress occurs when the wires go through a hot dip galvanization process. The zinc coating can reduce bond if the coating is thin because the coating can strip away easily. To avoid uncertainties due to the coating it was decided to remove it. The wire was submerged in a 0.1 Molar sodium bath, removing the zinc coating completely leaving only the bare steel wire. The average measured yield strength of bare wire was approximately 414 MPa (60 ksi) (Table 2-1).

The mass rig connection at the top of the column (Fig. 2-3) consisted of a rectangular concrete block 635 mm (25 in) high, 521 mm (20.5 in) long in the strong direction, and 559 mm (22 in) long in the weak direction. The mass rig was connected to the center of the block in the strong direction. An axial load was applied to the test specimen through a system of two hydraulic jacks and Dywidag prestressing bars. A steel I-beam, which was placed across the top of the block, supported the hydraulic jacks. The Dywidag bars extended from a base plate anchored in the footing up through the steel I-beam into the hydraulic jacks.

2.3.2 Footing Design

The footing of the test specimen represents the bent cap of the prototype column. The behavior of the bentcap was not being investigated in this study; therefore, the footing was overdesigned to prevent damage that might impact the test results of the test column.

The footing was designed as a rectangular spread footing. Details of the footing are shown in Figs. 2-5 and 2-6. The footing was 762 mm (30 in) high, 2438 mm (8 ft) long in the strong direction and 1829 mm (6ft) long in the weak direction. The steel reinforcement consisted of a top and bottom mat of ∅25 mm (#8) 90° hooked bars in both directions. Shear reinforcement was provided in the footing by placing ∅3 mm (#3) hooked ties at each at each intersection, the ties had a 90° hook at one end and a 270° hook at the other. The footing was fixed to the shake table through ten Dywidag prestressing bars. The Dywidag bars passed through the footing through ∅76 mm (3 in) vertical holes, into threaded couplers attached to the surface of the shake table, and stressed to 19.4 kN (4.36 kips).

2.3.3 Steel Jacket Retrofit Design

In general, the steel jacket retrofit was based on a compatibility relationship between the shear demand and the confinement capacity at the cross-section level. The detailed

method used to design the jacket is outlined in Refs. 5 and 17. The design considered shear strength, ductility, and constructability.

The steel jackets were designed in two segments leaving a physical discontinuity at the predicted plastic hinge location. The jacket was designed in an elliptical shape, in order to conform to the octagonal shape of the column. The jacket varied in a linear fashion along the height of the column in order to provide minimal gap between the column and the jacket. The jackets were of Grade 36 steel and had a thickness of 3.2 mm (0.125 in). The jackets were manufactured in half shells and assembled by placing them around the column and welding the shells together. After placing the jacket, grout was inserted in between the jacket and the column faces to ensure continuity. The grout thickness varied from 38 mm (1.5 in) to 64 mm (2.5 in). The jacket gap started at 441 mm (17.375 in) above the footing, and extended for 32 mm (1.25 in).

2.4 Selection and Design of FRP Jacket

The use of FRP jackets to retrofit highway bridge columns is becoming more accepted due to the high strength, light weight and the relative ease of application. The typical wrap consists of a fiber-reinforced plastic (FRP) which combines a fabric reinforcing material with a bonding agent. The fabric reinforcing material provides the composite wrap with its primary strength, while the bonding agent holds the reinforcing material together. The reinforcing material consists of uni-directional fibers which are arranged into a laminate by overlapping layers of reinforcing material in any direction to achieve the required strength. Due to the nature of the prototype columns, the choice of materials for this study required that an established, off the shelf, FRP system be used rather than creating a unique laminae.

In the previous studies of this series, the steel jacket retrofitted column performed well. However some flexural enhancement occurred which was undesirable. The flexural enhancement was due to a combination of the isotropic properties of the steel jacket, and the increase in the column cross-section due to the application of grout between the jacket and the column surface. FRP jackets minimize this problem since they are composed of uni-directional fibers that mainly strengthen the direction they are aligned. The uni-directional property allows the designer to uncouple the increase in shear capacity from flexural strength to a great extent. The FRP jacket is applied directly to the surface of the column, and does not require grout; therefore no appreciable increase in column cross-section is achieved. Some increase in flexural strength is encountered from the FRP jacket, but the increase is much less than that from a steel jacket.

2.4.1 Selection of FRP System and Supplier

Composite jackets used in the retrofit of highway bridge columns are generally composed of glass fiber-epoxy or carbon fiber-epoxy. There are a large number of suppliers who provide both the FRP materials and installation on highway bridge columns. However, there is a wide variation among composite jacket properties reported by different suppliers.

The reported material properties cannot be verified without knowing the exact composition of the fibers in the composite wrap, since the strength of the wrap is based on fiber size, quantity, and orientation. For the same fiber type, in general, the larger the fiber content, the higher the tensile strength of the composite, and the higher cost of the material. The fiber reinforcement can be composed of a single type of fiber or more than one type of fiber to enhance the flexibility and strength of the wrap. Each supplier creates their own patented recipe for their composite wrap fabric, creating large differences in material properties. A difference in material properties is expected among suppliers. However, care should be taken to ensure the supplier is reporting the material properties in accordance with accepted testing procedures such as ASTM D-3039[3].

The installation methods of composites vary between machine wrapping and hand wrapping of the columns. In machine wrapping, a robotic machine is used to apply a narrow strip of prepregnated material (with resin) around the column to create the FRP jacket. This method requires sufficient clearance under the bridge and around the column to physically install the robotic machine to the bent cap. Bridge I-1250 has many columns that are in a building that is located under the bridge, precluding the use of a robotic device. The hand wrapping method is ideal for columns within limited working spaces, as the fabric is installed in sheets wrapped around the column by hand. The key to this method is having sufficient expertise to ensure the material is properly installed on the column. The wrap must be sufficiently saturated with epoxy when placed on the column, completely flush with the column surface, preventing wrinkles and other effects that might cause voids in the composite jacket. Voids in the wrap severely impact the strength and durability of the jacket.

Installation expertise, therefore, becomes of prime importance in the selection of a supplier. Four composite suppliers companies were contacted. The supplier selected was Fyfe Co. LLC. The Fyfe system is currently approved by the California Department of Transportation[4] (CALTRANS), and other State DOT's. It was determined that one specimen would be retrofitted using carbon fiber-epoxy, and the other with glass fiber-epoxy. Two different materials were chosen due to their individual advantages. The carbon-fiber wrap has a very high tensile strength. It provides excellent resistance to environmental effects that are of great concern in a highway bridge application. The glass fiber-epoxy wrap has a lower tensile strength than carbon-fiber, requiring more layers of the material to provide the equivalent strength, however the glass fiber-epoxy system has been more widely used in highway applications due to its lower cost. The glass fiber-epoxy jacket system used on specimen FRG was Fyfe Co. LLC (SEH-51), and the carbon-fiber jacket system used on specimen FRC was Fyfe Co. LLC (SCH-51).

2.4.2 Design of Retrofit FRP Jacket

In the design of the FRP jacket for retrofit, shear strength, flexural enhancement, and constructability were considered. The goal of the retrofit was: (1) reduce the chance of brittle shear failure, (2) minimize the increased column flexural strength, (3) provide a jacket design compatible with the non-prismatic shape of the column.

The jacket was designed through consideration of the capacity and demand at the predicted plastic hinge location. The nominal shear capacity of the column (V_n) was

calculated by including contribution from concrete (V_c), and the transverse steel (V_s), using the CALTRANS method[4]. This method was chosen because it accounts for the reduced concrete strength capacity of the plastic hinge. The concrete shear strength includes the effects of compressive axial stress, displacement ductility demand, and level of column core confinement. The shear demand was calculated based on moment capacity and location of the plastic hinges.

The jacket thickness was designed for the difference between the column shear capacity and demand. The jacket design shear strength is outlined in Eqn. (2-1).

$$V_{Design} = \Omega_0 \cdot V_{Demand} - \phi \cdot (V_c + V_s) \quad (2\text{-}1)$$

This equation considers both an over-strength safety factor (Ω_0) and a strength reduction factor (ϕ) to account for the uncertainties of seismic loading effects and accurate estimation of shear capacity. The column design shear is then used to calculate the composite jacket thickness based on equilibrium of a typical column cross-section. The octagonal shape of the column was approximated as a circular column to account for the contribution of the jacket in a conservative manner. The Federal Highway Administration (FHWA) composite jacket design procedures were used to find the required thickness of the jacket[35]. The FHWA design equation was modified to only include passive confinement effects of the jacket. Equations (2-2) and (2-3) were used to derive the thickness of the jacket based on the jacket design shear, assuming a circular column relationship.

$$V_{Design} = \frac{\pi}{2} \cdot \left(\left(t_p \cdot E_p \right) \cdot \varepsilon_p \right) \cdot D \cdot cot(\theta) \quad (2\text{-}2)$$

$$t_j = \frac{2}{\pi} \cdot \left(\frac{V_{Design}}{\left(E_p \cdot \varepsilon_p \cdot D \cdot cot(\theta) \right)} \right) \quad (2\text{-}3)$$

Where:
- t_p = *Thickness of FRP jacket (passive component)*
- E_p = *Young's modulus of FRP jacket (passive component)*
- ε_p = *Design Strain of FRP jacket (passive component)*
- D = *Effective depth of FRP jacket*
- θ = *Design Shear crack failure inclination*

The FHWA method models the jacket as hoop reinforcement with the jacket area equivalent to the thickness of the jacket with a spacing height of unity (1 cm or 1 in). The thickness of the jacket (t_j) is calculated using Eqns. 2-1 through 2-3, given the plastic hinge location and composite wrap properties (Table 2-3). The thickness calculated must be rounded up to the typical minimal thickness of the installed jacket including epoxy therefore providing additional strength beyond that of the original design.

2.4.2.1 Specimen FRG

In specimen FRG, a Fyfe Co. LLC SEH-51 glass fiber-epoxy wrap was used to form the FRP jacket. The installed typical thickness of the SEH-51 wrap is 1.27 mm (0.05 in).

The calculated design thickness using Eqns. 2-1 through 2-3 was 3.48 mm (0.136 in), which translated to 3 wraps of the SEH-51. The wrap was not wound around the column, but rather placed in sequentially overlapping pieces of covering 270° around the weak axis in each sequence, as shown in Fig. 2-7. The jacket was composed of vertical segments of varying heights due to the geometry of the column. The maximum segment height was established so that the composite wrap would be flush with the surface of the column and not develop a large angle with respect to the horizontal axis that would increase flexural capacity of the column. A total of six segments were applied to the column, as shown in Fig. 2-8. In order to diminish the flexural enhancement of the specimen, the thickness of the wrap was reduced at the plastic hinge region. Two wraps were applied to the plastic hinge region, in a segment height of 102 mm (4 in), to promote failure in this region rather than allowing the shift of the plastic hinge. In the second phase of the study, it was found that the ideal failure zone occurred at the plastic hinge location, allowing maximum dissipation of seismic energy[5]. The top 203 mm (8 in) of the column was unwrapped simulating the effect of not wrapping the portion of the prototype column that extends into the grade.

2.4.2.2 Specimen FRC

In specimen FRC, a Fyfe Co. LLC SCH-51 carbon fiber-epoxy wrap was used to form the FRP jacket. The installed typical thickness of the SCH-51 is 1.0 mm (0.04 in). The calculated design thickness using Eqns. 2-1 through 2-3 was 1.1 mm (.04324 in), which translated to 2 wraps of the composite material. The wraps were applied to the column in segments similar to that of specimen FRG, as shown in Figure 2-9. The difference in material properties did not affect the number of segments or segment width. A total of six segments were applied to the column, as shown in Fig. 2-10. In a similar manner to specimen FRG, the flexural enhancement of the specimen was reduced by providing a reduced number of wraps the plastic hinge region. One wrap was applied to the plastic hinge region, in a segment height of 102 mm (4 in), to promote failure in the plastic hinge region. The top 203 mm (8 in) of the column was unwrapped.

2.5 Material Properties and Fabrication

2.5.1 Column and Footing

The construction of the test specimens endeavored to match the prototype bridge columns as closely as possible. The materials used in the prototype bridge consisted of grade 60 steel for longitudinal and transverse reinforcement. The rebar and steel wire used in the test specimens were tested in accordance with ACI 318 Section 3.5[2]. The results of these tensile tests are outlined in Table 2-1. The longitudinal reinforcement in the test specimens had an average yield strength of 461.9 MPa (67 ksi). The average yield strength of the wire used as transverse reinforcement was 413.6 MPa (60 ksi). The average yield stress for the steel in the prototype columns was 484 MPa (70.2 ksi).

The measured concrete compressive strength of the prototype column was specified as 40.3 MPa (5.85 ksi) in 1980. The estimated increase in strength over the 19 years since placing of the concrete is 20 percent, providing an estimate of the present compressive

strength as 48.3 MPa (7 ksi). The concrete compressive strength of the test specimens was measured in accordance with ASTM C-39[3]. A summary of the 7 day, 28 day, and test day strength of both the footing and column is shown in Table 2-2. The measured column concrete compressive strength on test day compares very well with the estimated current concrete strength of the prototype columns.

The two test specimens were constructed concurrently in the laboratory. The construction occurred in several separate phases, with the footing and column concrete poured separately. The formwork for the footing was assembled on a wood platform. A layer of form release was applied to the formwork to prevent binding of the concrete. The footing bar cages were pre-assembled adjacent to the formwork, and placed in the forms with a forklift. The cage was held upright and centered in the form using mortar chairs to ensure shifting of the cage would not occur during the concrete pour. The footing cage included four U-shaped hooks designed as lifting eyes constructed of ∅32 mm (#11) bars, which were placed after securing the bar cage. The longitudinal column reinforcement was then installed with a template to ensure that the column longitudinal bars were with a correct angle to form the column flare. The transverse column reinforcement was placed above and below the template for a length of 254 mm (10 in), to prevent shifting of the longitudinal rebar during the concrete pour. Twelve schedule 40 PVC pipes were placed vertically in the footing cage and tied in place to provide connection to the shake table. The PVC pipe measured ∅76 mm (3 in), by 762 mm (30 in) long. Two 305 mm (12 in) square forms with a depth of 38 mm (1.5 in) were secured to the bottom of the footing forms. The forms were positioned symmetrically about the column bars; such that when removed they would create a cavity to mount the axial load anchors for the Dywidag prestressing system in the bottom of the footing.

The footing concrete was supplied by a local ready-mix plant. The specified concrete mix provided 19 mm (0.75 in) maximum aggregate with a specified concrete strength of 41.36 MPa (6 ksi). The footings were poured in three lifts of 254 mm (10 in), mechanically vibrated during the pour. The surface was troweled to a smooth finish ensuring the footing surface was level in the formwork. A concrete slump of 76 mm (3 in) was measured in the middle of the pour. The footings were moist cured for 7 days, and achieved 28 day strength prior to pouring the concrete for the columns.

The column steel placement was completed after curing the footing concrete for three days. The transverse steel was extended through the height of the column and into the bottom portion of the top-of-column concrete block. Round plastic spacers were placed on the transverse steel throughout the column height to ensure a minimum cover of 19mm (0.75 in) was achieved. The column forms were assembled, coated with form release, and secured around the column. The top-of-column concrete block transverse reinforcement was assembled and four ∅38 mm by 521 mm (20.5 in) long PVC pipes were secured in the block horizontally to provide a connection point for the mass rig bolts. A template with four 27 mm (1.0625 in) bolts, which were 406 mm (16 in) long, was centered at the top of the concrete block to secure the axial loading beam in place. The column forms were centered on the footings and braced to ensure they would remain level in the horizontal and vertical directions during the concrete pour.

The column concrete was supplied by the same local ready-mix plant as the footing concrete. The specified concrete mix provided 9.5 mm (0.375 in) aggregate with a specified concrete strength of 44.8 MPa (6.5 ksi). A superplasticizer was added to the concrete mix prior to pouring to improve the concrete workability because of concerns over the congested reinforcement in the column. The superplasticizer has the effect of producing a flowing concrete that increases the slump. The columns were poured in approximately four lifts of 521 mm (20.5 in) and mechanically vibrated during the pour on the inside and outside of the formwork to prevent voids. The columns were moist cured for 7 days prior to removal of the formwork.

2.5.2 Composite Jacket

The composite jackets were installed by Fyfe Co. LLC certified installers. Both jackets were installed in the same day over a 12-hour period. The columns were prepared concurrently, and then the two jackets were installed sequentially, as shown in Fig. 2-11. The concrete surface of the columns was sanded with a grinder to reduce irregularities. The location of the individual composite wrap segments was drawn on the column with a marker to aide in the installation of the jacket. A base coat of epoxy was applied to the concrete surface of 3 mm (0.125 in) to provide a working platform for the jacket installation. The epoxy was a milky-white color that allowed the segment location lines to be seen. The surface epoxy was allowed to cure to a tacky state prior to installation of the composite wrap. The jacket was identical on both specimens with the exception of the composite fabric.

The jacket on Specimen FRG was installed first. During the curing process of the surface epoxy, the SEH-51 fabric was cut into the various segment sizes to allow quick installation. The segments were organized into the corresponding levels of wrap and impregnated with epoxy using a saturating machine. The jacket installation process began at the footing elevation working toward the top of the column. Each composite fabric strap was centered on the weak axis of the column and placed around the column 135° from the centerline of the weak axis. Figure 2-12 shows the typical application of a segment of wrap. The six segments of wrap on one side of the weak axis of the column were placed, and then the six on the opposite side of the column were placed overlapping the previously installed segments. After both sides of the jacket segments were applied to the column, the entire column/jacket surface was covered with an epoxy coat of 3 mm (0.125 in) to provide continuity between the layers of wrap. The process of applying the composite wrap was then continued until the specified three wrap thickness was installed on the column. A final coat of epoxy was then applied to the surface of the column to provide continuity and protection against environmental damage. The installation process creates an overlap on the ends of the column section of approximately 305 mm (12 in), consisting of a six wrap thickness. The suggested lap length of the supplier was a minimum of 152 mm (6 in) in order to fully develop the fibers in tension and prevent debonding. The lap length of 305 mm (12 in) was chosen due to the uncertainty of the effect of the octagonal column cross-section and non-prismatic column shape. The overlap was designed to provide sufficient development of the fibers in tension and prevent debonding.

The jacket on Specimen FRC was then installed in a similar manner with the exception of using the SCH-51 fabric, and providing a two wrap thickness over the height of

the column. All other details of the installation were identical including the use of the same epoxy for the SCH-51 fabric. After the installation of both jackets, test coupons were made of the composite wrap in accordance with ASTM D-3039[3]. A total of two test coupons were made from each jacket material. The jacket and the coupons were allowed 10 days to cure prior to placing the columns on the shake table. The coupons were tested following the tests of the column specimens, and the results are shown in Table 2-3.

2.6 Instrumentation

The test specimens were extensively instrumented to record bar strains, column curvature, column displacement, lateral forces, and the axial load. The test data were recorded on a *Pacific* data acquisition system at a rate of 200 samples per second (200 Hz).

A total of 83 strain gages were used in each specimen (FRG and FRC) to measure strain in the longitudinal rebar, transverse rebar, and composite jacket. Figures 2-13 through 2-15 show the longitudinal, transverse and composite jacket strain gage locations. The strain gage locations used within the test specimens FRC and FRG correspond to locations in specimens FA and FR to aid in the comparison of the retrofit schemes. The strain gages were manufactured by Tokyo Sokki Kenkyujo Co., Ltd. of Japan. Three different types of gages were used to instrument the column. The longitudinal reinforcement was instrumented with 10-mm (0.4-in) strain gage model (YL-10-5L). The transverse reinforcement was instrumented with a 2-mm (0.078-in) strain gage model (YL-2-5L). The composite jacket was instrumented with a 20-mm (.787-in) strain gage model (PFL-20-3L). The strain gages installed on the jacket were aligned with the uni-directional fibers in the jacket so that the measured strains would not have to be corrected to reflect fiber strain.

Curvature was measured through a series of *Novotechnik* transducers. Six 9.5-mm (0.375-in) threaded rods were installed on both sides of strong axis of the column 15 days after the composite jacket had been installed. The threaded rods begin at 241 mm (9.5 in) from the footing elevation and continue up to 971 mm (38.25 in) above the footing. The rods support the ends of the *Novotechnik* transducers allowing curvature to be calculated based on the displacement measured by the transducers. Figure 2-16 shows the location of the threaded rods and *Novotechnik* devices. A total of ten *Novotechnik* transducers were installed along the column surface with five on either side of the strong axis.

Load cells were used to measure the column axial loads. The axial loads were measured by placing load cells under the two hydraulic jacks in the Dywidag prestressing system. The lateral loads were measured through conversion of measured acceleration of the rigid link connecting the mass rig to the test specimen. The lateral load was calculated by multiplying the measured acceleration times the effective mass of the mass rig, including the P-delta effect of the mass rig on the lateral force applied to the column by the mass rig.

Column absolute displacement was measured relative to the laboratory wall using a *Temposonic* transducer attached to the top of the test specimen, at the level of the mass rig connection, as shown in Figure 2-17. The shake table displacement was measured by an

internal displacement transducer, which allowed the relative column displacement to be calculated as the difference between the absolute and table displacements.

2.7 Test Setup and Procedure

The specimens were tested in a similar fashion to the as-built and steel jacketed specimens. The column was rigidly attached to the shake table and a link connecting the column to the inertial mass. An earthquake history was used to drive a shake table and excite the test specimen. Figures 2-17 and 2-18 show the test setup.

The test specimen was centered and secured to the shake table. The lateral loading of the specimen was accomplished through the mass rig, which consisted of a pinned steel frame mechanism supporting concrete reaction blocks. The design of the mass rig is outlined in Ref. 12. The mass rig was connected to the specimen through the top block and a steel plate with a pinned rectangular steel tube, the other end of the tube was pinned to the mass rig through a steel plate. The mass rig supported four concrete reaction blocks each weighing 89 kN (20 kips). After the mass rig link was connected to the specimen, an axial load of 284.6 kN (64 kips) was applied through the hydraulic jack system. The hydraulic system consisted of two hydraulic jacks, connected to a pump and accumulator in series. The pump was engaged to provide the axial load and the accumulator was used to minimize the axial load fluctuation. The axial load was determined in accordance with the previous studies in the series, to represent typical axial load strain of a prototype column on the bridge. This loading was calculated as a function of an axial load index based on the column cross-sectional area and concrete compressive strength.

The earthquake history used to drive the shake table was the January 17, 1994 Northridge earthquake as measured at the Sylmar Hospital. This record was chosen due to it being representative of a typical earthquake in the western United States. Furthermore, analytical studies showed that this record would lead to high ductility demand thus allowing of the ultimate behavior testing (Section 2.2.3). Since the test specimen was a scaled model of the prototype column, the earthquake record had to be scaled to create a response in the test specimen that would parallel the prototype column. In addition, in order to fail the test specimen, the amount of column axial load differed from the inertial mass on the mass rig. The earthquake time step was scaled by a factor of 0.672 to account for the differences between the prototype and specimens[17].

The testing was completed by applying scaled versions of the strong motion accelerogram. The test of each column consisted of eleven events beginning with pre-yield loading and continuing until visible column failure occurred. The first event for both specimens began with 20% of the magnitude of the strong motion accelerogram. The events were incremented as shown in Tables 2-4 and 2-5. The final event in the testing process of both specimens occurred after apparent failure of the column; the purpose of running this event was to complete the test cycle and verify the apparent failure of the column.

Chapter 3

Test Procedure and Results

3.1 Introduction

This chapter presents the testing procedure and experimental results for the thirty-percent scale specimens tested on a shake table. The specimens described in this chapter consist of the as-built (FA), steel jacketed (FR), glass fiber-epoxy jacketed (FRG) and carbon fiber-epoxy jacketed (FRC). The test results for specimens (FA) and (FR) were previously reported in detail in Ref. 17. Selected data from that reference are used to review the relative merit of different retrofit methods. Testing was completed at the Bridge Engineering Laboratory at the University of Nevada, Reno.

3.2 Test Procedure and Methodology

The setup and test methods described in this section were similar for all four specimens tested on the shake table.

3.2.1 Test Setup

The cured specimen was lifted with a crane into position on the shake table, and placed on 38 mm (1.5 in) wooden spacers. The specimen footing was centered and loosely secured to the shake table using Dywidag prestressing bars. The bottom of the specimen footing was self-leveled using a grout with a specified 24-hour compressive strength of 68.9 MPa (10 ksi) which was allowed to cure 24 hours prior to stressing Dywidag bars to 24.1 MPa (3.5 ksi). Ten ϕ32 mm (1.25 in) Dywidag bars were used to anchor the footing to the table. The mass rig rigid link was connected to the top-of-column concrete block using four ϕ46 mm (1.8125 in) high strength bolts. The remaining external transducers were attached to the specimen, and the wires were extended and connected to the data acquisition system. The steel I-beam was secured in place on the top concrete block, and the hydraulic jack and Dywidag prestressing bar system were secured to the specimens. The hydraulic pump and accumulator were calibrated for the required axial load of 441.3 KPa (64 kips); and the axial load was set by energizing the hydraulic pump then verifying the result through the load cells and data acquisition system. The entire instrumentation system was checked to be functional and reset prior to specimen testing.

Fine tuning of the shake table system was accomplished through low level testing of the specimen prior to the test program. The fine tuning was necessary to improve the response of the shake table/specimen system as compared to the input earthquake base acceleration. The strong motion accelerogram was input into the data acquisition system,

which converted the accelerogram into a drive file that operates the shake table actuator. The shake table motion, without the specimen attached to the table, accurately represents the input strong motion accelerogram; however, the table response is affected by the stiffness and mass of the test specimen and tends not to model the input motion precisely. The difference between the input and actual table acceleration must be corrected to ensure the representative earthquake is adequately simulated by the shake table. Low level testing is completed through applying a series of random vibrations to the shake table, which allows the operator to filter any inadequacies in the response of the system. The amplitude of this vibratory motion is substantially below the predicted yield point of the specimen, with a maximum amplitude of 0.05 g. Therefore no degradation of the specimen occurs prior to the actual testing sequence. The goal of the fine tuning is to preserve the low frequency response of the input motion in the testing motion. Upon completion of this process the experimental procedure began, further analysis of the fine tuning process was done after the testing and is discussed in detail in Chapter 4.

3.2.2 Experimental Procedure

The test program involved excitation of the specimen with an earthquake acceleration history applied with increasing intensity until failure of the specimen occurred. The earthquake record used in this study was the 1994 Northridge earthquake as measured at the Sylmar Hospital (Fig. 3–1). This record was adjusted to account for the difference of scale of specimen and loading as discussed in Section 2.7, is shown in (Fig. 3-2). The record is referred to as both the 1994 Northridge earthquake and Sylmar earthquake in this document.

The expected column yield force was calculated for the test specimens using non-linear analysis that is presented in Chapter 4. This predicted yield force was used to determine a yield acceleration and to estimate the input earthquake amplitude that would yield the column. The test event sequence was then designed such that both the elastic and inelastic response of the column could be measured. The yield peak acceleration was predicted to be 0.26 g, which was approximately 40 percent of the peak acceleration of the earthquake record. The other events were then generally based on this event until failure. A complete list of all events for specimens FRG and FRC is shown in Tables 2-4 and 2-5. Specimens FA and FR were subjected to the same testing program as that applied to specimens FRG and FRC with the exception that the total number of events was influenced by the degradation of the specimen.

Each sequence of test events included snap back tests to measure the stiffness and damping of the test specimens during the test process. The snap back test was completed by pulling the shake table relative to the mass rig and suddenly releasing the hold which allowed the specimen to vibrate freely until viscous damping stopped the specimen motion. A hand jack and steel wire system was used to pull the specimen toward the mass rig up to a force of 13.3 kN (3 kips). The load in cable was measured with an inline load cell. Upon achieving the required load, the instrumentation system was started and the steel link in the wire system was cut to free the specimen. The rigid link acceleration of the specimen was recorded allowing the stiffness and damping to be calculated using a Fourier analysis. A snapback

test was performed before the test sequence began, at the expected yielding of the column, and well into the inelastic behavior of the column as shown in Table 2-4 and 2-5. The calculated frequency, damping, and period from the snapback measurements for all four specimens for the measured snapback events are shown in Table 3-1. A typical measured snapback acceleration record is shown in Fig. 3-3.

The frequency was determined from a Fourier analysis of each measured snapback acceleration record. Based on this frequency the specimen stiffness was calculated. The specimen viscous damping ratio was calculated from the measured acceleration using a logarithmic method. The snapback results show the retrofit methods FR, FRG, and FRC substantially increased the stiffness and frequency of each specimen relative to FA. The measured properties serve to compare the specimens initial state and relative amount of degradation during testing. However, the properties are not indicative of the measured response of the column due to the low level of force used to obtain the free vibration. Further discussion of the measured dynamic properties and methods used to calculate them is presented in Chapter 4.

3.2.3 Summary of Test Results for Specimens FA and FR

The results of tests for FA and FR are discussed in a brief manner in this section. The complete coverage of the findings can be found in Ref. 17. The significant measured results for these specimens are included in both tabular and graphical form in Section 3.4, in which a comparison of the three retrofit methods is made. The methods used to find the yield displacement and displacement ductility is presented in detail in Chapter 4. The measured data are labeled depending on the side of the column which is next to the mass rig ("near side of the column") or away from the mass rig ("far side of the column").

3.2.3.1 Specimen FA

The column yielded at a displacement of 25 mm (1.0 in) under a lateral load of 230.2 kN (51.75 kips). The peak lateral load was 254 kN (57.1 kips) and occurred during the fourth event. The maximum measured displacement was 137.9 mm (5.43 in) corresponding to a displacement ductility of $\mu_\Delta = 5.4$.

The plastic hinge developed at a distance from the footing of between 584 mm to 737 mm (23.0 in to 29.0 in) on the near side of the specimen; and 483 mm to 584 mm (19.0 in to 23.0 in) on the far side of the specimen in an unsymmetrical loading pattern consistent with loading. The hinge spread was substantial prior to failure on both sides of the column. Fracture of the outer most longitudinal steel occurred in the final event in the plastic hinge zone from 483 mm to 584 mm (19.0 in to 23.0 in) due to low-cycle fatigue.

The strains measured in the transverse steel showed yielding in the region of the plastic hinge. Yielding of the ties occurred after the fourth event corresponding to the full un-factored time history from the Northridge earthquake, which corresponds to a

displacement ductility of $\mu_\Delta = 3.5$. The specimen did not show shear failure. However extensive shear cracking was present at failure, and some of the transverse ties fractured in the final test event. Because of the extensive shear damage, it was determined that the columns need to be retrofitted.

3.2.3.2 Specimen FR

The steel jacket retrofit improved the seismic response of the column substantially. The column yielded at a displacement of 24 mm (0.95 in), at a lateral load of 325.4 kN (73.1 kips). The peak lateral load was achieved at 357.6 kN (80.4 kips), which occurred during the sixth event. The maximum displacement of the specimen was 167 mm (6.6 in), which corresponded to a displacement ductility of $\mu_\Delta = 6.9$. Figure 3-4 shows a comparison of the measured force-displacement envelopes for specimens FA and FR.

The plastic hinge was forced to develop between 425 mm and 457 mm (16.73 in to 18.0 in) from the footing due to the location of the gap in the jacket. The column failed due to fatigue at this elevation with longitudinal bar fracture. The measured strain in the lateral ties indicated the retrofit was successful even though some lateral ties yielded in the last event corresponding to a displacement ductility of $\mu_\Delta = 6.9$. The measured steel jacket strain showed yielding at the elevation just above the gap at 533 mm (21 in), occurring in the last event. Shear cracking was eliminated with the retrofit, and the seismic performance was excellent.

3.3 Test Results for Specimens FRG and FRC

The experimental results presented for the FRP-retrofitted specimens are the displacements, lateral forces, strains, and curvatures. The vast amount of data recorded during the test requires that only the critical data be detailed in this study. The data have been filtered to display significant data that are indicative of the effectiveness of the retrofit and general dynamic response of the column.

The strain gage locations for specimens FRG and FRC were identical using eighty-three strain gages in each specimen that consisted of eighteen longitudinal bar strain gages, twenty transverse tie strain gages, forty-five composite jacket strain gages (Figs. 2-13 through 2-15). Specimens FA and FR were instrumented similar to specimens FRG and FRC, consisting of identical numbers of gages on the longitudinal and transverse reinforcement; and twenty-eight strain gages on the steel jacket. The locations of the strain gages were identical within the columns. The curvature for all four specimens were measured using *Novotechnik* displacement transducers. The curvature was measured as an average value in between the threaded rods imbedded in the column composing a gage length. The gage lengths and elevations along the column height are shown in Figs. 2-16 and 2-18 for specimens FRG and FRC, respectively. The previously discussed "near side" and "far side" identifications are used to describe the side of the column with respect to the mass rig.

3.3.1 Specimen FRG

Specimen FRG was retrofitted with a glass fiber-epoxy jacket composed of six segments of a glass fiber-epoxy jacket with a primary thickness of three wraps 3.81 mm (0.15 in). The jacket was discontinuous at each segment as shown in Fig. 2–8, which provided a flexural failure path without compromising the jacket effectiveness in confinement.

The testing process lasted fourteen runs which included three pull back tests to measure degradation of the specimen, and eleven earthquake events to load the specimen to failure. The testing sequence amplified the earthquake strong motion accelerogram from 20 percent to 275 percent of the Sylmar record amplitude, as shown in Table 2-4. The input accelerogram is the target for the table to achieve for each test event. However the actual table acceleration varies due to the dynamic response of the table and specimen system as discussed in Section 3.2.2. The combined record of table target (input) acceleration for the eleven test events is shown in Fig. 3–5.

3.3.1.1 Description of Testing Process and Benchmarks

The target peak table acceleration for the first event was 0.12 which is 20 percent of the peak acceleration in the original Sylmar record. At this amplitude the column force was well below the yield force. The peak force achieved during the first event was 86.1 kN (19.4 kips) at a displacement of 4 mm (0.15 in). This event exceeded the cracking load of the concrete. However due to the jacket covering most of the column height, no visible damage was noted other than minor cracking of the epoxy on the jacket surface. The second event showed the longitudinal bars to be yielding with cracks beginning to develop at the joints of the jacket straps. A peak lateral force of 173.3 kN (39.0 kips) at a displacement of 13 mm (0.51 in) was recorded during this event.

The maximum lateral force was measured in event six with a peak lateral load of 341.1 kN (76.7 kips) at a displacement of 73 mm (2.89 in). The target peak acceleration was 0.9 g in this event. The specimen began to show extensive cracking in between the jacket segments, which appeared to be flexural cracking in the column propagating across the entire column cross-section. Figure 3-6 shows the cracking of the jacket and the concrete after the seventh event. The elevation just above the sign in the photo is 495 mm (19.5 in) above the footing.

The peak target table acceleration for the second to last event was 1.5 g (250 percent of the original Sylmar record). This event reached a peak lateral load of 321.8 kN (72.3 kips) at a displacement of 162 mm (6.38 in). The permanent deformation of the specimen after this event was 38 mm (1.5 in) an increase from 25 mm (1 in) at the end of the previous event. The large amount of permanent deformation after this event indicated the fracture of bars was imminent. The lateral load had only decreased 6 percent, however the cracks between the jacket segments had opened up to 3-mm (0.125-in).

The maximum target table acceleration in the final event was 1.75 g and resulted in the complete flexural failure of the specimen at the elevation of 495 mm (19.5 in). Figure 3-7 shows the collapsed specimen, being held in place by the mass rig system. In Figure 3-8 a close view of the failure detail shows the fracture of longitudinal bars. The concrete cover was completely disintegrated but was prevented from outward spalling due to the confinement of the jacket. The core concrete was cracked but did not appear to dilate to a great extent during the testing process. The transverse steel was completely intact and did not indicate failure of any kind.

The specimen was pushed upright and removed from the table. Figure 3-9 shows the extensive flexural cracking at each segment intersection along the column height. Each crack is approximately 3-mm (0.125-in) wide extending completely around the specimen circumference at the intersection of the segments of the jacket. The cracks in the jacket occurred either at the outmost intersection of the jacket segment, or at the overlapped intersection of the jacket segments. The white arrow in Fig. 3-10 points to a crack that appears to be through the center of the jacket segment at 1168 mm (46 in), this crack occurred at the overlap of the jacket segment, and was not indicative of column failure at this location. The sections shown in the Figs. 3-9 and 3-10 span from 140 mm (5.5 in) to 1200 mm (47.2 in) from the footing. The jacket was removed as shown in Fig. 3-10, which was taken from the same face as that is in Fig. 3-9. This figure shows extensive disintegration of the cover concrete in the region from 457 mm (18.0 in) to 559 mm (22.0 in), coinciding with the location that the column hinged when it failed. The flexural crack seen at 394 mm (15.5 in) occurred at the intersection of the jacket segments, and is similarly found at the other intersections of the jacket. Other spalling of concrete noted in Figs. 3-9 and 3-10 was due to the jacket removal process and the strong bond of the epoxy to the concrete. Figure 3-11 shows the side view of the column with the jacket removed. The right-hand side of the photo corresponds to the mass rig side of the specimen. The failure zone of spalled concrete is clearly seen with the longitudinal bar exposed between 457 mm (18.0 in) to 559 mm (22.0 in). The left-hand side of Fig. 3-11 shows extensive crushing of concrete that was primarily due to the final test event in which the column pivoted on this side. Close inspection of the specimen indicated no significant shear cracking in either the FRP jacket or the column.

3.3.1.2 Load and Displacement Histories

The displacements are measured relative to the table. The lateral forces shown were calculated from the link acceleration and mass rig weight, which included the P-delta force of the mass rig. The calculation of the lateral force is discussed in more detail in Chapter 4. The measured force-displacement hysteresis curves for the earthquake events are shown in Figs. 3-12 and 3-13. The first two events clearly show a linear behavior of the specimen. While events three through ten clearly show large energy dissipation through the wide hysteretic curves. The permanent deformation of the specimen increased with each event resulting in a shift of the hysteresis loops. Figure 3-14 shows the measured permanent displacement for each event. Based on the permanent deformations and the hysteresis curves it is clear that the specimen failed after the second to last event, corresponding to event ten.

The hysteresis curves for each event were used to calculate an average specimen stiffness based on the peak force and displacement at peak force from the starting point (chord stiffness) for each event. Table 3-2 shows the variation of the specimen stiffness over the testing events. The hysteresis curves were summarized by taking the peak force and corresponding displacement for each event, creating a force vs. displacement envelope as shown in Fig. 3-15. The two curves represent: (1) peak lateral force versus the corresponding displacement with respect to time, (2) peak lateral force versus the peak displacement without respect to time. The two curves coincide in the elastic region but deviate afterwards. The peak displacement achieved prior to failure of the specimen was 162 mm (6.84 in). The measured displacement for all the events is shown in Fig. 3-16.

3.3.1.3 Measured Strain

The strain gages were placed at the critical elevations within the column on the longitudinal and transverse steel. Their locations were based on the predicted failure region of the column and previous test results[5,17,37]. The visual mode of failure of the specimen was verified with the strain gage data.

The measured longitudinal bar strains were evaluated over the column height to determine the first yield and the plastic hinge elevation. Figure 3-17 shows the longitudinal bar strain envelopes over the column height for the far side of the specimen. In the figures, positive strain indicates compression, while the negative strain indicates tension. The bar yielded between the second and third events. The maximum strain measured prior to gage failure occurred at 13790 μs in event seven. The longitudinal bar strain on the near side of the specimen yielded after the second event, as shown in Fig. 3-18. Determination of the plastic failure location is more difficult on this side of the specimen due to the early failure of the gages. The instrumentation failed on the near side of the column due to the high tensile strains applied and sustained due to the permanent deformation of the specimen. The far side instrumentation lasted longer but failed as a consequence of the large tensile strains achieved in the higher amplitude events.

The transverse tie strains were broken into two groups: (1) center ties, (2) corner ties. The center ties were lapped at mid column across the strong axis of the column (Figs. 2-4 and 2-14). Strains in these ties were larger, in general, than the corner ties. The corner ties were hooped around the end of each side of the strong axis (Figs. 2-4 and 2-14). The peak strain envelopes for both groups of ties were plotted. However due to the failure of the gages at high displacements, only two sides of the specimen are shown in the figures. Figure 3-19 shows the lateral corner ties peak strain envelope located near the corner on the near side of the specimen. This figure shows all the strains were well below yield for all measured events prior to failure of the instrument. Figure 3-20 shows the strains for center ties on the far side of the specimen. This figure indicates all strains were also well below yielding.

Figures 3-21 and 3-22 show the jacket end and side strains envelopes over the column height respectively. The horizontal glass fiber-epoxy jacket strains were measured on five

sides of the column, mounted on the surface of the jacket at the outermost fiber. The critical strains developed at the extreme fiber of the end of the column strong axis corresponding to the lapped region of the composite straps and in the middle of the column where no overlap occurred. The glass fiber-epoxy jacket behavior is linear-elastic to failure with no "yield" point. The measured jacket strains were less than 50 percent of the ultimate strain of the jacket ($\varepsilon_u = 20900$ μs), and in most cases did not exceed the conservative design strain limit of $\varepsilon_d = 6000$ μs. The large increase in strain at the elevation of 533 mm (21 in) as compared to the other measurements indicates plastic hinge formation in this region from 356 mm to 660 mm (14.0 in to 26.0 in). Detailed comparison of measured strain locations is made in Section 3.4 for all specimens.

3.3.1.4 Measured Curvatures

The curvature was measured using *Novotechnik* displacement transducers attached to threaded rods imbedded in the specimen (Fig. 2-16). These instruments measured displacement changes over a gage length, and the data are the average curvatures between the threaded rods. During the testing, one of the threaded rods was loosened on the near rig side of the specimen giving inaccurate readings beyond the fifth event. Figure 3-23 shows the measured curvature envelopes over the height of the specimen. This figure shows the plastic hinge formation in two distinct locations on the specimen. The lower hinge region from 425 mm to 584 mm (16.5 in to 23.0 in) was located on the far side of the column. While an upper hinge region from 730 mm to 889 mm (28.75 in to 35.0 in) was located on the near side of the column. The asymmetrical hinging of the column was also seen in the testing of specimen FA, and is due to the unsymetric loading.

3.3.1.5 Measured Variation of Axial Force

The Dywidag prestressing system was used to apply the axial load to the specimens during the tests. The axial load was initially set at 284.6 kN (64 kips). However the hydraulic jacks did not respond rapidly enough during the test to maintain a constant load. The variation in axial load is shown in Fig. 3-24 for all eleven test events. The change in axial load during the test affects the flexural capacity of the column. A discussion of the effect of the axial load variation is presented in Section 4.2.2 and 4.2.3.

3.3.1.6 Comparison of Target and Achieved Table Peak Acceleration

The fine tuning process corrected a majority of the disparity between the input earthquake record and the actual table response. However some differences still occurred. Previous shake table tests indicated that the effect of difference in the input and output response of the shake table is minimal for the dominant frequency range of the test columns[12,17]. Figure 3-25 compares the envelope of the achieved peak table acceleration with the target peak acceleration. This figure indicates that the negative peak acceleration was well modeled by the shake table, but the positive acceleration was amplified from the

input record as much as 60 percent in the later events, providing a more symmetric loading to the specimen after the yield of the column. The large difference can be explained due to the changing stiffness of the specimen during the testing process that has the effect of nullifying some of the fine tuning process during the later events. A discussion of the effects of the variation in target and achieved peak accelerations is presented in Chapter 4.

3.3.2 Specimen FRC

Specimen FRC was retrofitted with a carbon fiber-epoxy jacket composed of six segments of a glass fiber-epoxy jacket with a primary thickness of two wraps 2.03 mm (0.08 in). The jacket was discontinuous at each segment as shown in Fig. 2–10.

The testing process lasted fourteen runs which included three pull back tests to measure degradation of the specimen and eleven earthquake events to load the specimen to failure. The testing sequence amplified the earthquake strong motion accelerogram from 20 percent to 250 percent of the Sylmar record amplitude, then reduced the amplitude level to 200 percent for the final event, as shown in Table 2-5. The combined record of table target (input) acceleration for the eleven test events is shown in Fig. 3-26.

3.3.2.1 Description of Testing Process and Benchmarks

The target peak table acceleration for the first event was 0.12 g which is 20 percent of the peak for the original Sylmar record. At this amplitude the column force was well below the yield force. The peak force achieved during the first event was 89.5 kN (20.1 kips) at a displacement of 5 mm (0.19 in). This event exceeded the cracking load of the concrete. However due to the jacket covering most of the column height, no visible damage was noted other than minor cracking of the epoxy on the jacket surface. The second event showed the longitudinal bars to be yielding, with cracks beginning to develop at the joints of the jacket straps. A peak lateral force of 182.0 kN (40.9 kips) at a displacement of 14 mm (0.54 in) was recorded during this event.

The maximum lateral force was measured in event six with a peak lateral load of 323.7 kN (72.8 kips) at a displacement of 77 mm (3.02 in). The target peak acceleration was 0.9 g in this event. The specimen began to show extensive flexural cracking between the jacket segments. Figure 3-27 shows the flexural cracking in the predicted plastic hinge region of the column. Due to the dark color of the jacket it is difficult to see the extent of the cracking in the photo. Specimen FRC developed a plastic hinge at both 495 mm (19.5 in) and 749 mm (29.5 in) from the footing.

The target table acceleration for the second to last event was 1.5 g (250 percent of the original Sylmar record). This event reached a peak lateral load of 298.7 kN (67.2 kips) at a displacement of 158 mm (6.2 in). The permanent deformation of the specimen after this event was 33 mm (1.3 in) an increase from 25 mm (1 in) at the end of the previous event. The large amount of permanent deformation after this event indicated the fracture of bars was

imminent. The lateral load had only decreased 7.8 percent, however the cracks between the jacket segments had opened up to 3-mm (0.125-in). The maximum target table acceleration in the final event was 1.2 g and resulted in the longitudinal bar fracture at 749 mm (29.5 in). The failure clearly indicated a plastic hinge region zones at both the 495 mm (19.5 in) and 749 mm (29.5 in) from the footing.

The specimen was pushed upright and removed from the table. The jacket was removed and is shown from two different perspectives in Figs. 3-28 and 3-29. Figure 3-28 shows a photo of the column from the weak axis. In the photo, the specimen has minor crushing of the cover concrete in the region from 219 mm (8.5 in) to 749 mm (29.5 in), with the largest amount of spalling concentrated at the higher elevation. The left side of the photo corresponds to the far side of the specimen. The flexural cracks are seen at all intersections of jacket segments as shown in Fig. 3-29. A large amount of the damage to the concrete surface was due to the removal of the jacket and the bond strength of the epoxy. Close inspection of the specimen indicated no significant shear cracking in either the FRP jacket or the concrete.

3.3.2.2 Load and Displacement Histories

The displacements discussed in this section are measured relative to the table. The lateral forces shown were calculated from the link acceleration and mass rig weight, which included the P-delta force of the mass rig.

The measured force-displacement hysteresis curves for the earthquake events are shown in Figs. 3-30 and 3-31. The first two events clearly show a linear behavior of the specimen. While events three through ten clearly shows large energy dissipation through the wide hysteresis curves. The permanent deformation of the specimen increased with each event resulting in a shift of the hysteresis curves. Figure 3-32 shows the measured permanent displacement for each event.

The hysteresis curves for each event were used to calculate an average specimen stiffness based on the peak force and displacement and peak force and the starting point (chord stiffness) for each event. Table 3-3 shows the variation of the specimen stiffness over the testing events. The hysteresis curves were summarized by taking the peak force and corresponding displacement for each event, creating a force vs. displacement envelope as shown in Fig. 3-33. The two curves represent: (1) peak lateral force versus the corresponding displacement with respect to time, (2) peak lateral force versus the peak displacement without respect to time. The two curves coincide in the elastic region but deviate afterward. The measured displacement for all events is shown in Fig. 3-34.

3.3.2.3 Measured Strains

The strain gages were placed at the critical elevations within the column on the longitudinal and transverse steel. Their locations were based on the predicted failure region

of the column and previous test results[5,17,37]. The visual mode of failure of the specimen was verified with the strain gage data.

The measured longitudinal bar strains were evaluated over the column height to determine the first yield and the plastic hinge elevation. In the figures, positive strain indicates compression and negative strain indicates tension. Figure 3-35 shows the longitudinal compression and tensile strain envelopes over the column height for the far side of the specimen. The bar yielded between the second and third events. The maximum strain measured prior to gage failure occurred at 9209 μs in event seven. Figure 3-36 shows the longitudinal bar strain envelopes on the near side of the specimen. The near side longitudinal bar yielded in tension in the third event and failed in the sixth. The instrumentation failed on the near side of the column due to the high tensile strains sustained early in the test due to the limitations of strain gages. The far side instrumentation lasted longer but failed as a consequence of the large tensile strains achieved in the higher amplitude events

The transverse tie strains were broken into two groups: (1) center ties, (2) corner ties. The center ties were lapped at mid column across the strong axis of the column (Figs. 2-4 and 2-14). Strains in these ties were larger, in general, than the corner ties. The corner ties were hooped around the end of each side of the strong axis (Figs. 2-4 and 2-14). The peak strain envelopes for both groups of ties were plotted. However due to the failure of the gages at high displacements only two sides of the specimen are shown in the figures. Figure 3-37 shows the lateral corner ties peak strain envelopes located near the corner on the near side of the specimen. This figure shows all the strains were well below yield for all measured events prior to failure of the instrument. Figure 3-38 shows the strains for the center tie on the far side of the specimen. This figure indicates all strains were also well below yielding.

Figures 3-39 and 3-40 show the jacket end and side strains envelopes over the column height respectively. The horizontal carbon fiber-epoxy jacket strains were measured on five sides of the column, mounted on the surface of the jacket at the outermost fiber. The critical strains developed at the end of the columns strong axis corresponding to the lapped region of the composite straps and in the middle of the column where no overlap occurred. The carbon fiber-epoxy jacket behavior is linear-elastic to failure with no "yield" point. The measured jacket strains were less than 50 percent of the ultimate strain of the jacket (ε_u = 8900 μs), and in most cases did not exceed the conservative design strain limit of ε_d = 6000 μs. The large increase in strain in the region of the jacket from 533 mm to 1092 mm (21 in to 43 in) as compared to the other measurements, indicates plastic hinge formation in this region, however due to strain gage failure, it is difficult to ascertain the precise failure elevation based on this data alone. Detailed comparison of measured strain locations is made in Section 3.4 for all specimens.

3.3.2.4 Measured Curvatures

The curvature was measured using *Novotechnik* displacement transducers attached to threaded rods imbedded in the specimen (Fig. 2-16). These instruments measured over a gage length, and hence the data are the average curvatures between the threaded rods. Figure

3-41 shows the measured curvature envelopes over the height of the specimen. This figure shows the plastic hinge formation in two distinct locations on the specimen corresponding to the region between 425 mm to 584 mm (16.5 in to 23.0 in) and 730 mm to 889 mm (28.75 in to 35.0 in). The lower hinge region from 425 mm to 584 mm (16.5 in to 23.0 in) was located on the far side of the column. While an upper hinge region from 730 mm to 889 mm (28.75 in to 35.0 in) was located on the near side of the column. The asymmetrical hinging of the column was also seen in the testing of specimens FA and FRG.

3.3.2.5 Measured Variation of Axial Force

The Dywidag prestressing system was used to apply the axial load to the specimens during the tests. The axial load was initially set at 284.6 kN (64 kips). However the hydraulic jacks did not respond rapidly enough during the test to maintain a constant load. The variation in axial load is shown in Fig. 3-42 for all eleven test events. The change in axial load during the test affects the flexural capacity of the column. A discussion of the effect of the axial load variation is presented in Section 4.2.2 and 4.2.3.

3.3.2.6 Comparison of Target Achieved and Table Peak Acceleration

The fine tuning process corrected a majority of the disparity between the input earthquake record and the actual table response. However some differences still occurred. Previous shake table tests indicated that the effect of difference in the input and output response of the shake table is minimal for the dominant frequency range of the test columns[12,17]. Figure 3-44 compares the envelope of the achieved peak table acceleration with the target peak acceleration. This figure indicates that the negative target peak acceleration exceeded the achieved peak acceleration by as much as 20 percent. The positive target peak acceleration was exceed by the achieved by as much as 60 percent. The large difference can be explained due to the changing stiffness of the specimen during the testing process that has the effect of nullifying some of the fine tuning process in the later events. A discussion of the effects of the variation in target and achieved peak accelerations is presented in Chapter 4.

3.4 Comparison of Retrofit Methods

The primary purpose of the retrofit was to provide sufficient shear capacity in the flared column with minimum increase in flexural capacity. The retrofit design had to ensure ease of installation due to the confined spaces around the prototype columns on bridge I-1250. In this and previous studies three retrofit materials were used to jacket the specimens: (1) steel (specimen FR), (2) glass fiber-epoxy (specimen FRG), and (3) carbon fiber-epoxy (specimen FRC). A comparison of the effectiveness of the retrofit methods was done using the measured forces, displacements, and strains. Detailed comparison of displacement ductility and flexural enhancement is presented in Chapter 4.

3.4.1 Measured Lateral Load and Deflection

A comparison of the lateral force envelopes for the four specimens, as shown in Figs. 3-44 and 3-45, indicates that the initial stiffness for the three retrofitted specimens was essentially identical. The primary difference was in the yield displacement. The yield displacement was determined by describing the force-displacement envelope in an elasto-plastic relationship. A line was extended from the origin to the data from the second event to describe the linear behavior; and a line modeling the plastic behavior was placed to balance the area under force-displacement envelope. The intersection of these two lines described the yield force and displacement. A more thorough discussion of this methodology is presented in Section 4.4. FRP jacketed specimens yielded between 23 mm to 25 mm (0.92 in to 1.0 in). This small difference in yield displacement leads to a slightly higher displacement ductility for the FRP jacketed specimens. The FRC specimen performed the best with a displacement ductility of $\mu_\Delta = 7.8$ at failure.

The ultimate lateral force achieved in the three retrofitted specimens indicated a significant increase in flexural capacity over the as-built specimen. Specimen FA reached an ultimate peak lateral load of 254 kN (57.1 kips), with three retrofits corresponding to an increase of 27.3% (FRC), 34.3% (FRG), 40.8% (FR) in peak lateral load. A large increase in flexural capacity is unwanted due to the impact of the higher forces on the column components such as the footing and bentcap structures, as well as shifting the loading of the bridge to possibly fail un-retrofitted columns. The FRP jacketing is not isotropic. Nonetheless, it provides some strength in its transverse direction which is minimized by the segmentation of the jacket. The relatively large increase in flexural strength of specimen FR is due to the isotropic properties of steel and increased cross-section of the specimen due to the grout filled gap between the column surface and steel jacket.

3.4.2 Measured Strains

A comparison of the measured strains was done for the bars in the vicinity of the plastic hinge region. The strain gages were at the same locations in the four specimens, therefore giving a good indication of the effectiveness of the jacket in redistributing the shear stress. Figures 3-46 to 3-48 show the longitudinal peak measured strain versus the peak displacement for each event at elevations of 279 mm (11 in), 546 mm (21.5 in), and 800 mm (31.5 in). The three figures show that the longitudinal steel yielded very early in the testing and reached very high strain levels prior to failure of the strain gages. The three retrofit methods confined the column core sufficiently to prevent premature failure of these bars. The difference in strain levels between the retrofit methods was not significant except in the case of specimen FR which at the 800 mm (31.5 in) elevation the bar did not yield until the sixth event.

The response of the transverse steel during the tests was the key indicator of a successful retrofit of the plastic hinge region from 546 mm (21.5 in) to 800 mm (31.5 in). This region was instrumented at three separate elevations as shown in Fig. 2-14. Figures 3-49 and 3-50 show the measured strain in the transverse reinforcement at 533 mm (21 in)

versus peak displacement for each event. Strain gages 16 and 18 show the effectiveness of the retrofit as the as-built specimen cross ties yield, and the retrofitted specimens are all well below yield. Since this elevation corresponded to the predicted failure zone and the measured plastic hinge region, the retrofit appears to be successful. The measured results indicate slightly better response from the FRP jacketed systems compared to the steel jacket. Figures 3-51 and 3-52 show the measured strain envelopes for transverse reinforcement at 660 mm (26 in). Strain gage 24 was installed on a corner tie and strain gage 22 was on the center tie. Strain gage 24 yielded in specimen FA just after the ultimate peak lateral load, the three retrofitted specimens show measured strains of much less than yield. Strain gage 22 indicates specimens FA and FR responded similarly nearly reaching yield in the last event, while specimens FRG and FRC are well below yield for the similar events. Figure 3-53 shows strain gage 27 at elevation 800 mm (31.5 in). This figure indicates all four specimens were below yield with the retrofitted specimens reaching less than 50 percent of yield.

The measured jacket strains are difficult to compare due to the difference in materials and their yield and ultimate strain capacities. The steel jacket was constructed of Grade 36 steel, however the measured properties of the jacket were substantially different with a measured yield stress of 382.6 KPa (55.5 ksi) corresponding to a yield strain of $\varepsilon_y = 1910\,\mu s$. The FRP systems are linear-elastic reaching an ultimate strain at failure without a clear yield point. The strains in these jackets are compared to their ultimate strain capacity and design strain capacity rather than yield. The measured ultimate strain is $\varepsilon_u = 20900\ \mu s$ for glass fiber composite, and $\varepsilon_u = 8200\ \mu s$ for carbon fiber composite. The design strain is $\varepsilon_u = 6000\ \mu s$ for both FRP specimens. The predicted plastic failure region is compared using the strain gages located at 533 mm (21 in) and 800 mm (31.5 mm), which were at identical locations in the three retrofitted specimens.

Figure 3-54 shows the measured strain at the end of the strong axis on the far side of the specimen at 533 mm (21 in). The steel jacket is well below yield at this location through the final event, while the FRP jackets are substantially higher. The glass fiber-epoxy jacket exceed the design strain in the final event but is substantially less than its ultimate strain; the carbon fiber-epoxy jacket is less than design strain in the final event, but is at approximately 50 percent of its ultimate. Figure 3-55 shows the measured strain on the end of the weak axis at 533 mm (21 in). The steel jacket has very small strains, while the FRP jackets are large but much less than ultimate strain. Specimen FRG exceeds the design strain but at the final event is less than 30 percent of the ultimate strain. Figures 3-56 and 3-57 show the measured jacket strains at 800 mm (31.5 in), indicating the steel jacket reached very small strains, and the FRP jackets reached higher strains but at levels much less than design strain. The only measured case of yielding of any of the jackets is shown in Fig. 3-58, in which the steel jacket exceed yield in the final event at 533 mm (21 in) from the footing.

Based on the measured strains, it appears that the three retrofit methods were very successful in reducing the strain level in the transverse ties. The steel jacket specimen (FR) yielded in the plastic hinge region, but in most other locations was much less than yield, while the FRP jacketed systems (FRG and FRC) reached higher strains and were generally more utilized during the tests.

3.5 Observations and Remarks

The thirty-percent scale specimens tested in the dynamic platform responded in a generally similar manner as the previous tests of the forty-percent scale specimens using quasi-static methods. The level of damage of the as-built specimen was greater due to the difference in the loading and unsymmetrical response of the column[17]. The earthquake loading allowed an accurate interpretation of the columns strength and capacity.

The experimental study indicates that the FRP jacketed systems provides an excellent alternative to the standard steel jacketing of concrete columns for increased seismic response in one-way non-prismatic flared columns. The two types of jackets used in this study show that the FRP jackets can be easily installed on non-prismatic columns in the field, and match or exceed the performance of steel jacketing. The installation limitation of steel requiring the expensive fabrication, insertion of grout, field welding are eliminated using FRP systems. The added benefit of the segmental composite jacket allows installation in very confined spaces where steel jacketing would require removal of the surrounding structural material proving very costly and time consuming.

The failure of the four thirty percent scale specimens occurred through low-cycle fatigue of the longitudinal rebar in the flared region of the specimen. This zone corresponds to the reduced number of longitudinal bars from 533 mm (21 in) to 800 mm (31.5 in), and is at the predicted plastic failure zone. The spreading of the plastic hinge was extensive in specimen FA, while it was much more controlled in specimens FR, FRG, and FRC due to the gap (or reduced number of layers) in the jackets. The as-built specimen (FA) developed extensive shear and flexural cracking prior to failure, with substantial spalling of cover concrete, which was all but eliminated by the three retrofit methods.

The dynamic measured properties of the specimens is described in Table 3-1 indicating the FRP jacket systems (FRG and FRC) increased the stiffness and frequency of the as-built specimen to a similar level seen in the steel jacketed system without increasing the cross-section of the column through insertion of grout. The degradation of the three retrofitted specimens was approximately the same over the eleven events with specimen failure occurring after 250 percent of the input earthquake motion, compared to the as-built specimen failure at 175 percent of the input earthquake motion. Clearly the retrofitted methods were successful at sufficiently delaying the failure of the specimen, and changing the failure mode to flexure from shear/flexure.

The measured strains of the four specimens indicates the three retrofit methods substantially reduced the lateral tie strain at all locations along the specimen height, extending the reserve shear strength of the column substantially. This is discussed in more detail Chapter 4. The as-built specimen (FA) developed severe shear cracking and spalling of concrete. The steel jacketed specimen (FR) had some shear cracking due to constraints of the grout and steel jacket allowing shear crack propagation. Specimens FRG and FRC essentially eliminated shear cracking due to the bonding of the composite wrap to the surface of the specimen. Note that the FRP jacket did not have a gap, but had a reduced number of

layers at the intended plastic hinge location. The presence of the composite helped reduce shear cracks at the locations where the gap in the steel jacket was placed.

The increase in flexural strength was unavoidable but controlled to a large extent by the design methods of the jacketing systems. Specimen FR used a physical gap to provide a failure plane and minimize flexural enhancement, however the 40 percent increase in flexural strength as compared to the as-built specimen indicates it was not as effective as desired. The FRP jacket systems (FRG and FRC) provided a reduced thickness of wraps at the plastic failure location to reduce the increase in flexural strength; however the experimental data indicates that the reduced thickness of composite wrap used in these specimens was not necessary as the segmented jacket allowed a clear flexural failure path.

A comparison of the two FRP systems shows that both systems performed equally well in the experimental study with a slight advantage in dynamic response shown by specimen FRC in both displacement ductility and minimization of flexural enhancement. The FRC system required less labor because it needed only two wraps of material amounting to approximately 2.03 mm (0.08 in) thickness, compared to specimen FRG with 3.81 mm (0.15 in) thick jacket. The less number of wraps and smaller relative thickness make the carbon fiber-epoxy material advantageous to install in very confined spaces due to the amount and cost of labor being proportional to the material thickness. The disadvantage of the FRC system is the cost being approximately twice that of the FRG system for a similar strength jacket.

The response of the retrofitted specimens indicate all three methods were effective in meeting the primary goal of increasing the shear strength of the as-built specimen. The increase in flexural strength in the retrofitted specimens was inevitable. However it was controlled by the gap (reduced thickness) in the jackets. The FRP jacketed specimens (FRG and FRC) seemed to slightly outperform the steel jacketed specimen (FR) based on displacement ductility and minimization of increase in flexural strength. With respect to ease of installation and reduced disruption to areas with limited access, however, the FRP jackets have a clear advantage.

Chapter 4

Analysis of Test Specimens

4.1 Introduction

This chapter presents the analytical studies of specimens FRG and FRC. The procedure and theory used to perform the analysis is discussed as well as a comparison of the experimental and theoretical responses of the test specimens. The effectiveness of the shake table modeling of the earthquake motion and variation of loading parameters is evaluated. The analysis was performed to determine: (1) dynamic modeling effectiveness, (2) force-deformation relationship, (3) predicted shear capacity, (4) contribution of FRP jacketing to the response.

4.2 Dynamic Modeling Considerations

The effectiveness of the shake table and axial loading system to model the earthquake loading was verified through rigorous analysis. An evaluation of the specimen response subjected to the actual table motion was done to determine if the levels of excitation were similar to those discussed in Section 2.7. In addition, the general spectral response of the four thirty percent scale specimens was compared to establish if the specimens had been subjected to comparable motions.

4.2.1 Shake Table Motions

The actual shake table motion is generally different from the input record prescribed in the shake table control system. This difference is due to the achieved response of the shake table being influenced by the dynamic properties of the specimen being tested. During the tests, the dynamic properties of the column changed due to the damage incurred by the specimen; thus making the initial tuning of the shake table as discussed in Section 3.2.1 ineffective. Upon completion of the testing, evaluation of the measured table acceleration and input motion was necessary to determine if the earthquake simulation modeled the actual input motion with reasonable accuracy.

The input earthquake accelerogram was compared to the measured table acceleration using a spectral analysis computer program *Spect*[31]. *Spect* was used to compare the pseudo acceleration response spectrum of the input earthquake accelerogram and the measured shake table acceleration to verify the period/frequency content of the signals. The program solves for the peak acceleration for a single-degree-of-freedom (SDOF) system given a period and damping ratio. The period range solved was from 0 to 4 seconds with the damping ratio of $\xi = 2\%$ for all calculations. Ideally the spectra would have similar fundamental periods and amplitudes for both the input and measured signals over the entire period range. The table

input accelerogram, 1994 Northridge Earthquake measured at Sylmar Hospital, was the same as the input signal discussed in Section 3.2.2 in which the time-scale of the record was adjusted for the scale of the specimen.

Figures 4-1 and 4-2 show the response spectrum for the two retrofitted specimens and table input signal for events one to eleven corresponding to 20% to 275% of the earthquake amplitude. The comparison shows the fundamental period of the base acceleration of the test specimens FRG and FRC ranges from 0.2 to 0.28 seconds (5 to 3.57 Hz), with a definitive peak at 0.2 seconds. The input earthquake accelerogram, adjusted for time-scale, has a fundamental period that ranges from 0.2 to 0.35 seconds (5 to 2.85 Hz). The experimental results in Tables 3-2 and 3-3 showed that the effective period of FRG and FRC was 0.5 seconds or higher during post yielding events (event 3 and after). Figures 4-1 and 4-2 show that the spectra for the actual motion for both specimens were generally very close indicating that both specimens were essentially subjected to the same motion. The figures also show that the achieved records deviated from the input target motion significantly. However, the differences are not critical as long as the achieved motions for both specimens were the same. The test specimens and the table input response spectra show a consistent behavior between the input and achieved accelerations in the predominant period range, which indicates the shake table was effective at modeling the input earthquake motion. The two FRP retrofitted specimens display a nearly identical spectral response for the periods from 0 to 2 seconds, showing that the comparison of experimental results of the force and displacement are reasonable between specimens FRG and FRC.

In order to compare the table motions for all four of the shake table specimens, the response spectra for the as-built specimen (FA) and the steel jacketed specimen (FR) were calculated for two percent damping and superimposed. Figures 4-3 and 4-4 show the response spectra for events four and six, corresponding to the peak or near peak responses of the specimens. Figure 4-3 shows a comparison of the four specimens for event four in which specimen FA reached its ultimate peak lateral load. For the effective period range of 0.46 and 0.92 seconds (Tables 3-2 and 3-3) the response of the four specimens is nearly identical with the exception of the magnitude of peak acceleration. Figure 4-4 shows the response spectra for event six for the four specimens, this event corresponds to the ultimate peak lateral load achieved in specimens FR, FRG, and FRC. In the effective period range all four specimens again show nearly identical responses. From this analysis it is apparent that the four specimens differ in dynamic properties to a small extent effecting the calculated psuedo acceleration, but their response justifies equal comparison between the specimens.

4.2.2 Variation in Axial Load

The testing of the specimens included applying an axial load proportionate with the load on a typical column found on the highway bridge being studied. The variation of axial loading that occurred in the testing process was due to the inefficiency of the hydraulic jacks and the accumulator of the prestressing system to compensate for the rapid column displacement caused by the earthquake loading. A typical variation of axial loading is experienced in lateral loading of a frame system that would occur in the prototype columns due to the interaction of the multi-column bentcap. However, studying this type of variation

in axial load is beyond the scope of this study. This analysis considers solely the variation in axial loading due to inefficiency of the loading system, which was not desired nor planned.

Tables 4-1 and 4-2 show a comparison of the measured maximum and minimum axial loads for specimens FRG and FRC, respectively. The variation in axial load for specimen FRG was from 79 percent to 212 percent of the target axial load of 284.6 kN (64 kips) and for specimen FRC from 75 percent to 188 percent of the target axial load. The difference in axial loading between specimens FRG and FRC is shown Fig. 4-5 for event six, which corresponds the ultimate peak lateral load in the specimens. Clearly the variation in axial load occurred during the same time intervals between specimens, implying that the change in flexural capacity occurred in a similar manner and at the same level in each specimen. Therefore, the increase in capacity in both specimens was similar.

Since the variation in axial loading was similar between specimens FRG and FRC, it was necessary to quantify the effect of the variation in axial load on column strength. A moment-curvature analysis was completed at the plastic hinge elevation to determine the variation of moment capacity with differing axial loads. The analysis was conducted by completing several iterations varying the axial load with each run. Figure 4-6 shows the variation in moment-curvature for specimen FRG using the maximum, minimum and target axial loads. The maximum moment for each run was then plotted versus the axial load to describe a moment-axial load interaction diagram. Figure 4-7 shows the column interaction diagram for specimen FRG. The figure indicates that even though the axial force varied as much as 212 percent, the flexural capacity increased approximately 9 percent. Figures 4-8 and 4-9 show similar moment-curvature and column interaction diagrams for specimen FRC. Both of the figures indicate a similar increase in flexural capacity of 9 percent at the maximum axial load. Since the variation in axial load was momentary, the increased flexural capacity of both specimens was assumed to be less than 9 percent. The minimum axial load for each specimen as shown in Figs. 4-7 and 4-9 indicates a reduction in flexural capacity for specimen FRG of 2 percent and for specimen FRC of 3 percent. Clearly the impact of the variation in axial load affected the strength of the specimens in a minimal manner.

4.2.3 Rate of Loading Effects on Test Specimen Strength

The measured strain rate on the specimens was found using the measured strain in the longitudinal bars. The measured strain for two consecutive points was divided by the time step to determine the average rate of change in the measured strain (strain rate). Figures 4-10 and 4-11 show the measured strain rate for the extreme longitudinal reinforcement in specimens FRG and FRC, for events one through five corresponding to 20 percent to 125 percent of the applied earthquake loading. Figures 4-10 and 4-11 indicate both specimens (FRG and FRC) achieved an average strain rate between 2,000 μs to 35,000 μs in the first five events, with the average strain rate calculated through statistical analysis of the strain rate history. High strain rates can cause a significant increase in the strength and stiffness of reinforced concrete columns that must be accounted for in the analysis of the test specimens[21].

4.2.3.1 Loading Rate Effect on Material Properties

The rate of loading of concrete can reduce or increase the maximum load achieved prior to failure or crushing. This phenomenon is exhibited in the testing of concrete cylinders with very slow loading rates (less than 10 μs/sec) the axial compressive strength is roughly 75-80% of the standard strength. With very high loading rates (15,000 to 20,000 μs/sec) the strength increases to approximately 110-115% of the standard strength[13,22]. Steel reinforcement experiences a similar increase of yield strength due to an increased rate of loading. Strain rates of greater than 10,000 μs can increase the yield strength by as much as ten percent[13].

In both concrete and steel the increase in strength is reduced under variable strain rate. However, this effect still needs to be considered. The effect of rate of loading in steel and concrete is typically accounted for in design through dynamic magnification factors that increase the compressive strength and stiffness of the structure. In the analytical part of this study, the measured compressive strength of the concrete and yield strength of longitudinal steel were increased by 10% to take into account the strain rate effect.

4.3 Force-Deformation Relationship

4.3.1 Computer Programs

The computer analysis of the specimens was completed using two special application programs in addition to standard spreadsheet and mathematical analysis software. The moment-curvature relationships were calculated using *RCMC*[37]. The theoretical earthquake response of the specimen was calculated using *RC-Shake*[12].

The computer program *RCMC* calculates the theoretical moment curvature for a reinforced concrete cross-section for a given axial load. The parameters of the program allow for consideration of both unconfined and confined concrete. The Mander et al. confinement model[15] was used. The failure of the cross-section is determined through the fracture of the first layer of steel, taking into consideration reduction of the effective depth of the section due to spalling of the cover concrete during the analysis. The program output includes the moment-curvature relationship as well as the strains in reinforcement.

RC-Shake is a computer program that calculates the dynamic response of a column modeled as a single-degree-of-freedom (SDOF) system. This program calculates the response of a column subjected to an earthquake record, considering both hysteretic and viscous damping, as well as the loading setup of the mass rig system. A degrading stiffness hysteresis model, called Q-hyst, models the nonlinear load-deformation response[26]. The input to the program requires a bi-linear load-displacement relationship (primary curve). The output of the program gives the force-displacement of the SDOF system.

4.3.2 Theoretical Lateral Deflection

The lateral deflection was based on a reinforced concrete cantilever column subjected to a lateral load. The components of deflection considered were flexure, shear, and bond slip:

$$\Delta_{Total} = \Delta_{Flexure} + \Delta_{Shear} + \Delta_{Bond\ Slip} \quad (4\text{-}1)$$

The components of the total deflection were determined separately and then added together. The following sections describe the theoretical methods used to calculate the components of the total deflection.

4.3.2.1 Flexural Deflection

The calculated curvature was used to determine the flexural deflection of the specimens by application of the moment area theorem as shown in Eqn. 4-2.

$$\Delta_{Flexure} = \int_a^b \varphi \cdot x \cdot dx \quad (4\text{-}2)$$

Where: φ = *Curvature*
x = *Shear span from center of load application to cross-section elevation*

Equation 4-2 quantifies the flexural deflection as the first moment of the area under the curvature diagram, between the two points of interest, with respect to the final point of interest. This equation was used to integrate column curvature from the top of the footing to the centerline of the applied load.

In this analysis, Eqn. 4-2 was applied to the calculated curvature data from *RCMC*. The moment-curvature relationship was calculated for various sections along the height of the column. The curvature corresponding to a given lateral load was then plotted versus the height of the column for the cross-sections. The first moment of the area under the curvature curve was calculated with *MathCad™* [16], using numerical integration to determine the flexural deflection for the lateral load considered.

4.3.2.2 Shear Deflection

The effect of shear deformation applies to deep structural members or cracked reinforced concrete members subjected to shear[20]. In this study the significant cracking of the specimens requires that shear deformation be considered. The shear deformation was calculated based on the shear stiffness derived by Park and Paulay in Ref. 20. The method considers a unit height of a cross-section of the column, with the deformation derived based on the shear stiffness (K_v) using a truss analogy. Equation 4-3 shows the shear stiffness relationship for a unit height on a column based on a shear crack inclination of 45°.

$$K_v = \frac{\rho_v}{1+4\cdot n\cdot \rho_v}\cdot E_s\cdot b_w\cdot d \qquad (4\text{-}3)$$

Where: K_v = *Shear stiffness for an element with a unit length*

ρ_v = *Shear reinforcement ratio* $\left(A_v/(b_w\cdot s)\right)$

n = *Modular Ratio (Es/Ec)*

E_s = *Young's modulus of shear reinforcement*

b_w = *Section width perpendicular to applied shear*

d = *Effective section depth*

A_v = *Area of shear reinforcement*

s = *Spacing of shear reinforcement along longitudinal axis*

The shear stiffness then is used to determine the total shear deflection (Δ_{Shear}), using Eqn. 4-4: where (V) is the applied shear force and (L) is the shear span.

$$\Delta_{Shear} = \frac{V\cdot L}{K_v} \qquad (4\text{-}4)$$

In this study the contribution of shear deformation was only considered at the predicted plastic hinge elevation of 533 mm (21 in), due to its considerable effect on the response of the specimen.

4.3.2.3 Bond Slip Deflection

The monolithic connection of the specimen requires consideration of the effect of bond slip on the total deflection. The method developed by Wehbe, et al. in Ref. 38 was used to calculate the bond slip deflection of the specimen. This method is applicable to reinforced concrete connections that have sufficient development to prevent bar pullout. Equation 4-5 shows the bond slip deflection relationship.

$$\Delta_{Bond\ Slip} = \theta_s\cdot L \qquad (4\text{-}5)$$

Where: θ_s = *Bond slip rotation at pivot point* $\left(\delta l/na_t\right)$

L = *Column shear span*

δl = *Longitudinal bar extension*

na_t = *Distance from the neutral axis to center of outermost tensile steel layer*

The longitudinal bar extension (δl) is determined by calculating the development length (l) and the basic bond strength (u) of the bar. Depending on the calculated strain of

the outermost steel layer in the column section, these values vary due to the strain profile, however the basic bond strength is assumed to remain constant as shown in Eqn. 4-6.

$$u = \frac{20 \cdot \sqrt{f'_c}}{d_b} \leq 5.5 \quad (MPa) \tag{4-6}$$

Where: f'_c = *Concrete compressive strength*
d_b = *Longitudinal bar diameter*

If the calculated strain is less than or equal to strain hardening, Eqns. 4-7 and 4-8 determine (δl), and lead to the calculation of the bond slip rotation (θ_s).

$$l = \frac{f_s \cdot d_b}{4 \cdot u} \tag{4-7}$$

$$\delta l = \frac{\varepsilon_s \cdot l}{2} \tag{4-8}$$

Where: f_s = *Calculated steel stress in outermost steel layer*
d_b = *Longitudinal bar diameter*
u = *Basic bond strength of longitudinal steel*
ε_s = *Calculated steel strain in outermost steel layer*

If the calculated steel strain is greater than strain hardening, two different development lengths must be considered: the development length at steel yielding (l_1), and the development length at the calculated stress (l_2). Eqns. 4-9 to 4–11 determine (δl), and lead to the calculation of the bond slip rotation (θ_s).

$$l_1 = \frac{(f_s - f_y) \cdot d_b}{4 \cdot u} \tag{4-9}$$

$$l_2 = \frac{f_y \cdot d_b}{4 \cdot u} \tag{4-10}$$

$$\delta l = \frac{\varepsilon_y \cdot l_2}{2} + \frac{(\varepsilon_s + \varepsilon_y) \cdot l_1}{2} \tag{4-11}$$

Where: f_s = *Calculated steel stress in outermost steel layer*
f_y = *Calculated steel yield stress in outermost steel layer*
d_b = *Longitudinal bar diameter*
u = *Basic bond strength of longitudinal steel*
ε_y = *Calculated steel yield strain in outermost steel layer*
ε_s = *Calculated steel strain in outermost steel layer*

4.3.3 Estimated Column Capacity Prior to Testing

The specimen flexural capacity was determined through a plastic analysis of the column using *RCMC* to calculate the moment-curvature relationship prior to the tests. The prediction was based on the target axial load of 284.6 kN (64 kips) taking into account the confining effects of the FRP jacket. The confined properties of the column were calculated using the compatibility relationship between the FRP jacket and the column core. The unconfined concrete properties were taken from Table 2-2 and the jacket properties were taken from Table 2-3. The non-prismatic shape of the column required that several cross-sections along the column be analyzed. The column was analyzed at eight locations along its height to determine the moment required to yield the cross-section. The yield moment was determined by using an elasto-plastic relationship to model the calculated moment-curvature without consideration to the dynamic modeling effects discussed in Section 4.2. The yield moment for each cross-section was then plotted versus the shear span, which is measured from the center of the applied load to the cross-section elevation. The demand on the column was determined by drawing a target line from the origin to the yield moment curve. The tangent point indicated the plastic moment and plastic hinge location. Figures 4-12 and 4-13 show this relationship for specimens FRG and FRC respectively. The plastic shear was determined by dividing the plastic moment by the shear span at the outermost point of the curve. From the figures it was noted that failure could occur at nearly any location between 533 mm to 800 mm (21 in to 31.5 in) from the footing, due to relative proximity of the plastic shear and moment capacity curves. Therefore the predicted plastic hinge length was determined to range from 533 mm to 800 mm (21 in to 31.5 in) from the footing, coinciding with the reduced number of longitudinal bars. The predicted plastic shear capacity (and thus lateral load capacity) was 245 kN (55.1 kips) for specimen FRG and 248.6 kN (55.9 kips) for specimen FRC, assuming a plastic hinge at 533 mm (21 in) from the footing.

4.3.4 Calculated Column Capacity

After the testing of specimens FRG and FRC, the column was re-analyzed to help explain the difference between the measured and predicted column capacity.

4.3.4.1 Specimen Stiffness

The primary load-deflection curve for each specimen was calculated based on the contribution of deflection components discussed in Section 4.3.2. A series of lateral loads were used to quantify a bi-linear stiffness relationship for specimens FRG and FRC. The linear range (first leg) was defined by a 177.9 kN (40 kips) lateral load, while the nonlinear range (second leg) being defined by a series of loads from 266.8 to 302.4 kN (60 to 68 kips): Where necessary the lateral forces were converted to an equivalent moment by multiplying the force by the shear span to the elevation of the cross-section being analyzed.

RCMC was used to determine the flexural component of deflection. The columns were analyzed at thirteen discrete elevations along the height of the specimen due to the non-prismatic shape of the column and the flexural contribution of the FRP jacket. The following

cross-sections were analyzed: (1) top and bottom of the column, (2) jacket segment discontinuities, (3) center of jacket segments, (4) termination of longitudinal bars.

The FRP jacket contributed both to the confinement of the column and flexural strength even though the composite fibers were essentially horizontal. The confining effect of the jacket was considered in a similar manner as in the pretest analysis. The flexural strength of the jacket was determined using the material properties listed in Table 2-3, as the strength at 90°. Figure 4-14 shows how the cross-section was modeled in *RCMC*. As each layer of jacket material failed it was removed from the model and the program was executed again until failure of all the layers of the jacket occurred. The jacket was modeled solely on the tension side of the column. The compressive strength of FRP jacketing can be substantial if buckling of the jacket fibers is prevented[9,14,32]. The compressive strength contribution by the FRP jacket was neglected in this study due to the jacket thickness and orientation of the uni-directional fibers. Section 4.6 discusses the FRP jacket contribution to the specimen strength in more detail.

Figures 4-15 and 4-16 show the calculated moment-curvature at each of the thirteen elevations analyzed for specimens FRG and FRC, respectively. In Figs. 4-15 and 4-16, the moment capacity of the middle of the jacket segments (127 mm, 305 mm, 623 mm, 877 mm, 1131 mm) reach a strength plateau prior to suddenly dropping off in strength and continuing until failure of the column. The plateau was due to the failure of one layer of the jacket, with the remaining layers staying intact. Figures 4-17 and 4-18 show samples of the calculated curvature versus column height for the 177.9 kN (40 kips) lateral load for specimens FRG and FRC, respectively. The flexural deflection for this load was then calculated using the procedures outlined in Section 4.3.2.1.

The shear and bond slip deflections were calculated using the procedures outlined in Sections 4.3.2.2 and 4.3.2.3. The elevation considered for the shear deformation was the plastic hinge elevation of 533 mm (21 in), while the elevation considered for the bond slip deflection was the column base. The calculations were made using the lateral loads described above. The calculated strains and stresses were taken from the moment curvature analysis completed for the flexural deflection calculation, and the measured steel properties in Table 2-1. The calculated force and displacement components are shown in Table 4-3. The loads listed in Table 4-3 (177.9 kN, 284.7 kN, 293.5 kN) correspond to the lateral forces which describe the primary load-deflection curve.

The two legs of the stiffness relationship were plotted based on the calculated force-displacement values, with the intersection of the legs defining the effective yield point of the column. Figures 4-19 and 4-20 show the estimated stiffness relationships for specimens FRG and FRC compared with the experimental force-deflection envelope. In Fig. 4-19 the calculated specimen stiffness and experimental force-deflection envelope for specimen FRG compare very well in the elastic range, indicating that the yield point of the column was calculated reasonably well. The inelastic range shows a consistent slope with the experimental results. However, the calculated ultimate load capacity is lower than the measured value. The difference between predicted and experimental load capacity is expected in the analysis since the dynamic effects discussed in Section 4.2 were not included.

Figure 4-20 shows the estimated specimen stiffness and experimental force-deflection envelope for specimen FRC. The predicted stiffness is essentially identical to specimen FRG with a slight difference in yield point as shown in Tables 4-5 and 4-6. Therefore, it is not surprising that the elastic stiffness compares well to the experimental force-displacement envelope for specimen FRC.

The similar strength of the specimens is evident in Figs. 4-19 and 4-20, as the stiffness relationships between specimen FRG and FRC are nearly identical. However the response of the specimens differed in ultimate capacity due substantially to the relative thickness of the jackets and their behavior under dynamic loading.

4.3.4.2 Calculated Force-Deflection and Displacement Responses

The calculated force deflection for the FRP jacketed specimens was completed using *RC-Shake*. The program input for both columns was the same with the exception of the column stiffness relationships and the input earthquake motions. The viscous damping ratio used was $\xi = 2\%$, and the power for the unloading stiffness ratio in the Q-hyst model was set at 0.25. The effective mass rig loading (M^*) was 447 kN (100.5 kips), with the overturning mass (W^*) at 426 kN (95.8 kips). The calculated bi-linear relationships described in Section 4.3.4.1 were used in the analysis.

The input earthquake record was the achieved table acceleration taken from each of the eleven events for each specimen. In order to model the multiple earthquake motions that the specimens had experienced, the table accelerations were spliced together into one large record. The output results were then separated to reflect an individual response of the column for each test event.

4.3.4.2.1 Specimen FRG

The calculated hysteretic curves of the specimen for events one to eleven are shown in Figs. 4-21 and 4-22. Hysteretic behavior began in event 5, and large energy dissipation was noted thereafter. Figures 4-23 and 4-24 compare the calculated and measured hysteresis curves for event six corresponding to the ultimate peak lateral load achieved in specimen FRG. The results show that the calculated and measured hysteresis curves have similar peak forces as well as showing large hysteretic energy dissipation. The calculated hysteresis curve, in Fig. 4-24, shows smaller deflections compared to the experimental data, which is believed to be due to the changing dynamic properties of the FRP jacket which were not modeled well through a simple bi-linear stiffness. The complexity of the segmental jacket system and stiffness changes documented from the snapback analysis shown in Table 3-1, indicate a more complex stiffness relationship is required.

Figure 4-25 compares the experimental and calculated peak lateral force-deflection envelopes for specimen FRG. The calculated yield and ultimate points of the column appear to fit the measured data very well, with the exception of the ultimate displacement and force

calculated being less than the experimental data. The difference in ultimate displacements is due to: (1) lack of permanent deformation in calculated response, (2) inability of *RC-Shake* to model damage effects related to permanent deformation. In the calculated force-displacement envelope, the limitations of the primary stiffness can account for a portion of the difference between experimental and calculated ultimate load capacity. The additional difference is thought to be due to the modeling of stiffness degradation. A comparison between the measured and ultimate force shows a 13 percent difference. However, the general trends in the analytical and experimental results are similar.

Figure 4-26 compares the total calculated and measured displacements for events one to eleven. Clearly, the experimental displacement record indicates permanent deformation with each successive event starting in event 4, while the calculated displacement does not show this effect. The peak displacement for each experimental event is substantially more than the calculated value. A detailed comparison of the measured and calculated responses for events 3 and 7 is made in Figs. 4-27 and 4-28. The figures indicate the measured and calculated displacement histories for events 3 and 7 have similar peaks and generally follow the same wave path. The measured response exceeds the calculated in magnitude, and the difference in permanent deformation is shown between the measured and calculated deflection history. The main difference between Fig. 4-27 and 4-28 is the increasing amount of permanent deformation not recorded in the calculated displacement.

4.3.4.2.2 Specimen FRC

The calculated hysteretic curves of the specimen for events one to eleven are shown in Figs. 4-29 and 4-30. In a similar manner to specimen FRG, the hysteretic behavior began in event 5 with large energy dissipation noted thereafter. The calculated and measured hysteresis curves for event six are shown in Figs. 4-31 and 4-32. The figures show that the curves compare well. The results show that the calculated and measured hysteresis curves have similar peak forces as well as showing large hysteretic energy dissipation. The calculated hysteresis curve, in Fig. 4-32, shows smaller deflections compared to the experimental data, which was consistent with the response of specimen FRG, and is attributed to the inadequacies of a simple bi-linear stiffness. As previously discussed, the complexity of the segmental jacket system indicates a more complex stiffness relationship is required.

Figure 4-33 compares the experimental and calculated peak lateral force-deflection envelopes for specimen FRC. The calculated yield and ultimate points of the column appear to fit the measured data very well, with the exception of the ultimate displacement and force calculated being less than the experimental data. The measured and calculated peak force varies by 10 percent. The difference in calculated and measured response is thought to be due to similar reasoning as described in Section 4.3.4.2.1. The general trends in the analytical and experimental results are similar.

Figure 4-34 compares the total calculated and measured displacements for events one to eleven. The experimental displacement record indicates permanent deformation with each successive event starting in event 4, while the calculated displacement does not show this

effect. The peak displacement for each experimental event is substantially more than the calculated value. A detailed comparison of the measured and calculated responses for events 3 and 7 is made in Figs. 4-35 and 4-36. The figures indicate the measured and calculated displacement histories for events 3 and 7 have similar peaks and generally follow the same wave path. The measured response exceeds the calculated in magnitude, and the difference in permanent deformation is shown between the measured and calculated deflection history. The main difference between Fig. 4-27 and 4-28 is the increasing amount of permanent deformation not recorded in the calculated displacement.

4.4 Column Behavior

The performance of a structural element under an applied load is measured by its ability to deform without a significant strength degradation[21]. This deformation is classified by the displacement ductility and drift ratio of the member. Displacement ductility is the ratio of the maximum displacement to the yield displacement, while drift is the ratio between maximum displacement and specimen height. It is essential to clearly define the yield point and maximum displacement of the structural element in order to calculate displacement ductility and drift. In the analysis, all four thirty percent scale specimens (FA, FR, FRG, FRC) were included in order to present a comparison among the retrofit schemes using a similar benchmark system.

The ductility relationship for the experimental data of the test specimens was determined approximating the force-displacement envelopes by an elasto-plastic relationship. The second test event was chosen as the last experimental event prior to the effective yielding of the column. A line was extended from the origin through that data point to emulate the elastic region. The remaining data points were approximated by another linear relationship representing the plastic region. The intersection of these lines determined the yield deflection and yield force of the test specimens. The maximum displacement was determined at the peak displacement in the second to last experimental event; corresponding to event six for specimen FA and event ten for specimens FR, FRG, and FRC. In the second to last event, the specimens had appeared to have failed. However, the measured lateral force demand did not show a large reduction from the ultimate peak lateral load. The last experimental event for all three retrofitted specimens involved loading the specimen to complete failure. The failure occurred during the last event with no useful clear failure point established. Using the second to last experimental event to determine the "ultimate displacement" of the specimens leads to a conservative estimate of the displacement ductility.

The yield point for the theoretical analysis was determined through a moment-curvature analysis of the test specimen, using a version of the effective yield force approach developed in the first study in this series[37]. The ultimate displacement was determined using the *RC-Shake* computer program, which underestimated maximum displacements due to the reasons discussed earlier.

4.4.1 Calculated and Measured Yield Points of the Specimens

The yield points for the four thirty percent scale specimens were calculated according to the procedures described above. The aforementioned factors: (1) axial load variation, (2) rate of loading effects, (3) flexural enhancement of FRP jacketing were included in the analysis.

Tables 4-4 and 4-5 show a comparison between the measured and calculated yield forces and displacements for all specimens. The data show that the calculated yield deflection was within 8 percent and 4 percent of the measured yield displacement for specimens FA and FR respectively. Specimens FRG and FRC showed a larger variation of 21 percent and 15 percent. The large discrepancy between experimental and calculated yield displacements in specimens FRG and FRC was due to the difficulty in approximating the stiffness contribution of the jacket. The comparison of measured and calculated yield force is shown in Table 4-5 for specimens FA, FR, FRG, and FRC. A comparison of specimens FA and FR indicate the ratio of calculated to experimental yield force was 0.96 and 0.81 respectively, while specimens FRG and FRC compared at 0.89 and 0.92.

4.4.2 Measured Displacement Ductility of Specimens

The displacement ductility was calculated as the ratio of the measured maximum displacement to the measured yield displacement. Table 4-6 shows the calculated displacement ductility for all specimens. Note that the values in the table do not show the ductility capacity. The actual ductility capacities are believed to be slightly higher. The maximum ductility achieved was by FRG and FRC at $\mu_\Delta = 7.4$ and $\mu_\Delta = 7.9$, respectively. In the as-built (FA) and steel jacketed (FR) specimens, smaller ductilities were found at $\mu_\Delta = 5.4$ and $\mu_\Delta = 6.9$ respectively. The displacement ductility levels achieved show that the retrofit of the as-built specimen was necessary and that all three retrofit methods improved the seismic response of the columns by nearly the same amount.

4.4.3 Measured Drift of Specimens

The drift was defined as the ratio of the maximum displacement to the height of the column measured to the footing. In this analysis, the specimen height was taken at 1778 mm (70 in), and the maximum displacement was from the second to last test event.

A comparison of the drifts for the four specimens is shown in Table 4-7, which indicates that all three retrofitted specimens showed greater than 9 percent drift in the second to last experimental event, while the as-built (FA) specimen achieved 7.7 percent. This large drift is consistent with the impending failure of a reinforced concrete column. Note that the calculated ductility and drift are still considered to be slightly conservative because the actual failure point could not be identified precisely.

4.5 Shear Capacity

As mentioned earlier, the columns of bridge I-1250 had a very small margin against shear failure and the retrofit design was mainly based on shear. Therefore the shear strength of the columns was of interest. In seismic design it is critical that the brittle failure of structural elements be avoided. Many different design procedures exist to ensure that shear failure does not dominate structural elements. In this study three different methods were used to determine the shear capacity of the specimens: (1) CALTRANS, (2) FHWA, and (3) Wehbe method.

4.5.1 CALTRANS Method

The nominal shear capacity (V_n) for ties and cross-ties is calculated according to Ref. 4, as shown in Eqn. 4-12.

$$V_n = V_c + V_s \tag{4-12}$$

Where: V_c = *Concrete nominal shear capacity*
V_s = *Steel nominal shear capacity*

The two components of the nominal shear capacity are steel and concrete strength, respectively, as shown in Eqns. 4-13 and 4-14. The shear capacity depends on two factors that describe displacement ductility, compressive axial stress, and confinement.

$$V_s = \frac{A_v \cdot f_y \cdot d}{s} \tag{4-13}$$

$$V_c = F_1 \cdot F_2 \cdot \sqrt{f'_c} \cdot A_e \leq 0.028 \cdot \sqrt{f'_c} \cdot A_e \quad (MPa) \tag{4-14}$$

Where: A_v = *Area of shear reinforcement*
f_y = *Yield strength of shear reinforcement*
d = *Distance from extreme concrete compression fiber to the centroid of tension reinforcement*
s = *spacing of shear reinforcement parallel to main reinforcement*
F_1 = *Factor that depends on level of confinement and displacement ductility (need not be taken less than 0.3)*

F_2 = *Factor that depends on the applied compressive axial stress*
A_e = *Effective concrete area (greater than or equal to 80% of gross area)*

The factors F_1 and F_2 can be interpolated from charts in Ref. 4, or can be calculated using Eqns. 4-15 and 4-16.

$$F_1 = \frac{\rho'' \cdot f_{yt}}{1.03} + 3.67 - \mu_\Delta \leq 3.0 \quad (MPa) \tag{4-15}$$

$$F_2 = \left(\frac{.5}{(6.895)}\right) \cdot P_1 + 1 \leq 1.5 \quad (MPa) \tag{4-16}$$

Where: $\rho'' = \dfrac{Volume\ of\ transverse\ reinforcement}{Volume\ of\ column\ core}$

f_{yt} = *Yield strength of transverse reinforcement*
μ_Δ = *Displacement Ductility Demand Ratio*
P_1 = Compressive Axial Stress (MPa)

4.5.2 FHWA Method

The nominal shear capacity for ties and cross ties considers the effect of the strength of concrete and lateral steel, as well as, a term for compressive axial stress according to Ref. 35, as shown in Eqn. 4-17.

$$V_n = V_c + V_t + V_p \tag{4-17}$$

Where: V_c = *Shear force carried by concrete*
V_s = *Shear force carried by truss action (lateral reinforcement)*
V_p = *Lateral component of compression strut in the column due to the applied axial load (arch action)*

The shear capacity of the concrete depends on the displacement ductility and can be found using Eqn. 4-18.

$$V_c = v_c \cdot A_e = k \cdot \sqrt{f'_c} \cdot A_e \tag{4-18}$$

Where: k = *0.29 in MPa units when $\mu_\Delta \leq 2$ and 0.1 in MPa units when $\mu_\Delta \geq 4$. For values ($2 < \mu_\Delta < 4$) linear interpolation is used.*
f'_c = *Concrete compressive strength*
A_e = *80% of the gross cross-section area*

Equation 4-19 shows the shear capacity of the transverse reinforcement, which considers a truss mechanism including a term for shear crack inclination.

$$V_t = \left(\frac{A_v \cdot f_y \cdot d}{s}\right) \cdot cot(\theta) \tag{4-19}$$

Where: A_v = *Area of shear reinforcement*
f_y = *Yield strength of shear reinforcement*
d = *Distance from extreme concrete compression fiber to the centroid of tension reinforcement*
s = *spacing of shear reinforcement parallel to main reinforcement*
θ = *Angle of shear crack*

The FHWA recommends the shear crack angle of $\theta = 30°$ be considered. However CALTRANS and ACI code suggest an angle of $\theta = 45°$.

The shear resistance due to axial load (V_p) is found from the horizontal component of strut that forms between the top and bottom of the column, as shown in Eqn. 4-20. For simplification, FHWA suggests that the axial load term (V_p) be taken as 20 percent of the applied axial load.

$$V_p = \left(\frac{(D-c)}{2 \cdot a}\right) \cdot P \qquad (4\text{-}20)$$

Where: D = *Section depth or diameter*
c = *Depth of the compressive zone at the bottom of the column*
a = *Total column length for a cantilever column (fixed-pinned)*
P = *Applied axial load*

4.5.3 Wehbe Method

This method is a hybrid of the CALTRANS and FHWA methods, as derived in Ref. 37. The nominal shear capacity combines the concrete (*Vc*) and the steel reinforcement (*Vs*) terms from the CALTRANS method, and the arch action term (V_p) from the FHWA method. The nominal shear capacity is shown in Eqn. 4-21.

$$V = V_c + V_s + V_p \qquad (4\text{-}21)$$

The (*Vc*) and (*Vs*) terms are taken directly from Section 4.5.1, while (V_p) is taken as 20 percent of the target axial load. The purpose of Eqn. 4-21 is to provide a reasonably accurate estimation of shear capacity by compensating for the underestimation of the CALTRANS method and the overestimation of the FHWA method[37].

4.5.4 Calculated Shear Capacities

The shear capacity for specimens FRG and FRC was calculated according to the methods outlined in Sections 4.5.1 through 4.5.3 for sections along the height of the specimen. All three methods were used to determine the shear capacity. The material properties used to calculate the shear capacity were from Tables 2-1 and 2-2. The shear

demand for each specimen was taken as the peak lateral load applied to the specimens during the experimental study. The peak lateral loads applied to specimens FRG and FRC were 341.1 kN (76.7 kips) and 323.7 kN (72.8 kips), respectively.

In order to compare the shear capacity and demands of specimens FRG and FRC, it was necessary to calculate the capacity of the specimen without the FRP jacket first. Figures 4-37 through 4-39 show the calculated CALTRANS, FHWA, and Webhe shear capacities over the height of the (un-retrofitted) specimen. Each capacity curve was calculated considering a range of displacement ductilities (μ_Δ) in order to determine the calculated shear capacity over the experimental procedure. The shear demand shown is the peak lateral load applied to the as-built specimen (FA) of 254 kN (57.1 kips). The calculated capacity varied due to the non-prismatic shape of the column and the displacement ductility used in the calculations. The displacement ductility was only varied within the predicted plastic hinge region of 533 mm (21 in) to 800 mm (31.5 in).

Figure 4-37 shows that the CALTRANS calculated specimen capacity predicts failure at a displacement ductility level of $\mu_\Delta = 6$. The CALTRANS method indicates sufficient shear capacity reserve at $\mu_\Delta = 4$ throughout the height of the column. The FHWA shear capacity is shown in Fig. 4-38. Since the FHWA method depends on the shear crack inclination (θ), as discussed in Section 4.5.2, this method was calculated for both the FHWA recommended shear crack angle $\theta = 30°$ and the standard shear crack angle $\theta = 45°$. Clearly using the recommended angle of $\theta = 30°$ indicates an excessively large column shear strength, while using $\theta = 45°$ reduces the overestimation of the shear capacity. In both cases the specimen is shown to have sufficient shear capacity. The FHWA method does not reduce the shear capacity for displacement ductilities greater than four, therefore neglects the further degradation of the shear capacity. The Wehbe shear capacity, as shown in Fig. 4-39, reveals similar results to the CALTRANS method, although there is a sufficient shear capacity at $\mu_\Delta = 6$. However, the margin against shear failure is indicated to be very small.

A comparison among the three analysis methods reveals that the CALTRANS method provides the lowest estimated the shear capacity, while the FHWA method provides the highest estimated the shear capacity at $\theta = 30°$. The Wehbe method offers a reasonable alternative between the CALTRANS and FHWA methods. This analysis shows that the as-built specimen lacks a sufficient margin against shear failure, and should be retrofitted.

The shear capacity of specimens FRG and FRC, including the contribution of the jacket, was calculated at the predicted plastic hinge location of 533 mm (21 in). The shear capacity was determined using the methods described in the previous sections. However, the assumed jacket shear capacity was added to the column shear capacity. The jacket shear capacity was calculated using Eqn. 2-2. The measured jacket properties from Table 2-3 were used, except that the design strain of $\varepsilon_d = 6000\ \mu s$ was used rather than the ultimate strain. The jacket thickness in the plastic hinge region was used corresponding to 2.54 mm (0.10 in) for specimen FRG, and 1.02 mm (0.04 in) for specimen FRC. Figures 4-40 and 4-41 show the comparison of calculated shear capacity including jacket strength and the measured load-deflection curve for specimens FRG and FRC, respectively. These figures indicate that both FRP jackets provided more than sufficient shear capacity to the specimen.

4.5.5 Estimated Shear Capacity

The estimated shear capacity was calculated based on the measured strains in the specimen transverse bars and FRP jacket. In the analysis the measured strains from the final test event were compared with the strain capacity of the materials to determine a residual shear capacity of the components of specimen. The measured strains in the transverse bars were compared to the yield strain, while the measured strains in the FRP jackets were compared to their ultimate strain. The residual strain capacity was then converted into shear force capacity by multiplying by the respective Young's modulus and effective area of the materials.

The estimated shear capacity of the specimens was calculated, at 533 mm (21 in) from the footing. The estimated and calculated shear capacity of the specimens is compared in Table 4-8 calculated with a displacement ductility of $\mu_\Delta = 6$. All three methods of shear calculation were used with the result expressed as a ratio of estimated to calculated capacities. The ratios for all methods indicate the shear capacities calculated were very close to the estimated. In the table, the calculated shear capacity of specimen FRG was slightly overestimated, while specimen FRC was slightly underestimated. The good correlation in results is thought to be due to the conservative design of the FRP jackets. A design strain was used to calculate the required thickness, thus underestimating the actual jacket capacity. This underestimation of the capacity allowed a large estimated reserve strength in the jacket, leading to the results shown in Table 4-8. In general, as shown in Figs. 3-40 and 3-41 the FHWA method overestimates shear capacity, while the CALTRANS method underestimates shear capacity. These trends are not seen in Table 4-8 due to the large impact of the jacket in the estimated shear capacity.

4.6 Contribution of FRP Jacket

The composite jackets of specimens FRG and FRC considerably improved the dynamic response of the as-built column. The experimental response of the specimens indicates that the jackets were highly effective in increasing the ductility level and the shear capacity of the specimens. Some unwanted flexural enhancement occurred, but the resulting shear demand was resisted by the jacket. The FRP jacket contributed to the mechanics of the column failure. The response of the jacket was influenced by the: (1) thickness, (2) segmental design, and (3) flexural enhancement of the transverse fibers.

The FRP jackets increased the initial (pre-yield) stiffness by approximately 25 percent based on the load-deflection envelopes (Fig 3-45). The calculated low-amplitude stiffness base on the measured frequencies in snap back tests show even a higher gain in stiffness (Tables 3-1 to 3-3). The greater force capacity of specimen FRG compared to specimen FRC, indicates a small difference in response of the specimens which is thought to be due to the difference in thickness between the composite jackets.

In the experimental study, the columns failed without visible sign of spalling of concrete or shear crack development due to FRP jacket preventing this behavior. The only

damage witnessed was flexural cracks that propagated along the segmental connections of the jacket and the eventual rupture of the longitudinal bars. The jacket led to flexural cracking at the discontinuity between segments. The segmental jacket design allowed rigid body rotation between the composite straps as indicated in the measured curvature in Figs. 3-22 and 3-41. The plastic hinges occurred at the intersection of these segments in both specimens FRG and FRC, showing that the discontinuity of the jacket should be considered in the design. It is suggested that the desired failure elevation of the column be controlled through the location of the jacket gap. The gap should be located such that it is concurrent with the desired failure location, to encourage plastic hinge development at this elevation. Conversely if failure is not desired in a specific location, such as a lap splice region, vertical overlap of the jacket segments is suggested to delay failure in this region.

In the analysis, the jacket was considered to work in tension and not under compression. The tensile strength of composite materials is well known. However the compressive strength effects are usually neglected in uni-directional fiber composites. This is due to the expected micro-buckling of the fibers limiting the compressive strength[32]. A discussion of the micro-buckling of composite fibers within the jacket is beyond the scope of this study. The compressive strength of the composites were neglected in this study due to a combination of the small jacket thickness and the segmental jacket design. The small number of composite wraps and the reduced number of wraps within the plastic hinge region could not prevent the material from the micro- buckling behavior. The segmental design is believed to have limited the development of the fibers in the longitudinal column direction preventing a shell-like response from occurring. Potentially some compressive strength was present prior to cracking of the epoxy surface. Table 2-3 shows that the epoxy has significant compressive strength and tensile strength compared to concrete, which impacts the initial flexural stiffness and un-cracked column properties. However since the composite fibers were not reinforced from buckling and the jacket was highly segmented, their long-term effect was minimized and therefore not considered in this study.

Chapter 5

Summary and Conclusions

5.1 Summary

The primary objective of this study was to develop and experimentally validate a seismic retrofit system utilizing available advanced composite fabrics for non-prismatic reinforced concrete bridge columns. The design criteria included minimizing flexural enhancement while ensuring constructability. The emphasis of the design was to increase the shear capacity within an appropriate level of safety. The validation of the design was accomplished through experimentally testing two thirty percent scale specimens retrofitted with FRP jacketing on a shake table.

This study is the fourth and final portion of the series outlining the seismic response and retrofit of bridge columns with structural flares. In the first study, a nonlinear analysis of several highway bridges located in Reno, Nevada was undertaken identifying the columns in bridge I-1250 as being of low margin of safety against shear failure. Bridge I-1250 is a sixteen-span reinforced concrete box girder structure, supported by a total of 94 one-way flared columns. This bridge was constructed in 1980 prior to many of the reforms in seismic design. The second phase included cyclic static testing of two forty percent scale as-built specimens[37]. This study showed the possibility of flexure/shear failure forming in the prototype column was high, and recommended retrofit of the column. As part of the second phase of the study, two forty percent scale specimens retrofitted with a steel jacket were tested under static cyclic loads[5]. From this study it was determined that the steel jackets were effective in controlling shear cracking and reducing strains in the transverse steel.

The third and fourth phases of the study series considered only the columns with high longitudinal steel ratio because they were more vulnerable to shear failure. The loading system used was a state-of-the-art shake table at the University of Nevada, Reno Bridge Engineering Laboratory. Due to limitations of the shake table, the scale of the specimens was reduced to thirty percent. Note that even with thirty percent scaling the cross-sectional dimension of the specimens at the end of the flare was 711 mm by 356 mm (28 in by 14 in). In the third study[17], two thirty percent scale specimens, one as-built (FA) and the other steel jacketed (FR) were tested. The fourth and final phase was the study reported in this document testing two additional thirty percent scale specimens, one retrofitted with a glass fiber-epoxy jacket (FRG) and the other retrofitted with a carbon fiber-epoxy jacket (FRC).

The design of the FRP jackets considered the effects of the octagonal cross-section and non-prismatic column shape. Since the primary purpose of the jacket was to enhance the column shear capacity, the composite fabric, consisting of uni-directional fibers, had to be oriented perpendicular to the column axis. This was done to ensure the contribution of the fibers would only increase the shear capacity without substantially increasing the flexural capacity of the column. Additionally, in a manner similar to leaving a gap in the steel

jacket, a weak section in the FRP jacket was designed to force flexural failure at the elevation of the predicted plastic hinge elevation. The weak section was designed to minimize the increase in flexural capacity of the column by reducing the number of composite wraps.

The shake table tests were performed in the strong direction of the column under a constant axial load. The shake table motion represented the 1994 Northridge earthquake recorded at Sylmar Hospital, with the timescale modified to account for the scale of the specimens. The testing was completed in stages applying from 20 percent to 275 percent of the earthquake amplitude over the eleven test events. The measured data included lateral loads, displacements, curvatures, and strains as well as the general column behavior during the test. The measured response of specimens FRG and FRC were compared with the results from specimens FA and FR to draw conclusions about the effectiveness of different retrofit methods.

An extensive analytical study of the columns was also included using moment-curvature and non-linear response history analyses. The theoretical analysis also included comparison of different methods to calculate the shear capacity. In the analysis specimens FA and FR were included to allow comparison of all the retrofit methods.

5.2 Conclusions

The main general observations and conclusions derived from this study are outlined below:

1. The method of using composite straps with lapped connections that was developed in this study was an effective method for retrofitting of non-prismatic columns. The segmental jacket design provided a means of encasing the column without reducing the effectiveness of the wrap, thus providing enhanced shear strength and column core confinement.

2. The glass fiber-epoxy specimen (FRG) and carbon fiber-epoxy specimen (FRC) were installed in a very simple manner. The level of work required to install the jackets was much less than is required of steel jacketing. The FRP jackets can easily be installed in tight locations under a bridge and can be used on non-prismatic bridge columns.

3. The FRP jacketed columns provided a large increase in shear capacity and ductility compared to the as-built specimens. The estimated shear capacity of each specimen exceeded the demand by approximately sixty percent.

4. The comparison between calculated and estimated shear capacities shows good correlation between CALTRANS, FHWA and Wehbe methods when considering the design strain of the jacket. Using the ultimate strain of the jacket overestimates the capacity.

5. The analytical model underestimated the flexural strength by ten percent even after the effects of strain rate, variation in axial load, and the jacket contribution to flexural strength were included.

6. The fairly large increase in flexural strength witnessed in the steel jacketed specimen (FR) was also seen in the FRP jacketed specimens but to a lesser extent. The segmental design of the FRP jacket helped reduce the increase in flexural strength of the column.

7. The measured displacement ductility and drift between the four specimens showed a minimum of 36 percent increase in ductility for the FRP jacketed specimens; and a 25 percent increase in drift. The FRP jacketed specimens slightly outperformed the steel jacketed specimen in these categories.

8. The FRP jackets outperformed the steel jackets in most measured criteria, with the exception of the steel jacketed specimen having a large reserve shear capacity due to the required overdesign of the jacket thickness for constructability.

9. All three retrofit methods achieved the goal of improving the seismic response of the column by increasing the shear capacity.

5.3 Recommendations

Based on the testing and analysis performed in this study the following recommendations are made with respect to the FRP jacketed specimens:

1. The design strain of $\varepsilon_d = 0.006$ should be used for Fyfe LLC glass fiber-epoxy and carbon fiber-epoxy jacket systems, rather than the ultimate strain or some other arbitrary value.

2. The segmentation of the jacket should be designed such that it encourages flexural failure at the desired elevation. Conversely, if flexural failure is not desired at an elevation, vertical overlap of the jacket is necessary to delay the failure at the segmental height.

3. The design of the jacket thickness for shear enhancement should include both an over-strength factor applied to the shear demand and a strength reduction factor applied to the shear capacity.

4. The increase in flexural capacity of a FRP jacketed column is depends on the: (1) orientation of the uni-directional fibers, (2) material strength of the composite straps, and (3) the number of wraps applied to the column. A combination of these effects should be considered in the calculated stiffness and flexural capacity of the column.

References

1. American Association of State Highway and Transportation Officials, "Standard Specifications for Highway Bridges," 15th Ed, Washington, D.C., 1992.

2. American Concrete Institute, "Building Code Requirements for Structural Concrete (ACI 318-95) and Commentary (ACI 318R-95)," Farmington Hills, 1995.

3. American Society for Testing and Materials, "Annual Book of ASTM Standards," Philadelphia, 1997.

4. California Department of Transportation, "Memo to Designers, 20-4," Engineering Service Center, Earthquake Engineering Branch, November 1998.

5. Caywood, C., Saiidi, M. S., and Sanders, D. H., "Seismic Retrofit of Flared Bridge Columns with Steel Jackets," Report No. 98-2, CCEER. Department of Civil Engineering, University of Nevada, Reno, June 1998.

6. Feng, M., and Bahng, E., "Damage Assessment of Jacketed RC Columns Using Vibration Tests," Journal of Structural Engineering, ASCE, Vol. 1254, No. 3, pp. 265-271, March 1999.

7. Gergely, I., Pantelides, C.P., Nuismer, R.J. and Reaveley, L.D., "Bridge Pier Retrofit Using Fiber-Reinforced Plastic Composites," Journal of Composites for Construction, ASCE, Vol. 2, No. 4, pp. 165-174, November 1998.

8. Hawkins, G. F. , Patel, N. R., and Steckel, G. L., "Failure Analysis of Highway Bridge Column Composite Overwraps," Proceedings of First International Conference on Composites in Infrastructure, Tucson, Arizona, pp. 1126-1140, January 1996.

9. Hull, D., and Clyne, T. W., "An Introduction to Composite Materials," 2nd Ed., Cambridge University Press, 1996.

10. Jin, L., Saadatmanesh, H., and Ehsani, M.R., "Seismic Retrofit of Existing Reinforced Concrete Columns by Glass-Fiber Composites," Proceedings of the Third Materials Engineering Conference (Infrastructure: New Materials and Methods of Repair), San Diego, California, pp. 758-763, November 1994.

11. Kent, D. C., and Park, R., "Flexural Members with Confined Concrete," Proceedings of the American Society of Civil Engineers (A.S.C.E), Vol. 97, No. ST7, pp. 1969-1990, July 1971.

12. Laplace, P., "Shake Table Testing of Flexure Dominated Reinforced Concrete Bridge Columns," M.S.C.E. Thesis, Department of Civil Engineering, University of Nevada, Reno, August 1999.

13. MacGregor, J. G., "Reinforced Concrete: Mechanics and Design," Prentice Hall, 1997.

14. Mallick, P. K., "Fiber-Reinforced Composites: Material, Manufacturing, and Design," 2nd Ed., Marcel Dekker, 1993.

15. Mander, J.B., Priestley, M.J.N., and Park, R., "Theoretical Stress-Strain Model for Confined Concrete Columns," ASCE Journal of Structural Engineering, Vol. 114, No. 8, pp. 1804-1826, August 1988.

16. "Mathcad 8 User's Guide," MATHSOFT, INC., Cambridge, MA, 1998.

17. McElhaney, B., "Shake Table Testing of Flared Bridge Columns with Steel Jacket Retrofit," M.S.C.E Thesis, Department of Civil Engineering, University of Nevada, Reno, August 1999.

18. Mirmiran, A. and Shahawy, M., "Behavior of Concrete Columns Confined by Fiber Composites," Journal of Structural Engineering, ASCE, Vol. 123, No. 5, pp. 583-590, May 1997.

19. "1994 Northridge Earthquake: Performance and Structures, Lifelines, and Fire Protection Systems," United States Department of Commerce, National Institute of Standards and Technology, Special Publication 862, May 1994.

20. Park, R., and Paulay, T., "Reinforced Concrete Structures," John Wiley & Sons, New York, 1975.

21. Paulay, T., and Priestley, M.J.N., "Seismic Design of Reinforced Concrete and Masonry Buildings," John Wiley & Sons, 1992.

22. Preistley, M.J.N., Seible, F., and Calvi, G. M., "Seismic Design and Retrofit of Bridges," John Wiley & Sons, 1996.

23. Priestley, M.J.N., Seible, F., Verma, R., and Xiao, Y., "Seismic Shear Strength of Reinforced Concrete Columns," Report No. SSRP 93/06, Department of Applied Mechanics and Engineering Sciences, University of California, San Diego, July 1993.

24. Priestley, M.J.N., Seible, F., and Uang, C.M., "The Northridge Earthquake of January 17, 1994: Damage Analysis of Selected Bridges," Report No. SSRP-94/06, Department of Applied Mechanics and Engineering Sciences, University of California, San Diego, La Jolla, California, February 1994.

25. Saadatmanesh, H., Ehsani, M.R., and Li, M.W., "Strength and Ductility of Concrete Columns Externally Reinforced with Fiber Composite Straps," ACI Structural Journal, Vol. 91, No. 4, pp. 434-447, July-August 1994.

26. Saiidi, M., "Hysteresis Model for Reinforced Concrete," Journal of Structural Division, Proceedings of the American Society of Civil Engineers (A.S.C.E), Vol. 108, No. ST5, pp. 1077-1087, May 1982.

27. Samaan, M., Mirmiran, A., and Shahawy, M., "Model of Concrete Confined by Fiber Composites," Journal of Structural Engineering, ASCE , Vol. 124, No. 9, pp. 1025-1031, September 1998.

28. Sanchez, A.V., Seible, F., and Priestley, M.J.N., "Solutions to Seismic Performance Problems of Flared Bridge Columns," Proceedings of the Second Symposium on Practical Solutions for Bridge Strengthening and Rehabilitation, The National Science Foundation, Kansas City, Missouri, pp. 93-102, March 24-25, 1997.

29. Seible F., and Priestley, M. J., "Retrofit of Rectangular Flexural Columns with Composite Fiber Jackets," Proceedings of the Second Annual Seismic Research Workshop, Sacramento, California, March 1993.

30. Seible, F., Priestley, M.J.N., Hegemier, G.A., and Innamorato, D., "Seismic Retrofit of RC Columns with Continuous Carbon Fiber Jackets," Journal of Composites for Construction, ASCE ,Vol. 1, No. 2, pp.52-62, May 1997.

31. "Spect", Computer Software (PC-Dos), Earthquake Engineering Class Notes (CE 679), University of Nevada, Reno, Instructor: R. Siddharthan, April 1998.

32. Swanson, S. R., "Design Methodology and Practices" Composites Engineering Handbook, Ed. P. K. Mallick, Marcel Dekker, pp. 1183-1206,1997.

33. "The Northridge Earthquake, January 17,1994 – Preliminary Reconnaissance Report," Earthquake Engineering Research Institute, Oakland, California, March 1994.

34. "The Continuing Challenge: The Northridge Earthquake of January 17, 1994," Report to the Director by Seismic Advisory Board, California Department of Transportation, October 1994.

35. U.S. Department of Transportation, "Seismic Retrofitting Manual for Highway Bridges," Federal Highway Administration, Pub. No. FHWA-RD-94-052, May 1995.

36. Wehbe N., and Saiidi, M.S., "Effects of Confined Core on Seismic Vulnerability of Reinforced Concrete Column with Structural Flares," ACI Special Publication (SP-187), Seismic Response of Concrete Bridges, 1998.

37. Wehbe, N.I, Saiidi, M.S., and Sanders, D. H., "Effects of Confinement and Flares on the Seismic Performance of Reinforced Concrete Bridge Columns," Report No. 97-2, CCEER. Department of Civil Engineering, University of Nevada, Reno, September 1997.

38. Wehbe, N. I., Saiidi, M., and Sanders, D. H., "Seismic Performance of Rectangular Bridge Columns with Moderate Confinement," ACI Structural Journal, Vol. 95, No. 2, March-April 1998.

39. Xiao, Y., Wu, H., and Martin, G.R., "Prefabricated Composite Jacketing of RC Columns for Enhanced Shear Strength," Journal of Structural Engineering, ASCE, Vol. 125, No. 3, pp. 255-264, March 1999.

TABLES

Table 2 - 1 Measured Tensile Strength of Steel Reinforcement

Bar Size	Yield Strain	Yield Stress MPa (ksi)	Ultimate Strain	Ultimate Stress MPa (ksi)
9.5 mm (#3)	0.00231	462 (67.0)	0.14	696 (101.0)
12.7 mm (#4)	0.00231	462 (67.0)	0.15	682 (99.0)
22.2 mm (#7)	0.00213	426 (61.7)	0.13	655 (95.0)
25.4 mm (#8)	0.00207	414 (60.0)	0.14	696 (101.0)
7 Gauge Wire 4.5 mm (.177 in)	0.00212	417 (60.5)	0.14	517 (75.0)

Table 2 - 2 Measured Concrete Compressive Strength

Footing

	Date	Sample #1	Sample #2	Sample #3	Average
7 Day	7/3/98	30.3 MPa (4400 psi)	29.5 MPa (4290 psi)	30.2 MPa (4390 psi)	30.0 MPa (4360 psi)
28 Day	7/24/98	35.1 MPa (5102 psi)	34.3 MPa (4980 psi)	36.0 MPa (5220 psi)	35.1 MPa (5100 psi)
Test 1	12/23/98	44.6 MPa (6472 psi)	43.9 MPa (6366 psi)	44.2 MPa (6420 psi)	44.2 MPa (6420 psi)

Note: Footing was poured on 6/26/98. Requested Properties were 6000 psi, 3/4" Aggregate.

Column

	Date	Sample #1	Sample #2	Sample #3	Average
7 Day	7/3/98	33.1 MPa (4810 psi)	30.9 MPa (4490 psi)	34.9 MPa (5075 psi)	33.0 MPa (4791 psi)
28 Day	7/24/98	45.4 MPa (6590 psi)	44.7 MPa (6490 psi)	44.8 MPa (6500 psi)	44.9 MPa (6526 psi)
Test 1	12/23/98	45.9 MPa (6666 psi)	49.6 MPa (7193 psi)	48.5 MPa (7039 psi)	48.0 MPa (6966 psi)
Test 2	1/7/99	48..5 MPa (7038 psi)	48.6 MPa (7056 psi)	46.5 MPa (6755 psi)	47.9 MPa (6950 psi)

Note: Column was poured on 8/3/98. Requested Properties were 6500 psi, 3/8" Aggregate.

Table 2 - 3 Composite Retrofit Measured and Specified Properties

	Fiberglass Epoxy**		
	Design****	Specified	Measured *
Tensile Modulus	20.7 GPa (3000 ksi)	27.6 GPa (4000 ksi)	24.3 Gpa (3520 ksi)
Ultimate Strain	0.60%	2.00%	2.09%
Ultimate Tensile Strength	124.0 MPa (18.0 ksi)	551.6 MPa (80.0 ksi)	521.4 MPa (75.62 ksi)
Strength at 90°	------	34.5 MPa (5.0 ksi)	------
Design Thickness	------	1.29 mm (.051 in)	------
Primary Fiber	------	E-Glass	------

	Carbon Fiber Epoxy***		
	Design****	Specified	Measured *
Tensile Modulus	65.5 Gpa 9500 ksi	68.9 Gpa (10000 ksi)	59.2 Gpa (8590 ksi)
Ultimate Strain	0.60%	1.00%	0.82%
Ultimate Tensile Strength	393.0 MPa (57.0 ksi)	689.5 MPa (100.0 ksi)	502.8 MPa (72.9 ksi)
Strength at 90°	------	34.5 MPa (5.0 ksi)	------
Design Thickness	------	1.04 mm (.041 in)	------
Primary Fiber	------	Carbon	------

	Cured Epoxy Matrix
	Specified
Tensile Strength	65.5 MPa (9.5 ksi)
Compressive Strength	241.3 MPa (35 ksi)
Flexural Strength	72.4 MPa (10.5 ksi)
Flexural Modulus	2.6 Gpa (375 ksi)
Bond Strength	21.4 MPa (3.1 ksi)

* Measured Properties in accordance with ASTM D3039

** TYFO® Fibrwrap® System (SEH-51). Uni-directional Fiberglass-Epoxy employing high-strength fibers in an epoxy matrix.

*** TYFO® Fibrwrap® System (SCH-51). Uni-directional Carbon Fiber-Epoxy employing high-strength fibers in an epoxy matrix.

**** Design Properties based on Caltrans Memo to Designers, and Federal Highway Specifications.

Table 2 - 4 Specimen FRG Test Event Schedule

Run Number	Motion	Comments/Purpose
1	Quick Release	Measure Frequency/Damping
2	0.2 x Slymar	Tuning Aquisition System
3	0.4 x Slymar	Column Yield
4	Quick Release	Measure Frequency/Damping
5	0.75 x Slymar	----------
6	1.0 x Slymar	----------
7	1.25 x Slymar	----------
8	1.5 x Slymar	----------
9	Quick Release	Measure Frequency/Damping
10	1.75 x Slymar	----------
11	2.0 x Slymar	----------
12	2.25 x Slymar	----------
13	2.5 x Slymar	----------
14	2.75 x Slymar	----------

Table 2 - 5 Specimen FRC Test Event Schedule

Run Number	Motion	Comments/Purpose
1	Quick Release	Measure Frequency/Damping
2	0.2 x Slymar	Tuning Aquisition System
3	0.4 x Slymar	Column Yield
4	Quick Release	Measure Frequency/Damping
5	0.75 x Slymar	----------
6	1.0 x Slymar	----------
7	1.25 x Slymar	----------
8	1.5 x Slymar	----------
9	Quick Release	Measure Frequency/Damping
10	1.75 x Slymar	----------
11	2.0 x Slymar	----------
12	2.25 x Slymar	----------
13	2.5 x Slymar	----------
14	2.0 x Slymar	----------

Table 3 - 1 Measured Dynamic Properties from Snapback Testing
30% Scale Specimens

Snapback 1

	Specimen			
	FA	FR	FRG	FRC
Period (sec)	0.40	0.20	0.25	0.25
Frequency (Hz)	2.50	5.00	3.93	4.07
Stiffness Kn/mm (k/in)	11.4 (64.9)	45.5 (259.5)	28.0 (160.3)	30.0 (171.7)
Damping (%)	-------	-------	1.34	1.33

Snapback 2

	Specimen			
	FA	FR	FRG	FRC
Period (sec)	0.50	0.30	0.26	0.28
Frequency (Hz)	2.00	3.33	3.80	3.60
Stiffness Kn/mm (k/in)	7.3 (41.5)	20.2 (115.3)	26.3 (149.9)	23.6 (134.5)
Damping (%)	-------	-------	3.54	3.09

Snapback 3

	Specimen			
	FA	FR	FRG	FRC
Period (sec)	0.50	0.50	0.43	0.44
Frequency (Hz)	2.00	2.00	2.33	2.27
Stiffness Kn/mm (k/in)	7.3 (41.5)	7.3 (41.5)	9.9 (56.3)	9.3 (53.3)
Damping (%)	-------	-------	3.83	3.30

Note: Data for specimens FA and FR are taken from previous study which did not include calculation of damping.

Table 3 - 2 Measured Dynamic Properties from Hysteresis Specimen FRG

Event		Stiffness KN/mm (Kip/in)	Natural Frequency Hz	Natural Period sec.
-------	Snapback 1	28.0 (160.3)	3.93	0.25
1	0.2 x Sylmar	17.9 (102.0)	3.14	0.32
2	0.4 x Sylmar	12.5 (71.2)	2.62	0.38
-------	Snapback 2	26.3 (149.9)	3.80	0.26
3	0.75 x Sylmar	8.7 (49.5)	2.18	0.46
4	1.0 x Sylmar	7.6 (43.6)	2.05	0.49
5	1.25 x Sylmar	4.9 (28.0)	1.64	0.61
6	1.5 x Sylmar	3.5 (20.3)	1.40	0.71
-------	Snapback 3	9.9 (56.3)	2.33	0.43
7	1.75 x Sylmar	3.1 (17.9)	1.31	0.76
8	2.0 x Sylmar	2.6 (14.7)	1.19	0.84
9	2.25 x Sylmar	2.4 (13.5)	1.14	0.88
10	2.5 x Sylmar	2.2 (12.3)	1.09	0.92

Table 3 - 3 Measured Dynamic Properties from Hysteresis Specimen FRC

Event		Stiffness KN/mm (Kip/in)	Natural Frequency (Hz)	Natural Period (sec)
------	Snapback 1	30.0 (171.7)	4.067	0.25
1	0.2 x Sylmar	18.1 (103.6)	3.16	0.32
2	0.4 x Sylmar	12.5 (71.3)	2.62	0.38
------	Snapback 2	23.6 (134.5)	3.6	0.28
3	0.75 x Sylmar	8.7 (49.5)	2.18	0.46
4	1.0 x Sylmar	7.2 (41.0)	1.99	0.50
5	1.25 x Sylmar	4.3. (24.4)	1.53	0.65
6	1.5 x Sylmar	4.3 (24.8)	1.55	0.65
------	Snapback 3	9.3 (53.3)	2.267	0.44
7	1.75 x Sylmar	3.2 (18.5)	1.34	0.75
8	2.0 x Sylmar	2.5 (14.5)	1.18	0.85
9	2.25 x Sylmar	2.3 (13.3)	1.13	0.88
10	2.5 x Sylmar	2.2 (12.3)	1.09	0.92

Table 4 - 1 Comparison of Measured and Design Peak Axial Force (Specimen FRG)

Event	Maximum Axial Force (kN)	Ratio of Maximum Axial Force to Design Axial Force	Minimum Axial Force (kN)	Ratio of Minimum Axial Force to Design Axial Force
1	288.7	1.01	274.4	0.96
2	309.6	1.09	272.4	0.96
3	363.0	1.28	242.4	0.85
4	385.7	1.36	239.1	0.84
5	431.0	1.51	226.4	0.80
6	485.7	1.71	223.8	0.79
7	503.1	1.77	231.0	0.81
8	507.5	1.78	237.4	0.83
9	519.1	1.82	239.1	0.84
10	520.4	1.83	242.1	0.85
11	604.5	2.12	161.3	0.57

Table 4 - 2 Comparison of Measured and Design Peak Axial Force (Specimen FRC)

Event	Maximum Axial Force (kN)	Ratio of Maximum Axial Force to Design Axial Force	Minimum Axial Force (kN)	Ratio of Minimum Axial Force to Design Axial Force
1	295.8	1.04	284.5	1.00
2	322.1	1.13	273.8	0.96
3	377.7	1.33	240.2	0.84
4	401.7	1.41	232.9	0.82
5	451.5	1.59	217.0	0.76
6	498.2	1.75	214.0	0.75
7	511.1	1.80	220.2	0.77
8	520.9	1.83	224.4	0.79
9	523.1	1.84	233.6	0.82
10	536.5	1.88	231.9	0.81
11	488.0	1.71	250.9	0.88

Table 4 - 3 Calculated Displacement Components for Specimens (FRG and FRC)

Specimen FRG

	Calculated Deflection (mm)			
Load (kN)	Flexural	Shear	Bond Slip	Total
177.9	8.1	2.5	1.0	11.6
284.7	42.9	4.0	2.8	49.8
293.6	67.9	4.2	2.9	75.0

Specimen FRC

	Calculated Deflection (mm)			
Load (kN)	Flexural	Shear	Bond Slip	Total
177.9	8.0	2.5	1.0	11.5
284.7	45.5	4.0	2.8	52.4
293.6	79.3	4.2	2.9	86.4

Table 4 - 4 Comparison of Measured and Calculated Yield Displacements

Column Specimen	Measured Yield Displacement (mm)	Calculated Yield Displacement (mm)	Ratio of Calculated to Measured
As-built (FA)	25.40	23.48	0.92
Steel Jacketed (FR)	24.13	24.92	1.03
Fiberglass-Epoxy (FRG)	23.37	17.82	0.76
Carbon Fiber-Epoxy (FRC)	22.10	17.83	0.81

Table 4 - 5 Comparison of Measured and Calculated Yield Forces

Column Specimen	Measured Yield Force (kN)	Calculated Yield Force (kN)	Ratio of Calculated to Measured
As-built (FA)	230.20	218.70	0.95
Steel Jacketed (FR)	325.40	262.00	0.81
Fiberglass-Epoxy (FRG)	310.10	275.60	0.89
Carbon Fiber-Epoxy (FRC)	300.00	273.40	0.91

Table 4 - 6 Comparison of Measured Displacement Ductility

Column Specimen	Yield Displacement (mm)	Ultimate Displacement (mm)	Displacement Ductility
As-built (FA)	25.40	137.92	5.4
Steel Jacketed (FR)	24.13	167.13	6.9
Fiberglass-Epoxy (FRG)	23.37	172.97	7.4
Carbon Fiber-Epoxy (FRC)	22.10	173.74	7.9

Table 4 - 7 Comparison of Measured Drift Percent

Column Specimen	Column Height (mm)	Ultimate Displacement (mm)	Drift %
As-built (FA)	1778.0	137.92	7.8
Steel Jacketed (FR)	1778.0	167.13	9.4
Fiberglass-Epoxy (FRG)	1778.0	172.97	9.7
Carbon Fiber-Epoxy (FRC)	1778.0	173.74	9.8

Table 4 - 8 Comparison of Estimated and Calculated Shear Capacities

	Ratio of Estimated to Calculated Shear Capacity# at μ_Δ - 6		
	CALTRANS Method	FHWA Method	Wehbe Method
FRC	1.04	1.03	1.04
FRG	0.93	0.94	0.94

FIGURES

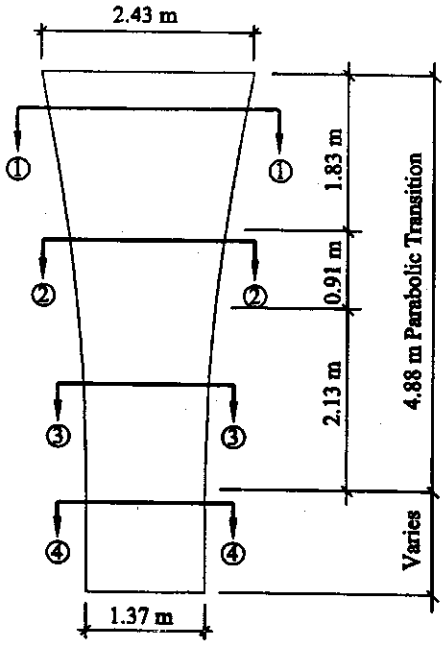

Figure 2 - 1 Elevation of Prototype Bridge Column

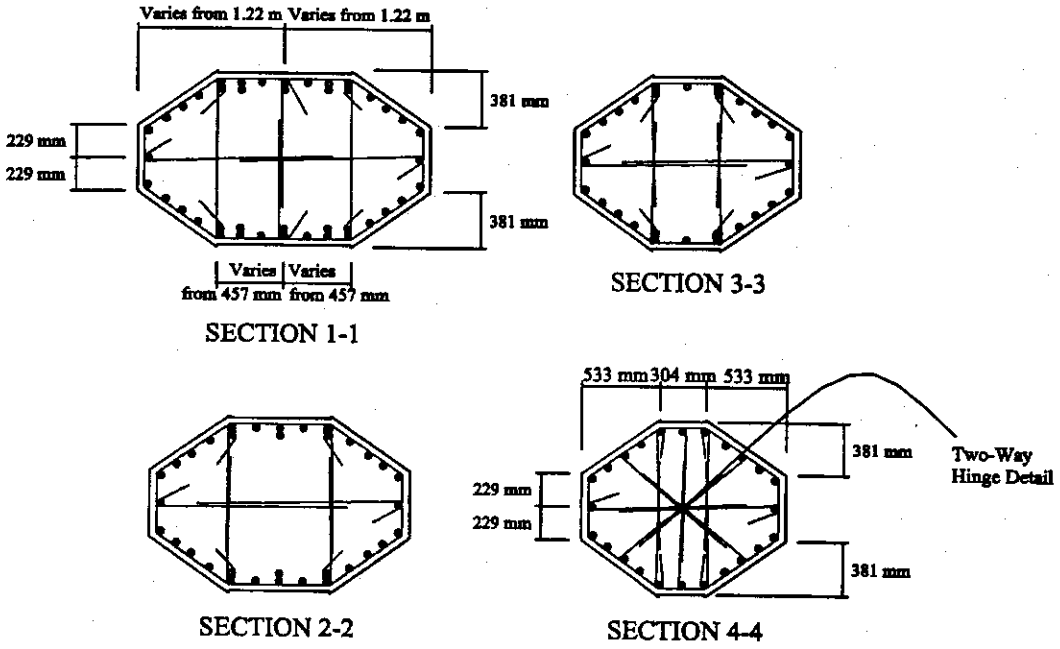

Note: Longitudinal bars are 36 mm (#11), Transverse ties are 13 mm (#4) at 102 mm (4 in) spacing.

Figure 2 - 2 Typical Cross-Section of Prototype Column

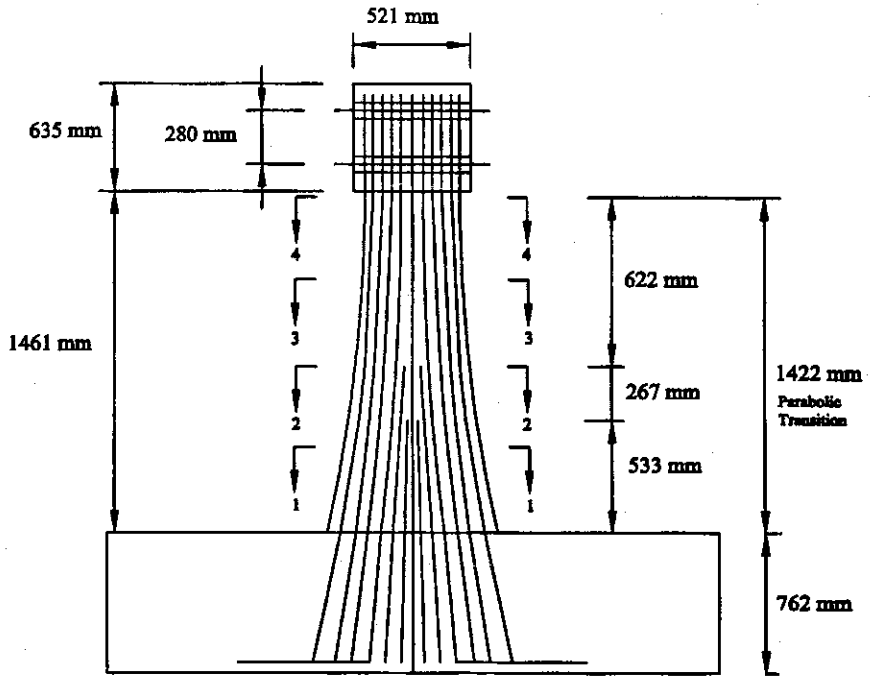

Figure 2 - 3 Elevation of Thirty Percent Scale Test Specimen

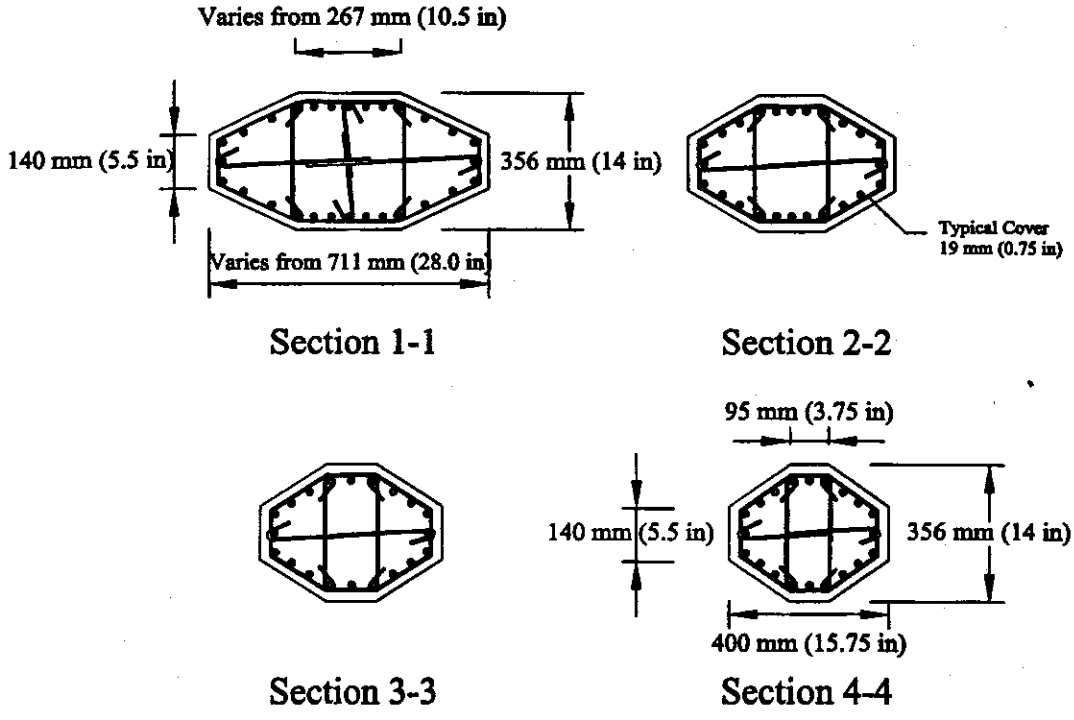

Figure 2 - 4 Typical Cross-Section of Thirty Percent Scale Test Specimen

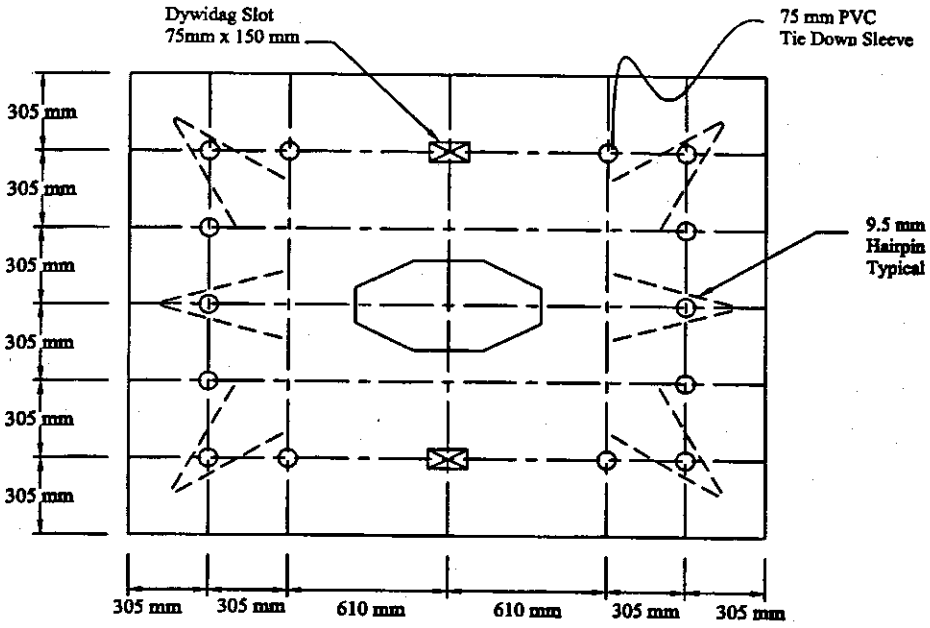

Figure 2 - 5 Plan View of Test Specimen Footing

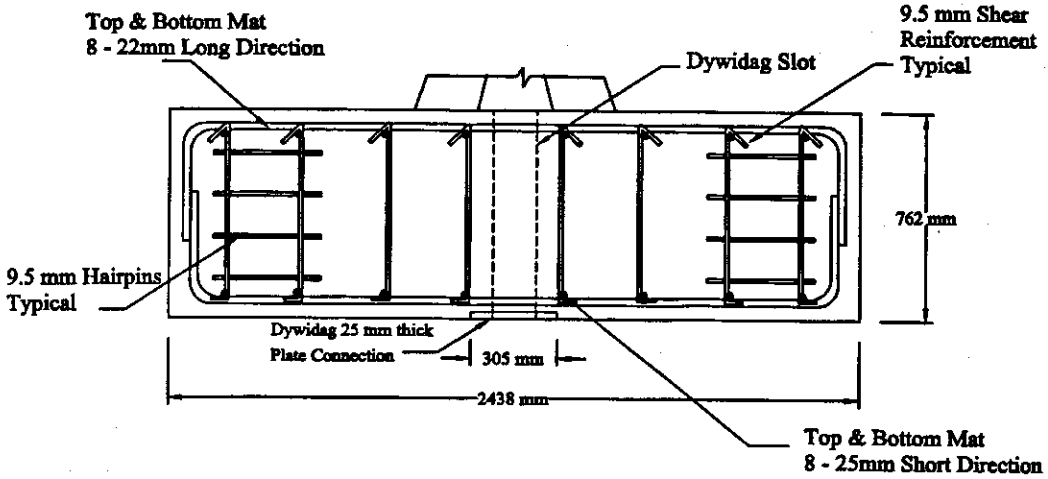

Figure 2 - 6 Elevation of Test Specimen Footing

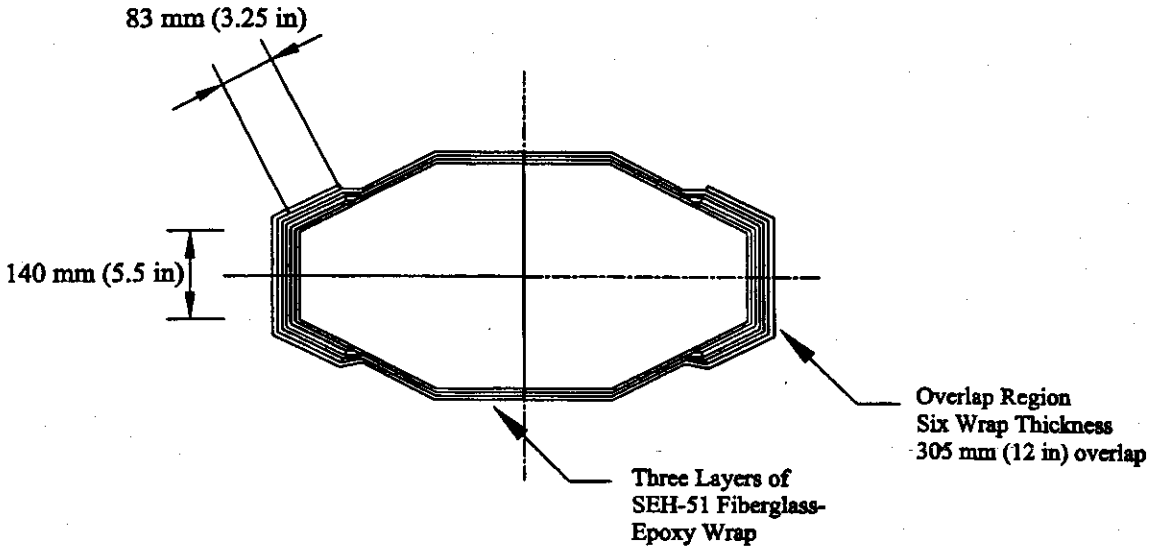

Figure 2 - 7 Typical FRG Jacketed Test Specimen Cross-Section

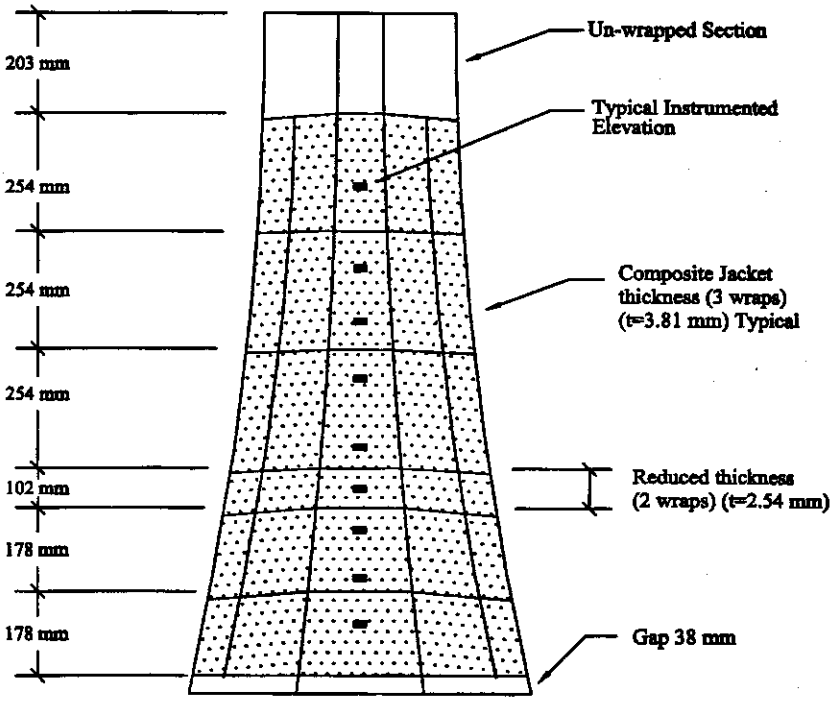

Figure 2 - 8 Elevation of FRG Jacketed Test Specimen

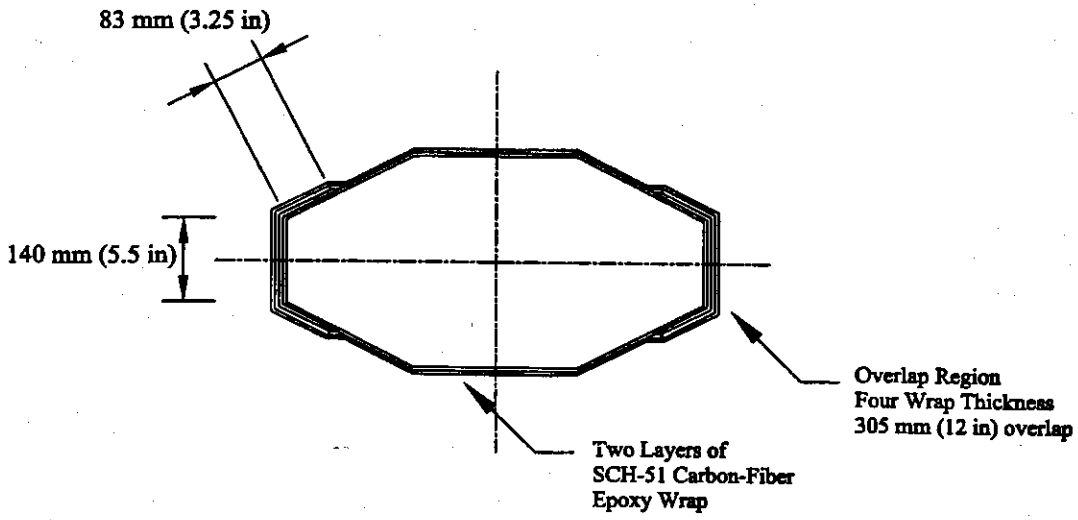

Figure 2 - 9 Typical FRC Jacketed Test Specimen Cross-Section

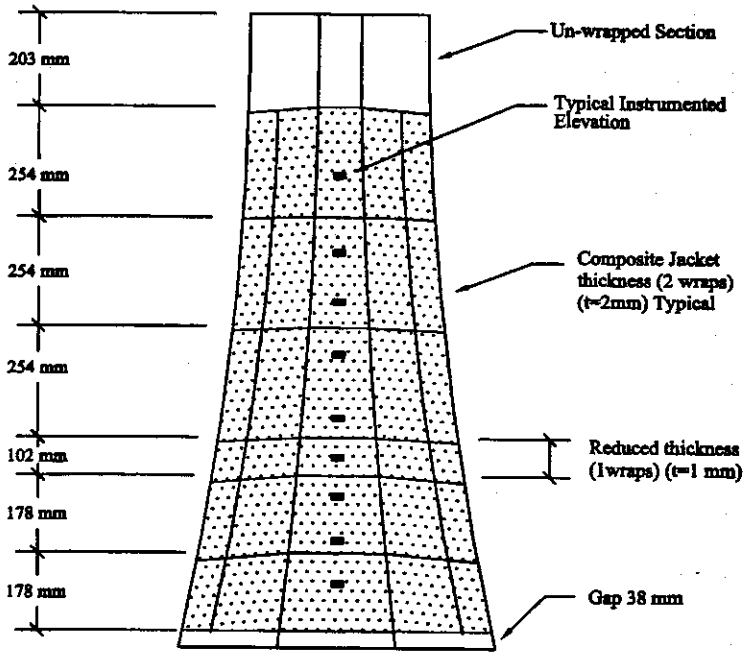

Figure 2 - 10 Elevation of FRC Jacketed Test Specimen

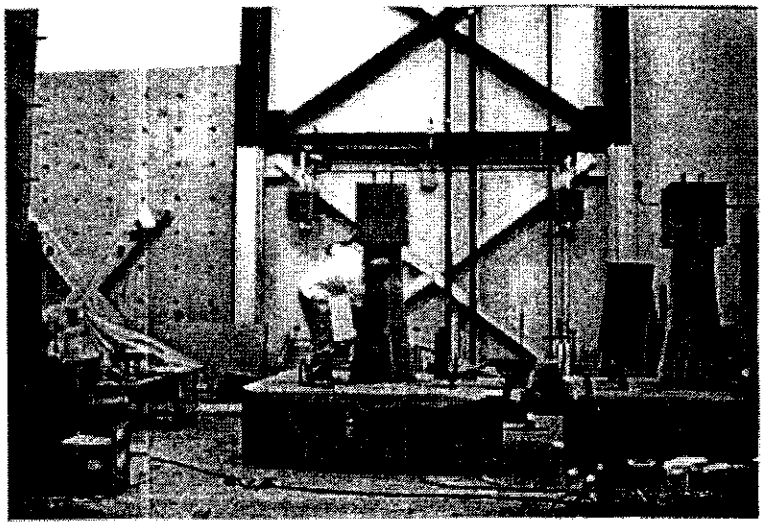

Figure 2 - 11 Column Surface Preparation

Figure 2 - 12 Composite Fabric Installation

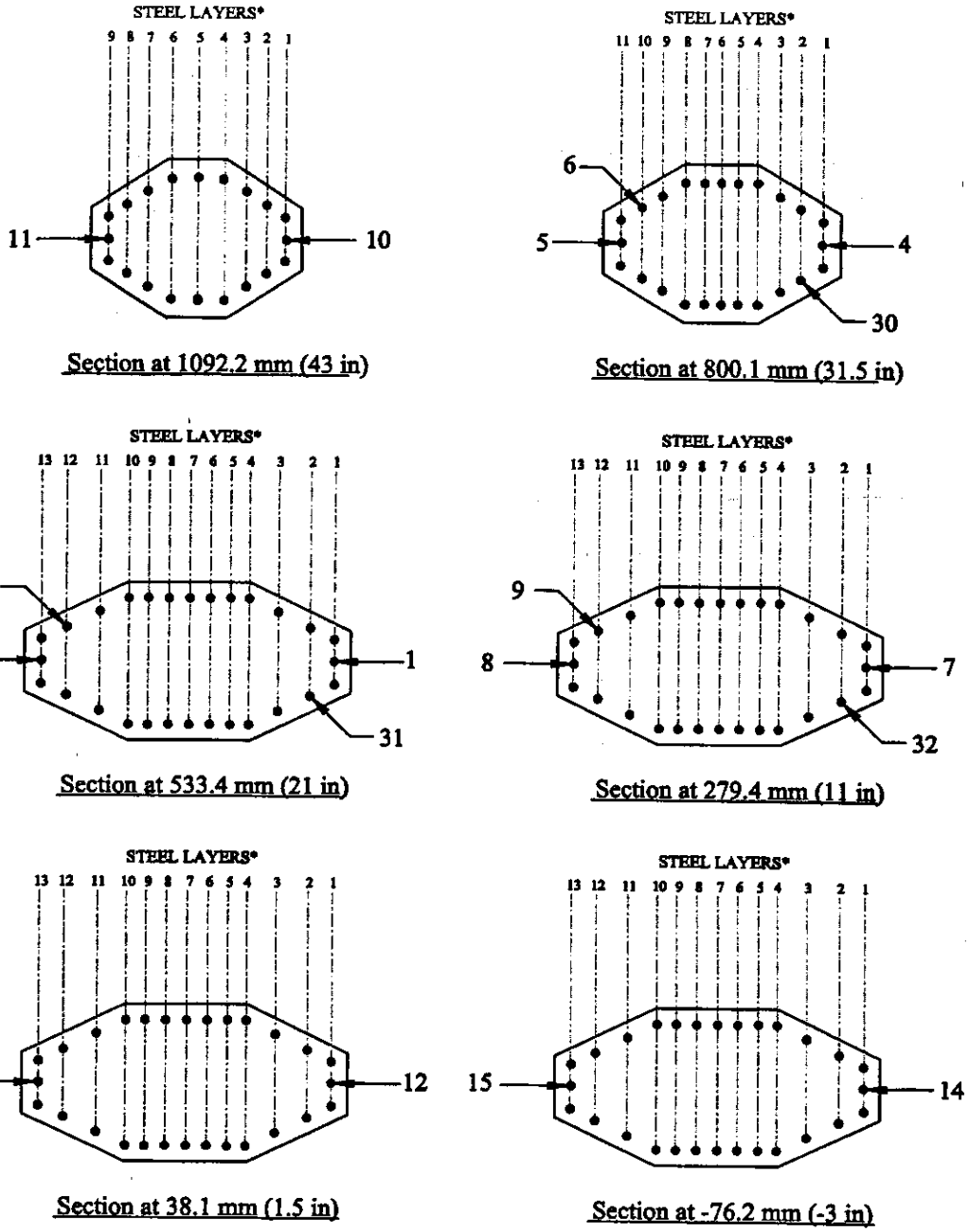

*Note: Steel layer #1 coincides with the side of the test specimen closest to the mass rig as shown in the test setup figures. Previous reports indicated layer #1 was in the pull direction, and the highest number layer was in the push direction.

Figure 2 - 13 Strain Gage Locations on Longitudinal Rebar

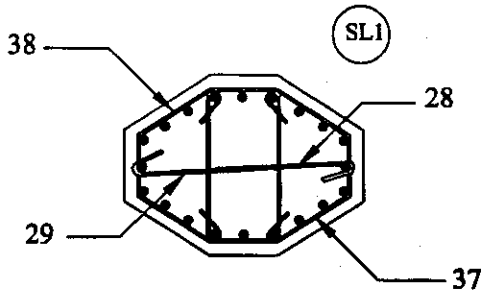

Section at 1092.2 mm (43 in)

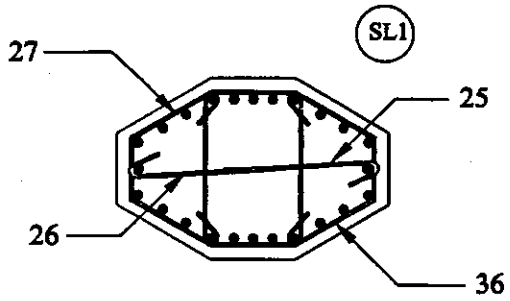

Section at 800.1 mm (31.5 in)

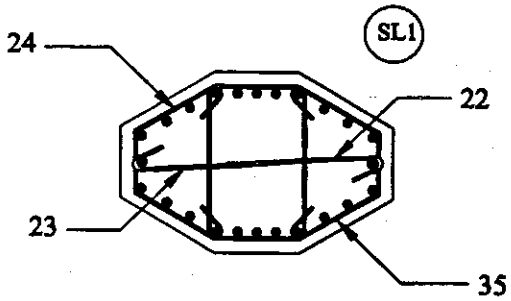

Section at 660.4 mm (26 in)

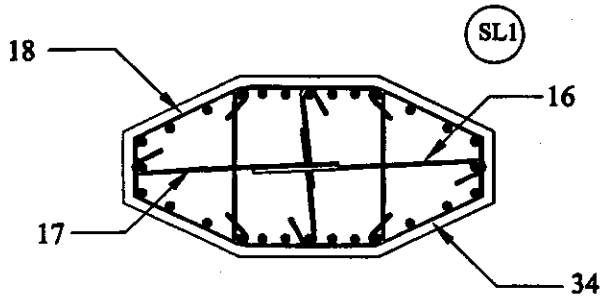

Section at 533.4 mm (21 in)

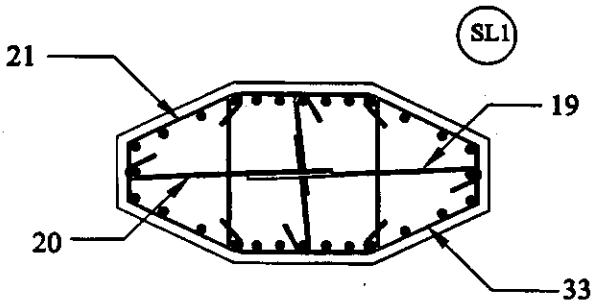

Section at 279.4 mm (11 in)

Note: SL1 refers to the first layer of steel as shown in the longitudinal rebar strain gage locations. The first steel layer coincides with the side of the test specimen closest to the mass rig as shown in the test setup figures.

Figure 2 - 14 Tranverse Steel Strain Gage Locations for Specimens FRG and FRC

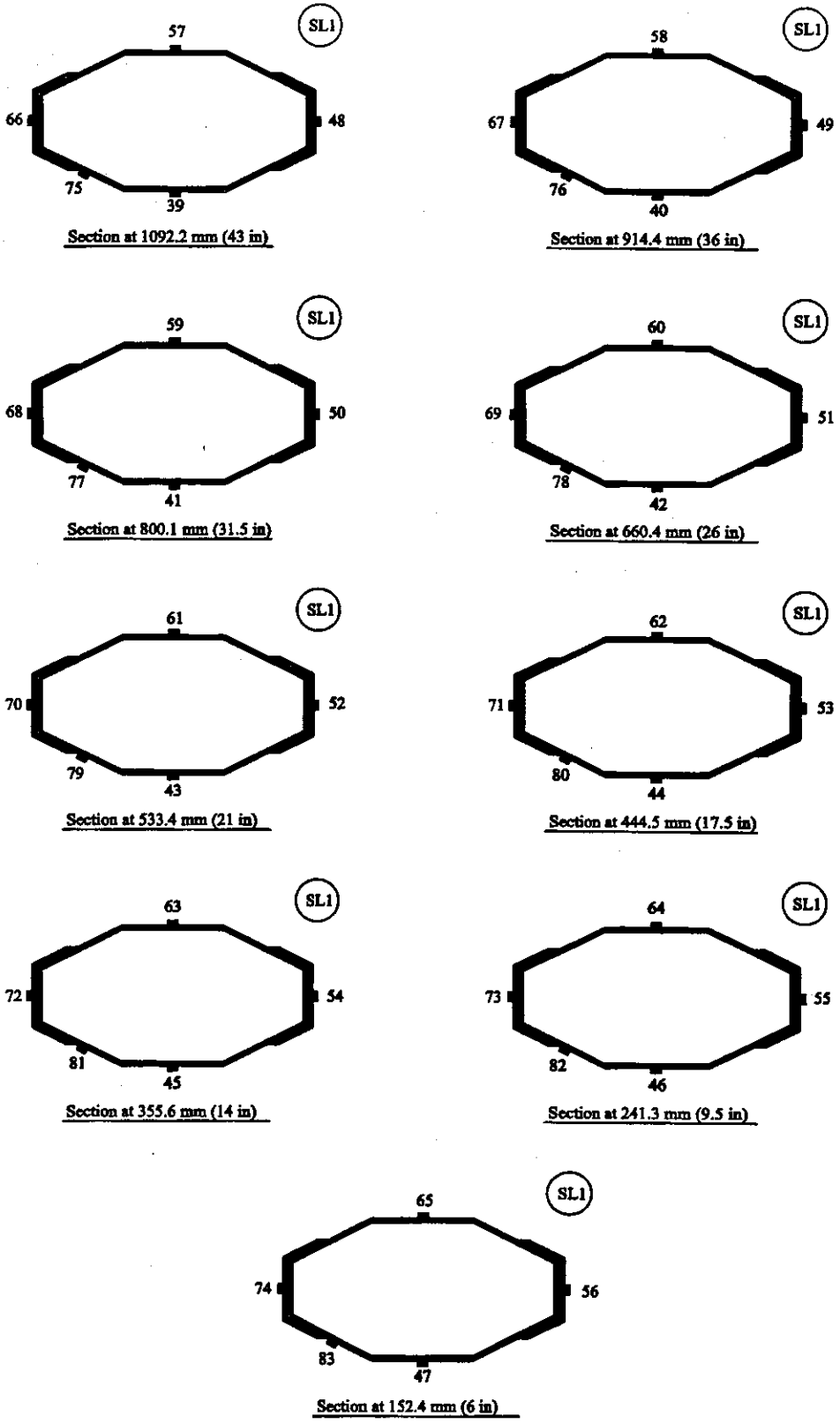

Figure 2 - 15 Composite Jacket Strain Gage Locations Specimen FRG and FRC

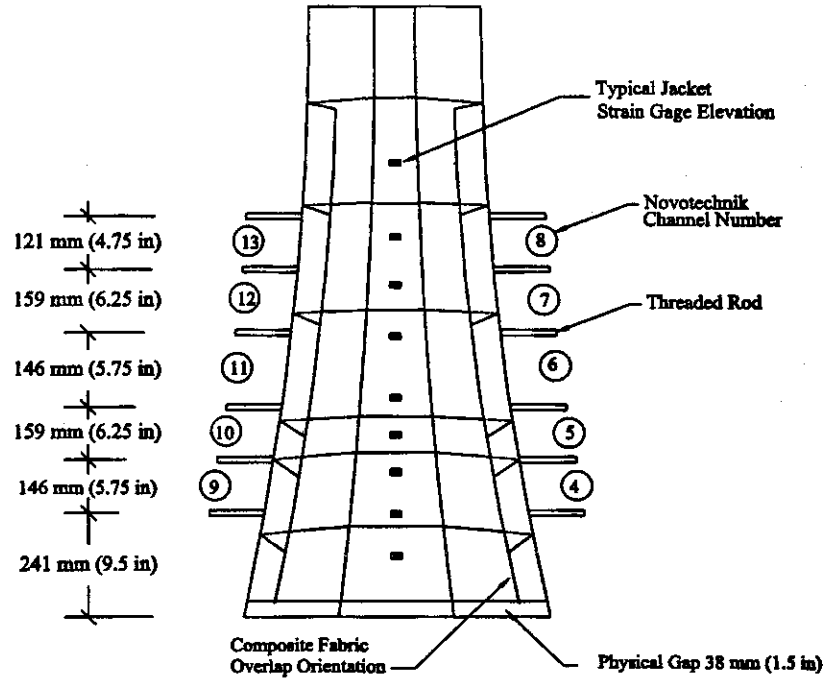

Figure 2 - 16 Novotechnick Transducer Locations Specimens FRG and FRC

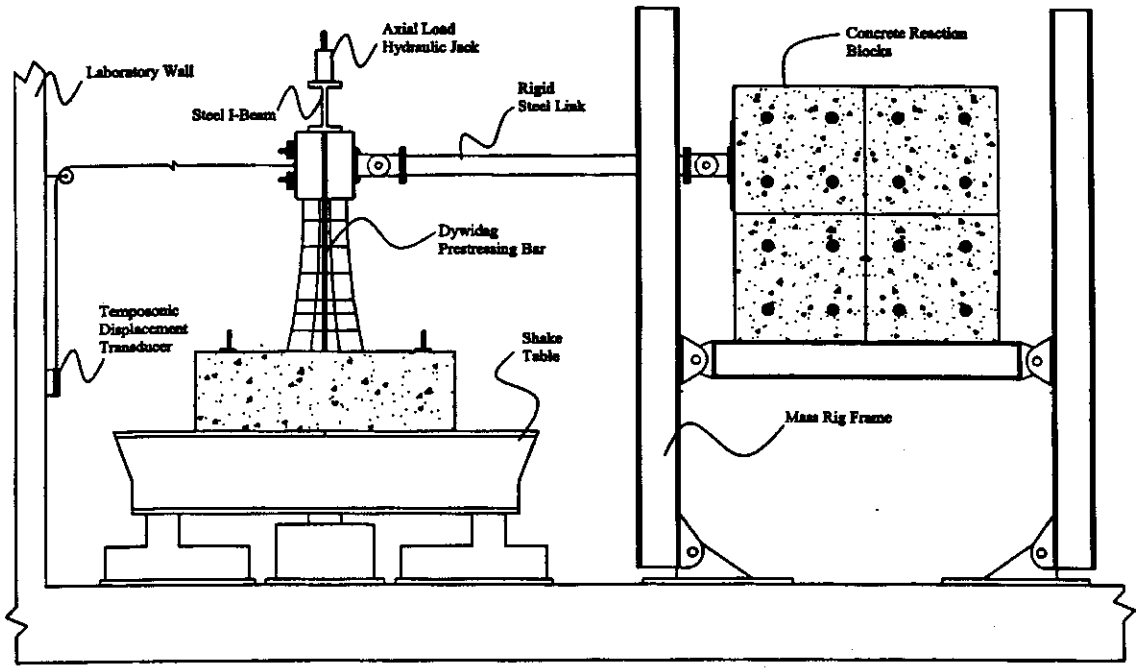

Figure 2 - 17 Shake Table Test Setup

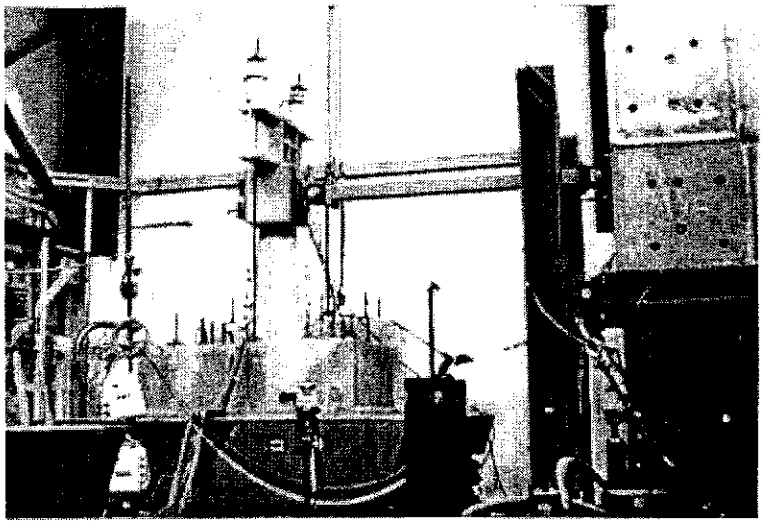

Figure 2 - 18 Test Setup

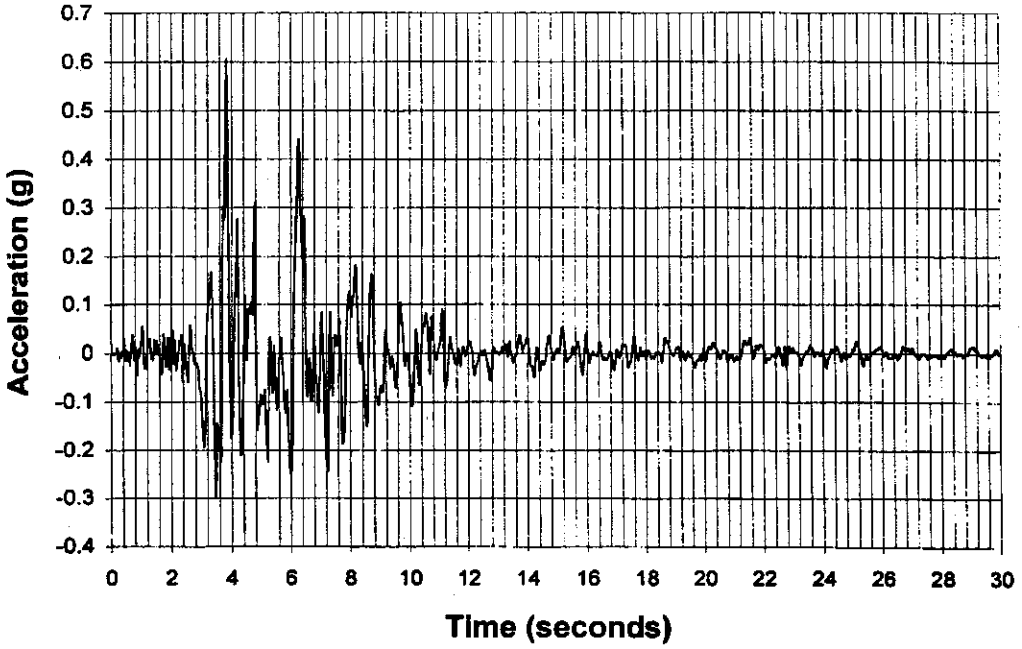

Figure 3 - 1 Strong Motion Accelerogram from 1994 Northridge Earthquake Measured at Sylmar Hospital

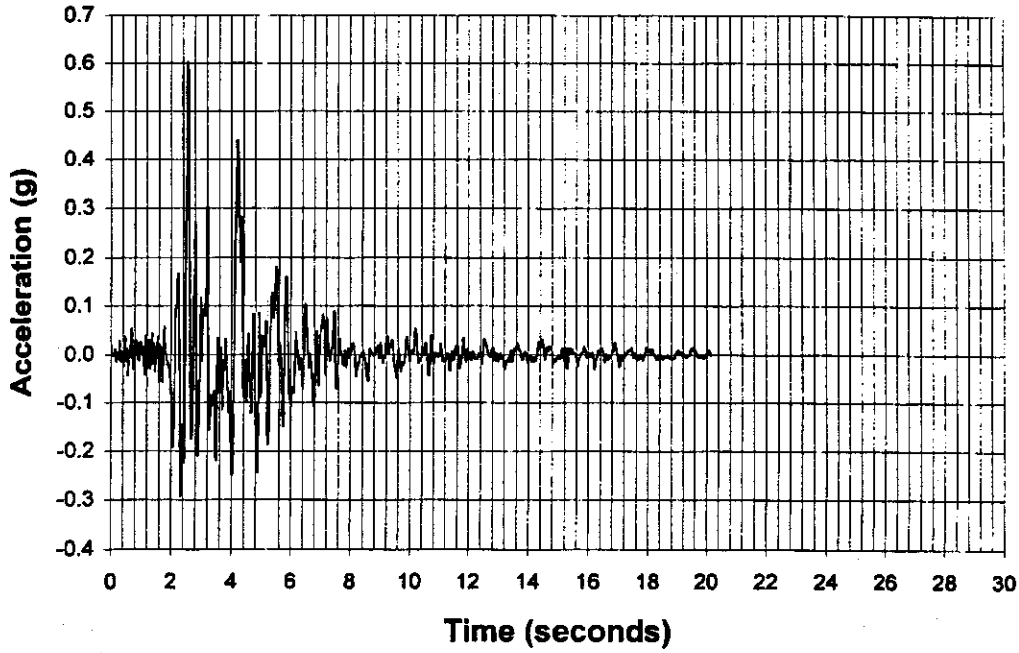

Figure 3 - 2 Shake Table Input Accelerogram of 1994 Northridge Earthquake (Sylmar Record)

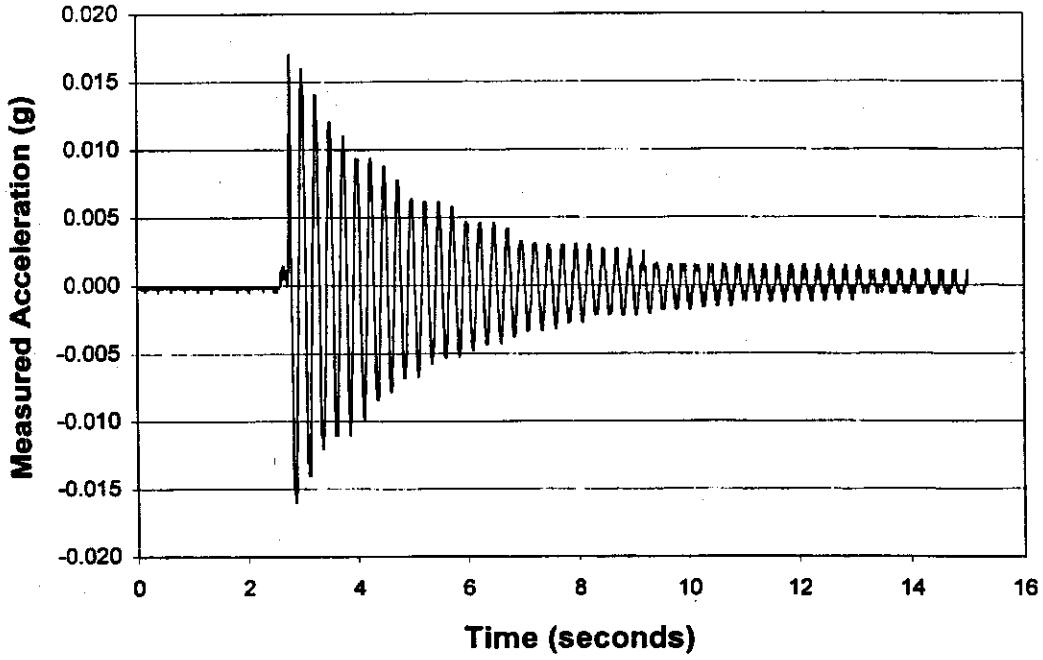

Figure 3 - 3 Typical Measured Acceleration from Snapback Test

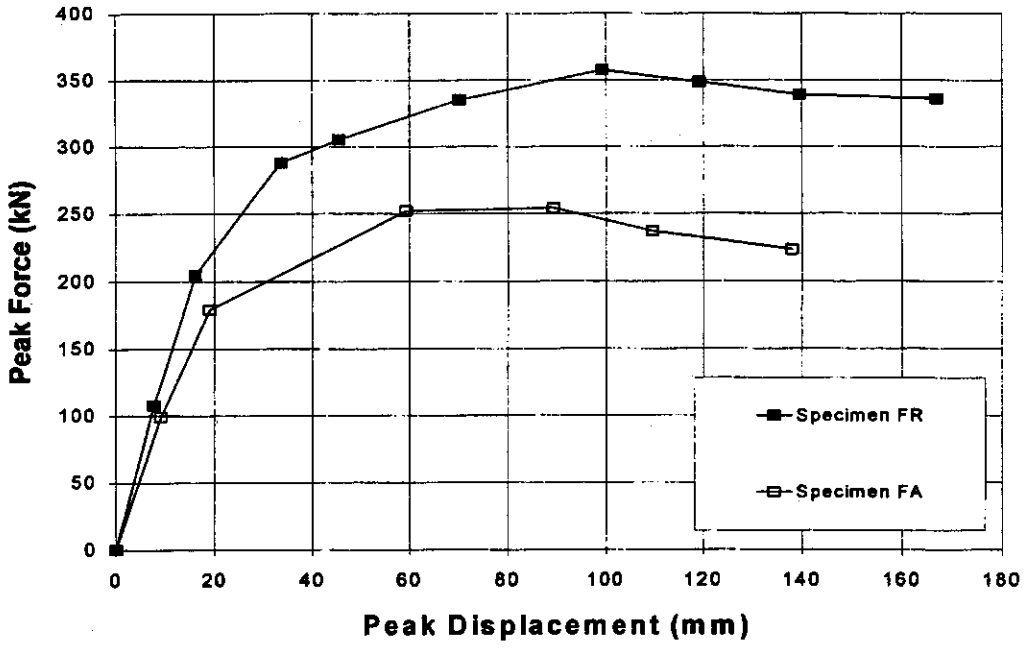

Figure 3 - 4 Peak Force vs. Peak Displacement Envelopes for Specimens FA and FR

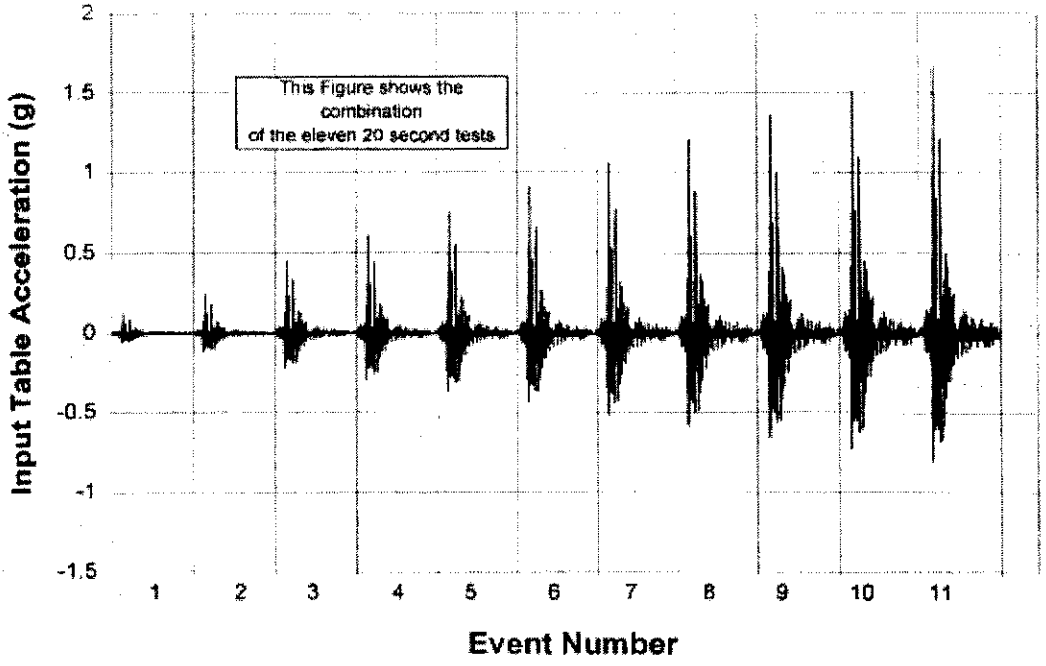

Figure 3 - 5 Shake Table Combined Event Input Acceleration Specimen FRG

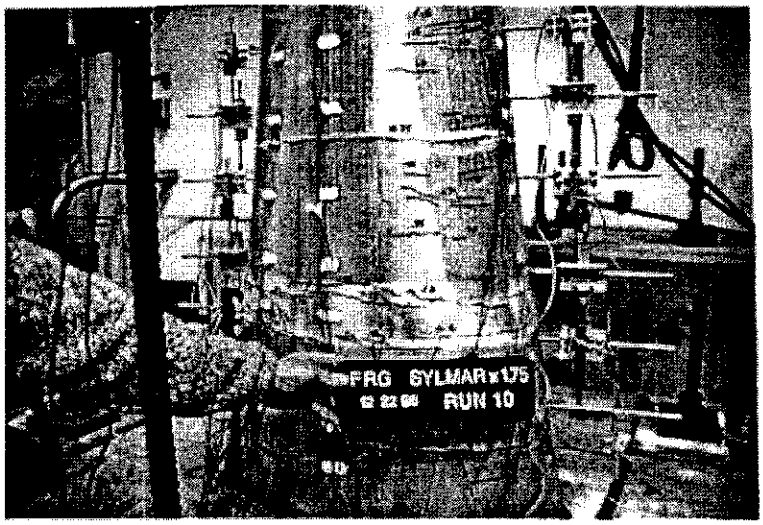

Figure 3 - 6 Specimen FRG Jacket Cracking at 1.75 x Sylmar (Event 7)

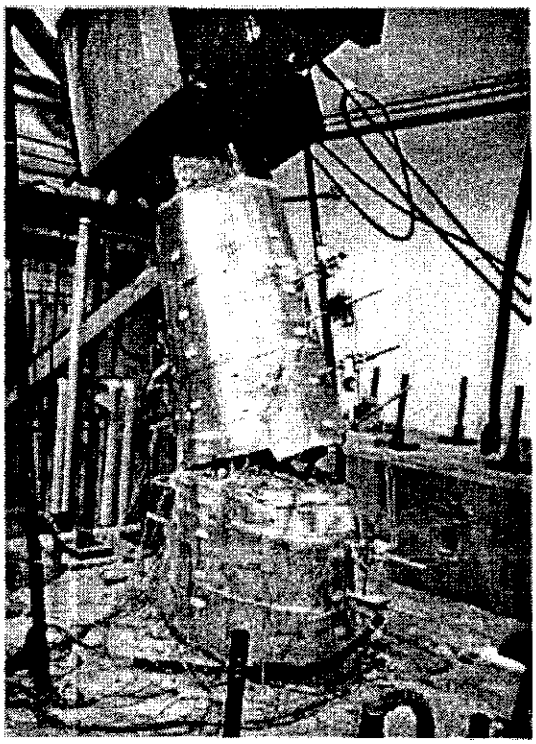

Figure 3 - 7 Collapse of Specimen FRG after Event 11

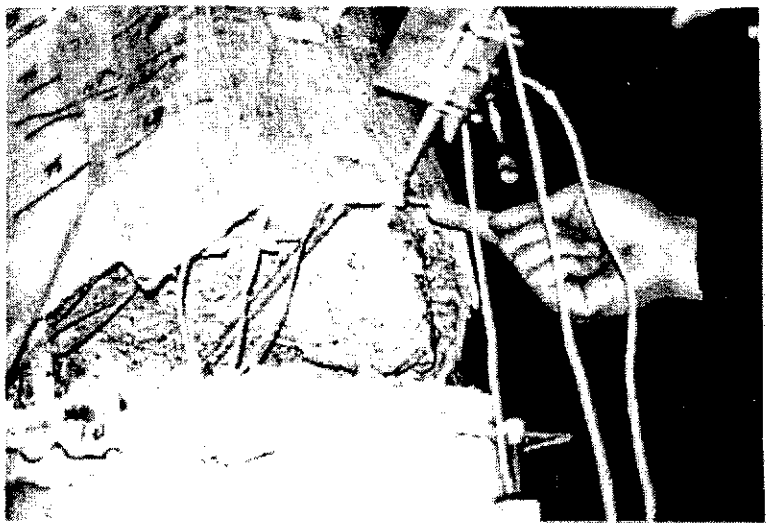

Figure 3 - 8 Specimen FRG at Elevation 495 mm (19.5 in) after Collapse

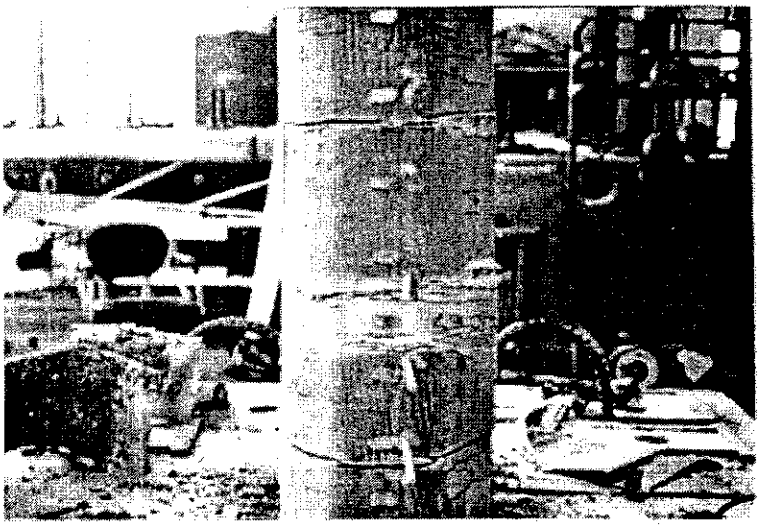

Figure 3 - 9 Specimen FRG before Removal of Jacket

Figure 3 - 10 Specimen FRG after Jacket Removal from 241 mm to 800 mm (9.5 in to 31.5 in) above Footing Elevation

Figure 3 - 11 Specimen FRG with Jacket Removed from Weak Axis

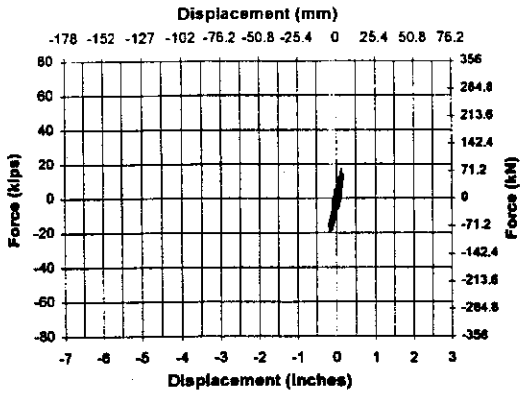

0.2 x Sylmar Event 1

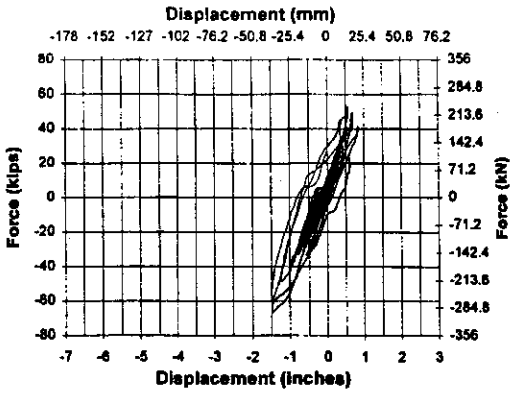

1.0 x Sylmar Event 4

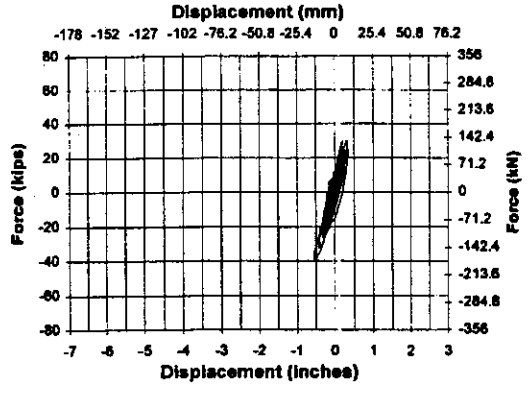

0.4 x Sylmar Event 2

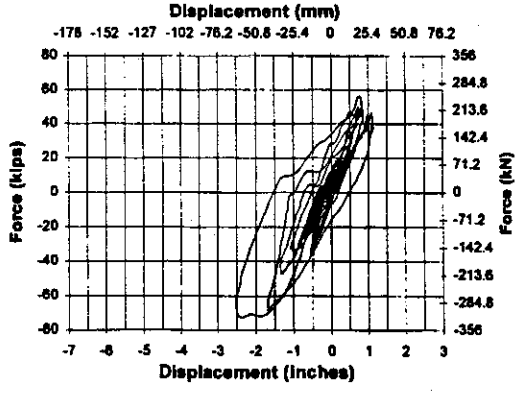

1.25 x Sylmar Event 5

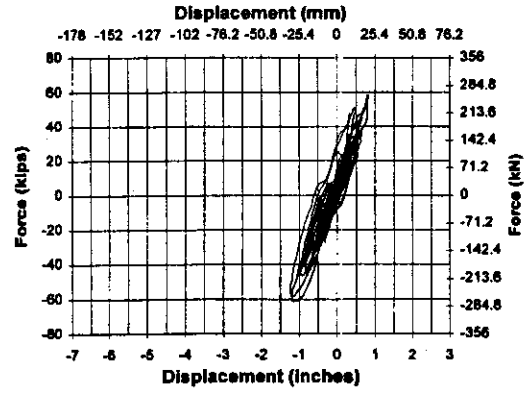

0.75 x Sylmar Event 3

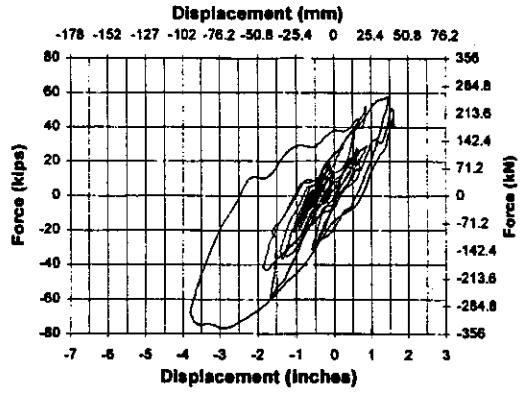

1.5 x Sylmar Event 6

Figure 3 - 12 Force vs. Displacement Hysteresis Specimen FRG Events 1-6

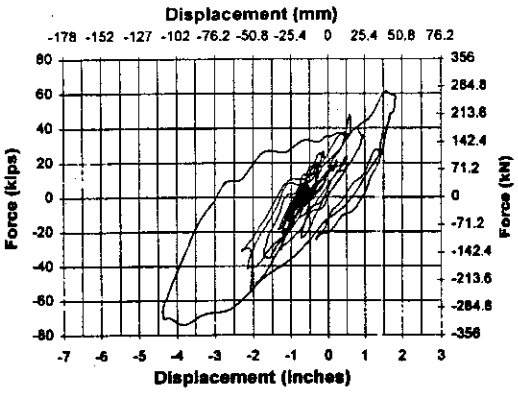

1.75 x Sylmar Event 7

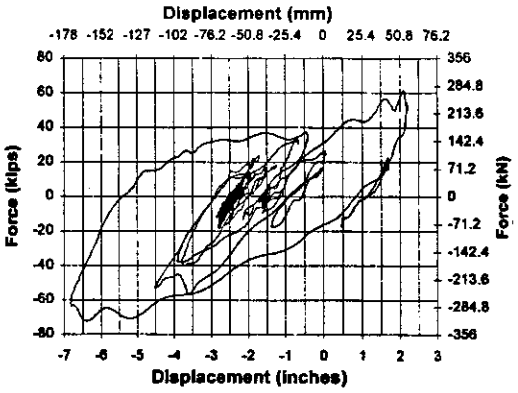

2.5 x Sylmar Event 10

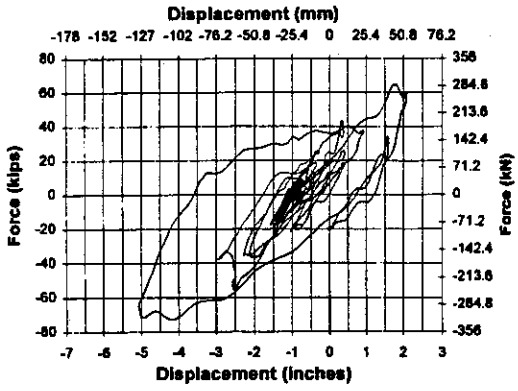

2.0 x Sylmar Event 8

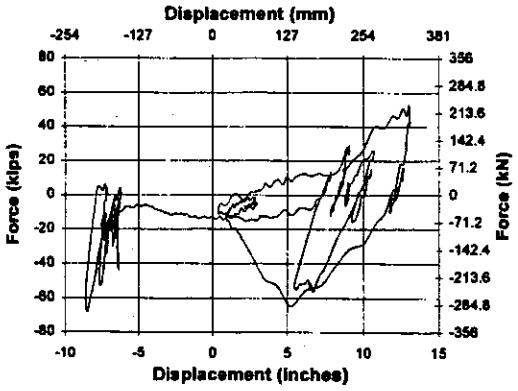

2.75 x Sylmar Event 11

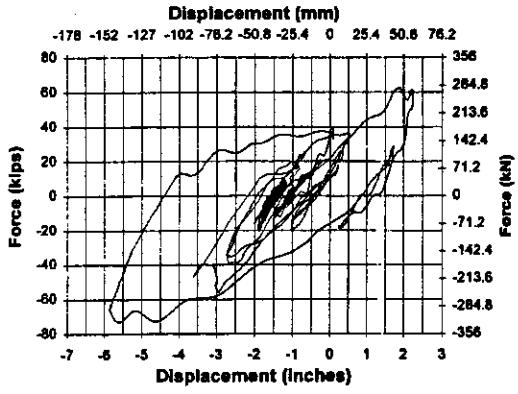

2.25 x Sylmar Event 9

Figure 3 - 13 Force vs. Displacement Hysteresis Specimen FRG Events 7-11

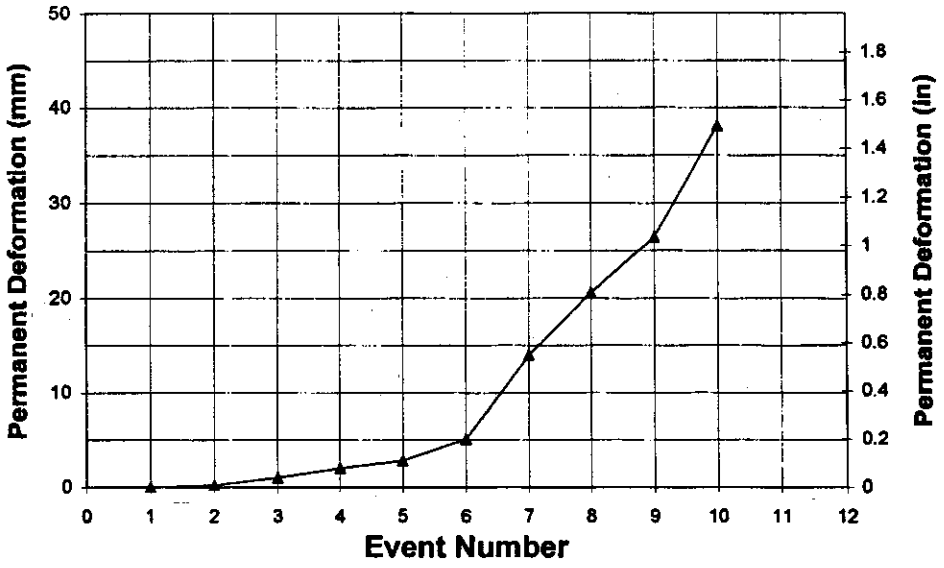

Figure 3 - 14 Measured Permanent Deformation after each Event Specimen FRG

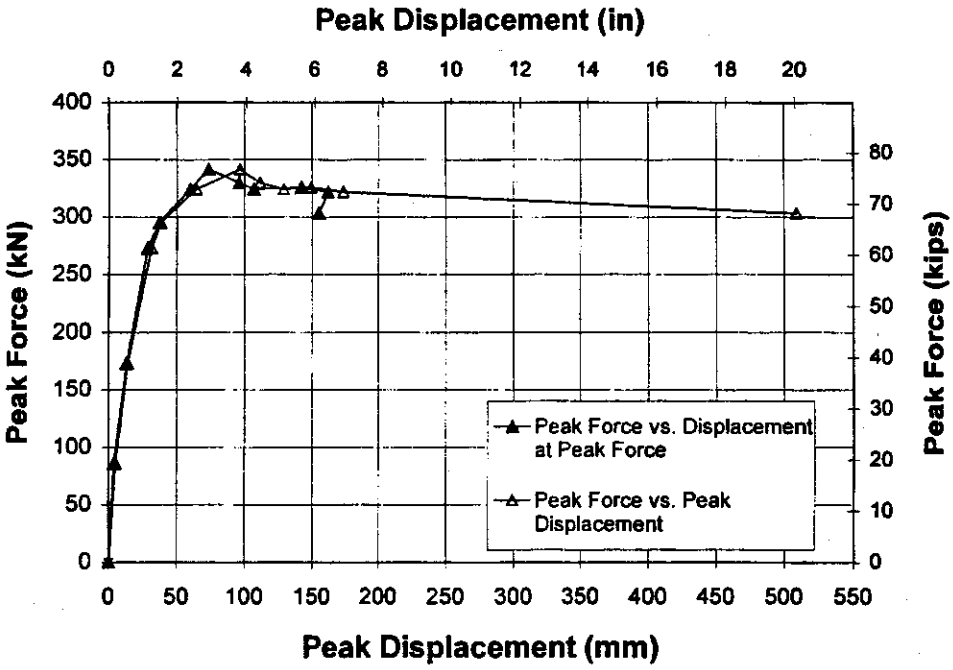

Figure 3 - 15 Force vs. Displacement Envelopes Specimen FRG

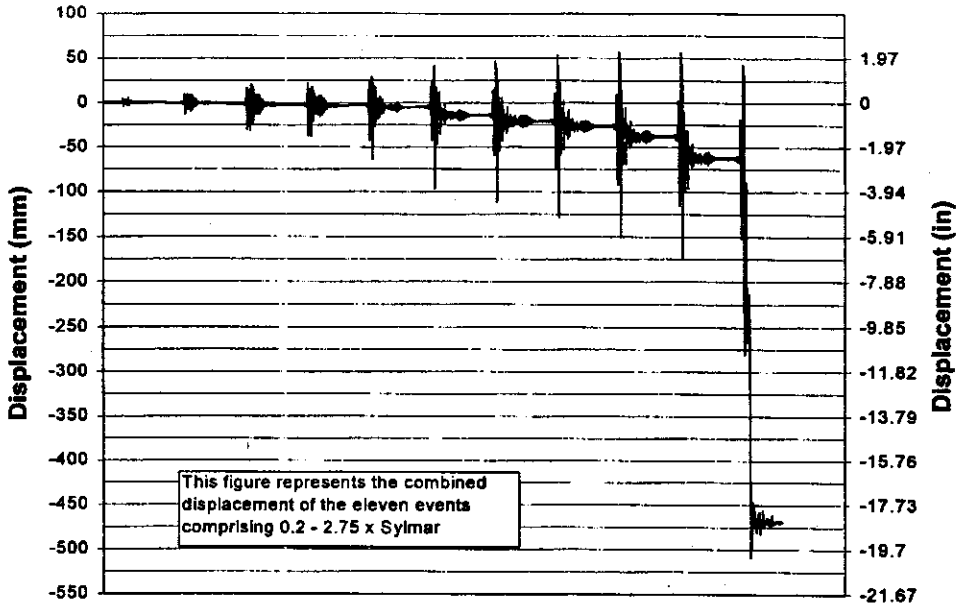

Figure 3 - 16 Combined Displacement Events 1-11 Specimen FRG

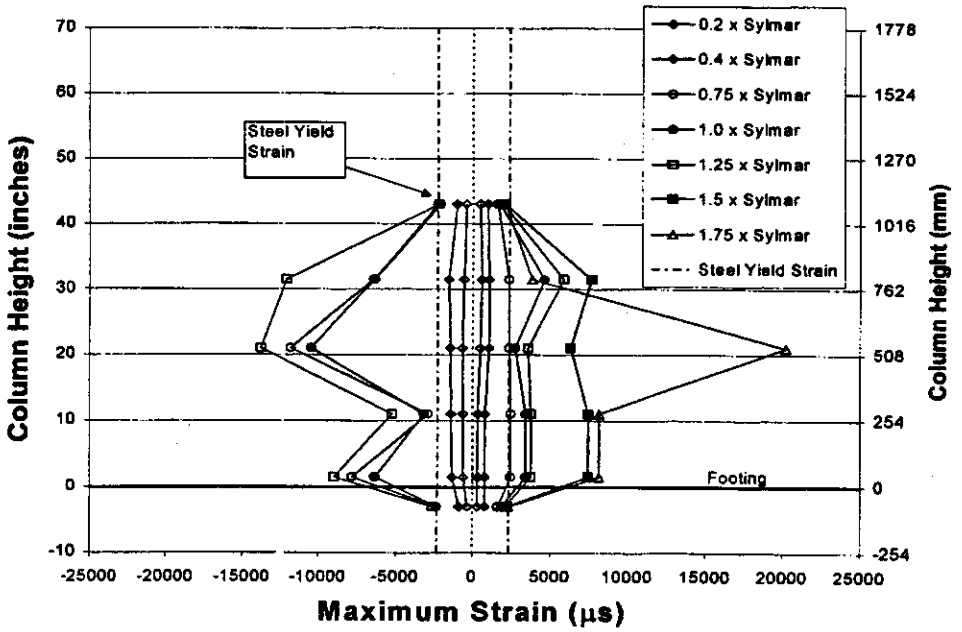

Figure 3 - 17 Longitudinal Bar Strain Envelopes (Far Side) Specimen FRG

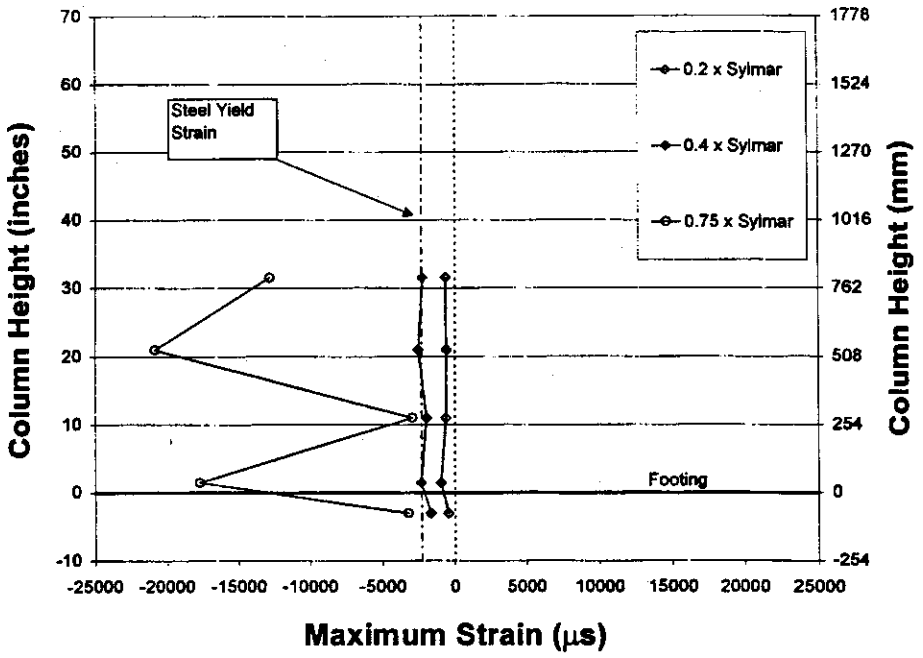

Figure 3 - 18 Longitudinal Bar Strain Envelopes (Near Side) Specimen FRG

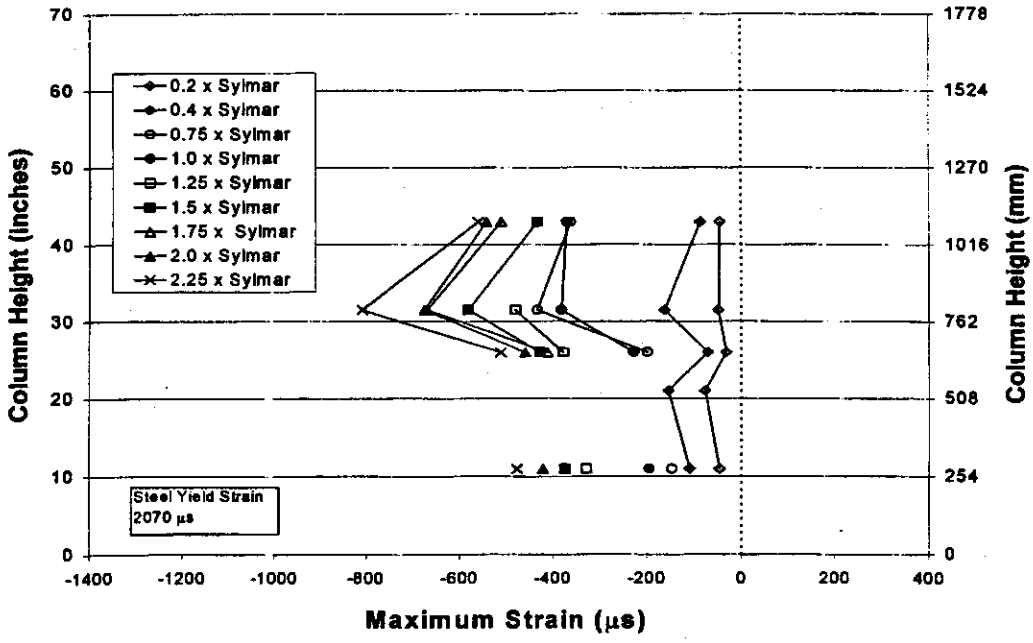

Figure 3 - 19 Corner Tie Strain Envelopes Specimen FRG

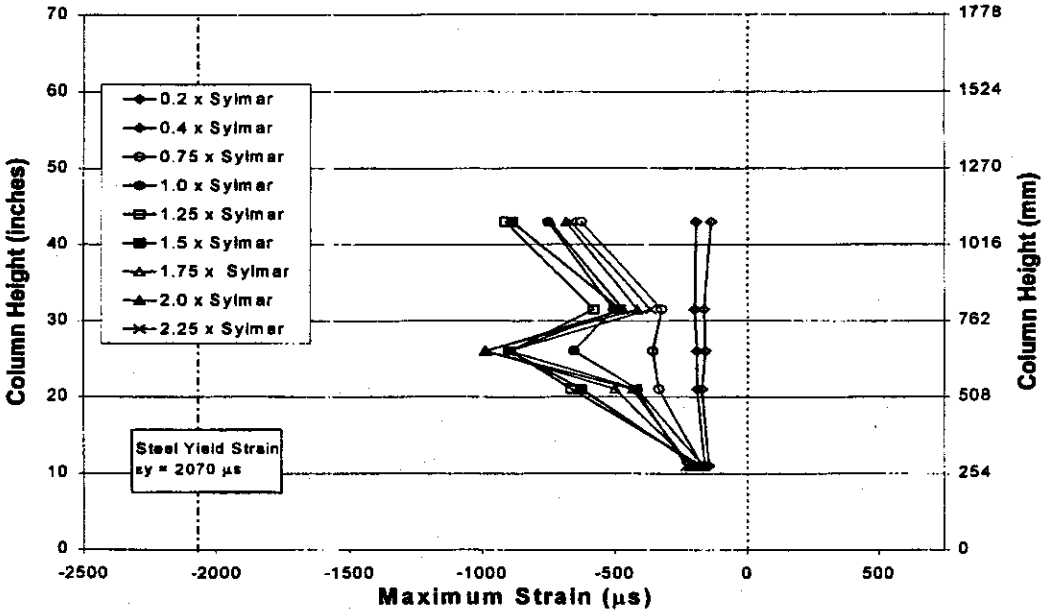

Figure 3 - 20 Center Tie Strain Envelopes Specimen FRG

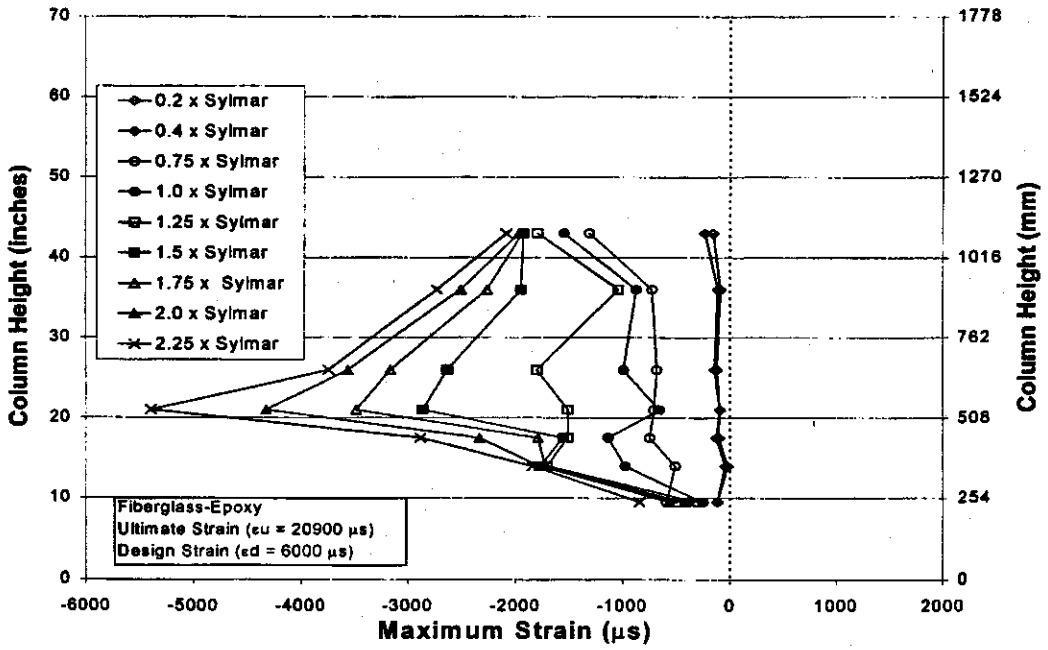

Figure 3 - 21 Jacket End Strain Envelopes Specimen FRG

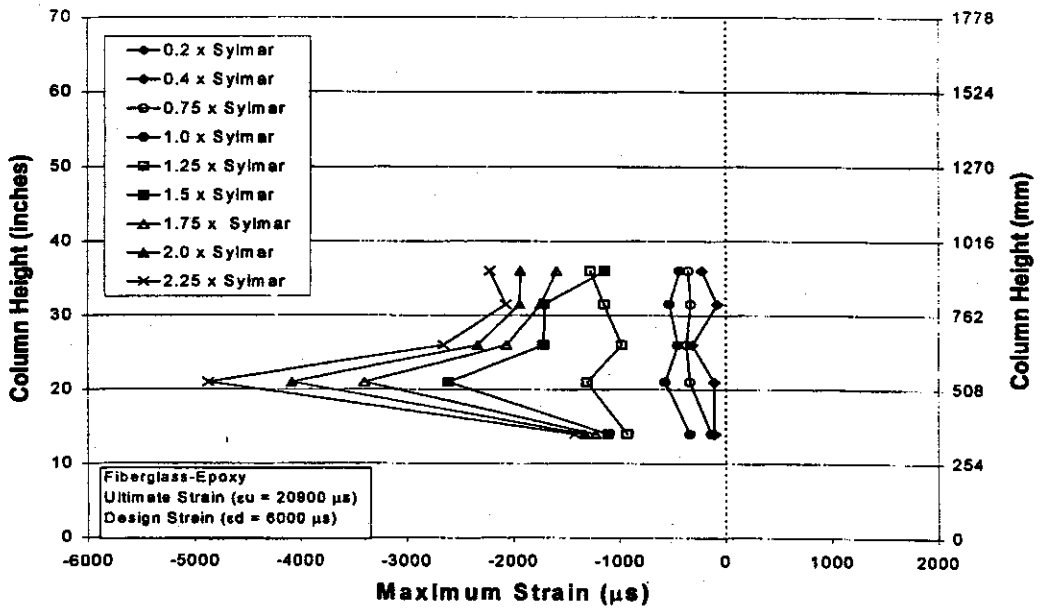

Figure 3 - 22 Jacket Side Strain Envelopes Specimen FRG

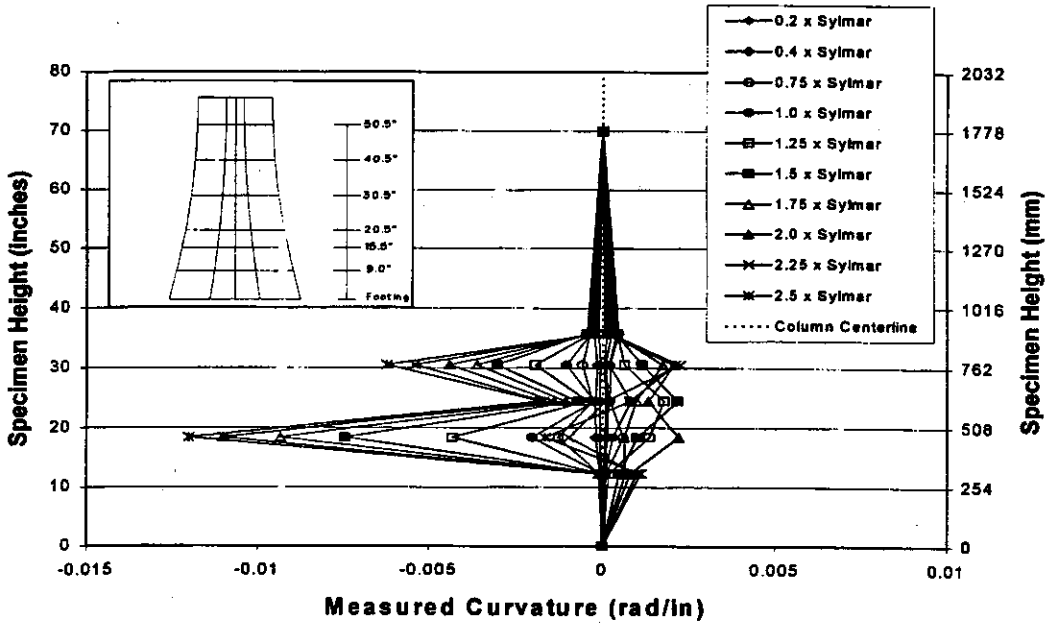

Figure 3 - 23 Measured Curvature Envelopes Specimen FRG

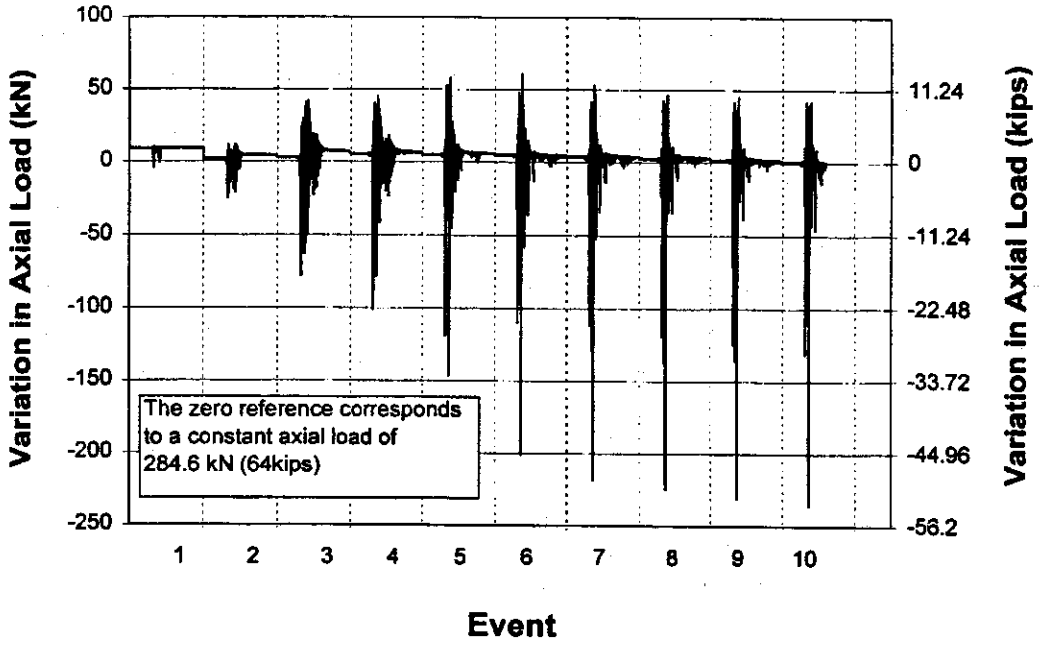

Figure 3 - 24 Variation in Axial Load Events 1-10 Specimen FRG

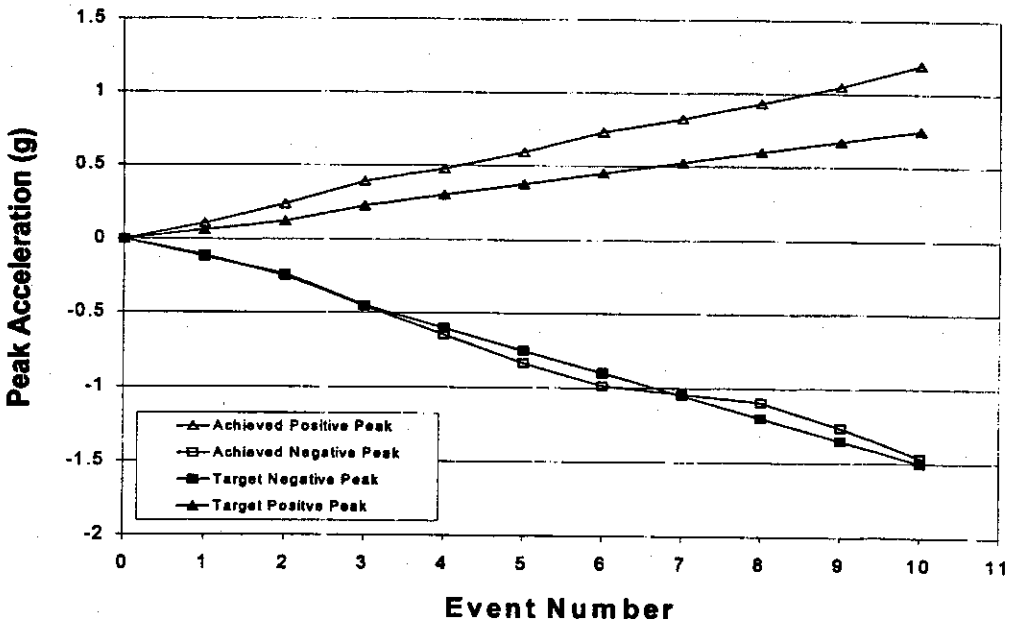

Figure 3 - 25 Comparison of Measured and Calculated Peak Acceleration (FRG)

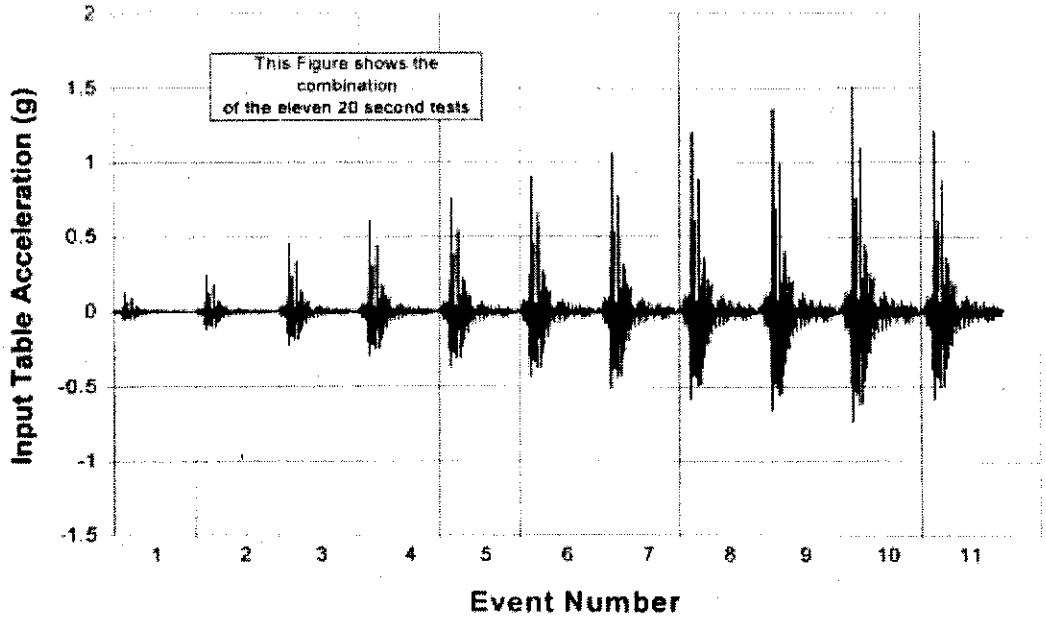

Figure 3 - 26 Shake Table Combined Input Acceleration Specimen FRC

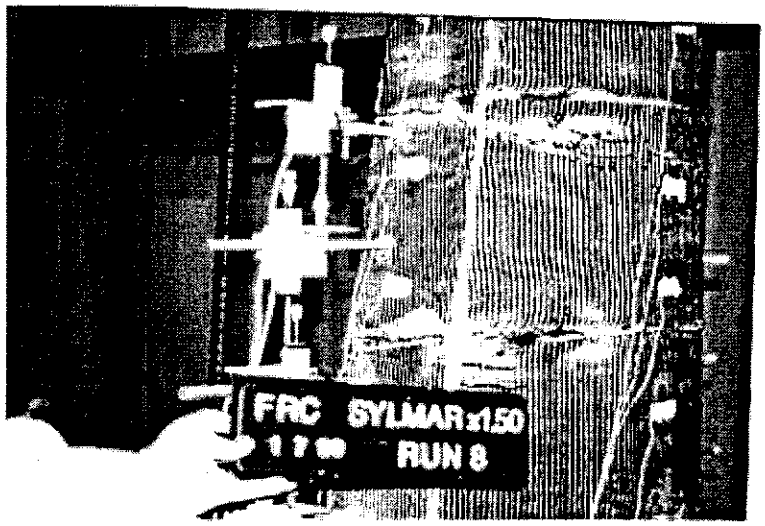

Figure 3 - 27 Specimen FRC Jacket Cracking at 1.5 x Sylmar (Event 6)

Figure 3 - 28 Specimen FRC with Jacket Removed from Weak Axis

Figure 3 - 29 Specimen FRC after Jacket Removal from 241 mm to 800 mm (9.5 in to 31.5 in) above Footing Elevation

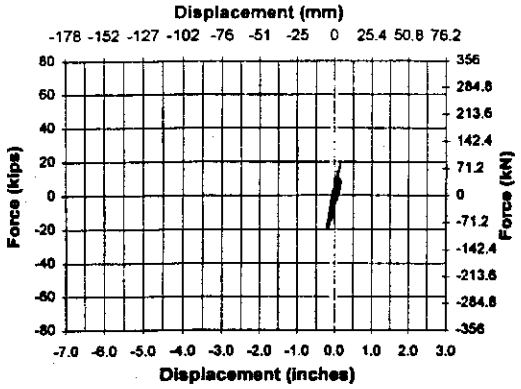

0.2 x Sylmar Event 1

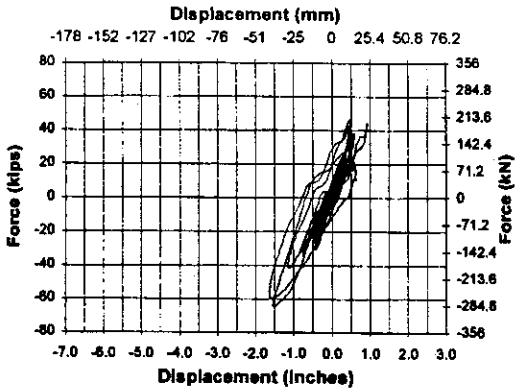

1.0 x Sylmar Event 4

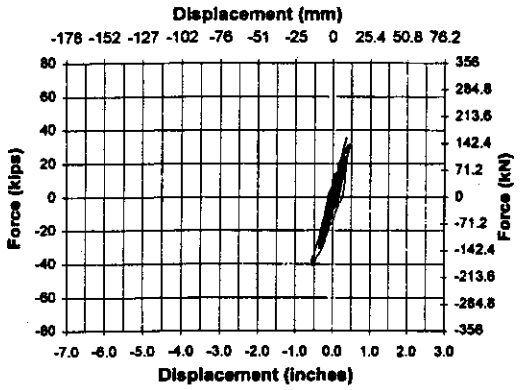

0.4 x Sylmar Event 2

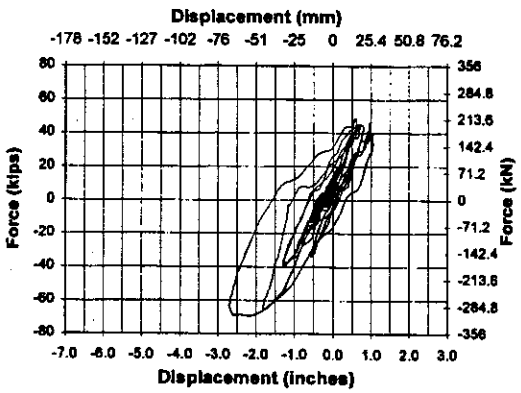

1.25 x Sylmar Event 5

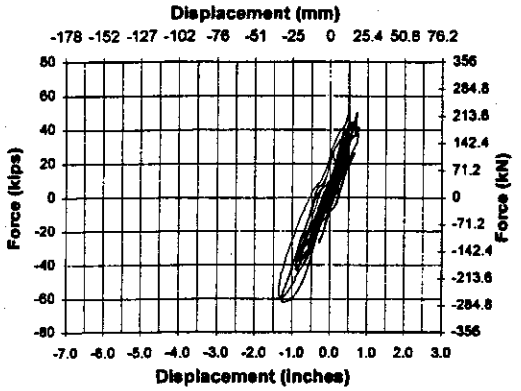

0.75 x Sylmar Event 3

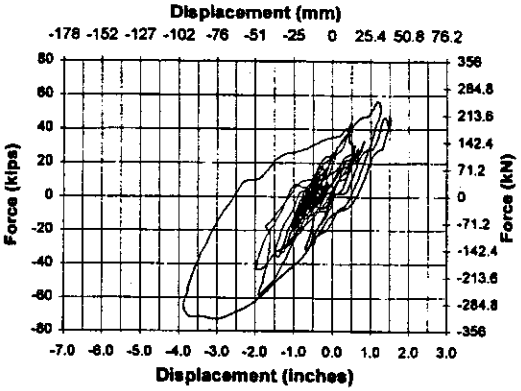

1.5 x Sylmar Event 6

Figure 3 - 30 Force vs. Displacement Hysteresis Specimen FRC Events 1-6

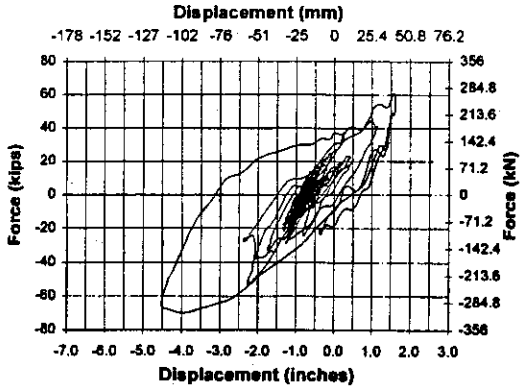

1.75 x Sylmar Event 7

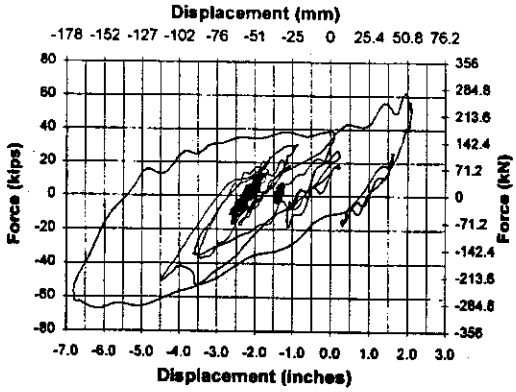

2.5 x Sylmar Event 10

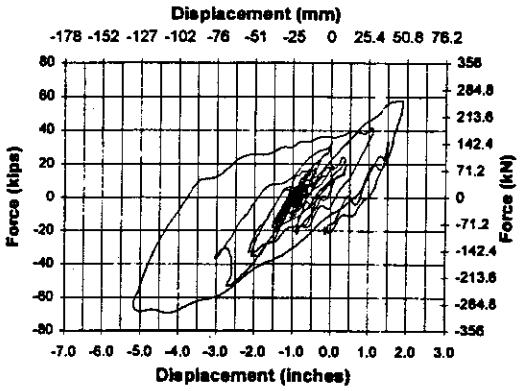

2.0 x Sylmar Event 8

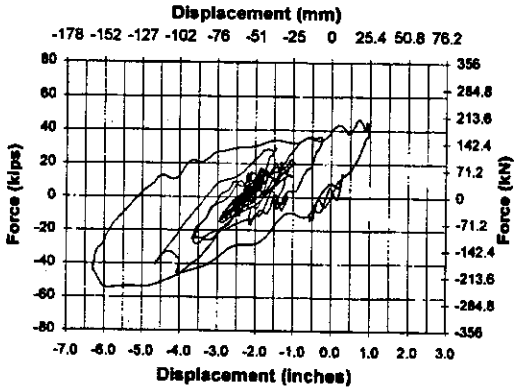

2.0 (2) x Sylmar Event 11

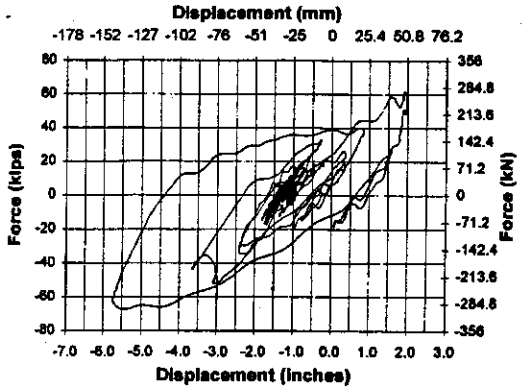

2.25 x Sylmar Event 9

Figure 3 - 31 Force vs. Displacement Hysteresis Specimen FRC Events 7-11

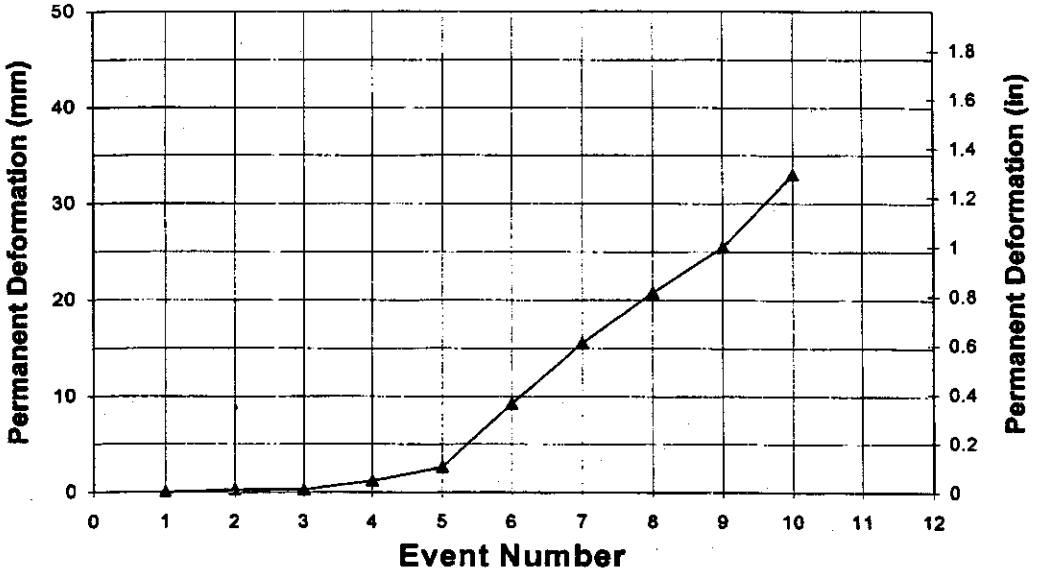

Figure 3 - 32 Measured Permanent Deformation after each Event Specimen FRC

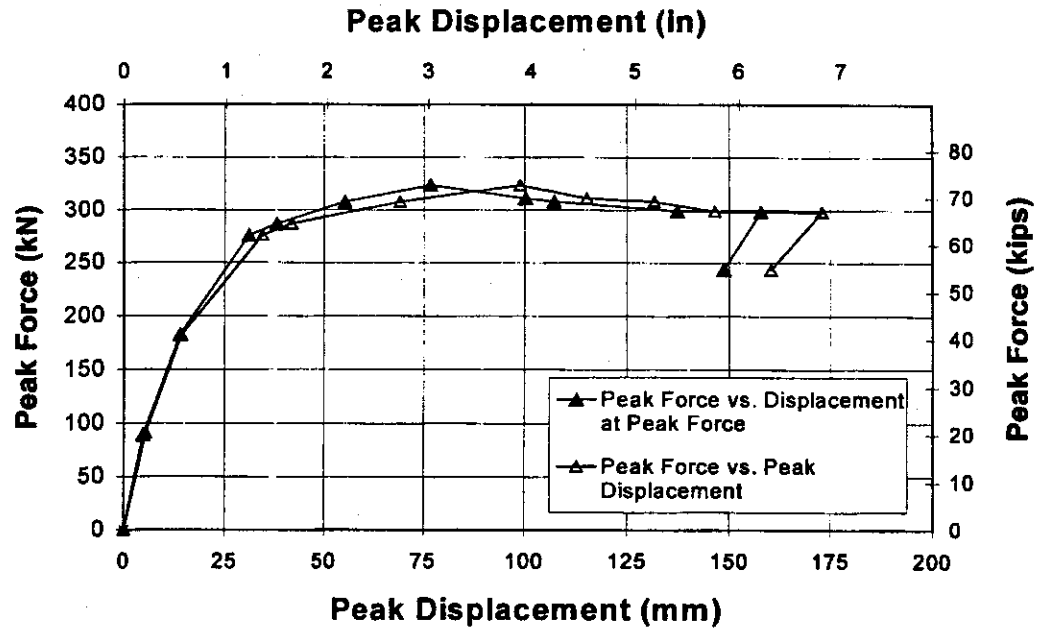

Figure 3 - 33 Force vs. Displacement Envelopes Specimen FRC

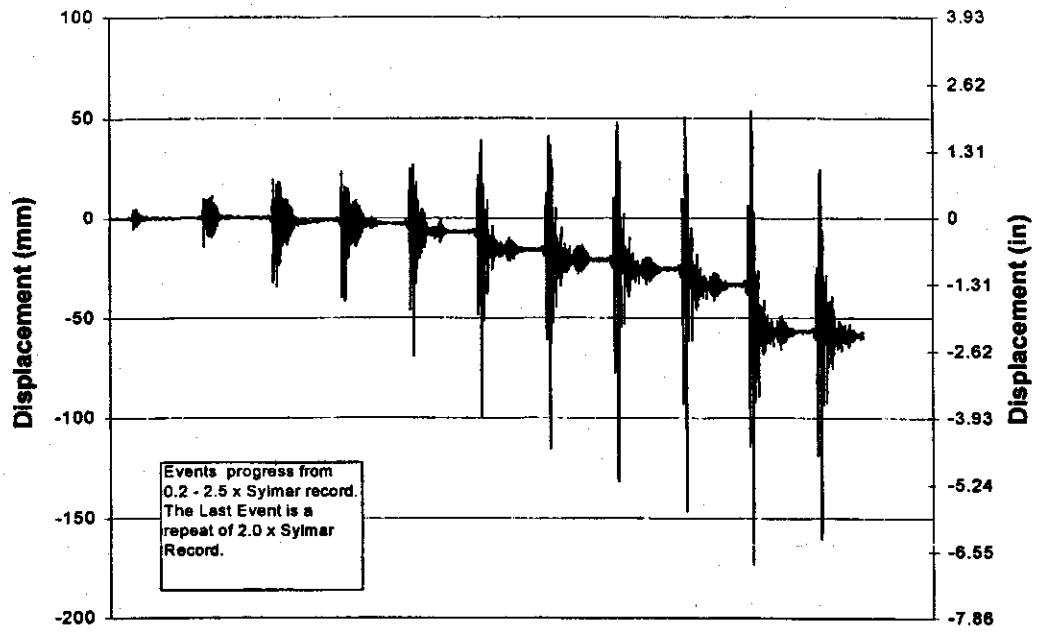

Figure 3 - 34 Combined Displacement Events 1-11 Specimen FRC

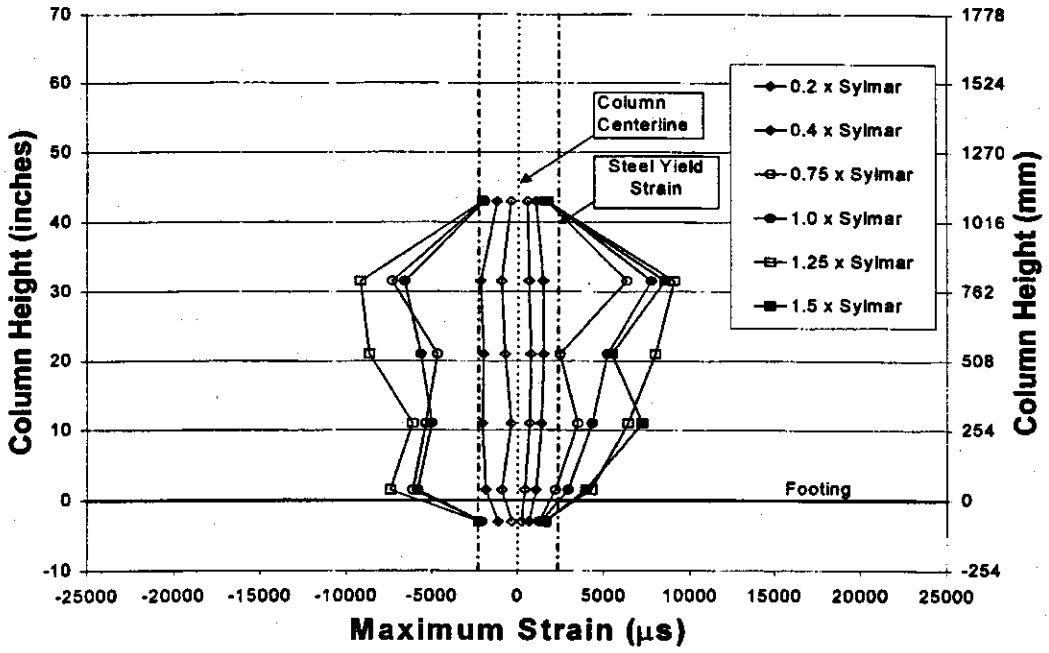

Figure 3 - 35 Longitudinal Bar Strain Envelopes (Far Side) Specimen FRC

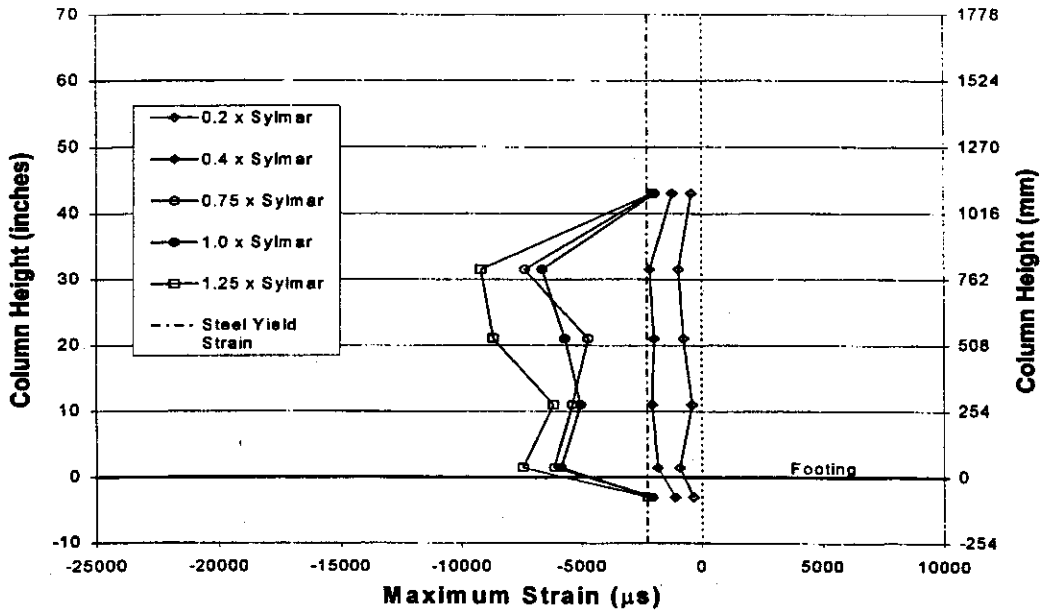

Figure 3 - 36 Longitudinal Bar Strain Envelopes (Near Side) Specimen FRC

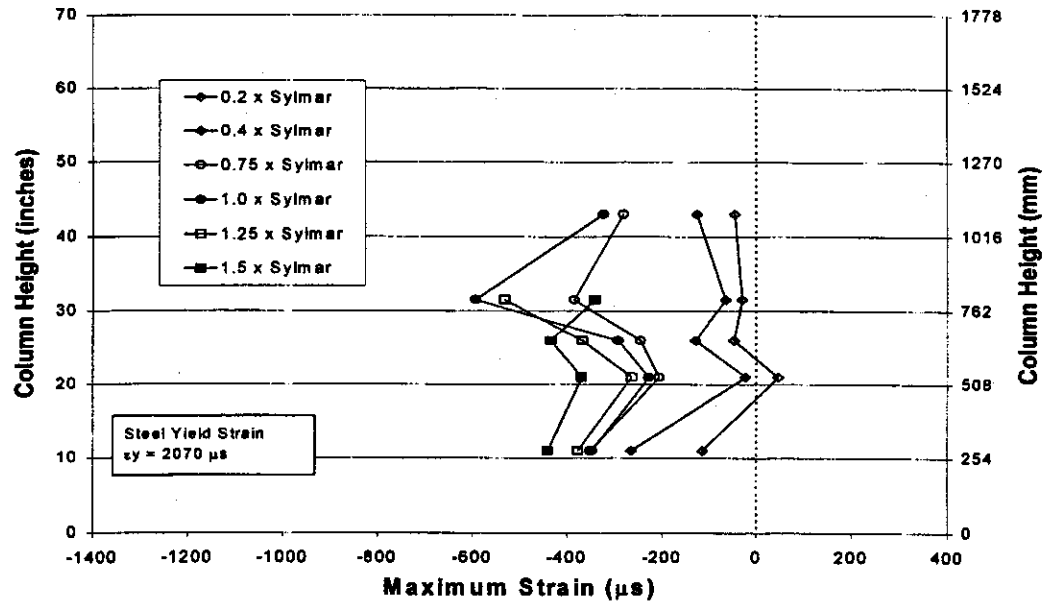

Figure 3 - 37 Corner Tie Strain Envelopes Specimen FRC

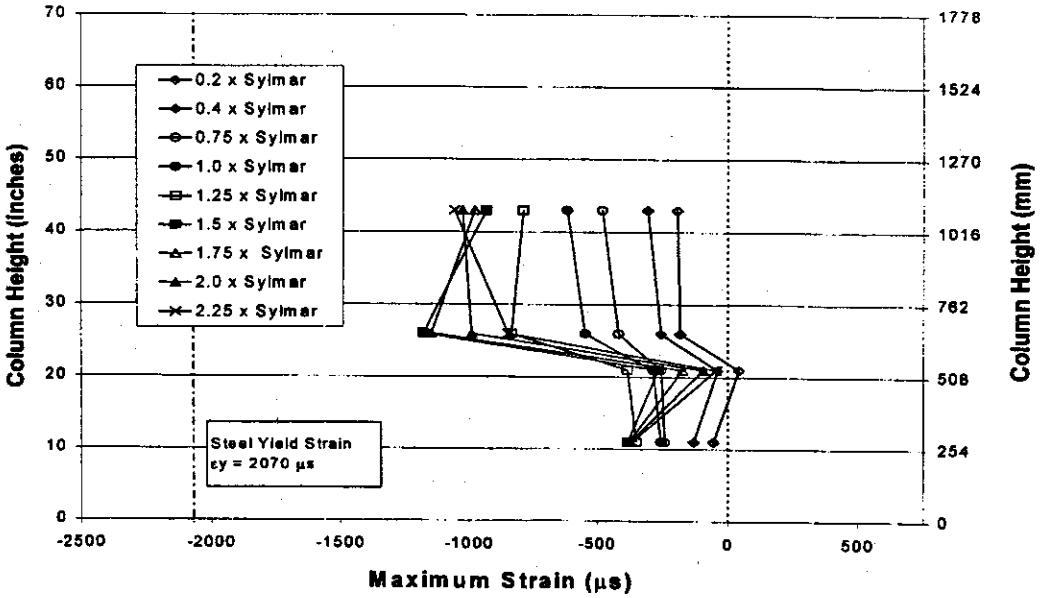

Figure 3 - 38 Center Tie Strain Envelopes Specimen FRC

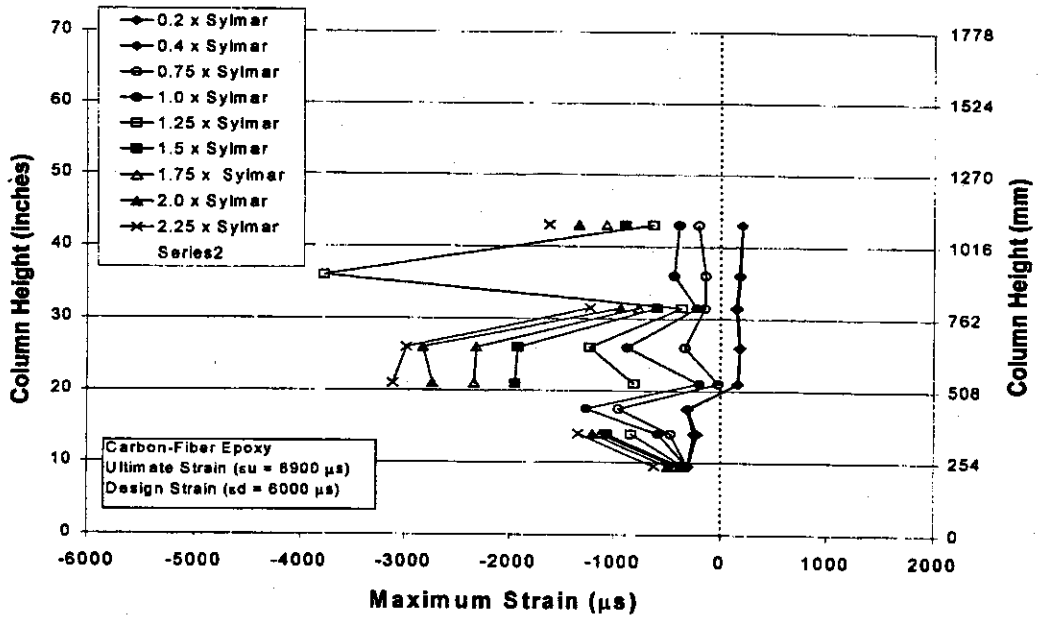

Figure 3 - 39 Jacket End Strain Envelopes Specimen FRC

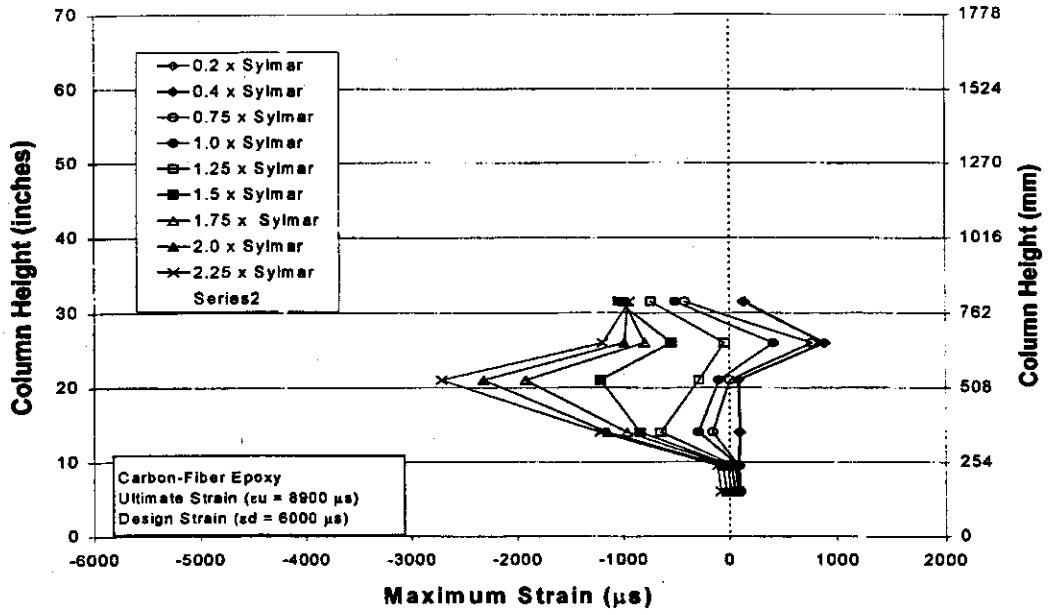

Figure 3 - 40 Jacket Side Strain Envelopes Specimen FRC

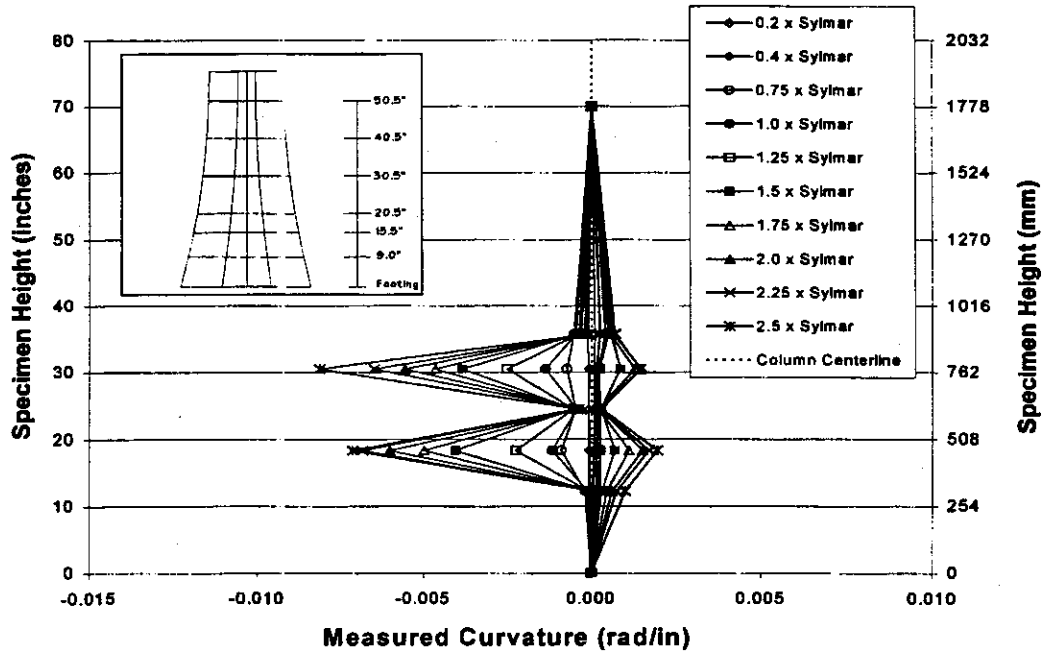

Figure 3 - 41 Measured Curvature Envelopes Specimen FRC

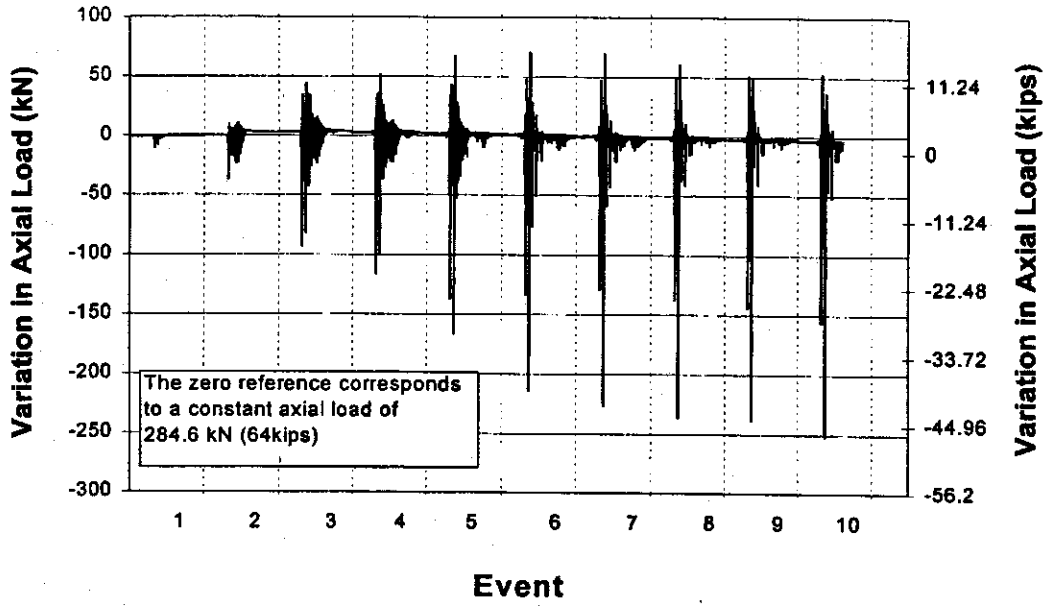

Figure 3 - 42 Variation in Axial Load Events 1-10 Specimen FRC

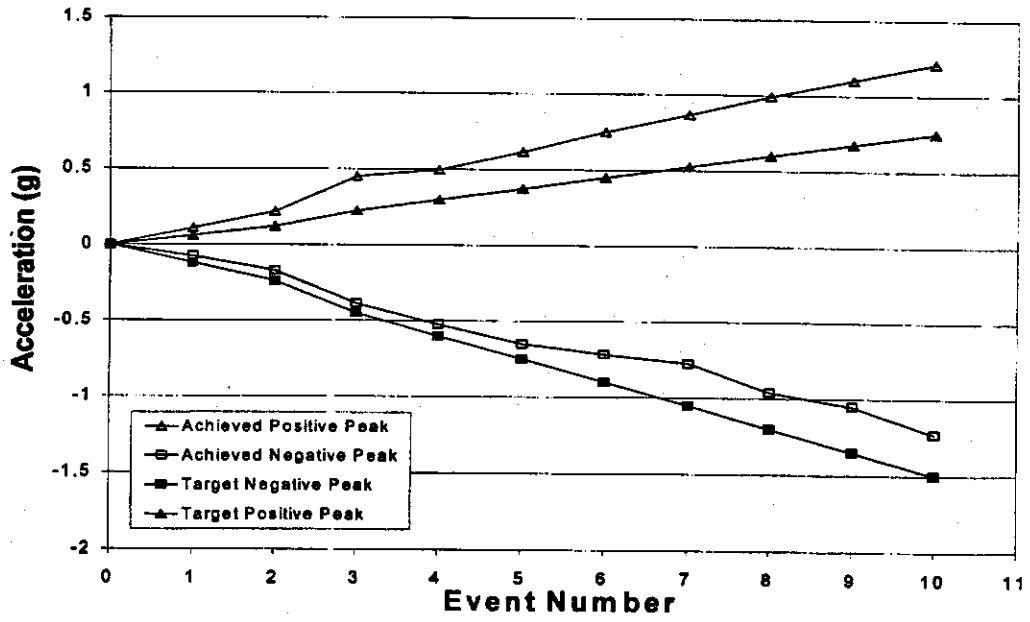

Figure 3 - 43 Comparison of Measured and Calculated Peak Acceleration (FRC)

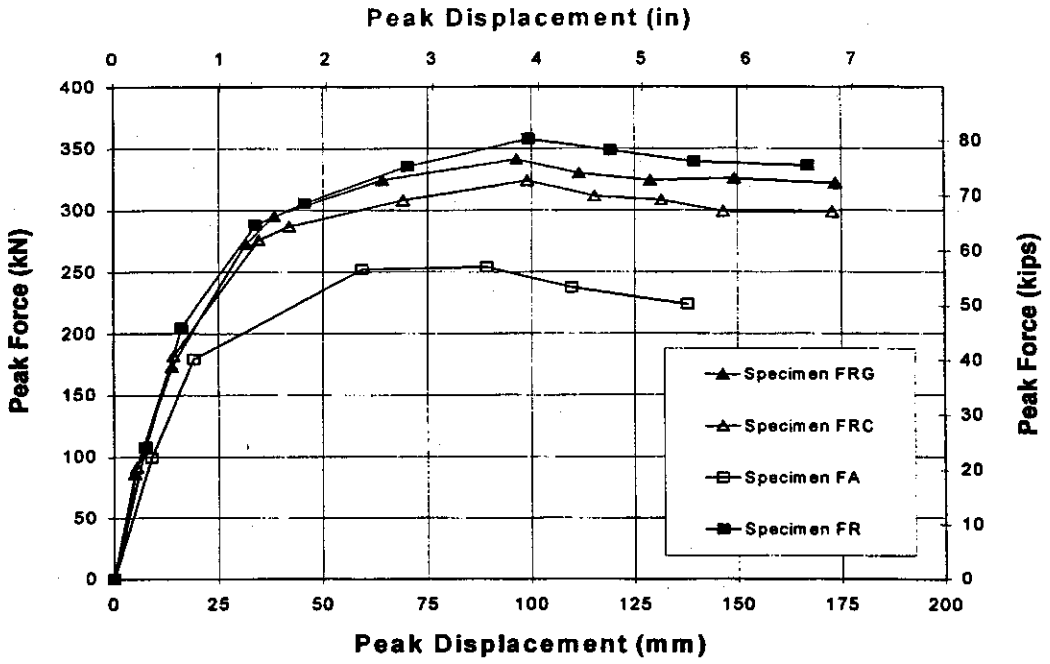

Figure 3 - 44 Peak Force vs. Peak Displacement Envelopes

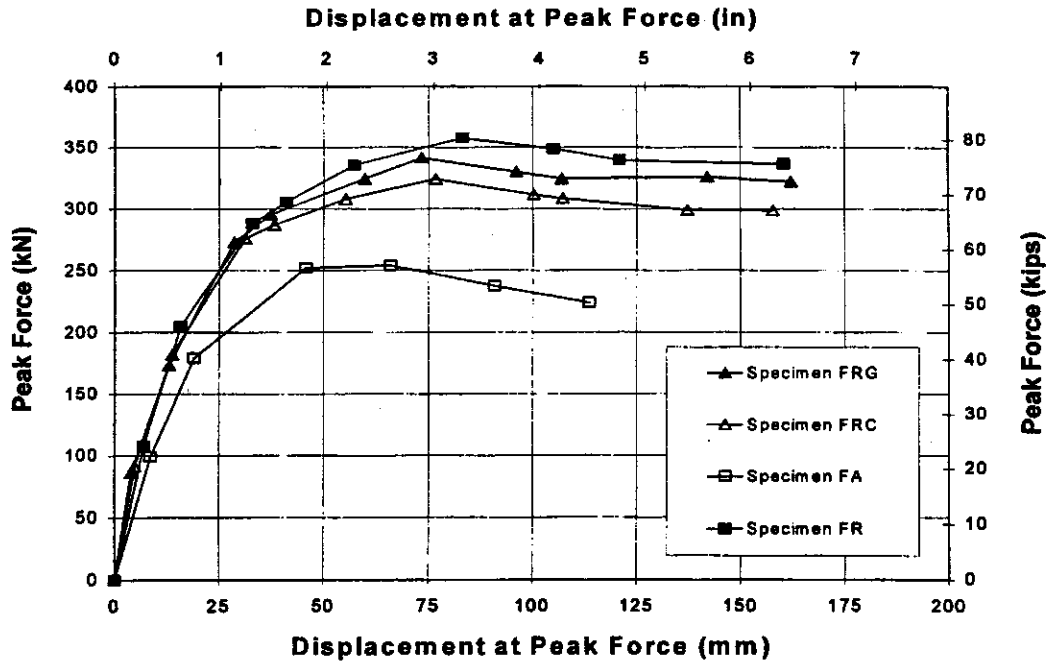

Figure 3 - 45 Peak Force vs. Displacement at Peak Force Envelopes

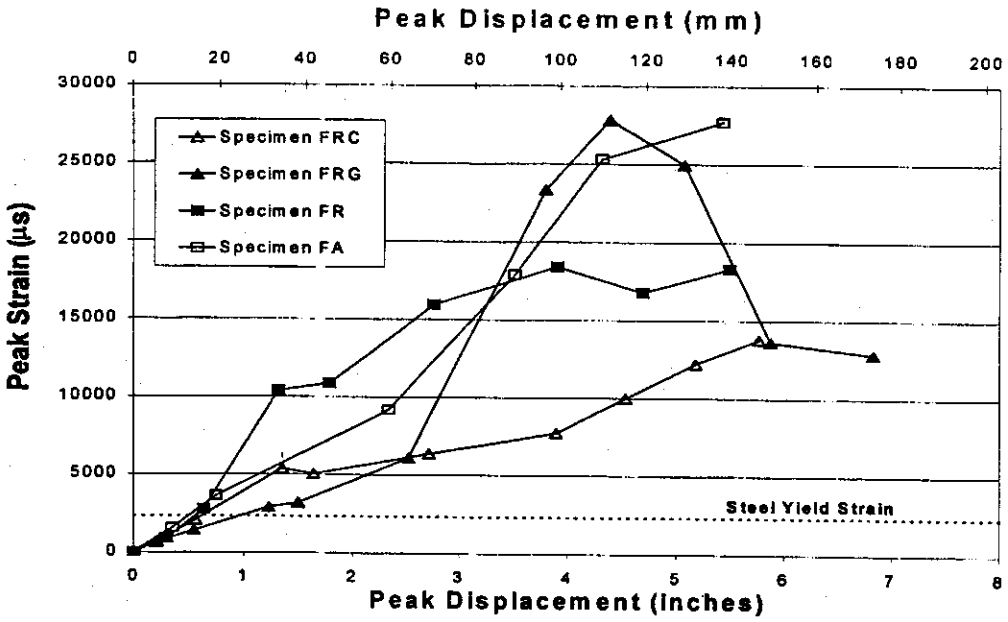

Figure 3 - 46 Longitudinal Bar Strain vs. Displacement at Elevation 279 mm (11 in) SG 11

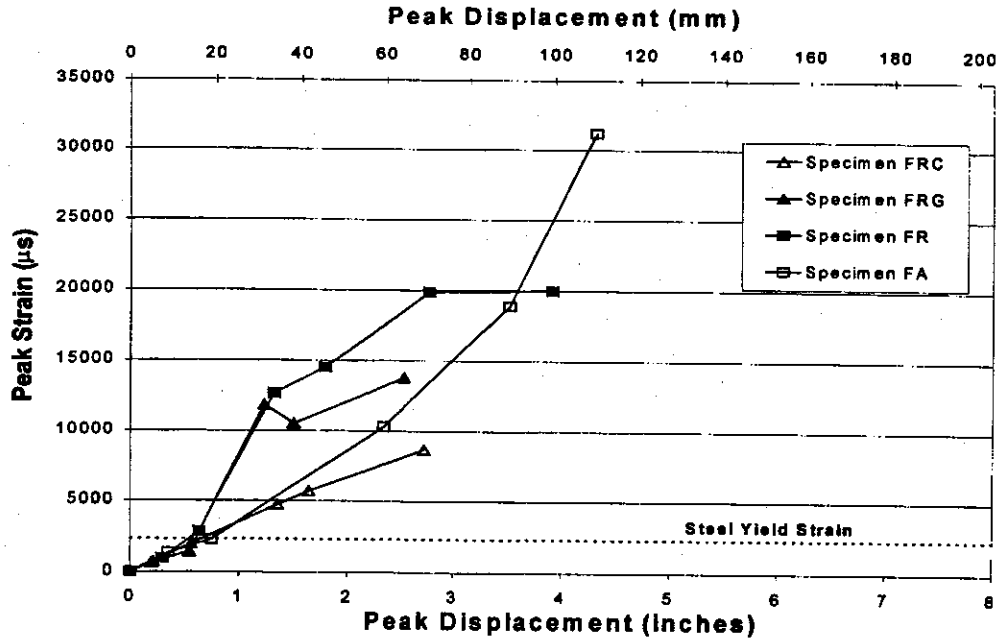

Figure 3 - 47 Longitudinal Bar Strain vs. Displacement at Elevation 533 mm (21 in) SG 16

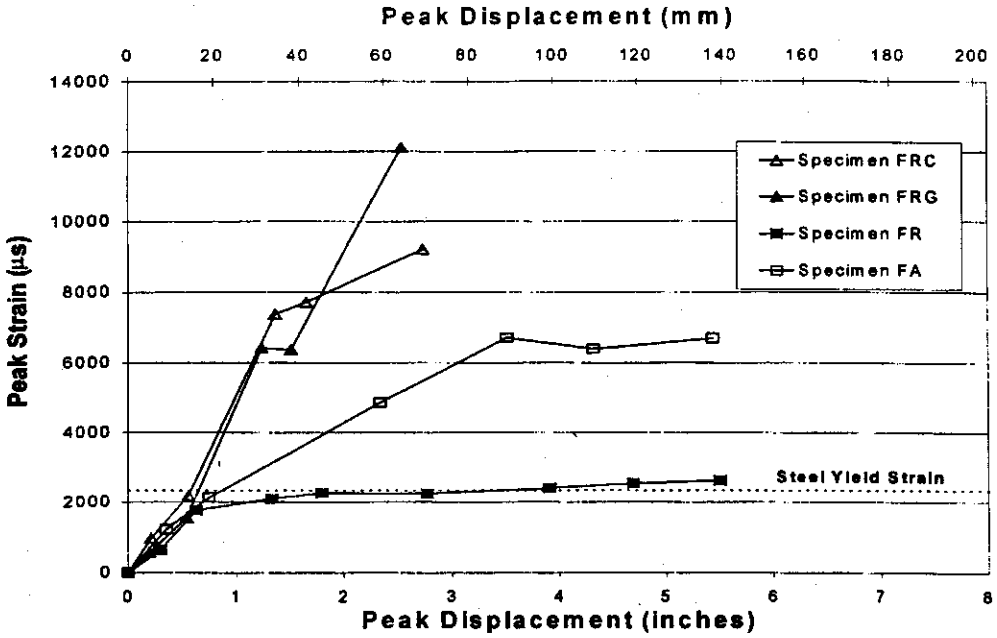

Figure 3 - 48 Longitudinal Bar Strain vs. Displacement at Elevation 800 mm (31.5 in) SG 5

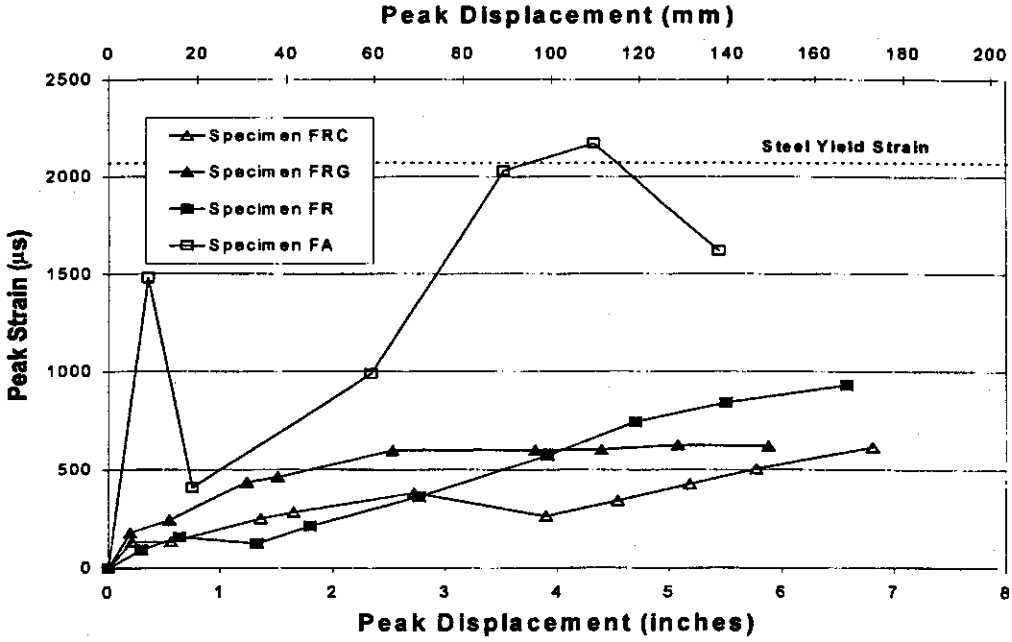

Figure 3 - 49 Transverse Bar Strain vs Displacement at Elevation 533 mm (21 in) SG 16

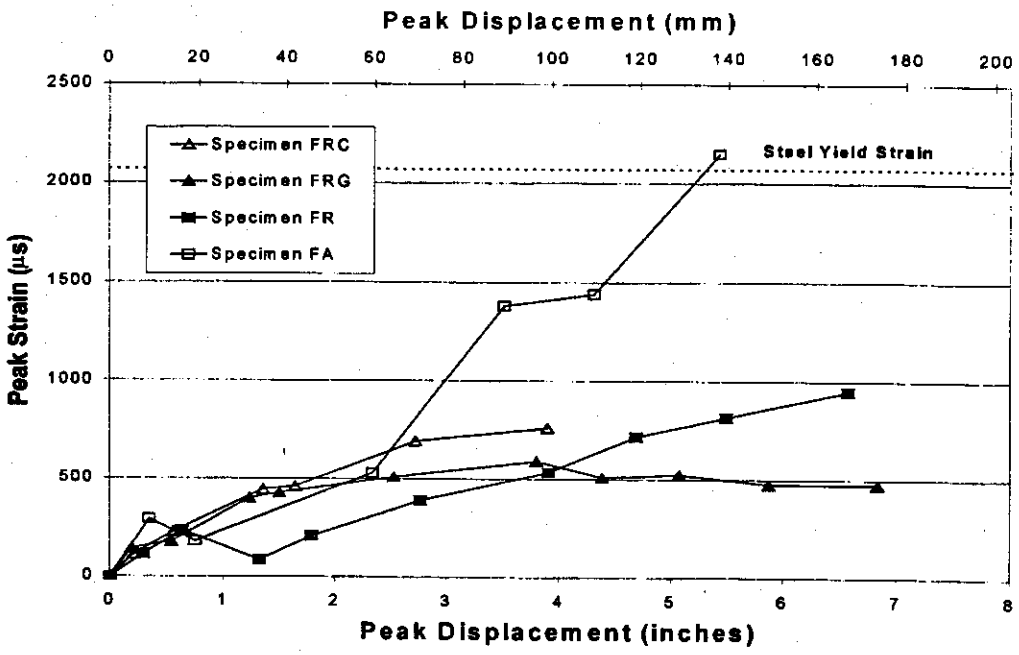

Figure 3 - 50 Transverse Bar Strain vs. Displacement at Elevation 533 mm (21 in) SG 18

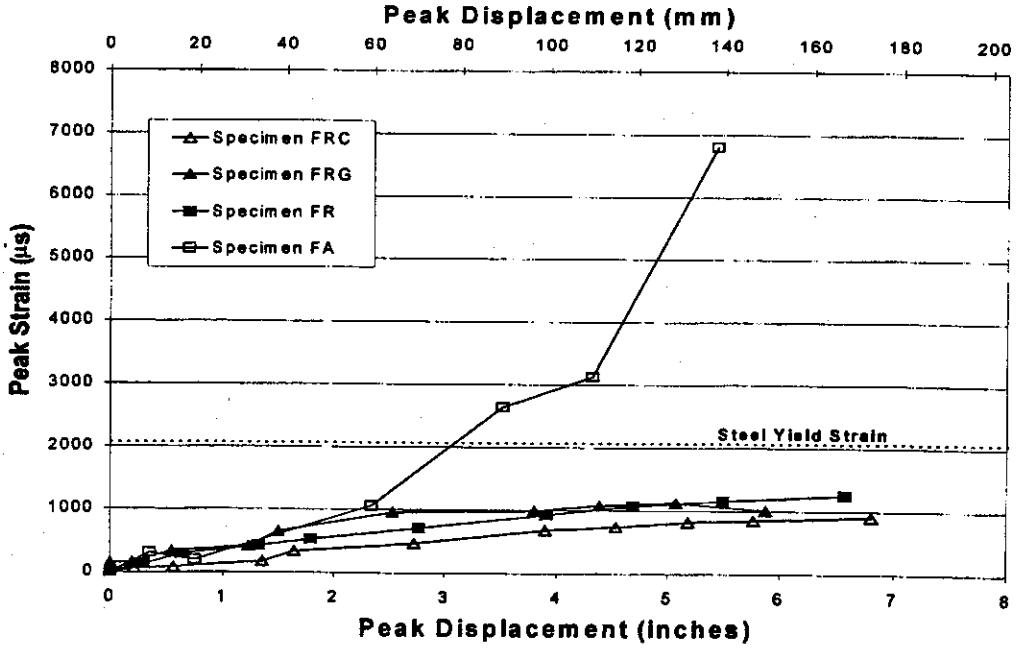

Figure 3 - 51 Transverse Bar Strain vs. Displacement at Elevation 660 mm (26 in) SG 24

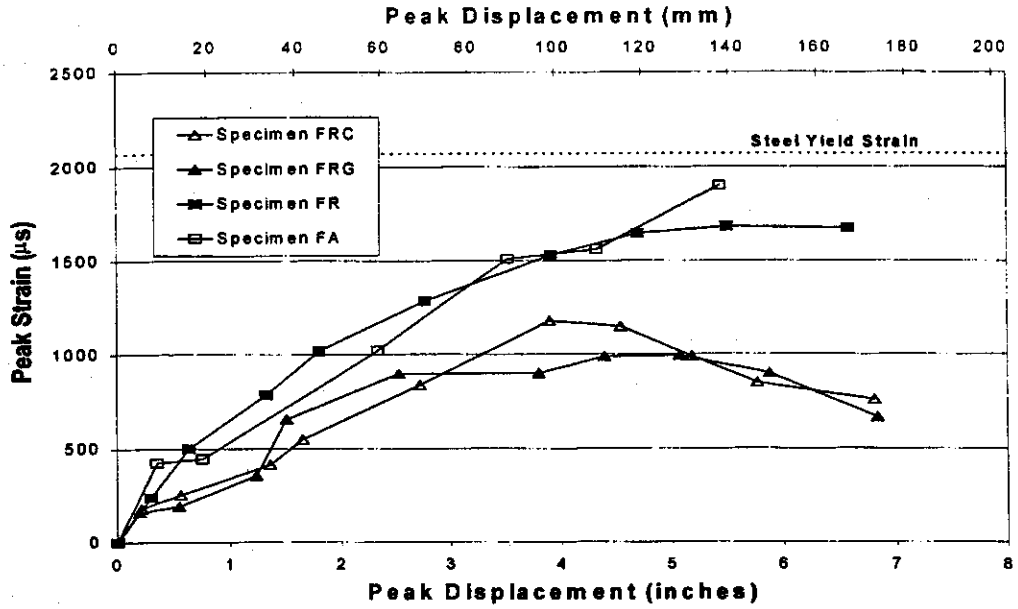

Figure 3 - 52 Transverse Bar Strain vs. Displacement at Elevation 660 mm (26 in) SG 22

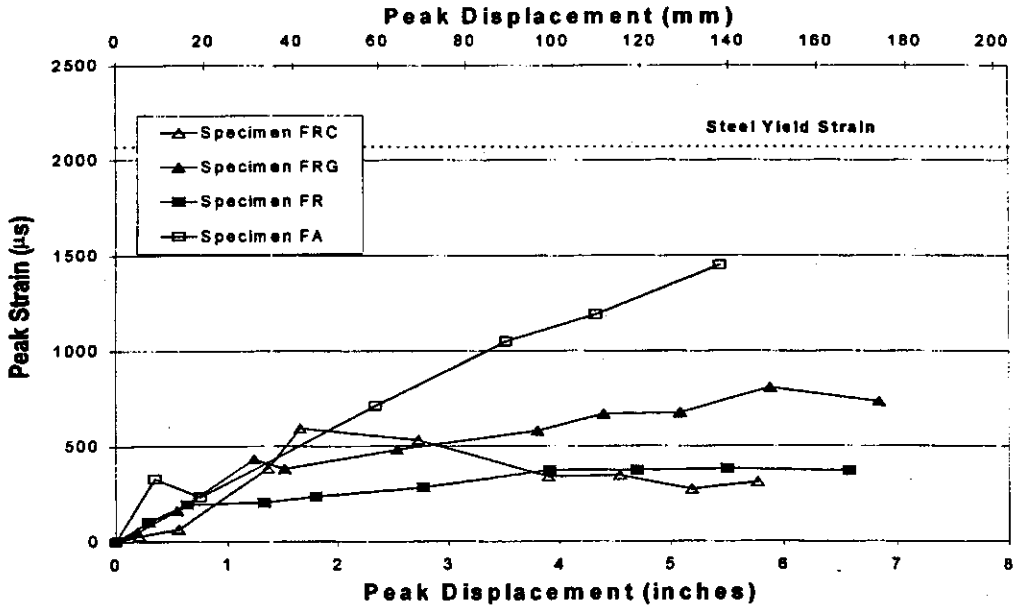

Figure 3 - 53 Transverse Bar Strain vs. Displacement at Elevation 800 mm (31.5 in) SG 27

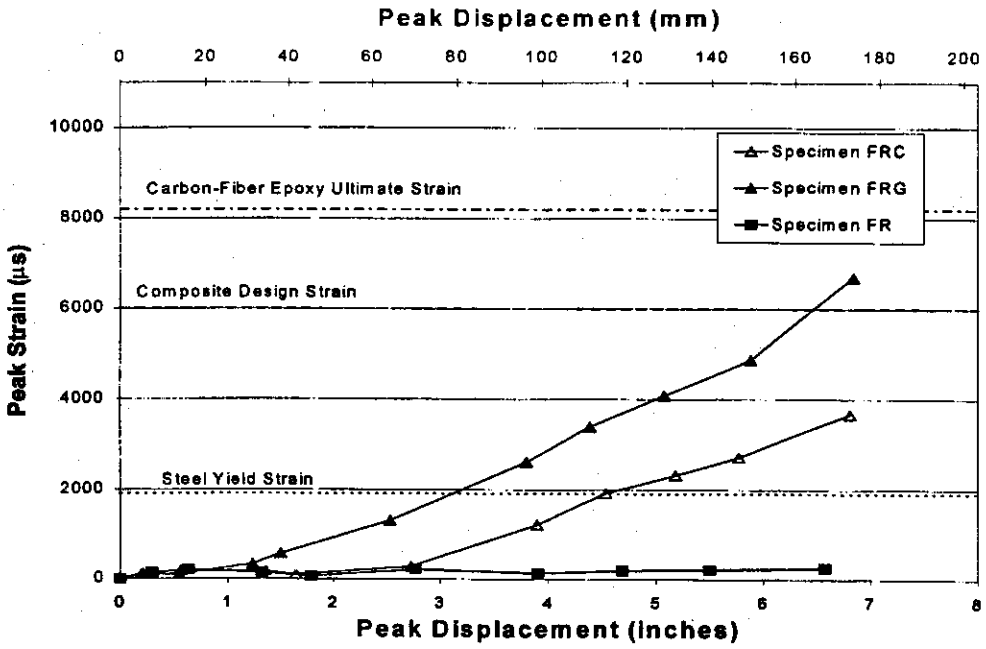

Figure 3 - 54 Jacket End Strain vs. Displacement at Elevation 533 mm (21 in) SG 62

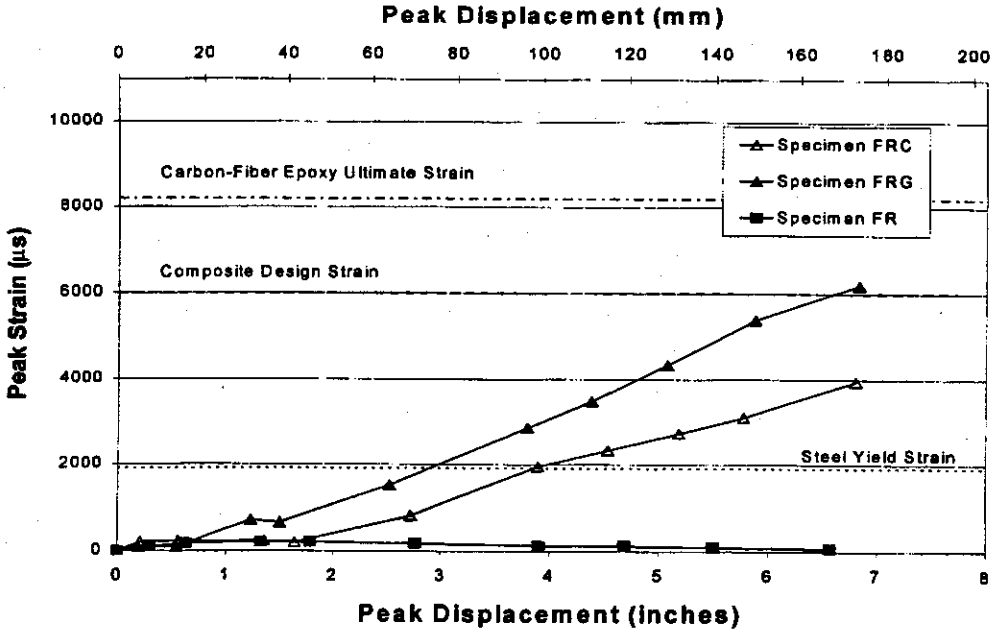

Figure 3 - 55 Jacket Side Strain vs. Displacement at Elevation 533 mm (21 in) SG 80

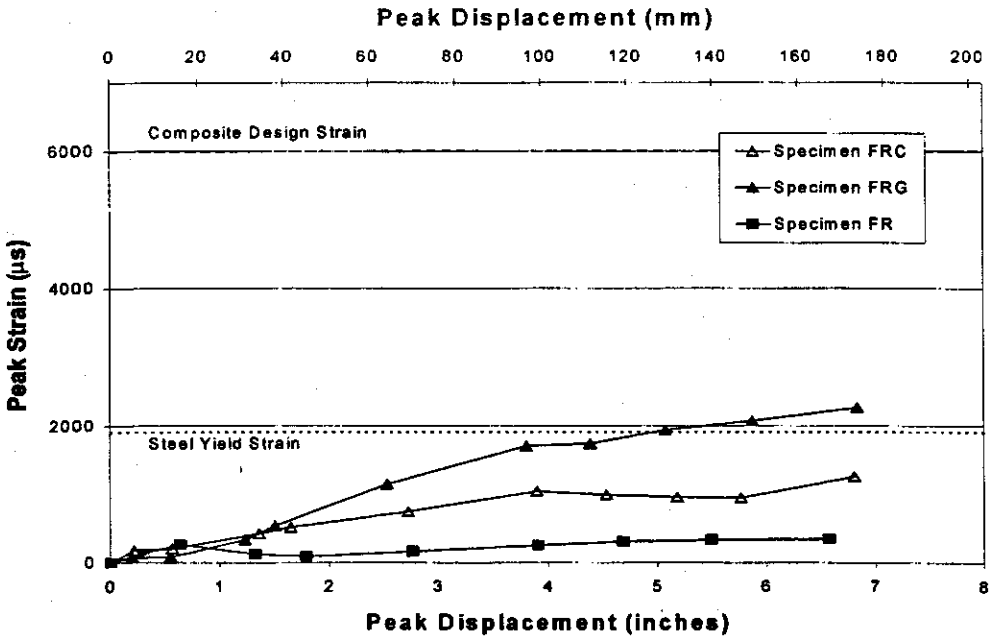

Figure 3 - 56 Jacket End Strain vs. Displacement at Elevation 800 mm (31.5 in) SG 60

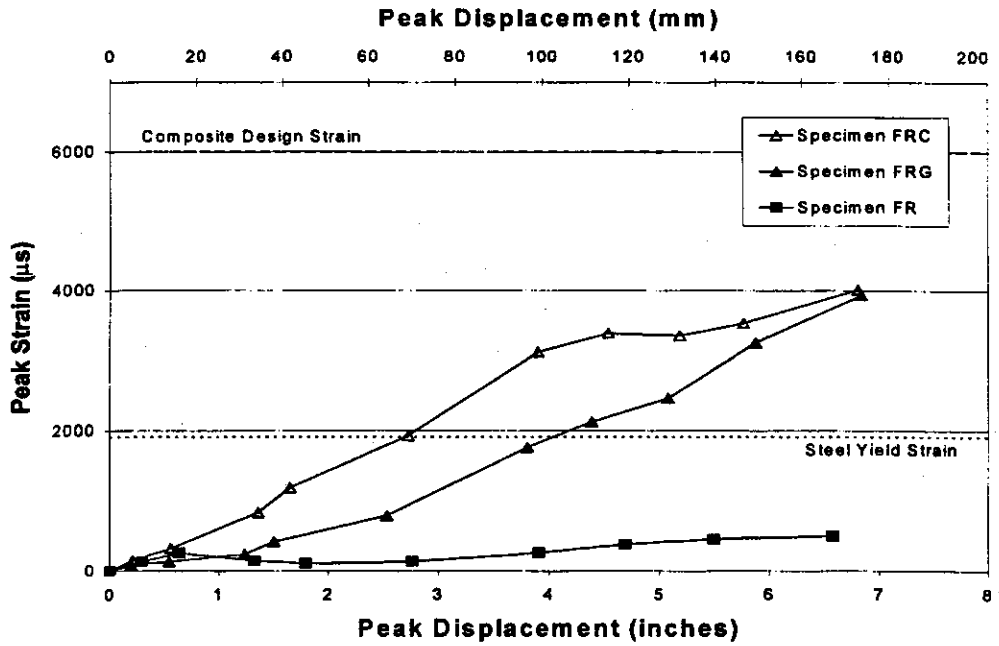

Figure 3 - 57 Jacket Side Strain vs. Displacement at Elevation 800 mm (31.5 in) SG 87

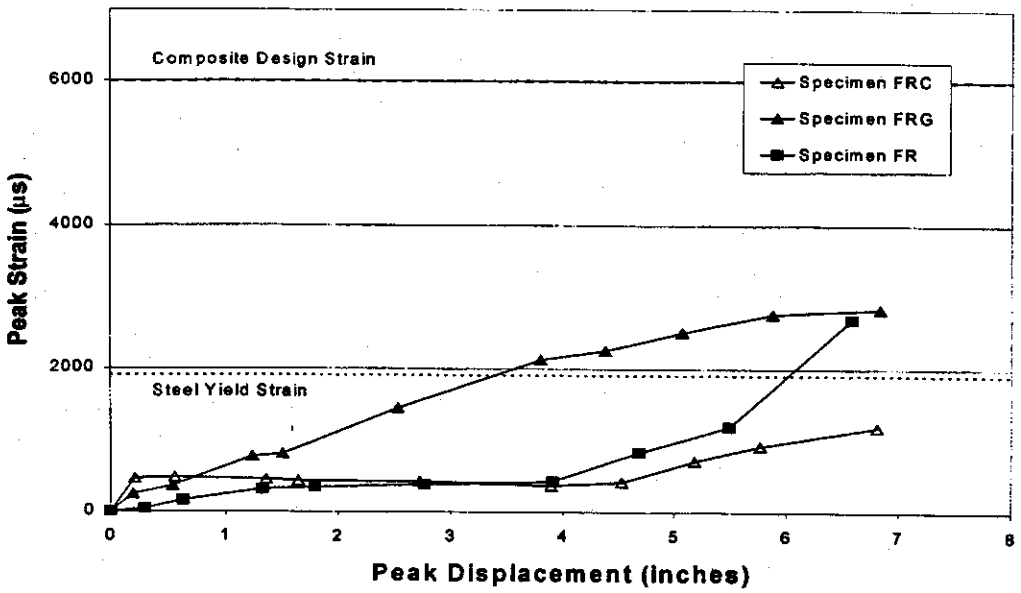

Figure 3 - 58 Jacket End Strain vs. Displacement at Elevation 533 mm (21 in) SG71

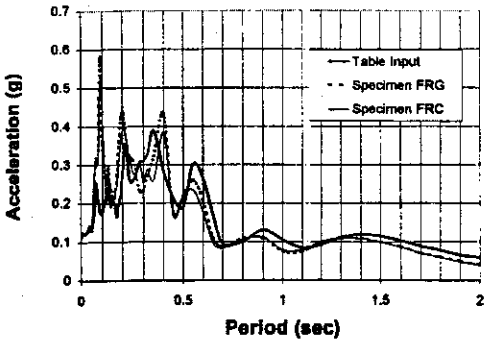

0.2 x Sylmar Event 1

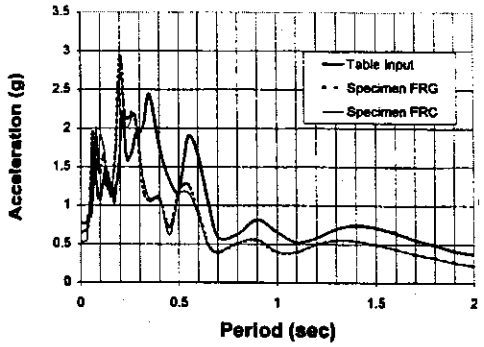

1.0 x Sylmar Event 4

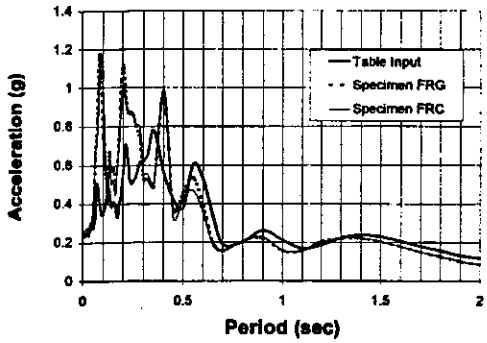

0.4 x Sylmar Event 2

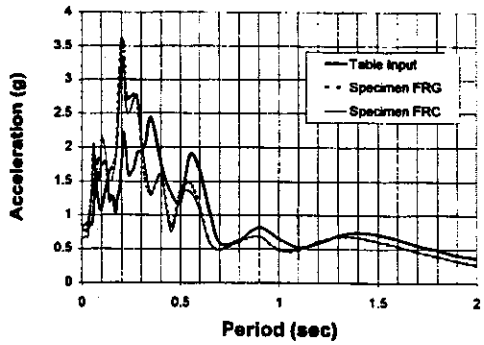

1.25 x Sylmar Event 5

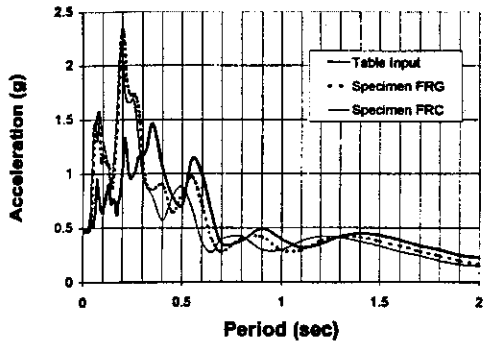

0.75 x Sylmar Event 3

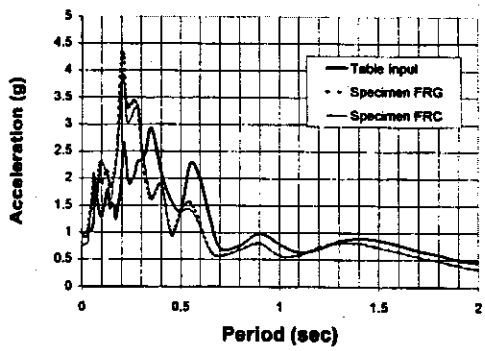

1.5 x Sylmar Event 6

Figure 4 - 1 Response Spectrum for Events 1-6 (Specimens FRG and FRC)

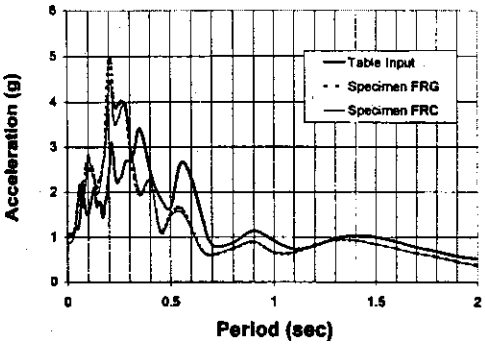

1.75 x Sylmar Event 7

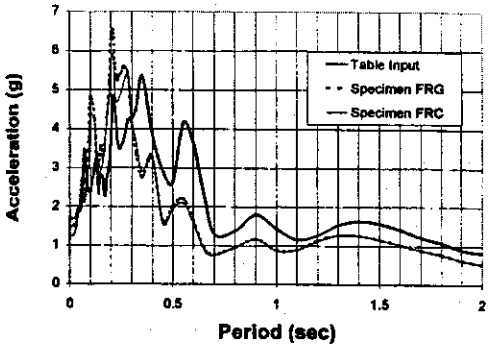

2.5 x Sylmar Event 10

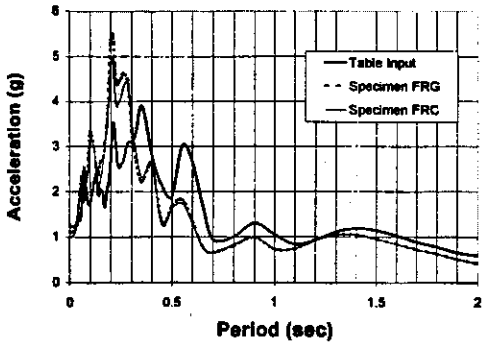

2.0 x Sylmar Event 8

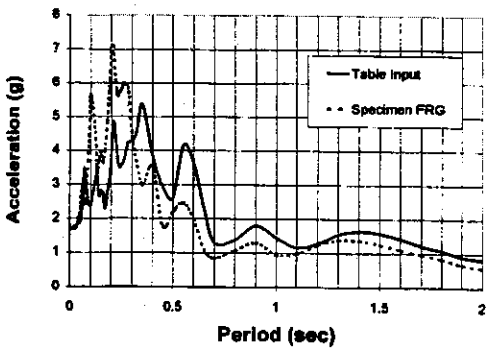

2.75 x Sylmar Event 11

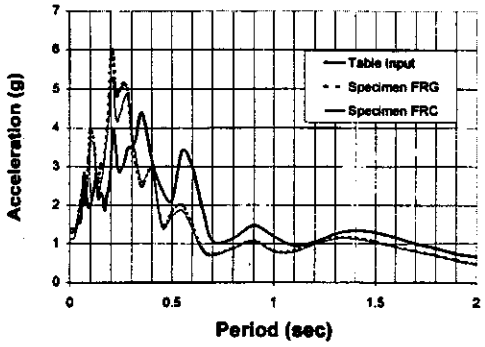

2.25 x Sylmar Event 9

Figure 4 - 2 Response Spectrum for Events 7-11 (Specimens FRG and FRC)

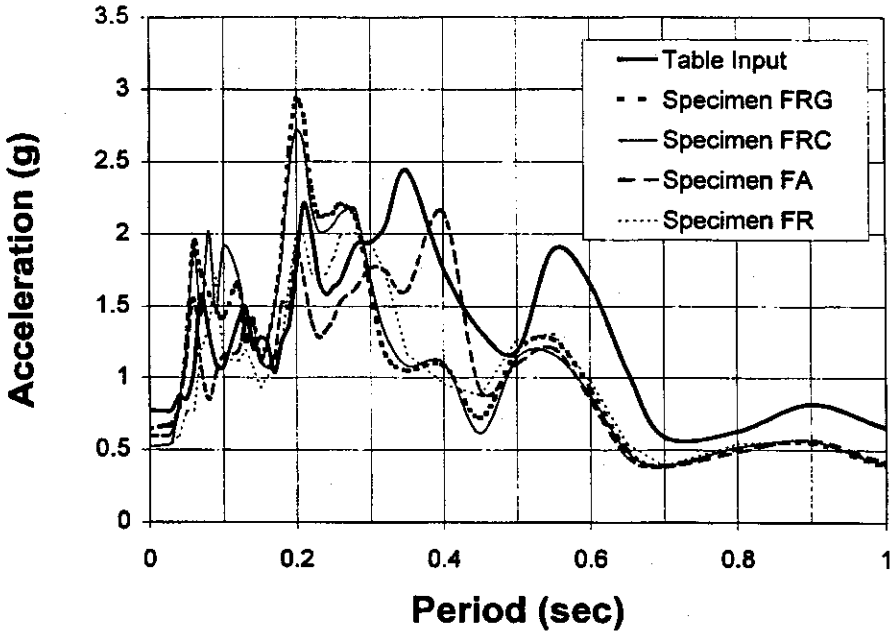

Figure 4 - 3 Response Spectra for Event 4 (1.0 x Sylmar) All Specimens

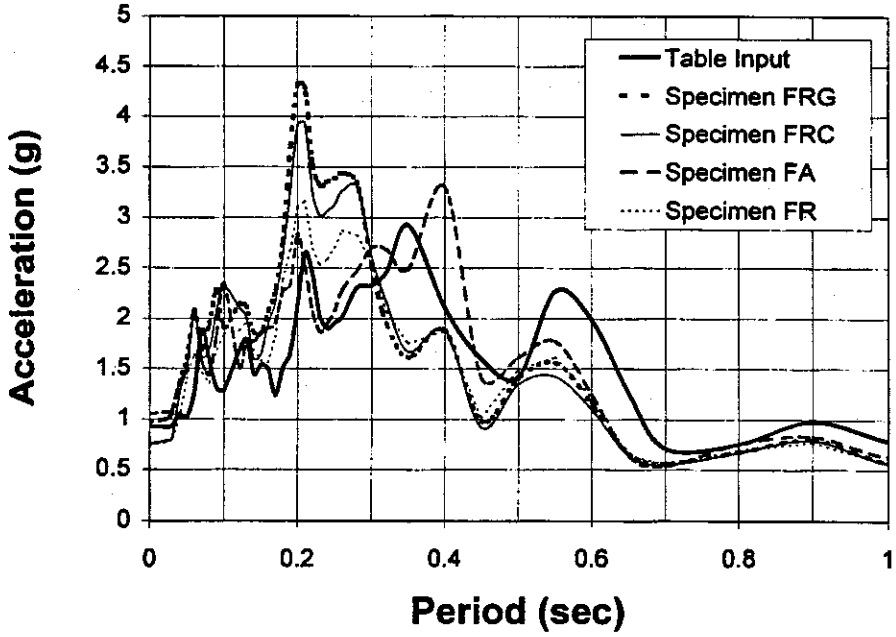

Figure 4 - 4 Response Spectra for Event 6 (1.5 x Sylmar) All Specimens

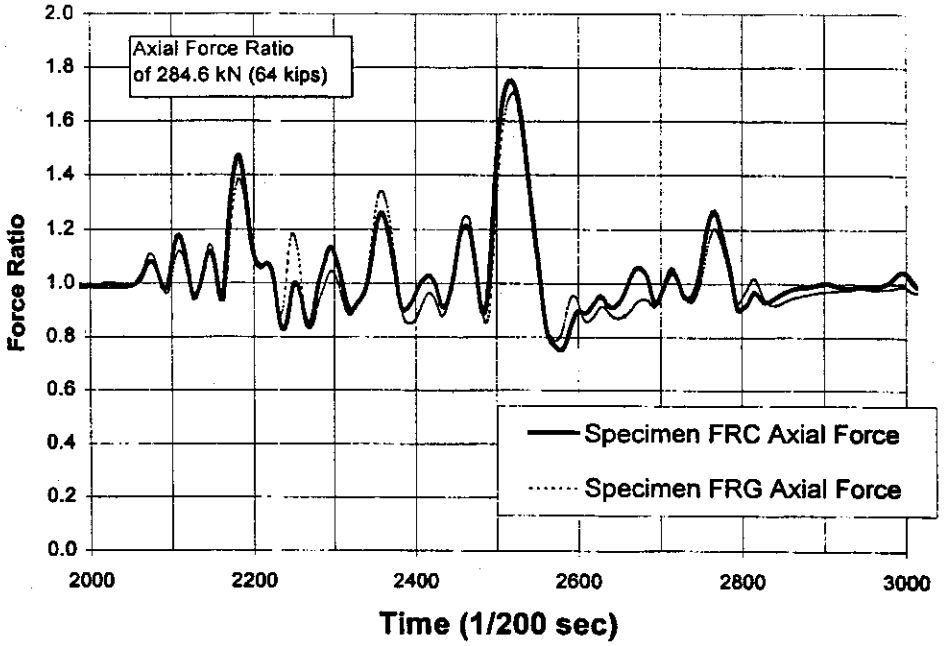

Figure 4 - 5 Comparison of Variation of Axial Load for Event 6 (FRG and FRC)

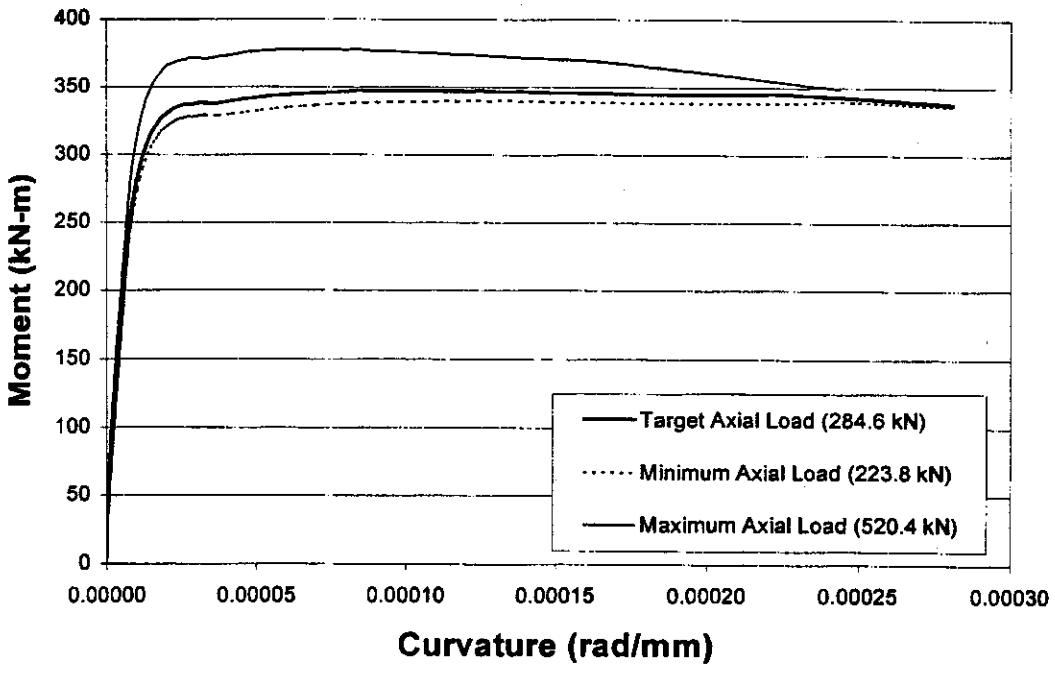

Figure 4 - 6 Variation in Moment-Curvature for Effect of Axial Load (FRG)

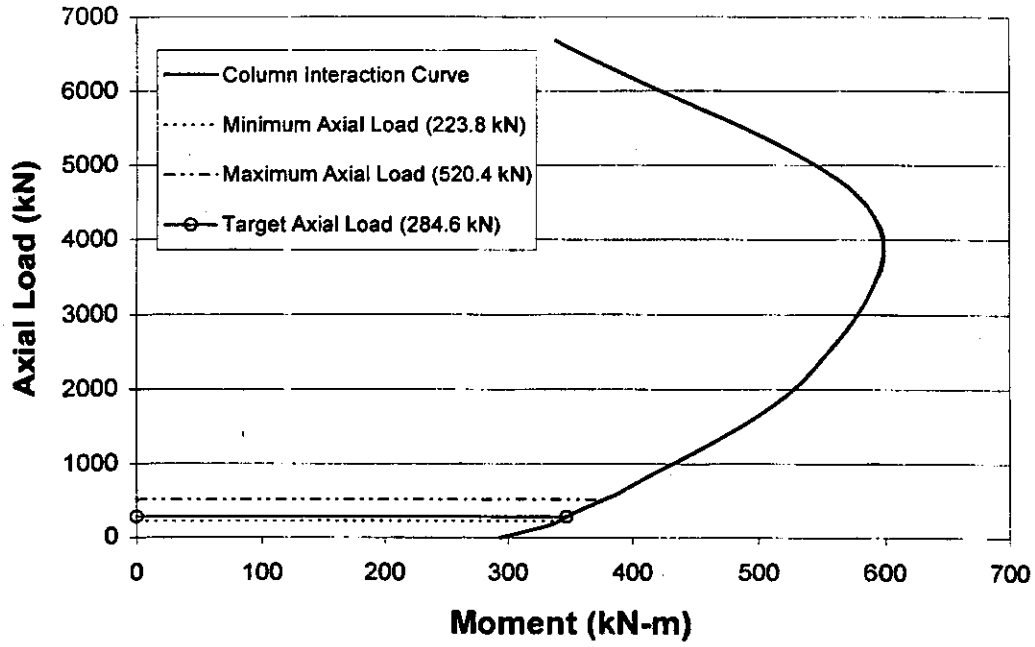

Figure 4 - 7 Column Interaction Diagram (FRG)

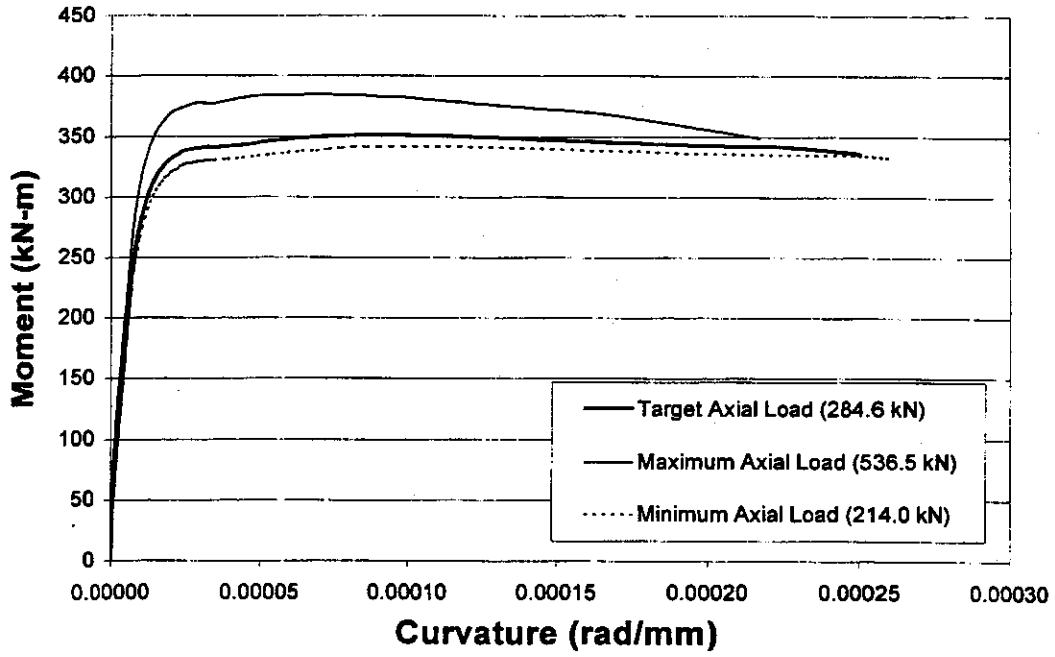

Figure 4 - 8 Variation of Moment-Curvature from Effect of Axial Load (FRC)

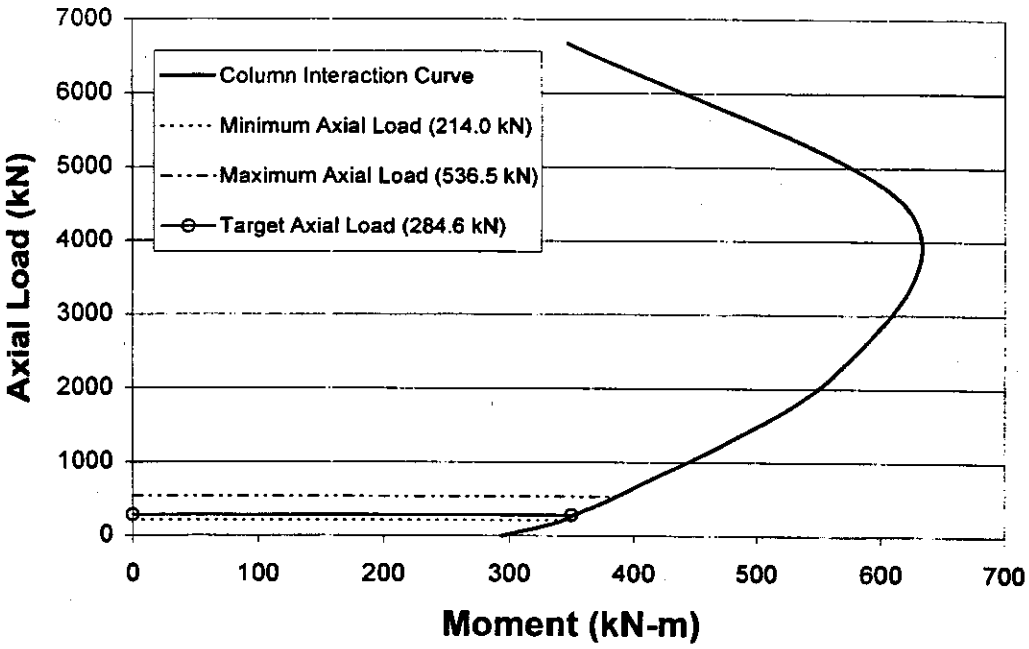

Figure 4 - 9 Column Interaction Diagram (FRC)

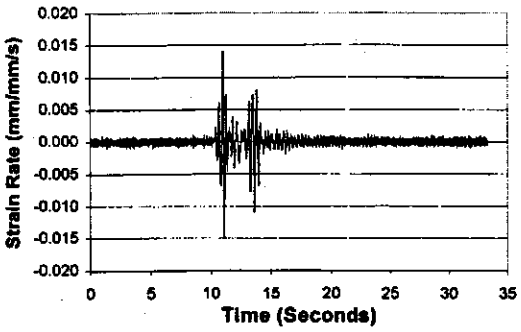

0.2 x Sylmar Event 1

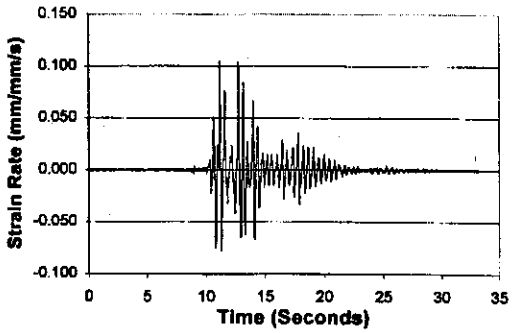

1.0 x Sylmar Event 4

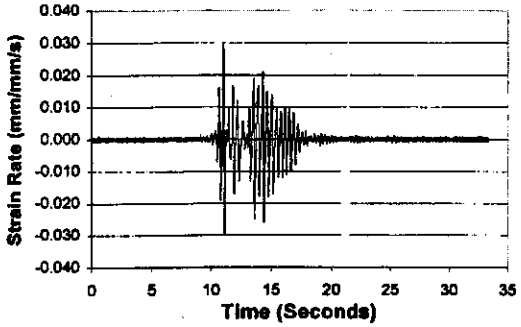

0.4 x Sylmar Event 2

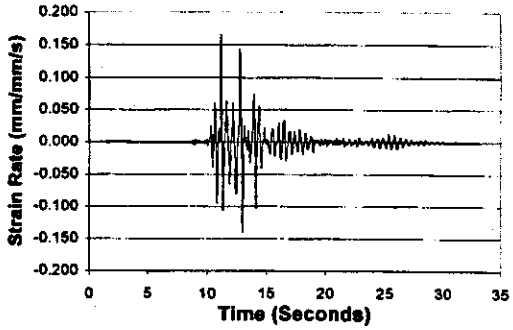

1.25 x Sylmar Event 5

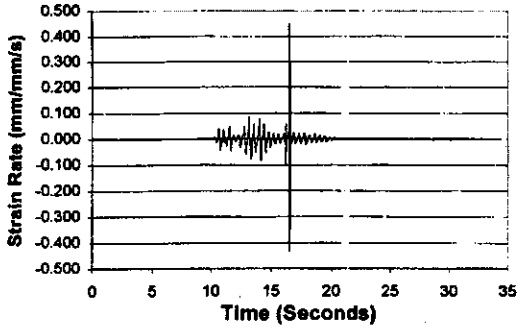

0.75 x Sylmar Event 3

Figure 4 - 10 Measured Strain Rate Events 1-5 (Specimen FRG)

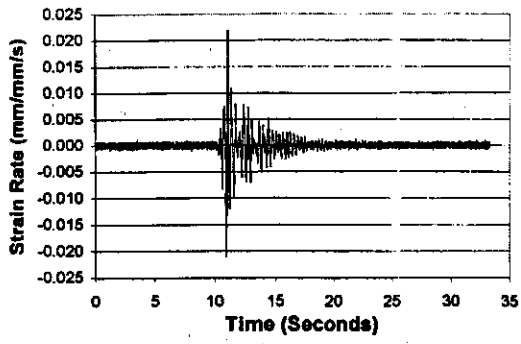

0.2 x Sylmar Event 1

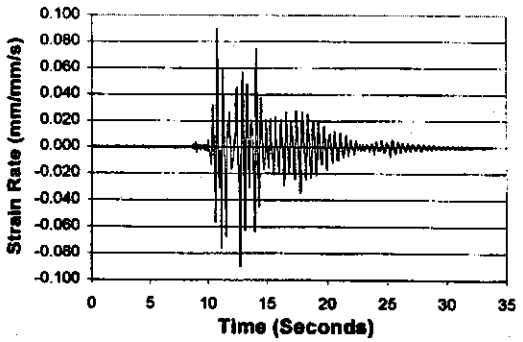

1.0 x Sylmar Event 4

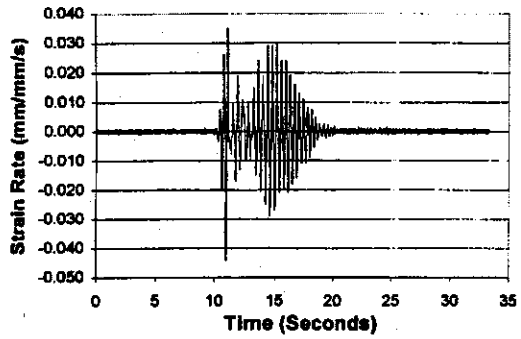

0.4 x Sylmar Event 2

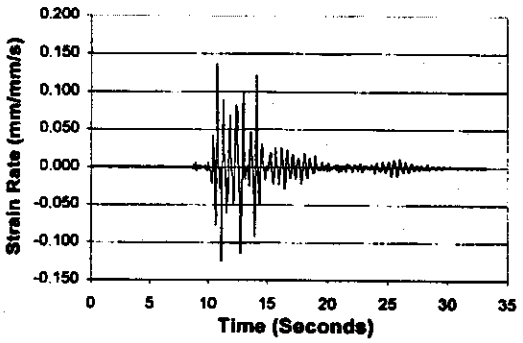

1.25 x Sylmar Event 5

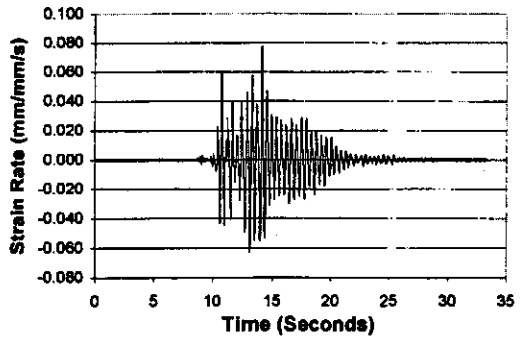

0.75 x Sylmar Event 3

Figure 4 - 11 Measured Strain Rate Events 1-5 (Specimen FRC)

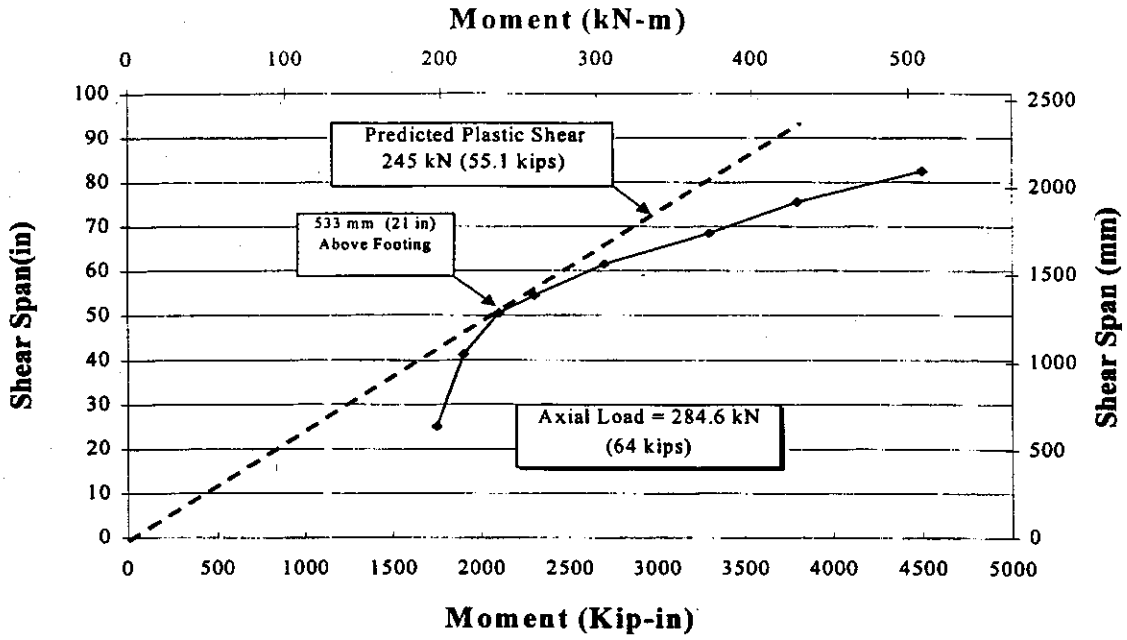

Figure 4 - 12 Predicted Moment Capacity (Specimen FRG)

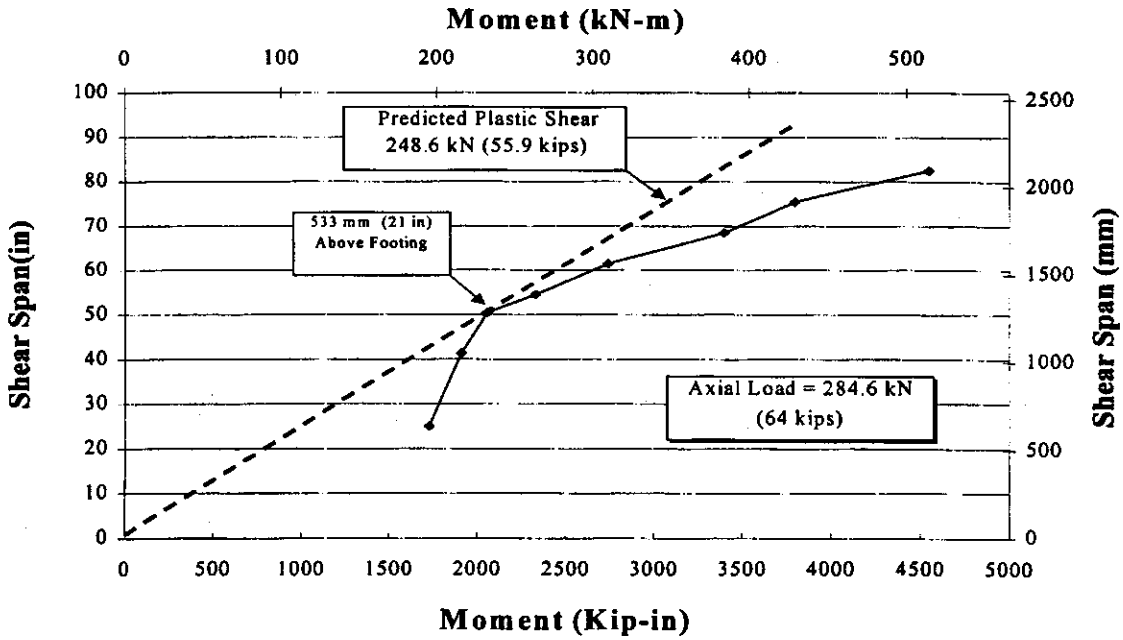

Figure 4 - 13 Predicted Moment Capacity (Specimen FRC)

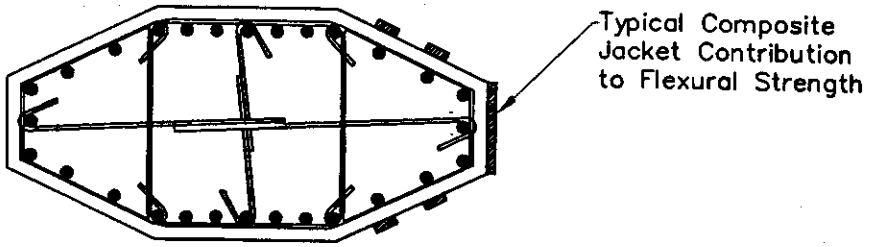

* Model Used in RCMC

Figure 4 - 14 Model of FRP Jacket for Flexural Enhancement in *RCMC*

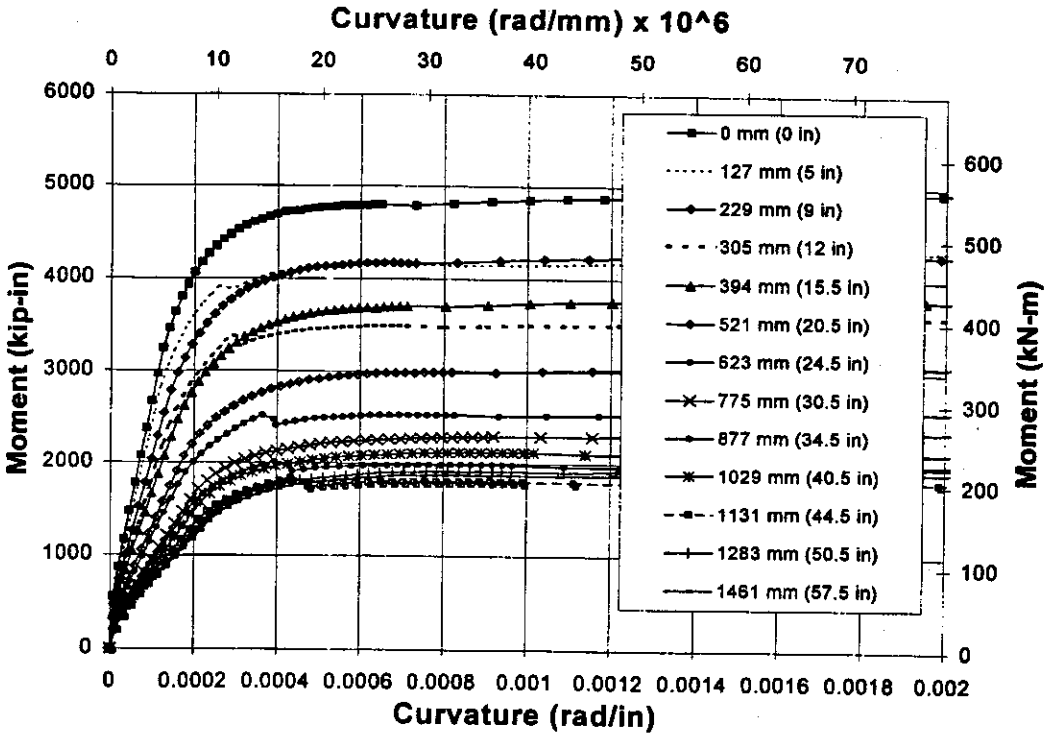

Figure 4 - 15 Moment vs. Curvature for Specimen FRG

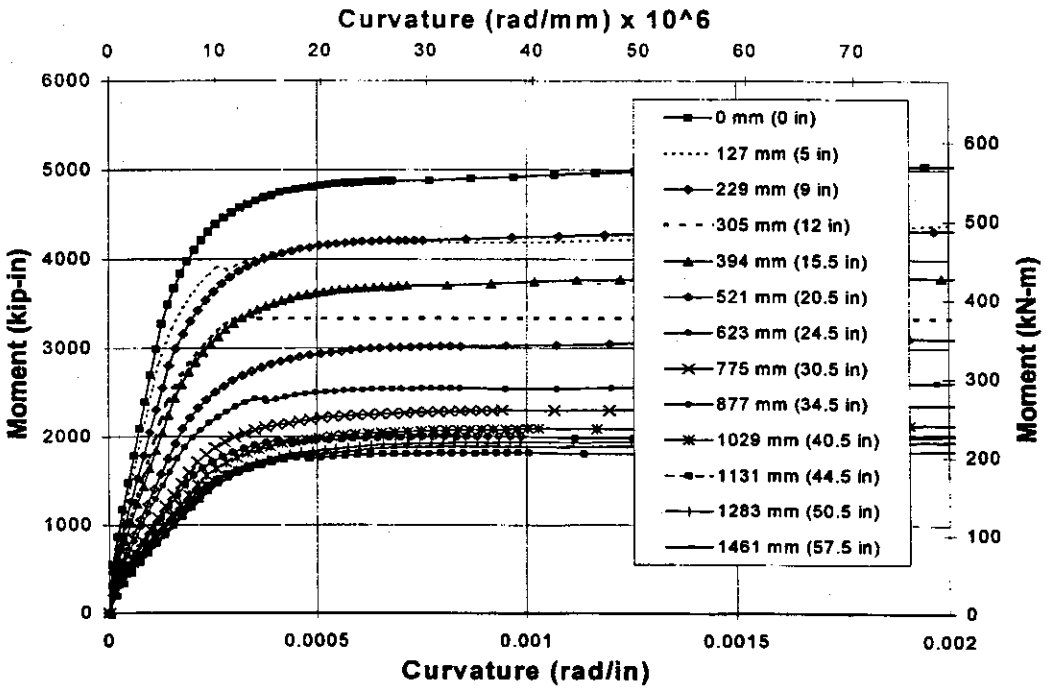

Figure 4 - 16 Moment vs. Curvature for Specimen FRC

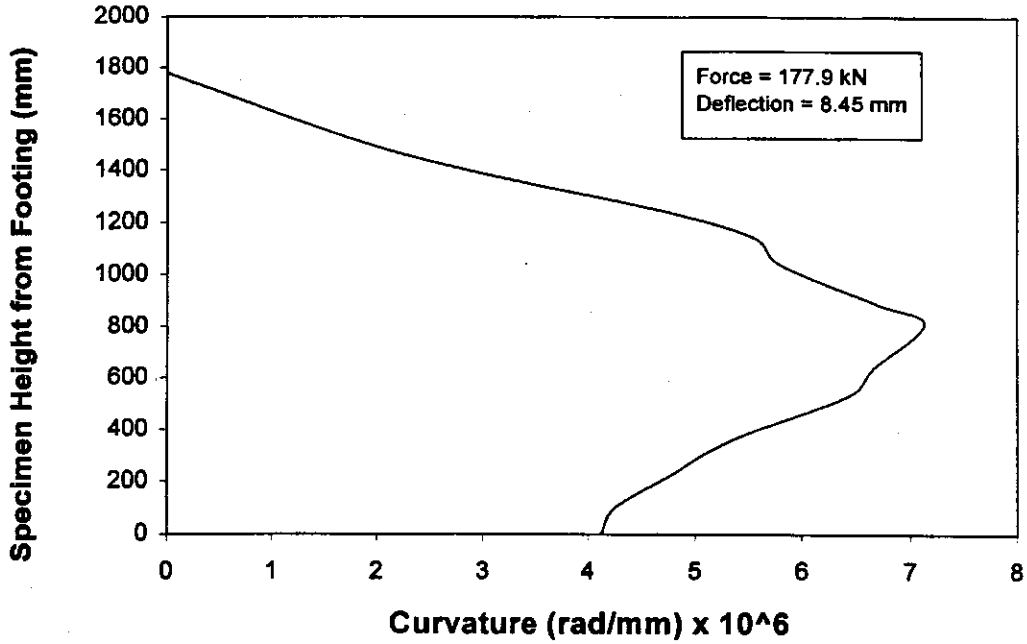

Figure 4 - 17 Calculated Curvature vs. Specimen Height for Flexural Deflection Calculation (Specimen FRG)

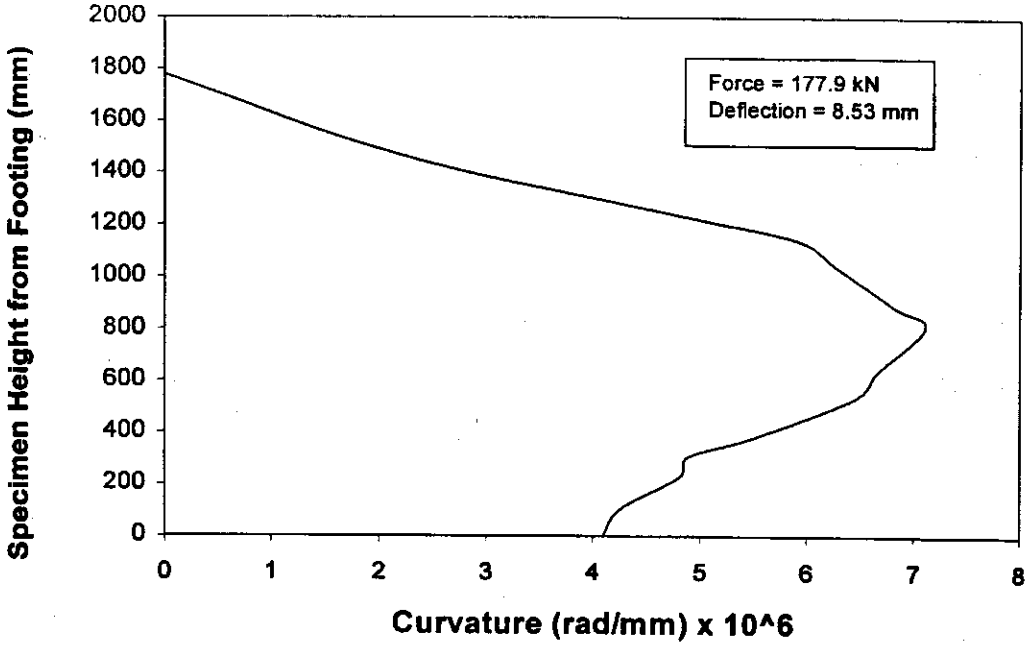

Figure 4 - 18 Calculated Curvature vs. Specimen Height for Flexural Deflection Calculation (Specimen FRC)

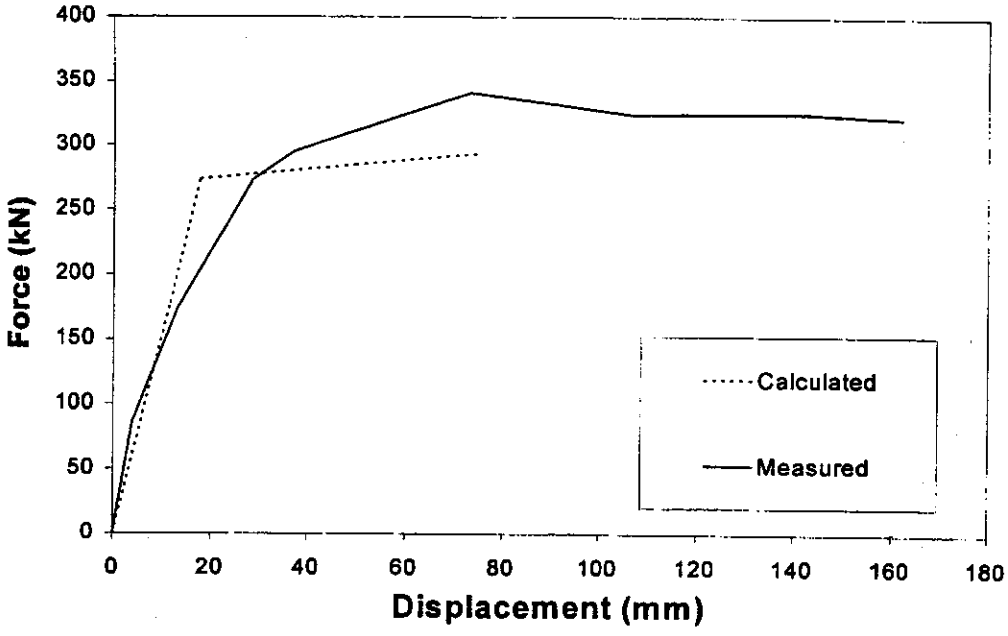

Figure 4 - 19 Comparison of Calculated Stiffness and Measured Force-Displacement Envelope (Specimen FRG)

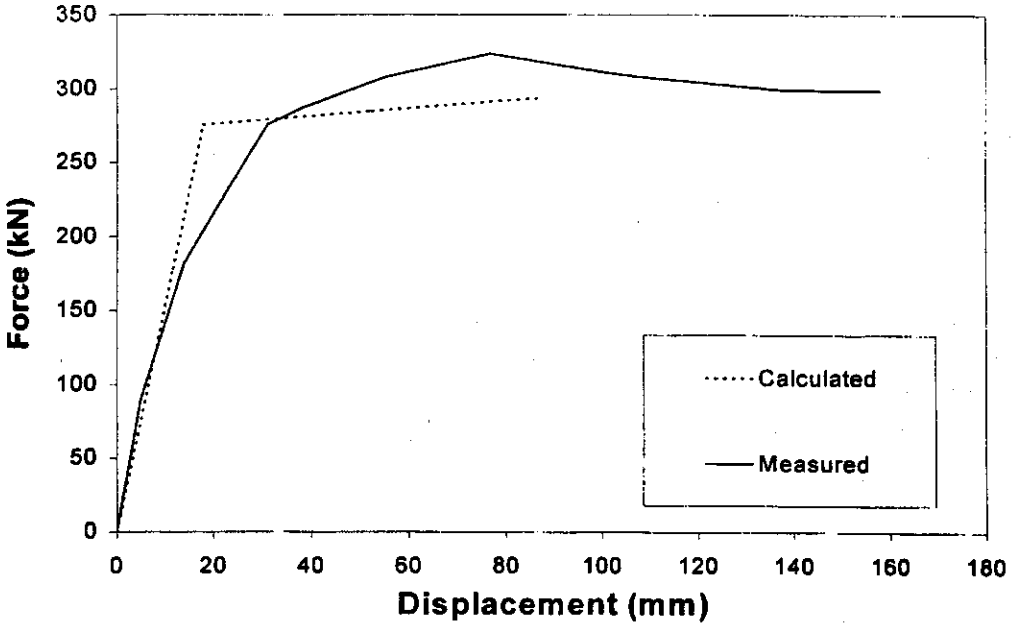

Figure 4 - 20 Comparison of Calculated Stiffness and Measured Force Displacement Envelope (Specimen FRC)

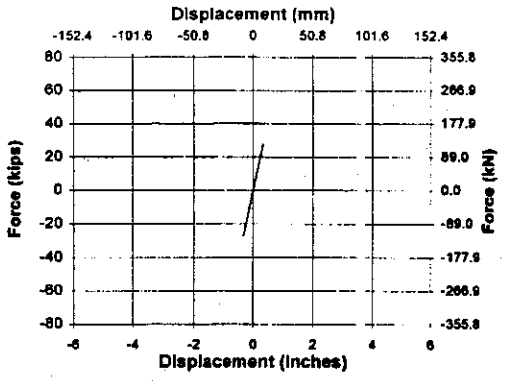

0.2 x Sylmar Event 1

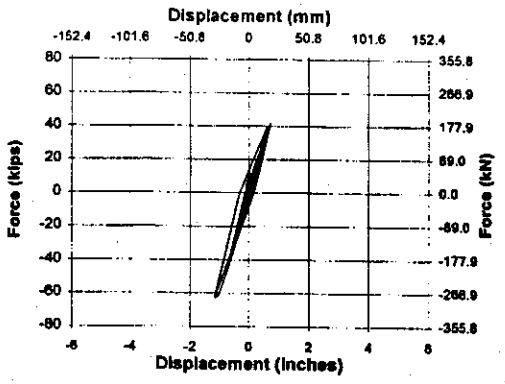

1.0 x Sylmar Event 4

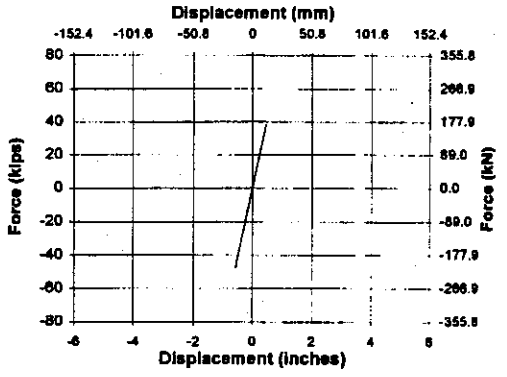

0.4 x Sylmar Event 2

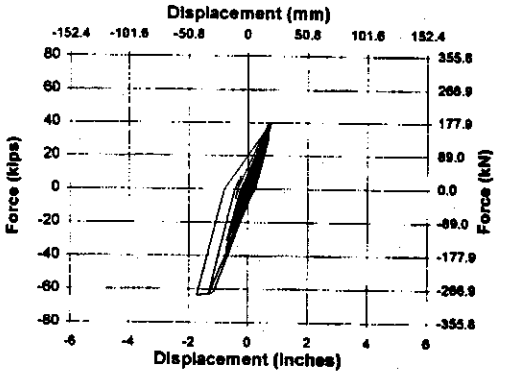

1.25 x Sylmar Event 5

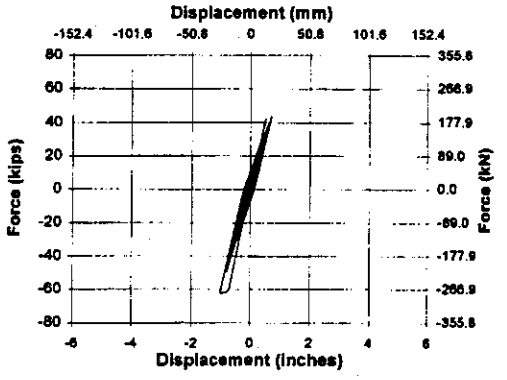

0.75 x Sylmar Event 3

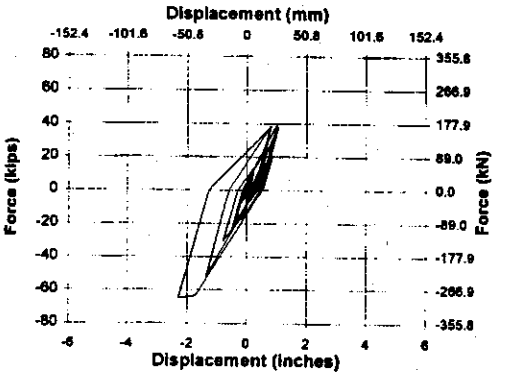

1.5 x Sylmar Event 6

Figure 4 - 21 Analytical Force vs. Displacement Hysteresis Events 1-6 (Specimen FRG)

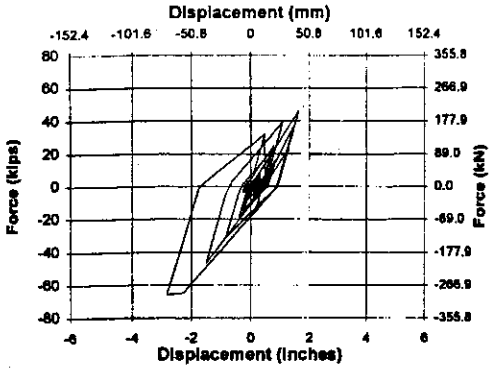

1.75 x Sylmar Event 7

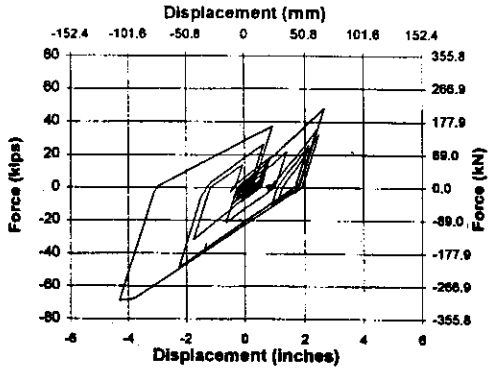

2.5 x Sylmar Event 10

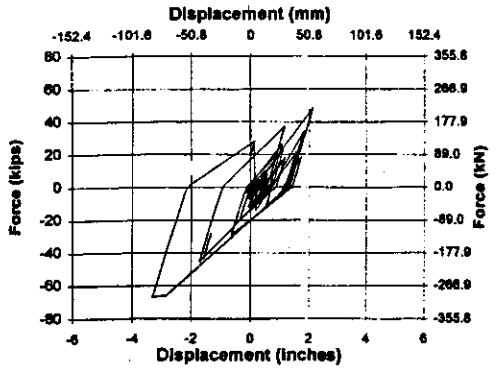

2.0 x Sylmar Event 8

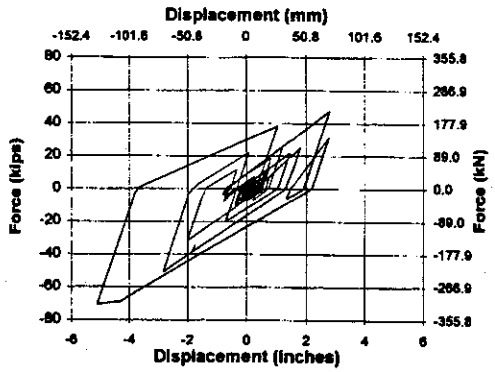

2.75 x Sylmar Event 11

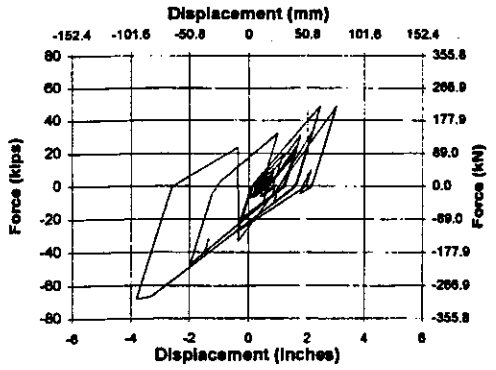

2.25 x Sylmar Event 9

Figure 4 - 22 Analytical Force vs. Displacement Hysteresis Events 7-11 (Specimen FRG)

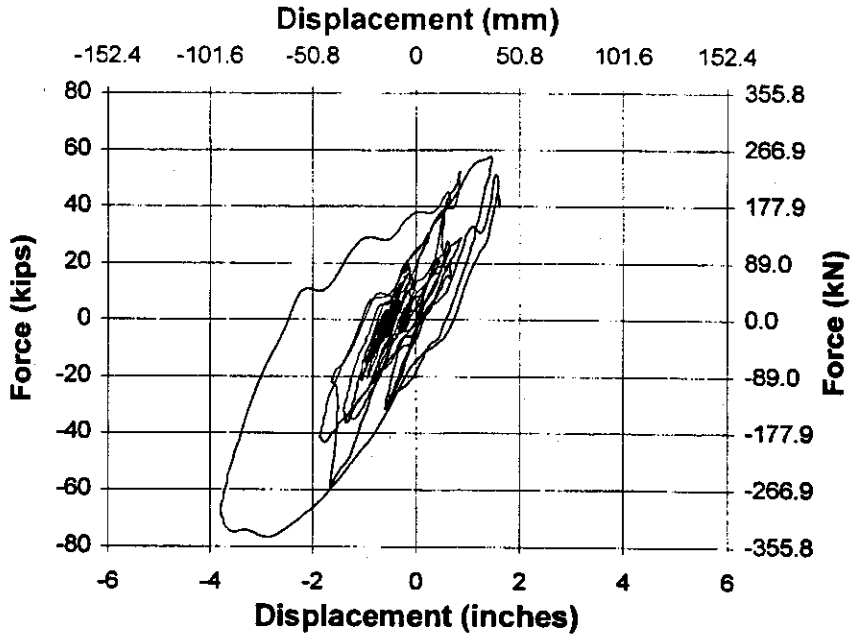

Figure 4 - 23 Measured Force vs. Displacement Hysteresis Event 6 (Specimen FRG)

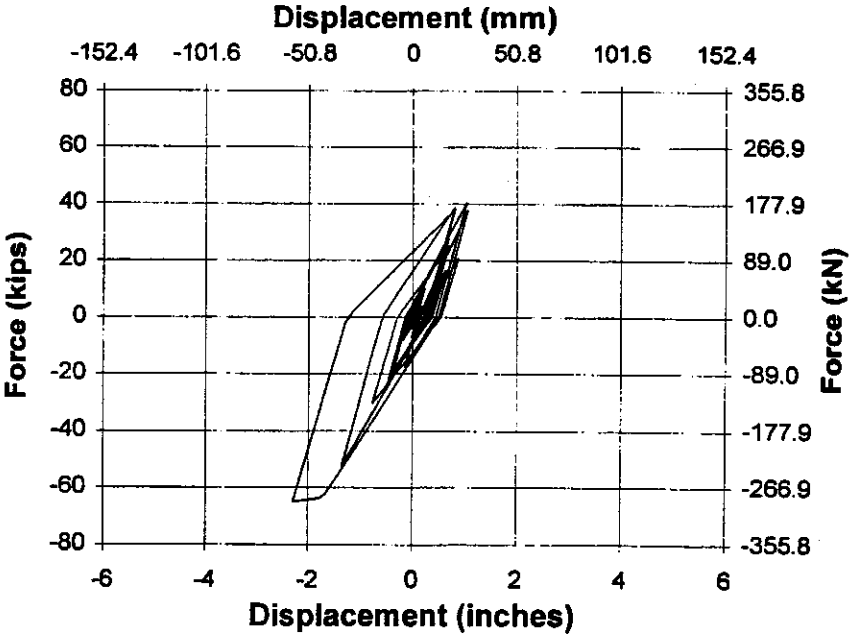

Figure 4 - 24 Calculated Force vs. Displacement Hysteresis Event 6 (Specimen FRG)

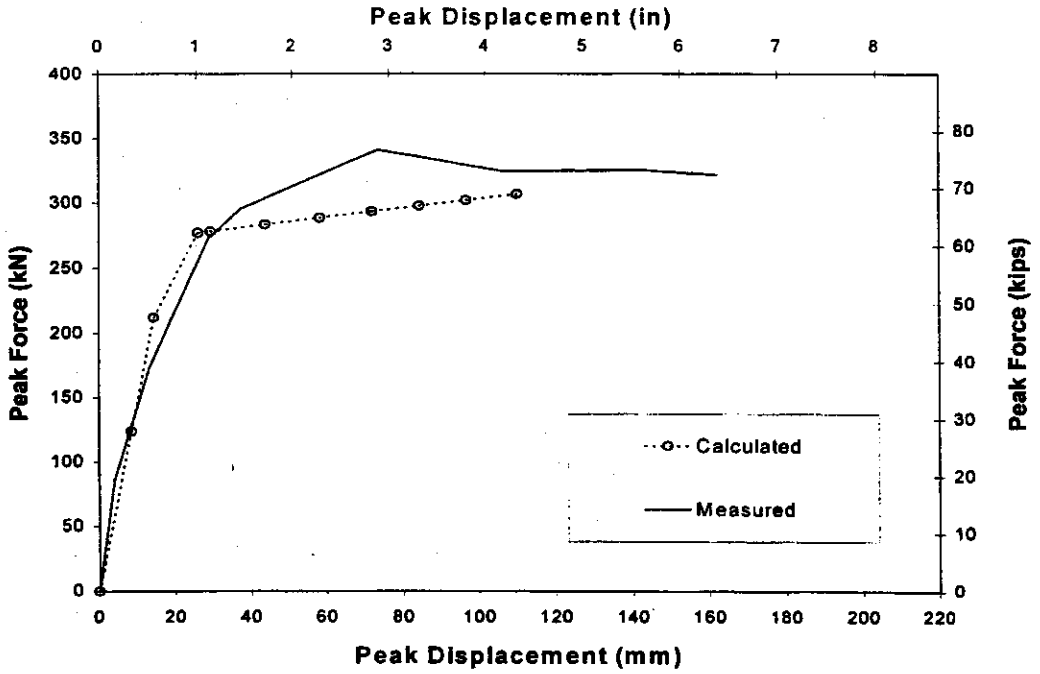

Figure 4 - 25 Comparison of Measured and Calculated Force-Displacement Envelopes (Specimen FRG)

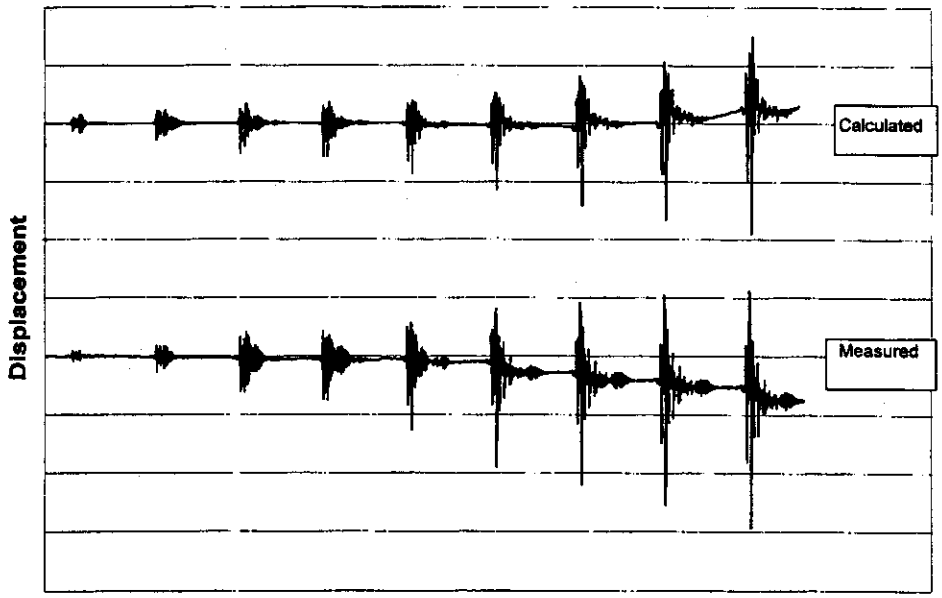

Figure 4 - 26 Measured and Calculated Combined Displacement Events 1-9 (Specimen FRG)

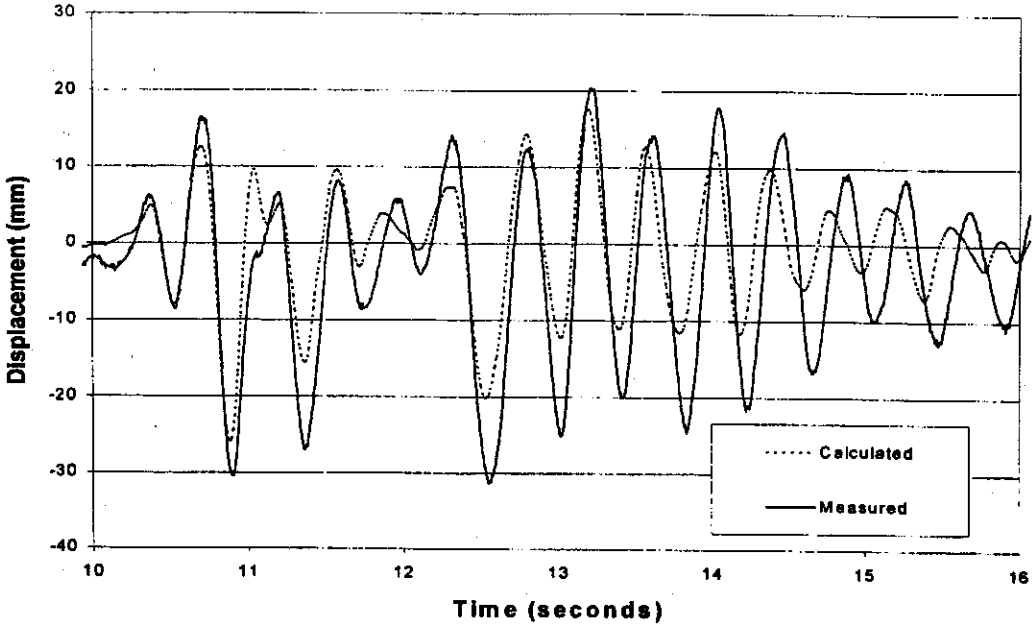

Figure 4 - 27 Calculated and Measured Displacement Histories for Event 3 from 10 to 16 seconds (Specimen FRG)

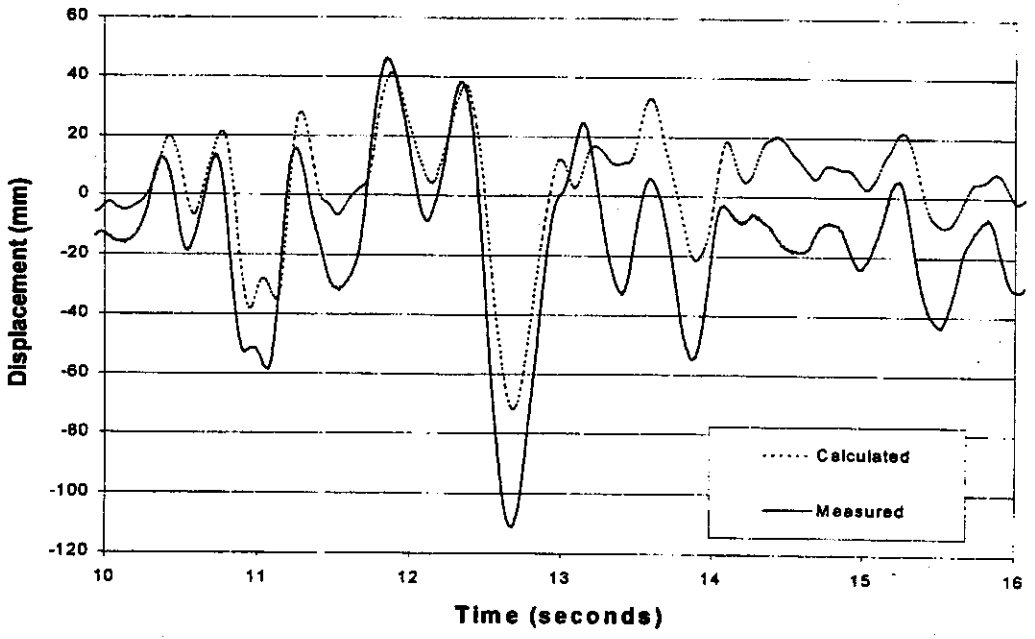

Figure 4 - 28 Calculated and Measured Displacement Histories for Event 7 from 10 to 16 seconds (Specimen FRG)

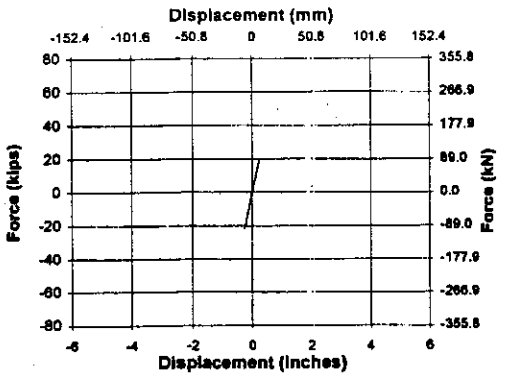

0.2 x Sylmar Event 1

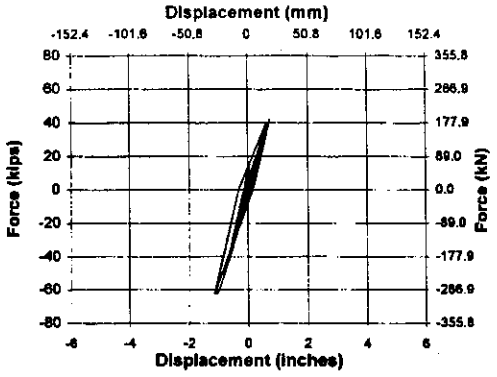

1.0 x Sylmar Event 4

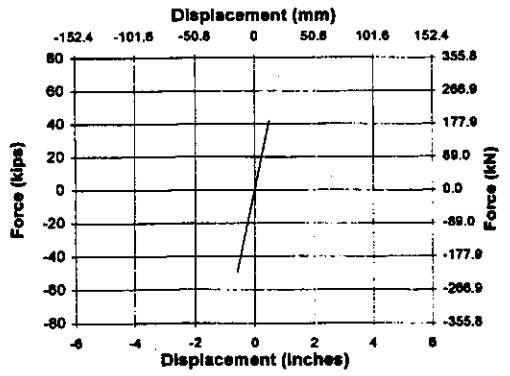

0.4 x Sylmar Event 2

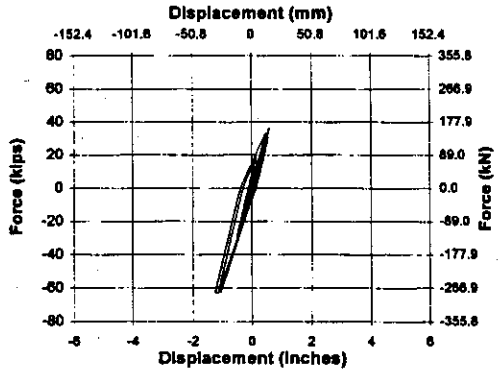

1.25 x Sylmar Event 5

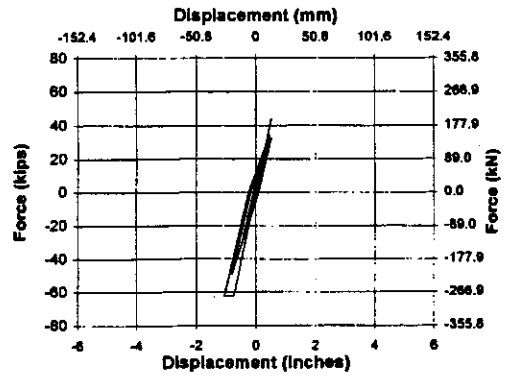

0.75 x Sylmar Event 3

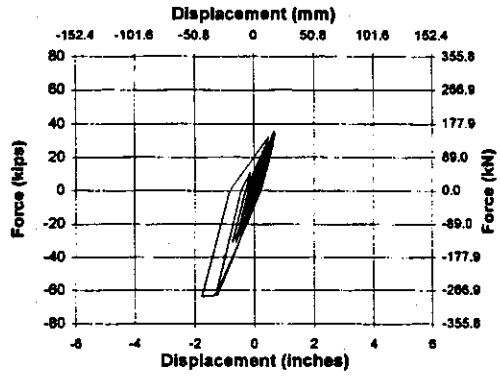

1.5 x Sylmar Event 6

Figure 4 - 29 Analytical Force vs. Displacement Hysteresis Events 1-6 (Specimen FRC)

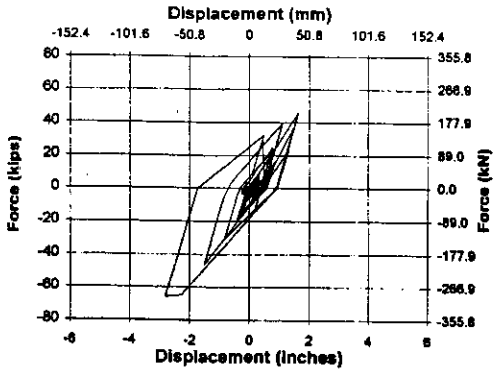

1.75 x Sylmar Event 7

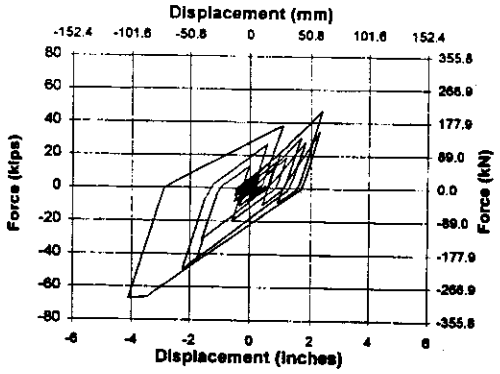

2.5 x Sylmar Event 10

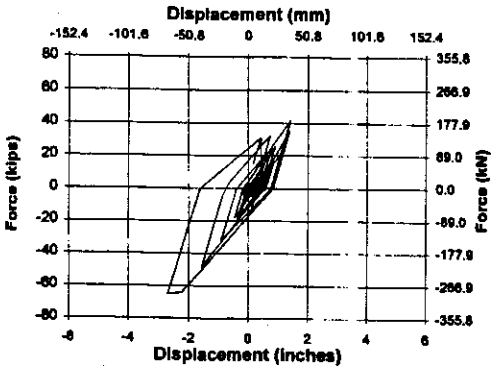

2.0 x Sylmar Event 8

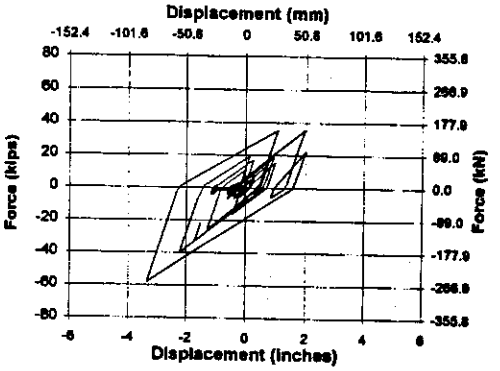

2.0 (2) x Sylmar Event 11

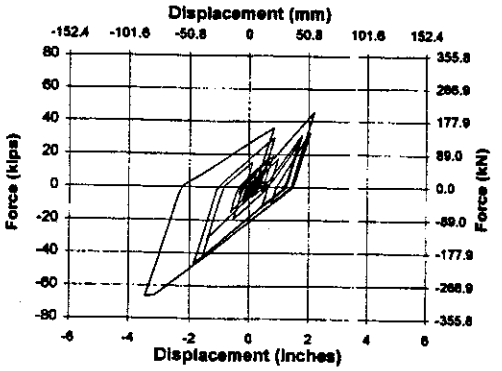

2.25 x Sylmar Event 9

Figure 4 - 30 Analytical Force vs. Displacement Hysteresis Events 7-11 (Specimen FRC)

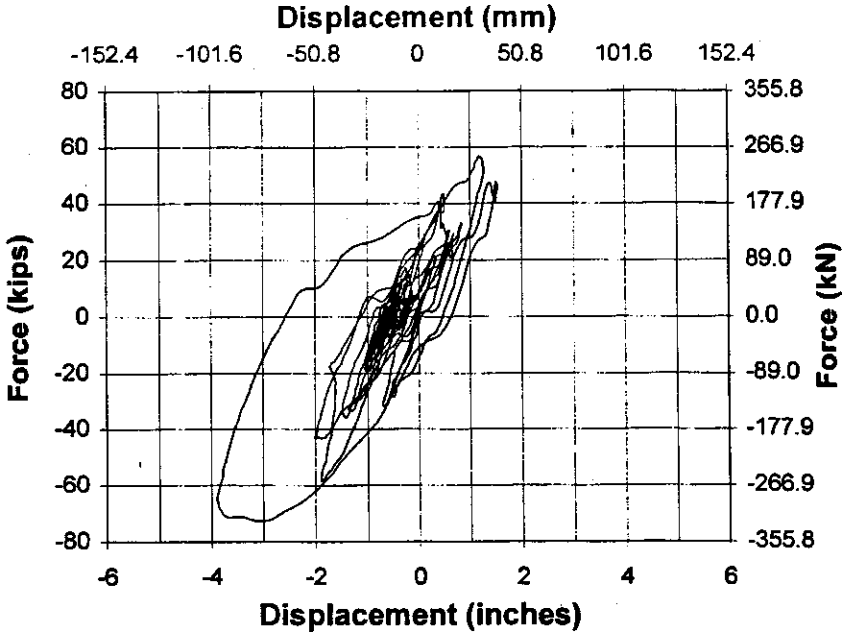

Figure 4 - 31 Measured Force vs. Displacement Hysteresis Event 6 (Specimen FRC)

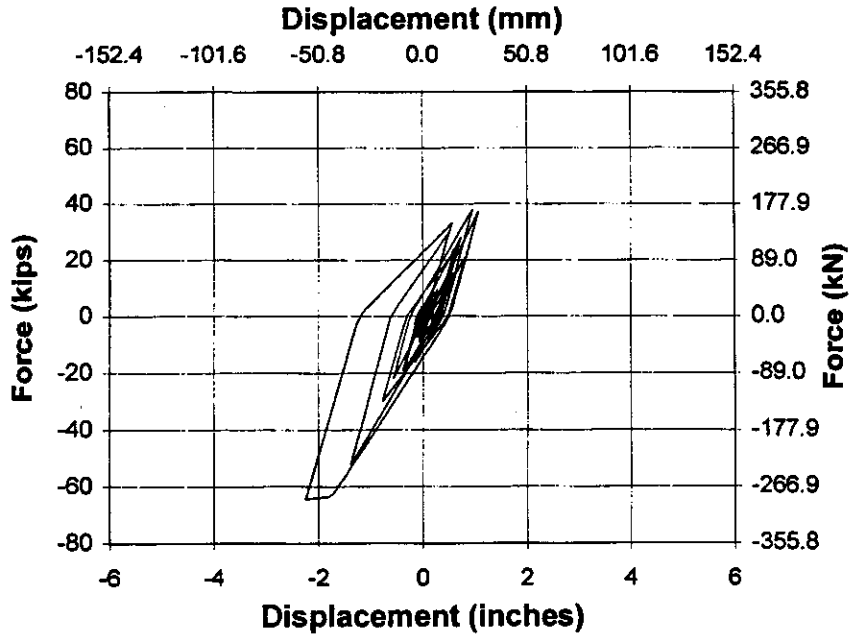

Figure 4 - 32 Calculated Force vs. Displacement Hysteresis Event 6 (Specimen FRC)

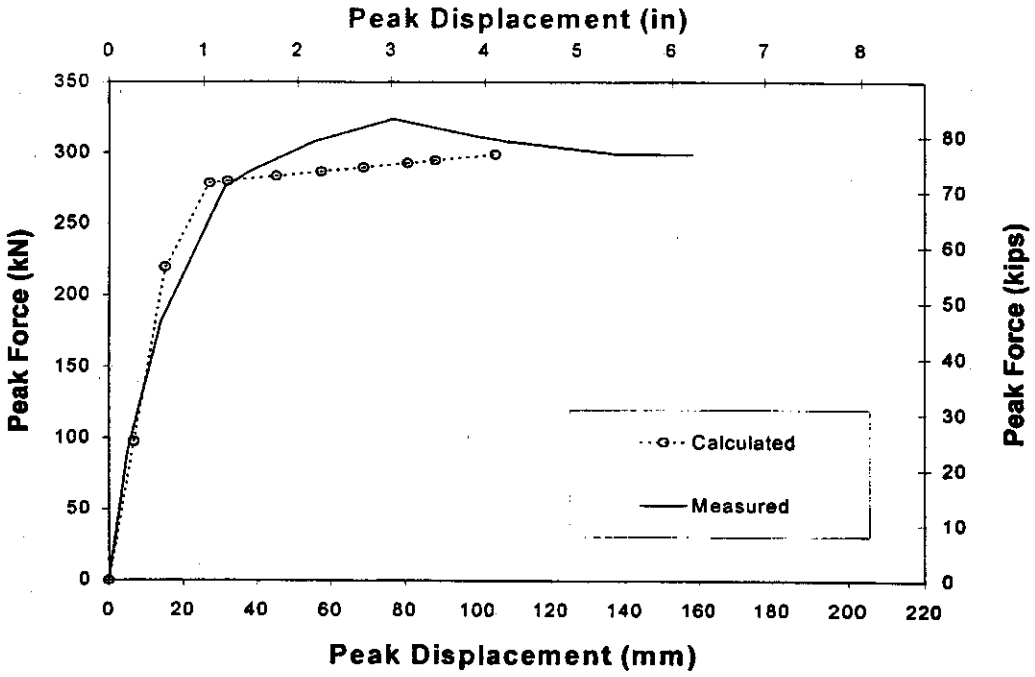

Figure 4 - 33 Comparison of Measured and Calculated Force-Displacement Envelopes (Specimen FRC)

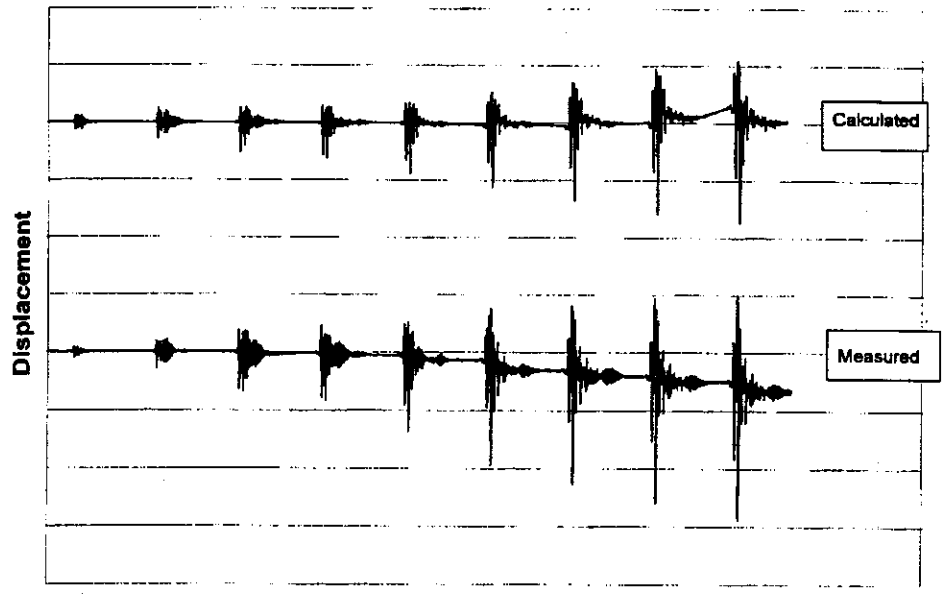

Figure 4 - 34 Measured and Calculated Combined Displacement Events 1-9 (Specimen FRC)

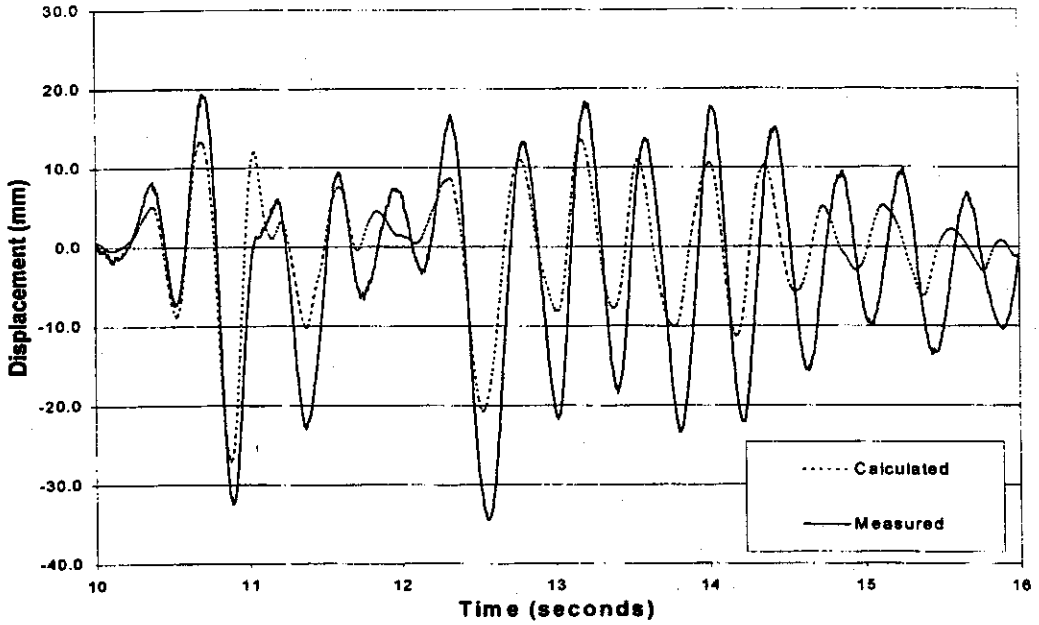

Figure 4 - 35 Calculated and Measured Displacement Histories for Event 3 from 10 to 16 seconds (Specimen FRC)

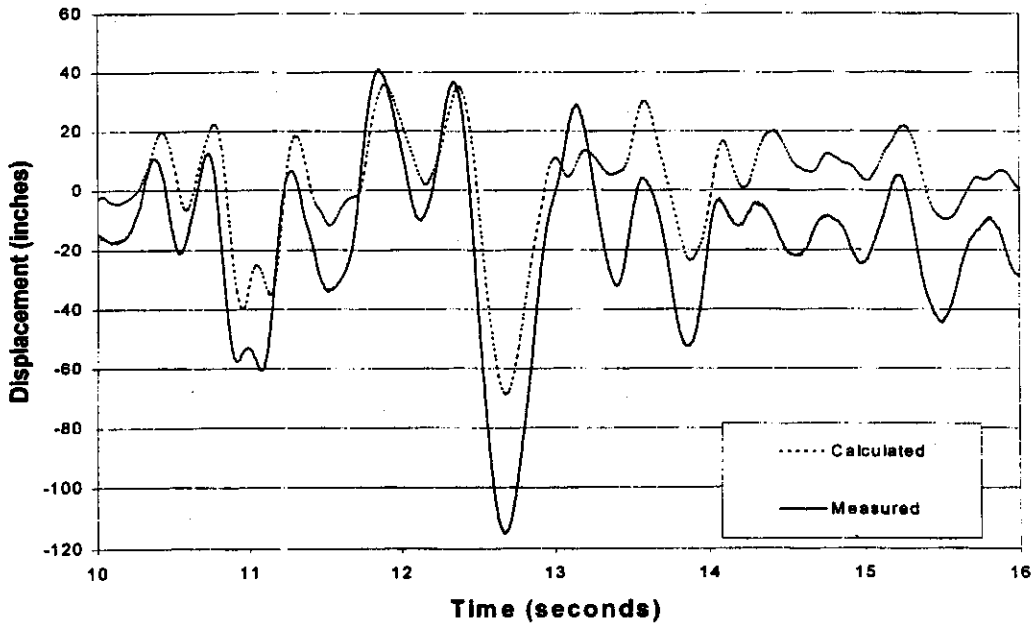

Figure 4 - 36 Calculated and Measured Displacement Histories for Event 7 from 10 to 16 seconds (Specimen FRC)

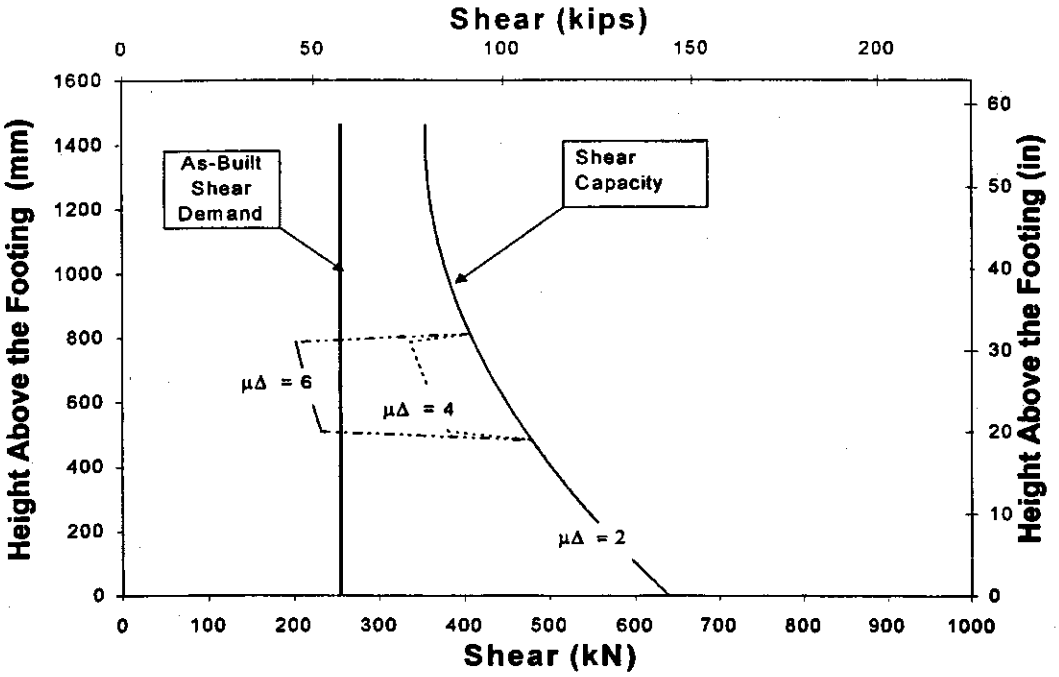

Figure 4 - 37 CALTRANS Shear Capacity over Height of Un-retrofitted Specimen

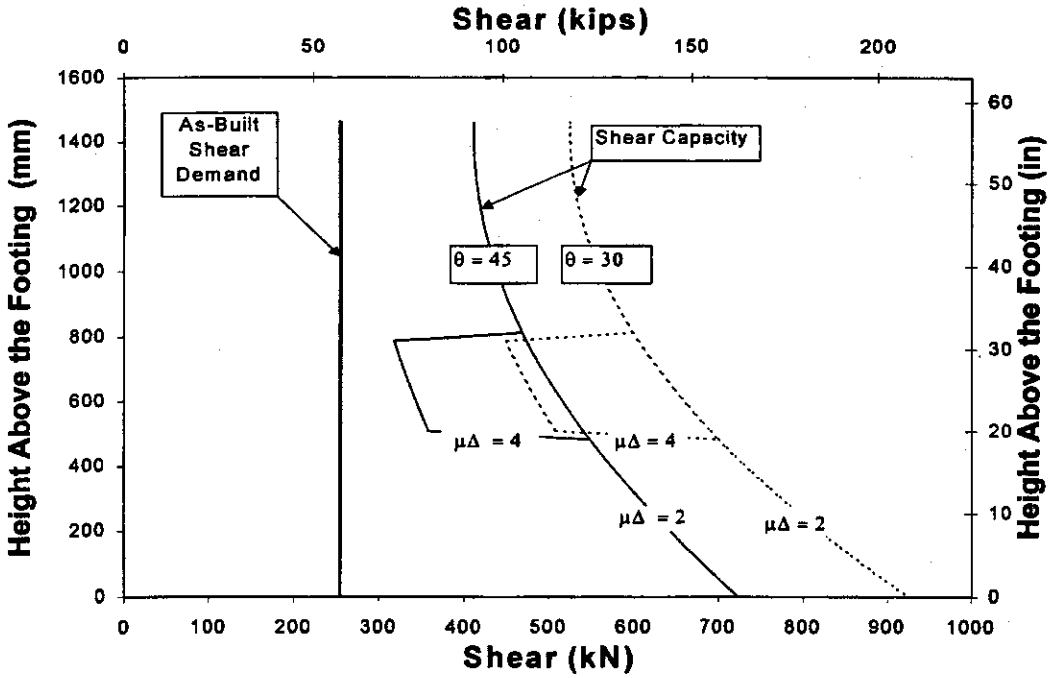

Figure 4 - 38 FHWA Shear Capacity over Height of Un-retrofitted Specimen

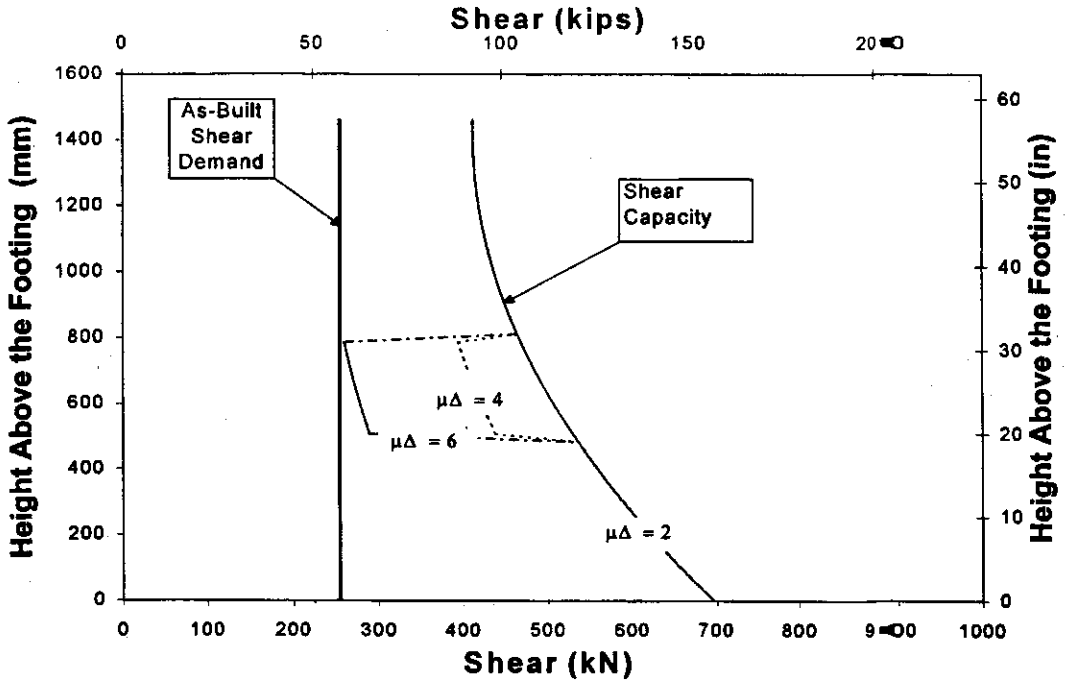

Figure 4 - 39 Wehbe Shear Capacity over Height of Un-retrofitted Specimen

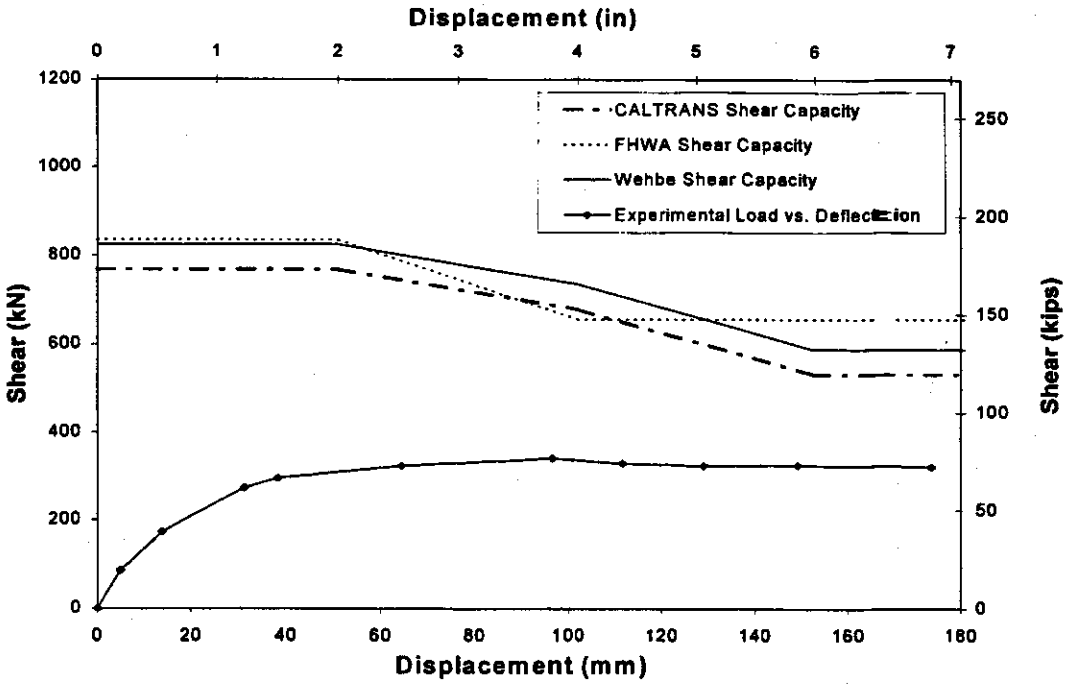

Figure 4 - 40 Shear Capacity of Specimen FRG at Plastic Hinge Region

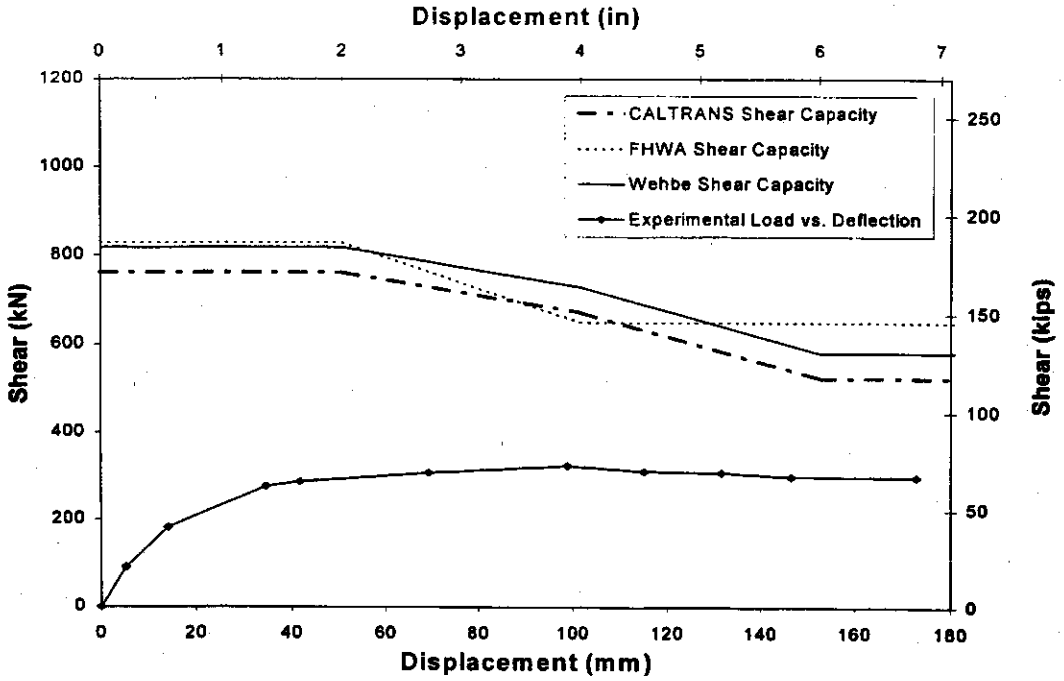

Figure 4 - 41 Shear Capacity of Specimen FRC at Plastic Hinge Region

LIST OF CENTER FOR CIVIL ENGINEERING EARTHQUAKE RESEARCH (CCEER) PUBLICATIONS

Report No.	Publication
CCEER-84-1	Saiidi, M., and R. Lawver, "User's Manual for LZAK-C64, A Computer Program to Implement the Q-Model on Commodore 64," Civil Engineering Department, Report No. CCEER-84-1, University of Nevada, Reno, January 1984.
CCEER-84-2	Douglas, B. and T. Iwasaki, "Proceedings of the First USA-Japan Bridge Engineering Workshop," held at the Public Works Research Institute, Tsukuba, Japan, Civil Engineering Department, Report No. CCEER-84-2, University of Nevada, Reno, April 1984.
CCEER-84-3	Saiidi, M., J. Hart, and B. Douglas, "Inelastic Static and Dynamic Analysis of Short R/C Bridges Subjected to Lateral Loads," Civil Engineering Department, Report No. CCEER-84-3, University of Nevada, Reno, July 1984.
CCEER-84-4	Douglas, B., "A Proposed Plan for a National Bridge Engineering Laboratory," Civil Engineering Department, Report No. CCEER-84-4, University of Nevada, Reno, December 1984.
CCEER-85-1	Norris, G. and P. Abdollaholiaee, "Laterally Loaded Pile Response: Studies with the Strain Wedge Model," Civil Engineering Department, Report No. CCEER-85-1, University of Nevada, Reno, April 1985.
CCEER-86-1	Ghusn, G. and M. Saiidi, "A Simple Hysteretic Element for Biaxial Bending of R/C Columns and Implementation in NEABS-86," Civil Engineering Department, Report No. CCEER-86-1, University of Nevada, Reno, July 1986.
CCEER-86-2	Saiidi, M., R. Lawver, and J. Hart, "User's Manual of ISADAB and SIBA, Computer Programs for Nonlinear Transverse Analysis of Highway Bridges Subjected to Static and Dynamic Lateral Loads," Civil Engineering Department, Report No. CCEER-86-2, University of Nevada, Reno, September 1986.
CCEER-87-1	Siddharthan, R., "Dynamic Effective Stress Response of Surface and Embedded Footings in Sand," Civil engineering Department, Report No. CCEER-86-2, University of Nevada, Reno, June 1987.
CCEER-87-2	Norris, G. and R. Sack, "Lateral and Rotational Stiffness of Pile Groups for Seismic Analysis of Highway Bridges," Civil Engineering Department, Report No. CCEER-87-2, University of Nevada, Reno, June 1987.
CCEER-88-1	Orie, J. and M. Saiidi, "A Preliminary Study of One-Way Reinforced Concrete Pier Hinges Subjected to Shear and Flexure," Civil Engineering Department, Report No. CCEER-88-1, University of Nevada, Reno, January 1988.
CCEER-88-2	Orie, D., M. Saiidi, and B. Douglas, "A Micro-CAD System for Seismic Design of Regular Highway Bridges," Civil Engineering Department, Report No. CCEER-88-2, University of Nevada, Reno, June 1988.
CCEER-88-3	Orie, D. and M. Saiidi, "User's Manual for Micro-SARB, a Microcomputer Program for Seismic Analysis of Regular Highway Bridges," Civil Engineering Department, Report No. CCEER-88-3, University of Nevada, Reno, October 1988.

CCEER-89-1 Douglas, B., M. Saiidi, R. Hayes, and G. Holcomb, "A Comprehensive Study of the Loads and Pressures Exerted on Wall Forms by the Placement of Concrete," Civil Engineering Department, Report No. CCEER-89-1, University of Nevada, Reno, February 1989.

CCEER-89-2 Richardson, J. and B. Douglas, "Dynamic Response Analysis of the Dominion Road Bridge Test Data," Civil Engineering Department, Report No. CCEER-89-2, University of Nevada, Reno, March 1989.

CCEER-89-2 Vrontinos, S., M. Saiidi, and B. Douglas, "A Simple Model to Predict the Ultimate Response of R/C Beams with Concrete Overlays," Civil Engineering Department, Report NO. CCEER-89-2, University of Nevada, Reno, June 1989.

CCEER-89-3 Ebrahimpour, A. and P. Jagadish, "Statistical Modeling of Bridge Traffic Loads - A Case Study," Civil Engineering Department, Report No. CCEER-89-3, University of Nevada, Reno, December 1989.

CCEER-89-4 Shields, J. and M. Saiidi, "Direct Field Measurement of Prestress Losses in Box Girder Bridges," Civil Engineering Department, Report No. CCEER-89-4, University of Nevada, Reno, December 1989.

CCEER-90-1 Saiidi, M., E. Maragakis, G. Ghusn, Y. Jiang, and D. Schwartz, "Survey and Evaluation of Nevada's Transportation Infrastructure, Task 7.2 - Highway Bridges, Final Report," Civil Engineering Department, Report No. CCEER 90-1, University of Nevada, Reno, October 1990.

CCEER-90-2 Abdel-Ghaffar, S., E. Maragakis, and M. Saiidi, "Analysis of the Response of Reinforced Concrete Structures During the Whittier Earthquake 1987," Civil Engineering Department, Report No. CCEER 90-2, University of Nevada, Reno, October 1990.

CCEER-91-1 Saiidi, M., E. Hwang, E. Maragakis, and B. Douglas, "Dynamic Testing and the Analysis of the Flamingo Road Interchange," Civil Engineering Department, Report No. CCEER-91-1, University of Nevada, Reno, February 1991.

CCEER-91-2 Norris, G., R. Siddharthan, Z. Zafir, S. Abdel-Ghaffar, and P. Gowda, "Soil-Foundation-Structure Behavior at the Oakland Outer Harbor Wharf," Civil Engineering Department, Report No. CCEER-91-2, University of Nevada, Reno, July 1991.

CCEER-91-3 Norris, G., "Seismic Lateral and Rotational Pile Foundation Stiffnesses at Cypress," Civil Engineering Department, Report No. CCEER-91-3, University of Nevada, Reno, August 1991.

CCEER-91-4 O'Connor, D. and M. Saiidi, "A Study of Protective Overlays for Highway Bridge Decks in Nevada, with Emphasis on Polyester-Styrene Polymer Concrete," Civil Engineering Department, Report No. CCEER-91-4, University of Nevada, Reno, October 1991.

CCEER-91-5 O'Connor, D.N. and M. Saiidi, "Laboratory Studies of Polyester-Styrene Polymer Concrete Engineering Properties," Civil Engineering Department, Report No. CCEER-91-5, University of Nevada, Reno, November 1991.

CCEER-92-1 Straw, D.L. and M. Saiidi, "Scale Model Testing of One-Way Reinforced Concrete Pier Hinges Subject to Combined Axial Force, Shear and Flexure," edited by D.N. O'Connor, Civil Engineering Department, Report No. CCEER-92-1, University of Nevada, Reno, March 1992.

CCEER-92-2 Wehbe, N., M. Saiidi, and F. Gordaninejad, "Basic Behavior of Composite Sections Made of Concrete Slabs and Graphite Epoxy Beams," Civil Engineering Department, Report No. CCEER-92-2, University of Nevada, Reno, August 1992.

CCEER-92-3 Saiidi, M. and E. Hutchens, "A Study of Prestress Changes in A Post-Tensioned Bridge During the First 30 Months," Civil Engineering Department, Report No. CCEER-92-3, University of Nevada, Reno, April 1992.

CCEER-92-4 Saiidi, M., B. Douglas, S. Feng, E. Hwang, and E. Maragakis, "Effects of Axial Force on Frequency of Prestressed Concrete Bridges," Civil Engineering Department, Report No. CCEER-92-4, University of Nevada, Reno, August 1992.

CCEER-92-5 Siddharthan, R., and Z. Zafir, "Response of Layered Deposits to Traveling Surface Pressure Waves," Civil Engineering Department, Report No. CCEER-92-5, University of Nevada, Reno, September 1992.

CCEER-92-6 Norris, G., and Z. Zafir, "Liquefaction and Residual Strength of Loose Sands from Drained Triaxial Tests," Civil Engineering Department, Report No. CCEER-92-6, University of Nevada, Reno, September 1992.

CCEER-92-7 Douglas, B., "Some Thoughts Regarding the Improvement of the University of Nevada, Reno's National Academic Standing," Civil Engineering Department, Report No. CCEER-92-7, University of Nevada, Reno, September 1992.

CCEER-92-8 Saiidi, M., E. Maragakis, and S. Feng, "An Evaluation of the Current Caltrans Seismic Restrainer Design Method," Civil Engineering Department, Report No. CCEER-92-8, University of Nevada, Reno, October 1992.

CCEER-92-9 O'Connor, D., M. Saiidi, and E. Maragakis, "Effect of Hinge Restrainers on the Response of the Madrone Drive Undercrossing During the Loma Prieta Earthquake," Civil Engineering Department, Report No. CCEER-92-9, University of Nevada, Reno, February 1993.

CCEER-92-10 O'Connor, D., and M. Saiidi, "Laboratory Studies of Polyester Concrete: Compressive Strength at Elevated Temperatures and Following Temperature Cycling, Bond Strength to Portland Cement Concrete, and Modulus of Elasticity," Civil Engineering Department, Report No. CCEER-92-10, University of Nevada, Reno, February 1993.

CCEER-92-11 Wehbe, N., M. Saiidi, and D. O'Connor, "Economic Impact of Passage of Spent Fuel Traffic on Two Bridges in Northeast Nevada," Civil Engineering Department, Report No. CCEER-92-11, University of Nevada, Reno, December 1992.

CCEER-93-1 Jiang, Y., and M. Saiidi, "Behavior, Design, and Retrofit of Reinforced Concrete One-way Bridge Column Hinges," edited by D. O'Connor, Civil Engineering Department, Report No. CCEER-93-1, University of Nevada, Reno, March 1993.

CCEER-93-2 Abdel-Ghaffar, S., E. Maragakis, and M. Saiidi, "Evaluation of the Response of the Aptos Creek Bridge During the 1989 Loma Prieta Earthquake," Civil Engineering Department, Report No. CCEER-93-2, University of Nevada, Reno, June 1993.

CCEER-93-3 Sanders, D.H., B.M. Douglas, and T.L. Martin, "Seismic Retrofit Prioritization of Nevada Bridges,"

Civil Engineering Department, Report No. CCEER-93-3, University of Nevada, Reno, July 1993.

CCEER-93-4 Abdel-Ghaffar, S., E. Maragakis, and M. Saiidi, "Performance of Hinge Restrainers in the Huntington Avenue Overhead During the 1989 Loma Prieta Earthquake," Civil Engineering Department, Report No. CCEER-93-4, University of Nevada, Reno, June 1993.

CCEER-93-5 Maragakis, E., M. Saiidi, S. Feng, and L. Flournoy, "Effects of Hinge Restrainers on the Response of the San Gregorio Bridge During the Loma Prieta Earthquake," (in final preparation) Civil Engineering Department, Report No. CCEER-93-5, University of Nevada, Reno.

CCEER-93-6 Saiidi, M., E. Maragakis, S. Abdel-Ghaffar, S. Feng, and D. O'Connor, "Response of Bridge Hinge Restrainers During Earthquakes -Field Performance, Analysis, and Design," Civil Engineering Department, Report No. CCEER-93-6, University of Nevada, Reno, May 1993.

CCEER-93-7 Wehbe, N., Saiidi, M., Maragakis, E., and Sanders, D., "Adequacy of Three Highway Structures in Southern Nevada for Spent Fuel Transportation, Civil Engineering Department, Report No. CCEER-93-7, University of Nevada, Reno, August 1993.

CCEER-93-8 Roybal, J., Sanders, D.H., and Maragakis, E., "Vulnerability Assessment of Masonry Public Buildings in the Reno-Carson City Urban Corridor," Civil Engineering Department, Report No. CCEER-93-8, University of Nevada, Reno, May 1993.

CCEER-93-9 Zafir, Z. and Siddharthan, R., "MOVLOAD: A Program to Determine the Behavior of Nonlinear Horizontally Layered Medium Under Moving Load," Civil Engineering Department, Report No. CCEER-93-9, University of Nevada, Reno, August 1993.

CCEER-93-10 O'Connor, D.N., Saiidi, M., and Maragakis, E.A., "A Study of Bridge Column Seismic Damage Susceptibility at the Interstate 80/U.S. 395 Interchange in Reno, Nevada," Civil Engineering Department, Report No. CCEER-93-10, University of Nevada, Reno, October 1993.

CCEER-94-1 Maragakis, E., B. Douglas, and E. Abdelwahed, "Preliminary Dynamic Analysis of a Railroad Bridge," Report CCEER-94-1, January 1994.

CCEER-94-2 Douglas, B.M., Maragakis, E.A., and Feng, S., "Stiffness Evaluation of Pile Foundation of Cazenovia Creek Overpass," Civil Engineering Department, Report No. CCEER-94-2, University of Nevada, Reno, March 1994.

CCEER-94-3 Douglas, B.M., Maragakis, E.A., and Feng, S., "Summary of Pretest Analysis of Cazenovia Creek Bridge," Civil Engineering Department, Report No. CCEER-94-3, University of Nevada, Reno, April 1994.

CCEER-94-4 Norris, G.M. and Madhu, R., "Liquefaction and Residual Strength of Sands from Drained Triaxial Tests, Report 2," Civil Engineering Department, CCEER-94-4, University of Nevada, Reno, August 1994.

CCEER-94-5 Saiidi, M., Hutchens, E., and Gardella, D., "Prestress Losses in a Post-Tensioned R/C Box Girder Bridge in Southern Nevada," Civil Engineering Department, CCEER-94-5, University of Nevada, Reno, August 1994.

CCEER-95-1 Siddharthan, R., El-Gamal, M., and Maragakis, E.A., "Nonlinear Bridge Abutment Stiffnesses:

Formulation, Verification, and Design Curves," Civil Engineering Department, CCEER-95-1, University of Nevada, Reno, January 1995.

CCEER-95-2 Norris, G.M., Madhu, R., Valceschini, R., and Ashour, M., "Liquefaction and Residual Strength of Loose Sands from Drained Triaxial Tests," Report 2, Civil Engineering Department, Report No. CCEER-95-2, University of Nevada, Reno, February 1995.

CCEER-95-3 Wehbe, N., Saiidi, M., Sanders, D., and Douglas, B., "Ductility of Rectangular Reinforced Concrete Bridge Columns with Moderate Confinement,"Civil Engineering Department, Report No. CCEER-95-3, University of Nevada, Reno, July 1995.

CCEER-95-4 Martin, T., Saiidi, M., and Sanders, D., "Seismic Retrofit of Column-Pier Cap Connections in Bridges in Northern Nevada," Civil Engineering Department, Report No. CCEER-95-4, University of Nevada, Reno, August 1995.

CCEER-95-5 Darwish, I., Saiidi, M., and Sanders, D., "Experimental Study of Seismic Susceptibility of Tapered Bridge Column-Footing Connections," Civil Engineering Department, Report No. CCEER-95-5, University of Nevada, Reno, September 1995.

CCEER-95-6 Griffin, G., Saiidi, M., and Maragakis, E., "Nonlinear Seismic Response of Isolated Bridges and Effects of Pier Ductility Demand," Civil Engineering Department, Report No. CCEER-95-6, University of Nevada, Reno, November 1995.

CCEER-95-7 Acharya, S., Saiidi, M., and Sanders, D., "Seismic Retrofit of Bridge Footings and Column-Footing Connections," Report for the Nevada Department of Transportation, Civil Engineering Department, Report No. CCEER-95-7, University of Nevada, Reno, November 1995.

CCEER-95-8 Maragakis, E., Douglas, B., and Sandirasegaram, U., "Full-Scale Field Resonance Tests of a Railway Bridge," A Report to the Association of American Railroads, Civil Engineering Department, Report No. CCEER-95-8, University of Nevada, Reno, December 1995.

CCEER-95-9 Douglas, B., Maragakis, E., and Feng, S., "System Identification Studies on Cazenovia Creek Overpass," Report for the National Center for Earthquake Engineering Research, Civil Engineering Department, Report No. CCEER-95-9, University of Nevada, Reno, October 1995.

CCEER-96-1 El-Gamal, M.E. and Siddharthan, R.V., "Programs to Computer Translational Stiffness of Seat-Type Bridge Abutment," Civil Engineering Department, Report No. CCEER-96-1, University of Nevada, Reno, March 1996.

CCEER-96-2 Labia, Y., Saiidi, M., and Douglas, B., "Evaluation and Repair of Full-Scale Prestressed Concrete Box Girders," A Report to the National Science Foundation, Research Grant CMS-9201908, Civil Engineering Department, Report No. CCEER-96-2, University of Nevada, Reno, May 1996.

CCEER-96-3 Darwish, I., Saiidi, M., and Sanders, D., "Seismic Retrofit of R/C Oblong Tapered Bridge Columns with Inadequate Bar Anchorage in Columns and Footings," A Report to the Nevada Department of Transportation, Civil Engineering Department, Report No. CCEER-96-3, University of Nevada, Reno, May 1996.

CCEER-96-4 Ashour, M., Pilling, P., Norris, G., and Perez, H., "The Prediction of Lateral Load Behavior of Single Piles and Pile Groups Using the Strain Wedge Model," A Report to the California Department of

Transportation, Civil Engineering Department, Report No. CCEER-96-4, University of Nevada, Reno, June, 1996.

CCEER-97-1 Maragakis, E., Douglas, B., and Sandirasegaram, U. "Full-Scale Field Resonance Tests of a Railway Bridge," A Report to the Association of American Railroads, Civil Engineering Department, University of Nevada, Reno, May, 1996.

CCEER-97-2 Wehbe, N., M. Saiidi, and D. Sanders, "Effects of Confinement and Flares on the Seismic Performance of Reinforced Concrete Bridge Columns," Civil Engineering Department, University of Nevada, Reno, Report No. CCEER-97-2, September, 1997.

CCEER-97-3 Darwish, I., M. Saiidi, G. Norris, and E. Maragakis, "Determination of In-Situ Footing Stiffness Using Full-Scale Dynamic Field Testing," A Report to the Nevada Department of Transportation, Structural Design Division, Carson City, Nevada, Report No. CCEER-97-3, University of Nevada, Reno, October, 1997.

CCEER-97-4 Not Published.

CCEER-97-5 Isakovic, T., M. Saiidi, and A. Itani, "Influence of new Bridge Configurations on Seismic Performance," Department of Civil Engineering, University of Nevada, Reno, Report No. CCEER-97-5, September, 1997.

CCEER-98-1 Itani, A., "Cyclic Behavior of "as Built" Laced Members With End Gusset Plates on the San Francisco Bay Bridge", Center for Civil Engineering Earthquake Research, Department of Civil Engineering, University of Nevada, Reno, Nevada, Report No. CCEER-98-1, March, 1998.

CCEER-98-2 Norris, G., and M. Ashour, "Liquefication and Undrained response evaluation of Sands from Drained Formulation", Center for Civil Engineering Earthquake Research, Department of Civil Engineering, University of Nevada, Reno, Nevada, Report No. CCEER-98-2, May, 1998.

CCEER-98-3 Qingbin, C., B.M. Douglas, E. Maragakis, and I.G. Buckle, "Extraction of Nonlinear Hysteretic Properties of Seismically Isolated Bridges from Quick-Release Field Tests", Center for Civil Engineering Earthquake Research, Department of Civil Engineering, University of Nevada, Reno, Nevada, Report No. CCEER-98-3, June, 1998.

CCEER-98-4 Maragakis, E., B.M. Douglas, and C. Qingbin, "Full-Scale Field Capacity Tests of a Railway Bridge", Center for Civil Engineering Earthquake Research, Department of Civil Engineering, University of Nevada, Reno, Nevada, Report No. CCEER-98-4, June, 1998.

CCEER 98-5 Itani, A., B. Douglas, and J. Woodgate, "Cyclic Behavior of Richmond-San Rafael Retrofitted Tower Leg", Center for Civil Engineering Earthquake Research, Department of Civil Engineering, University of Nevada, Reno, Nevada, Report No. CCEER-98-5, June, 1998.

CCEER 98-6 Moore, R., M. Saiidi, and A. Itani, "Seismic Behavior of New Bridges with Skew and Curvature", Center for Civil Engineering Earthquake Research, Department of Civil Engineering, University of Nevada, Reno, Nevada, Report No. CCEER-98-6, October, 1998.

CCEER 98-7 Itani, A., and A. Dietrich, "Cyclic Behavior of Double Gusset Plate connections", Center for Civil Engineering Earthquake Research, Department of Civil Engineering, University of Nevada, Reno, Nevada, Report No. CCEER-98-7, December, 1998.

CCEER 99-1 Caywood, C., M. Saiidi, and D. Sanders, "Seismic Retrofit of Flared Bridge Columns with Steel Jackets," Civil Engineering Department, University of Nevada, Reno, Report No. CCEER-99-1, February 1999.

CCEER 99-2 Mangoba, N., M. Mayberry, and M. Saiidi, "Prestress Loss in Four Box Girder Bridges in Northern Nevada," Civil Engineering Department, University of Nevada, Reno, Report No. CCEER-99-2, March 1999.

CCEER 99-3 Abo-Shadi, N., M. Saiidi, and D. Sanders, "Seismic Response of Bridge Pier Walls in the Weak Direction," Civil Engineering Department, University of Nevada, Reno, Report No. CCEER-99-3, April 1999.

CCEER 99-4 Buzick, A. and M. Saiidi, "Shear Strength and Shear Fatigue Behavior of Full-Scale Prestressed Concrete Box Girders," Civil Engineering Department, University of Nevada, Reno, Report No. CCEER-99-4, April 1999.

CCEER 99-5 Randall, M., M. Saiidi, E. Maragakis, and T. Isakovic, "Restrainer Design Procedures for Multi-Span Simply-Supported Bridges," Civil Engineering Department, University of Nevada, Reno, Report No. CCEER-99-5, April 1999.

CCEER 99-6 Wehbe, N., and M. Saiidi, "User's Manual for RCMC v 1.2- A Computer Program for Moment-Curvature Analysis of Confined and Unconfined Reinforced Concrete Sections," Civil Engineering Department, University of Nevada, Reno, Report No. CCEER-99-6, May 1999.

CCEER-99-7 Burda, J. and A. Itani, "Studies of Seismic Behavior of Steel Base Plates," Civil Engineering Department, University of Nevada, Reno, Report No. CCEER-99-7, May 1999.

CCEER-99-8 M. Ashour and G. Norris, "Refinement of the Strain Wedge Model Program," Civil Engineering Department, University of Nevada, Reno, Report No. CCEER-99-8, March 1999.

CCEER-99-9 Dietrich, A., and A. Itani, "Cyclic Behavior of Laced and Perforated Steel Members on the San Francisco-Oakland Bay Bridge," Civil Engineering Department, University of Nevada, Reno, . Reno, Report No. CCEER-99-9, December 1999.

CCEER 99-10 Itani, A., and A. Dietrich, "Cyclic Behavior of Built Up Steel Members and their Connections," Civil Engineering Department, University of Nevada, Reno, Report No. CCEER-99-10, December 1999.

CCEER 99-11 Itani, A., and J. Woodgate, "Axial and Rotational Ductility of BuiltUp Structural Steel Members," Civil Engineering Department, University of Nevada, Reno, Report No. CCEER-99-11, December 1999.

CCEER 99-12 Sgambelluri, M., Sanders, D.H., and Saiidi, M., "Behavior of One-Way Reinforced Concrete Bridge Column Hinges in the Weak Direction," Report No. 99-12, Department of Civil Engineering, University of Nevada, Reno, December 1999.

CCEER 99-13 Laplace, P., Sanders, D.H., Douglas, B, and Saiidi, M. "Shake Table Testing of Flexure Dominated Reinforced Concrete Bridge Columns," Report No. 99-13, Department of Civil Engineering, University of Nevada, Reno, December 1999.

CCEER 99-14 Itani, A., J. A. Zepeda, and E. A. Ware "Cyclic Behavior of Steel Moment Frame Connections for the Moscone Center Expansion," Civil Engineering Department, University of Nevada, Reno, Report No. CCEER-99-14, December 1999.

CCEER 00-1 Ashour, M., and Norris, G. "Undrained Lateral Pile and Pile Group Response in Saturated Sand", Civil Engineering Department, University of Nevada, Reno, Report No. CCEER-00-1, May 1999. January 2000.

CCEER 00-2 Saiidi, M. and Wehbe, N., "A Comparison of Confinement Requirements in Different Codes for Rectangular, Circular, and Double-Spiral RC Bridge Columns," Civil Engineering Department, University of Nevada, Reno, Report No. CCEER-00-2, January 2000.

CCEER 00-3 McElhaney, B., M. Saiidi, and D. Sanders, "Shake Table Testing of Flared Bridge Columns With Steel Jacket Retrofit," Civil Engineering Department, University of Nevada, Reno, Report No. CCEER-00-3, January 2000.

CCEER 00-4 Martinovic, F., M. Saiidi, D. Sanders, and F. Gordaninejad, "Dynamic Testing of Non-Prismatic Reinforced Concrete Bridge Columns Retrofitted with FRP Jackets," Civil Engineering Department, University of Nevada, Reno, Report No. CCEER-00-4, January 2000.